

NORTHWESTERN UNIVERSITY

Synthesis and Characterization of Isoprene-Derived Organosulfates  
And Other Atmospherically-Relevant Molecules

A DISSERTATION

SUBMITTED TO THE GRADUATE SCHOOL  
IN PARTIAL FULFILLMENT OF THE REQUIREMENTS

for the degree

DOCTOR OF PHILOSOPHY

Field of Chemistry

By

Jonathan Gregory Varelas

EVANSTON, ILLINOIS

December 2021

## Abstract

### Synthesis and Characterization of Isoprene-Derived Organosulfates and Other Atmospherically-Relevant Molecules

Jonathan Gregory Varelas

Secondary organic aerosol (SOA) particles are a class of highly abundant atmospheric constituents that represent a substantial fraction of carbon within the climate system. A subset of naturally-occurring SOA particles are formed through atmospheric oxidation of biogenic volatile organic compounds (BVOCs), forming oxygenated products of lower volatility that can partition into the condensed phase and subsequently exposed to a variety of aqueous phase transformations. Particulate SOA, and aerosols generally, are thought to have a substantial impact on the radiative budget of the planet, yet their chemical and physical complexity preclude the accurate analysis of these systems and the carbon-based molecules from which they are derived. Adding further convolution is the presence of atmospheric pollutants emitted through anthropogenic activity, such as sulfur dioxide and nitrogen oxides. The interaction between biogenic SOA and man-made pollutants can result in numerous chemical transformations of organic compounds within SOA, one of which is the formation of carbon-based compounds bearing sulfate ester functionality, or organosulfates. Despite the molecular complexity of species within atmospheric aerosols, organosulfates derived from isoprene, the largest non-methane source of atmospheric carbon, has been suggested to be the most dominant and ubiquitous organic compound bearing sulfate ester moieties. However, a lack of authentic chemical standards hampers the accurate study of the formation, properties and atmospheric fate of isoprene-derived organosulfates.

In this thesis, we report a synthetic methodology to access organosulfates derived from a highly prevalent oxidation product of isoprene known as isoprene epoxydiol (IEPOX). The

development of this method allows for facile access to all possible regiochemical and stereochemical isomers of this family of compounds. Efforts were directed in the preparation of these species as ammonium salts, which are suggested to be relevant to the natural formation of IEPOX-derived organosulfates in the atmosphere. The generation of these compounds also allowed for evaluation of their chemical and physical properties through the use of several analytical methods. Through the measurement of aqueous pH, a general trend of compound acidity was established, correlating strongly with steric congestion of the sulfate ester functionality. The inherent stability of each compound was investigated in both aqueous and acidic media using time-point nuclear magnetic resonance (NMR). It was found that the tertiary isomers of the IEPOX-derived organosulfates exhibited degradation, while the remaining compounds were stable under aqueous and acidic conditions. It is our hope that the preparation of this series of compounds, and our preliminary analysis of their chemical properties, will be a useful avenue of study within the atmospheric and organic synthesis communities.

In addition to our efforts concerning IEPOX-derived organosulfates, isotopologues of  $\alpha$ -pinene, a highly abundant atmospheric terpene, were synthesized using site-specific deuteration to install deuterium atoms at various positions along the carbon backbone. These labeled species are currently being used in several ongoing domestic and international collaborative efforts to characterize the various atmospheric oxidation pathways of gas phase  $\alpha$ -pinene.

---

Prof. Regan J Thomson and Prof. Franz M. Geiger

Research Advisors

## Acknowledgements

This thesis would not have been possible without the persistent support of my colleagues, collaborators and loved ones throughout these last few years.

Firstly, I would like to thank my research advisors Prof. Regan Thomson and Prof. Franz Geiger. Regan and Franz – I am continually in awe of your command of the subject matter, passion for research and scientific brilliance. You have both provided me with unbelievable encouragement, saint-like patience and mentorship during this process, and there is no way I can repay you for all that I have learned. I am incredibly proud and grateful to have had you both as my advisors. It hasn't been easy, but I thank you both for the knowledge and experience I received from being a student in your research groups. I also extend my gratitude to the other members of my thesis committee Prof. Karl Scheidt and Prof. Rick Silverman for their advice and feedback during departmental milestones.

I also thank my undergraduate advisor Prof. Seann Mulcahy. Seann – you are the reason I even considered graduate school in the first place, and your love of organic chemistry set the stage for me. Thank you for the inspiration. And a huge thank you to the other students in the Mulcahy research group I had the pleasure of working with as an undergraduate at Providence College.

I extend my deepest gratitude to all of the Thomson and Geiger group members, past and present. Whether we worked closely or not, your support made this experience incredibly rewarding. For group members who have moved on – Dr. Mary Alice Upshur, Dr. Ariana Gray Be, Dr. Dawning Liu, Dr. Naomi Dalchand, Dr. Hilary Chase, Dr. Paul Ohno, Dr. Jennifer Rote, Dr. James Hudson Tryon – or who are still here – Aleia, Aidan, Jana, Israel, Rebekah, Jenny, Anhia – you are all brilliant and amazing, and I wish you all nothing but success and happiness.

Additional thanks to friends outside of my research groups – Dr. Jason “the Chad” Khoury, Dr. Tyler Pearson and Becky.

I want to extend my appreciation to the other two members of ‘the Three Musketeers’ Dr. Marvin Vega and Dr. Emily Robinson – thank you both for the friendship, support and laughs while you were both here, and an even bigger thanks for talking me off the ledge multiple times (Emily, I’ll always be thankful for our frantic walk-and-talks around the third floor of Tech). And to Dr. Abdallah Diagne, thanks for being an amazing friend and offering your support even after graduating, as well as thanks for our three-hour podcasts in which we over-analyze movies more than any human being probably should.

To my friends from home and from college, thank you for all of the support during this experience. James, thanks for the long political talks and unexpected calls. To my friends in Special Guest, especially Gio, thank you for providing some levity on many dark days. Ron, Nick, Scottie and Jamesy: thanks for the late nights playing Call of Duty and for the endless supply of dark humor and memes.

To my family, you all have given me a tremendous amount of love and encouragement during the last few years, and I cannot thank you enough for all of the support. Lacey, Paige, Granny Mo, and new additions to our family, Jason and Spencer – you are all the best.

To my brother, Andrew – thank you for being my best friend, for always offering some much-needed perspective after a tough day in the lab, and for encouraging me to not take myself so seriously. You are an incredible role model and I hope to be as fiercely intelligent and resourceful as you as I step out into the professional world. I love you, dude.

Mom and Dad – I could write an entire separate thesis about how much I love and cherish you both and how much I appreciate all that you’ve done for me. Your love and willingness to

help have made me feel as if I'm home with you despite being across the country. I mean it when I say that I don't know if I could have done any of this without you both behind me. Thank you for being an endless support system, and I am so proud to be your son. I love you both.

And, finally, to my girlfriend Sarah. You met me early in this endeavor, and I cannot tell you how grateful I am that I'm finishing it with you by my side. It is crazy to think that you've spent the most time with me during this process, and you are one of the biggest reasons I've stayed sane – relatively. During this challenging time, you've seen me at my best, and you've seen me at my absolute lowest, and you still continue to love me and show me patience and kindness. I owe you the world for all that you've done for me in the past few years, and I can't find the words to describe the gratitude, admiration and respect that I have for you. I love you, and thank you for everything.

**List of Abbreviations**

(NH <sub>4</sub> ) <sub>2</sub> SO <sub>4</sub>	ammonium sulfate
2-MG	2-methylglyceric acid
Ac	acetyl
Ac <sub>2</sub> O	acetic anhydride
ATOFMS	aerosol time-of-flight mass spectrometry
Bn	benzyl
BnBr	benzyl bromide
BVOC	biogenic volatile organic compound
CCN	cloud condensation nuclei
CI	chemical ionization
CID	collision-induced dissociation
CIMS	chemical ionization mass spectrometer
D <sub>2</sub> O	deuterium oxide
D <sub>2</sub> SO <sub>4</sub>	<i>d</i> <sub>2</sub> -sulfuric acid
DCM	dichloromethane
DDQ	2,3-dichloro-5,6-dicyano-1,4-benzoquinone
di	deionized
DIPEA	diisopropylethylamine
DMAP	4-dimethylaminopyridine
DMF	<i>N,N</i> -dimethylformamide
DMSO	dimethyl sulfoxide

eq. or Equiv	equivalence
ESI	electrospray ionization
Et	ethyl
EtOH	ethanol
FTIR	Fourier-transform infrared spectrometry
GC	gas chromatography
H <sub>2</sub>	hydrogen gas
H <sub>2</sub> SO <sub>4</sub>	sulfuric acid
HEC	Harvard environmental chamber
HILIC	hydrophilic interaction liquid exchange chromatography
HO	hydroxyl radical
HOM	highly oxygenated molecules
HPLC	high performance liquid chromatography
HR	high resolution
HRMS	high-resolution mass spectrometry
HSO <sub>3</sub> Cl	chlorosulfonic acid
ICR	ion cyclotron resonance
IEPOX	isoprene epoxydiol
IR	infrared
ISOPOOH	hydroxyhydroperoxide
KOH	potassium hydroxide
LA-SPAMS	laser ablation single particle aerosol mass spectrometry
LC	liquid chromatography

M	molar, or molarity
$m/z$	mass-to-charge ratio
MACR	methacrolein
MAE	methacrylic acid epoxide
$m$ CPBA	<i>meta</i> -chloroperbenzoic acid
Me	methyl
MeOH	methanol
MPAN	methacroyl peroxyxynitrate
MS	mass spectrometry
$\text{Na}_2\text{CO}_3$	sodium carbonate
$\text{Na}_2\text{S}_2\text{O}_7$	sodium pyrosulfate
$\text{NaBH}_4$	sodium borohydride
$\text{NaH}$	sodium hydride
$\text{NaOD}$	sodium deuterioxide
$\text{NaOH}$	sodium hydroxide
$\text{NEt}_3$	triethylamine
$\text{ng m}^{-3}$	nanograms per cubic meter
$\text{NH}_3$	ammonia
$\text{NH}_4\text{HCO}_2$	ammonium formate
$\text{NMe}_3$	trimethylamine
NMR	nuclear magnetic resonance
$\text{NO}_3$ -CIMS	nitrate-based chemical ionization mass spectrometer
$\text{NO}_x$	nitrogen oxides

NTP	natural temperature and pressure
O <sub>3</sub>	ozone
PAH	polycyclic aromatic hydrocarbons
PDT	pendant drop tensiometry
PhCHO	benzaldehyde
PM <sub>2.5</sub>	fine particulate matter
PMB	<i>para</i> -methoxybenzyl
POA	primary organic aerosol
Pyr, or Py	pyridine
QTOFMS	quadrupole time-of-flight mass spectrometry
RO <sub>2</sub>	peroxyradical
SDS	sodium dodecyl sulfate
SeO <sub>2</sub>	selenium dioxide
SFG	sum frequency generation
SLS	sodium lauryl sulfate
SO <sub>2</sub>	sulfur dioxide
SO <sub>3</sub>	sulfur trioxide
SOA	secondary organic aerosol
TBA	tetrabutylammonium
TBAF	tetrabutylammonium fluoride
TBSCl	<i>tert</i> -butyldimethylsilyl chloride
<i>t</i> BuOOH	<i>tert</i> -butyl hydroperoxide
TCE	trichloroethyl

Tg yr <sup>-1</sup>	teragrams per year
THF	tetrahydrofuran
ToF	time-of-flight
TOPAS	Tunable optical parametric amplifier set-up
TQD	triple quadrupole mass spectrometry
VOC	volatile organic compound

**Table of Contents**

<b>Abstract.....</b>	<b>2</b>
<b>Acknowledgements .....</b>	<b>4</b>
<b>List of Abbreviations .....</b>	<b>7</b>
<b>List of Schemes.....</b>	<b>19</b>
<b>List of Tables .....</b>	<b>21</b>
<b>Chapter 1 Chemical Properties, Prevalence, and Relevance of Organosulfates within the Atmosphere.....</b>	<b>22</b>
<b>1.2 Prevalence of Organosulfate Compounds .....</b>	<b>28</b>
<b>1.2.1 Commercial applications of Organosulfates .....</b>	<b>28</b>
<b>1.2.2 Organosulfates within Natural Products and Biological Systems.....</b>	<b>30</b>
<b>1.3 Organosulfates within the Atmosphere .....</b>	<b>32</b>
<b>1.3.1 Isoprene (IEPOX)–Derived Organosulfates.....</b>	<b>35</b>
<b>1.3.2 Organosulfates Derived from Other BVOCs .....</b>	<b>44</b>
<b>1.3.3 Organosulfates Derived from Aromatic Compounds.....</b>	<b>46</b>
<b>1.4 Detection, Identification and Measurement of Organosulfates.....</b>	<b>48</b>
<b>1.4.1 Offline Methods.....</b>	<b>48</b>
<b>1.4.2 Online Methods .....</b>	<b>50</b>
<b>1.5 Conclusions and Scope of Work .....</b>	<b>51</b>
<b>Chapter 2 Synthesis of IEPOX-derived Organosulfates .....</b>	<b>54</b>

	13
<b>2.1 Synthetic Approaches Towards Sulfate Esters .....</b>	<b>55</b>
<b>2.1.1 Chlorosulfonic Acid .....</b>	<b>56</b>
<b>2.1.2 Sodium pyrosulfate .....</b>	<b>56</b>
<b>2.1.3 Sulfuric acid.....</b>	<b>57</b>
<b>2.1.4 Sulfur trioxide–amine complexes .....</b>	<b>58</b>
<b>2.2 Past Syntheses of Atmospherically relevant Organosulfates as Chemical Standards</b>	<b>61</b>
<b>2.3 Development of a Regioselective and Stereocontrolled Synthesis of IEPOX-derived Organosulfates.....</b>	<b>66</b>
<b>2.3.1 Synthesis of <i>anti</i>-IEPOX-derived organosulfates.....</b>	<b>68</b>
<b>2.3.2 Synthesis of <i>syn</i>-IEPOX-derived organosulfates .....</b>	<b>73</b>
<b>2.3.3 Challenges in the Synthesis of IEPOX-derived Organosulfates .....</b>	<b>77</b>
<b>2.4 Conclusions.....</b>	<b>91</b>
<b>2.5 Experimentals.....</b>	<b>91</b>
<b>2.5.1 General Information.....</b>	<b>91</b>
<b>2.5.2 Synthetic Procedures .....</b>	<b>92</b>
<b>Chapter 3 Evaluation of Stability and Acidity of IEPOX-Derived Organosulfates .....</b>	<b>118</b>
<b>3.1 Inherent Acidity of IEPOX-derived Organosulfates .....</b>	<b>119</b>
<b>3.1.1 Measurement of pH values for IEPOX-derived Organosulfate Compounds.....</b>	<b>121</b>
<b>3.2 Stability of IEPOX-derived Organosulfates.....</b>	<b>127</b>
<b>3.2.1 Time-Point NMR Spectra of IEPOX-derived Organosulfates .....</b>	<b>129</b>
<b>3.2.2 Efforts to Synthesize Hypothesized Decomposition Product III-11 .....</b>	<b>135</b>

	14
<b>3.3 Conclusions.....</b>	<b>140</b>
<b>3.4 Experimental Information .....</b>	<b>142</b>
<b>Chapter 4 Future Directions Regarding IEPOX-derived Organosulfates &amp; Synthesis and Analysis of Isotopically-labelled Terpenes .....</b>	<b>143</b>
<b>4.1 Ongoing Work and Future Directions of IEPOX-derived Organosulfates.....</b>	<b>144</b>
<b>4.1.1 Surface Specific Analysis of IEPOX-derived Organosulfates – Sum Frequency Generation Spectroscopy and Pendant Drop Tensiometry .....</b>	<b>144</b>
<b>4.1.2 Uptake of <math>\alpha</math>-pinene-derived Semivolatile Organic Compounds by Organosulfate Particles.....</b>	<b>150</b>
<b>4.2 Synthesis of <math>\alpha</math>-Pinene Isotopologues .....</b>	<b>152</b>
<b>4.2.1 Using Selective Deuteration for the Investigation of <math>\alpha</math>-Pinene-derived HOM... </b>	<b>153</b>
<b>4.2.2 Unimolecular reactions of Peroxy Radicals Formed in Oxidation of <math>\alpha</math>-pinene via Hydroxyl Radicals.....</b>	<b>158</b>
<b>4.3 Probing Synergy of Atmospheric Oxidation Products Through <math>^{13}\text{C}</math> Isotopic-Labeling .....</b>	<b>166</b>
<b>4.4 Conclusions.....</b>	<b>169</b>
<b>References.....</b>	<b>170</b>
<b>Appendix.....</b>	<b>192</b>

## List of Figures

<b>Figure 1.1</b> The emission of BVOCs into the atmosphere and their subsequent atmospheric oxidation generates chemical species of lower volatility, leading to partitioning from the gas phase to the condensed aerosol phase. ....	24
<b>Figure 1.2</b> Radiative forcing estimates of various atmospheric constituents and their uncertainties of influence relative to 1750. Figure adapted from IPCC, 2013.....	26
<b>Figure 1.3</b> Several natural products and biologically-relevant compounds bearing sulfate esters as functional groups. ....	31
<b>Figure 1.4</b> The emission of BVOC and their resulting SOA constituents can interact with anthropogenic pollutants resulting in the generation of organosulfates, or sulfate esters .....	33
<b>Figure 1.5</b> Sector share of anthropogenic sulfur dioxide emissions measured from 2005–2014. Figure adapted from Fioletov et al, 2016.....	34
<b>Figure 1.6</b> Proposed structures of isoprene–derived organosulfates throughout the literature....	40
<b>Figure 1.7</b> The suite of possible structures of IEPOX–derived organosulfates attributed to $m/z$ 215. ....	41
<b>Figure 1.8</b> A collection of organosulfates proposed to form from $\alpha$ -pinene and $\beta$ -pinene oxidation products.....	45
<b>Figure 1.9</b> The emission of aromatic compounds from urbanized areas can contribute to the formation of aromatic organosulfates. ....	47
<b>Figure 2.1</b> A general synthetic strategy to access organosulfates via masked sulfate esters and subsequent deprotection.....	60
<b>Figure 2.2</b> The eight IEPOX-derived organosulfates.....	67
<b>Figure 2.3</b> The overall synthetic methodology to access IEPOX-derived organosulfates.....	68

<b>Figure 2.4</b> NMR spectrum of <i>anti</i> organosulfate <b>II-31</b> in $d_6$ -DMSO showing a substantial ammonium impurity at $\delta$ 7.45 ppm.....	81
<b>Figure 2.5</b> NMR spectrum of protected ammonium salt <b>II-59</b> in $d_6$ -DMSO with appropriate equimolar ammonium signal at $\delta$ 7.05 ppm.....	86
<b>Figure 2.6</b> General representation of the Prevost dihydroxylation to afford <i>anti</i> vicinal diols. ..	87
<b>Figure 3.1</b> The suite of IEPOX-derived organosulfates prepared as ammonium salts. ....	121
<b>Figure 3.2</b> Pictorial representation of pH and pD values measured for the suite of IEPOX-derived organosulfates and the parent tetraols. pD values are listed in parentheses under pH values. Data taken from <b>Table 3.1</b> . ....	126
<b>Figure 3.3</b> Rationalization of the observed trend of acidity shown by the IEPOX-derived organosulfates through differing degrees of intramolecular hydroxyl interactions between the primary, secondary and tertiary isomers. ....	127
<b>Figure 3.4</b> Representation of the formation of the IEPOX-derived organosulfates from acidic uptake of <i>trans</i> - $\beta$ -IEPOX and subsequent attack of sulfate, and several chemical byproducts of decomposition of the IEPOX-derived species. ....	130
<b>Figure 3.5</b> NMR spectra of <i>syn</i> tertiary organosulfate <b>III-4</b> in D <sub>2</sub> O. Experimental duration was 30 days, with the bottom spectrum taken at day and the top taken at day 30. Both spectra are normalized to the signal intensity of the deuterium oxide peak at 4.79 ppm. Disappearance of the methylene signal at 3.63 ppm was used as the baseline for decomposition. ....	132
<b>Figure 3.6</b> Spectra of <i>syn</i> tertiary sulfate <b>III-3</b> and decomposition to the corresponding 2-methyltetraol held <i>in vacuo</i> using a laboratory-grade pump. ....	133
<b>Figure 3.7</b> NMR spectra of <i>anti</i> tertiary organosulfate <b>III-8</b> in D <sub>2</sub> O and the hypothesized chemical transformation leading to the signal formed at 9.24 ppm. ....	134

**Figure 3.8** Comparison of NMR spectrum of *anti* tertiary organosulfate **III-8** in D<sub>2</sub>O with simulated <sup>1</sup>H NMR spectra of several potential decomposition products, including **III-11** and its enol tautomeric forms (**III-21**). Spectra for each compound were simulated using the native NMR calculation plug-in within *MestrelNova*<sup>TM</sup> NMR processing software. The confidence interval of the calculations is reported to be 95%. The relevant spectral window is shown from ~5.8 ppm – 13 ppm. The aldehydic proton of **III-11** is highlighted in blue, and the olefinic proton attributed to the enol tautomer **III-21** is highlighted in red. .... 139

**Figure 3.9** Comparison of the <sup>1</sup>H and <sup>13</sup>C NMR spectra of *anti* tertiary organosulfate **III-8** in D<sub>2</sub>O and corresponding mechanistic explanation. The spectral windows for the proton and carbon spectra were 6.0 – 10 ppm and 145 – 205 ppm respectively. The proton and carbon spectra were taken at t = 20 days. The 9.28 ppm and 198.84 ppm peaks highlighted in blue are suggested to be due to **III-11**, and 6.67 ppm and 154.12 ppm highlighted in red due to tautomer **III-21**. .... 140

**Figure 4.1** Energy diagram depiction of SFG.  $\omega$  represents the frequency of each incident light field.  $\omega_{IR}$  represents the frequency of a tunable IR light field, and  $\omega_{vis}$  represents a visible light field.  $\omega_{SFG}$  represents the sum frequency of the two incident light fields. .... 146

**Figure 4.2** SFG spectra of the IEPOX-derived organosulfates and the *syn* and *anti* tetraols. Each sample was spin-coated on an SiO<sub>2</sub> window and was measured in triplicate. The spectra were collected using *ssp* polarization. .... 148

**Figure 4.3** On the left, an image of the pendant drop tensiometry instrument. On the right, an enlarged view of a pendant drop of a sample solution generated using a syringe. Figure adapted from Gray Bé et al 2017, courtesy of Dr. Ariana Gray Bé. .... 150

**Figure 4.4** The two organosulfates derived from IEPOX used in the study of  $\alpha$ -pinene-derived SVOC uptake in collaboration with Harvard University. .... 152

- Figure 4.5** The proposed autoxidation pathways of  $\alpha$ -pinene via ozonolysis and subsequent oxidations. Figure adapted from Iyer et al, 2021. Each of the pathways of oxidation produce structurally-unique peroxy radicals which are vital intermediates in the formation of HOM. Deuteration at certain positions of the  $\alpha$ -pinene skeleton (marked in red and blue) will assist in the elucidation of which peroxy radicals are formed and their relative rates by measuring the exchange of deuterium atoms. .... 155
- Figure 4.6** Diagram of the experimental set-up to probe HOM formation of  $\alpha$ -pinene ozonolysis courtesy of the Ehn group at University of Helsinki. .... 157
- Figure 4.7** The three isotopologues of  $\alpha$ -pinene **IV-4**, **IV-11** and **IV-12** synthesized to probe the unimolecular reactions of the  $\alpha$ -pinene-derived peroxy radicals. .... 160
- Figure 4.8** Instrument schematic of the GC-ToF-CIMS. Figure exported from Xu et al, 2018 with permission from Dr. Lu Xu..... 161
- Figure 4.9** Potential mechanisms of synergy between pinanediol **IV-21** and glyoxal **IV-22** and the subsequent formation of complex organic species. .... 167

## List of Schemes

<b>Scheme 1.1</b> Commercial production of sodium dodecyl sulfate (SDS).....	29
<b>Scheme 1.2</b> Formation pathway towards isoprene-derived organosulfates and other isoprene-derived oxidation products under low NO <sub>x</sub> conditions, adapted from Surratt et al, 2010.....	37
<b>Scheme 1.3</b> Formation pathway towards isoprene-derived organosulfates and other isoprene-derived oxidation products under high NO <sub>x</sub> conditions, adapted from Lin et al, 2013. ....	39
<b>Scheme 2.1</b> Synthesis of organosulfates via sulfation of an alcohol using chlorosulfonic acid. .	56
<b>Scheme 2.2</b> Synthesis of organosulfates via sulfation of an alcohol using sodium pyrosulfate. .	57
<b>Scheme 2.3</b> Synthesis of organosulfates via epoxide opening using sulfuric acid. ....	57
<b>Scheme 2.4</b> Synthesis of organosulfates using sulfuric acid and dicyclohexylcarbodiimide. ....	58
<b>Scheme 2.5</b> Synthesis of organosulfates using sulfur trioxide amine adducts. ....	59
<b>Scheme 2.6</b> Synthesis of aryl organosulfates utilizing a masked sulfate ester strategy disclosed by Liu and coworkers, 2004.....	61
<b>Scheme 2.7</b> Syntheses of various organosulfates believed to be derived from isoprene. ....	63
<b>Scheme 2.8</b> Syntheses of various organosulfates derived from $\alpha$ - and $\beta$ - pinene and limonene. 65	65
<b>Scheme 2.9</b> Syntheses of aromatic organosulfates.....	66
<b>Scheme 2.10</b> Synthesis of <i>anti</i> IEPOX-derived organosulfates <b>II-34</b> and <b>II-32</b> . ....	70
<b>Scheme 2.11</b> Synthesis of <i>anti</i> IEPOX-derived organosulfates <b>II-31</b> and <b>II-33</b> .....	72
<b>Scheme 2.12</b> Synthesis of <i>syn</i> IEPOX-derived organosulfates <b>II-30</b> and <b>II-28</b> . ....	74
<b>Scheme 2.13</b> Synthesis of primary <i>syn</i> IEPOX-derived organosulfates <b>II-27</b> and <b>II-29</b> .....	76
<b>Scheme 2.14</b> Initial final steps in the synthetic route towards <i>syn</i> primary organosulfate <b>II-27</b> . 78	78
<b>Scheme 2.15</b> Revised method of sulfation in the synthesis of <i>syn</i> primary organosulfate <b>II-27</b> . 79	79

<b>Scheme 2.16</b> Depiction of hypothetical isolation of pyridinium salt <b>II-58</b> and subsequent counterion metathesis followed by hydrogenolysis to yield <b>II-59</b> . .....	85
<b>Scheme 3.1</b> Initial synthetic route to access aldehyde <b>III-11</b> . .....	135
<b>Scheme 3.2</b> A revised synthetic route towards <b>III-11</b> utilizing various protecting groups. ....	136
<b>Scheme 3.3</b> An additional revised synthetic route towards aldehyde <b>III-11</b> . .....	138
<b>Scheme 4.1</b> Synthesis of $\alpha$ -pinene <b>IV-3</b> and <b>IV-4</b> . .....	156
<b>Scheme 4.2</b> Oxidation of $\alpha$ -pinene via hydroxyl radical, the subsequent generation of RO <sub>2</sub> species <b>IV-8</b> , <b>IV-9</b> , <b>IV-10</b> , and three potential unimolecular reactions from <b>IV-9</b> . The overall rate of unimolecular reactions is given by $k_{\text{uni}} = k_{1,5\text{H}} + k_{1,6\text{H}} + k_{\text{endo}}$ .....	160
<b>Scheme 4.3</b> The oxidation of $\alpha$ -pinene isotopologues <b>IV-4</b> , <b>IV-11</b> , and <b>IV-12</b> to form deuterated derivatives of <b>IV-9</b> and the unimolecular reactions relevant to each deuterium-labelled compound. ....	163
<b>Scheme 4.4</b> Synthesis of $\alpha$ -pinene isotopologue <b>IV-12</b> . .....	165
<b>Scheme 4.5</b> Synthesis of $\alpha$ -pinene isotopologue <b>IV-11</b> . .....	165
<b>Scheme 4.6</b> Intended synthetic route to generate labeled pinanediol <b>IV-23</b> . .....	169

**List of Tables**

<b>Table 2.1</b> Efforts to remove ammonium impurity from <i>anti</i> primary sulfate <b>II-31</b> using a variety of purification methods.....	83
<b>Table 2.2</b> Conditions for the reaction screen of Prevost dihydroxylation of <b>II-60</b> to afford <b>II-61</b> . For all entries, the hydrolysis conditions were dissolution in 3.0 M KOH (Concentration of <b>II-60</b> in solution: 0.5 M). Entries marked with blue utilized molecular sieves in the introduction of I <sub>2</sub> . .....	88
<b>Table 2.3</b> Conditions for the opening of epoxide <b>II-36</b> to afford <b>II-61</b> .....	90
<b>Table 3.1</b> pH and pD measurements of the suite of IEPOX-derived organosulfates <b>III-1,2,...,8</b> , and the parent <i>syn</i> and <i>anti</i> tetraols <b>III-9</b> and <b>III-10</b> respectively. All measurements done in triplicate. Ambient temperature for all measurements was 20.3 °C.....	125
<b>Table 3.2</b> Summary of observed lifetimes of the suite of IEPOX-derived organosulfates via time-point NMR under aqueous and acidic conditions.....	130

**Chapter 1**

Chemical Properties, Prevalence, and Relevance of Organosulfates within the Atmosphere

## 1.1 Introduction - Organic Atmospheric Aerosols

The topic of climate change has long perplexed the scientific community due to the number of factors influencing global temperatures within the atmosphere. Apart from the canonical forcings that have been well-studied, such as emission of carbon dioxide and other greenhouse gases, there are a number of atmospheric constituents that remain poorly understood. As climate change is one of the most dire threats facing the planet, a comprehensive view of all relevant factors is essential to understanding the causes, stakes and potential courses of action related to rising global temperatures.<sup>1</sup> Among these poorly understood constituents are atmospheric aerosols.

Atmospheric aerosols are defined as gaseous suspensions of solid or liquid matter and are emitted from a plethora of natural and anthropogenic sources.<sup>1-3</sup> Biogenic aerosols, including emissions from large forested areas, sea spray and gases from volcanic eruption, account for the majority of aerosols in the atmosphere (appx. 90% by mass).<sup>4</sup> Depending on their particular type and characteristics, aerosols exhibit a wide range of properties that influence the global energy budget, such as scattering and absorbing radiation and seeding cloud condensation.<sup>2-4</sup>

Of particular interest to atmospheric scientists and organic chemists alike are carbon-based atmospheric aerosols. Gaseous organic species constitute the majority of fine particulate matter in both natural and industrial environments,<sup>2, 5</sup> and can generally be categorized into two distinct groups. Primary organic aerosols (POA) are gaseous organic species that are emitted directly into the atmosphere without further chemical transformation, including fossil fuel combustion, suspensions of soil particulates and plant debris, biomass burning and emissions via volcanic eruption. Distinct from primary organic aerosol, secondary organic aerosols (SOA) constitutes the majority of carbon in the atmosphere. SOA is defined as the resultant material from the

atmospheric oxidation of volatile organic compounds (VOCs) originating from both natural sources, named biogenic volatile organic compounds (BVOCs), and anthropogenic sources. The oxidation of these compounds via interactions with atmospheric oxidants such as ozone and hydroxyl radical can lead to structural diversification through the incorporation of oxygen atoms, and thus generate species of lower volatility able to partition from the gas phase into the condensed liquid phase (**Figure 1.1**).<sup>2, 5</sup>

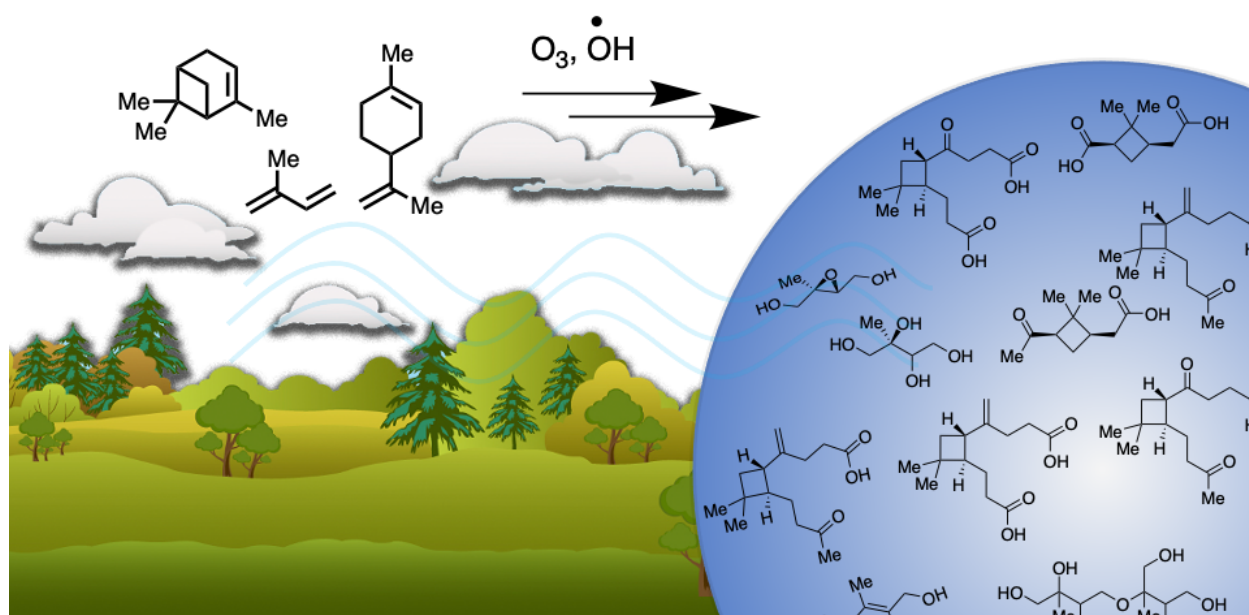


**Figure 1.1** The emission of BVOCs into the atmosphere and their subsequent atmospheric oxidation generates chemical species of lower volatility, leading to partitioning from the gas phase to the condensed aerosol phase.

The chemical and physical properties of SOA has been extensively studied to elucidate their potential effect on the atmosphere, climate system,<sup>2-5</sup> and human health.<sup>6-8</sup> However, the high degree of variability in factors such as the VOC precursor, the level of oxidation, and the reactivity of molecular constituents has made the standardized study of SOA challenging. As such, the accurate modeling of SOA within the climate system with respect to atmospheric chemistry, transport processes and ultimate fate within the atmosphere remains elusive, adding to the uncertainty of the properties of aerosols in climate-related processes such as global temperature rise and radiative forcing (RF) (**Figure 1.2**), two measures to which aerosols contribute a substantial uncertainty.<sup>1</sup> In addition, the vast number and variety of molecules within SOA makes the understanding of climate-relevant properties of aerosols even more challenging to study. According to several atmospheric field studies utilizing mass spectrometry, it is estimated that up to 100,000 chemically distinct compounds are able to be detected.<sup>4, 9-12</sup> Without a robust library of authentic chemical standards, the accurate identification and study of these compounds within SOA will remain inconclusive.

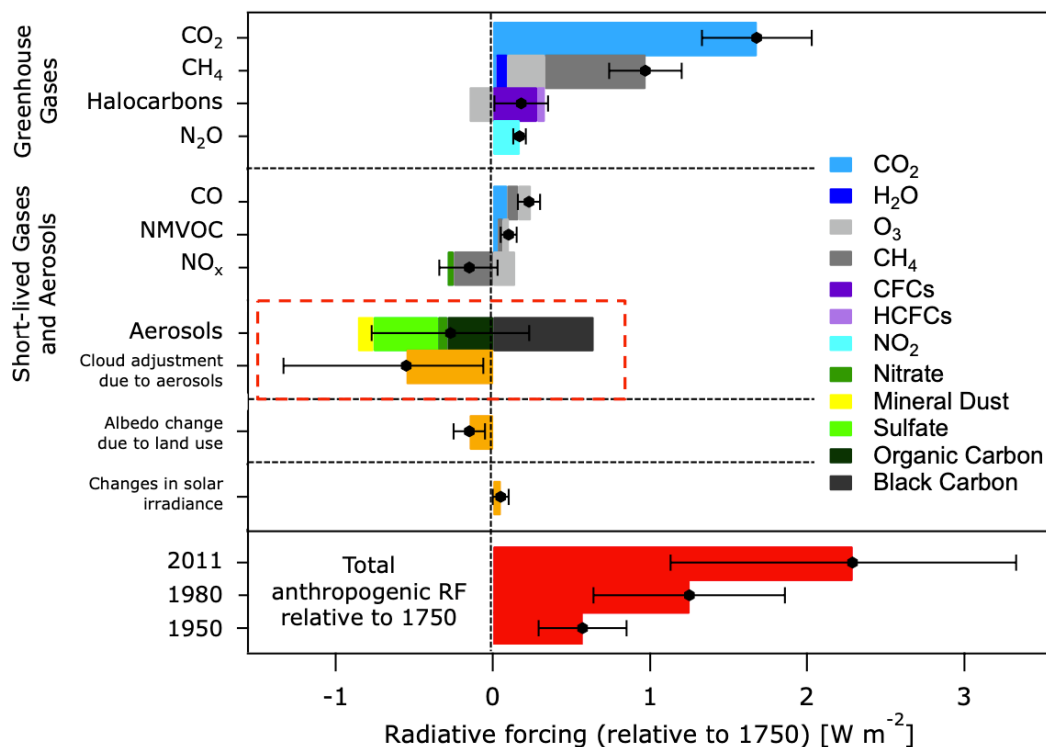


**Figure 1.2** Radiative forcing estimates of various atmospheric constituents and their uncertainties of influence relative to 1750. Figure adapted from IPCC, 2013.

Adding even further to the complexity surrounding SOA constituents is the presence of byproducts of anthropogenic pollution, such as inorganic species containing sulfur and nitrogen. Organic species within SOA are more highly reactive compared to their unsaturated terpenoid parent molecules due to the incorporation of oxygen atoms onto the carbon backbone of VOC precursors.<sup>13-15</sup> As such, the chemical composition of SOA is highly fluxional due to environmental influences within the surrounding atmosphere. Taking a closer look at one of these factors, sulfur dioxide ( $\text{SO}_2$ ) is emitted into the atmosphere through a variety of sources. While the main natural source of  $\text{SO}_2$  in the atmosphere is gaseous emission from volcanic eruption, there

are numerous anthropogenic sources of SO<sub>2</sub> emission such as the burning of fossil fuels by power plants, industrial processes concerning metal extraction from ore, and emissions from locomotives, ships and other transportation vehicles.<sup>16-18</sup> In the gas phase, SO<sub>2</sub> is subject to atmospheric oxidation and generates sulfate anion, typically undergoing conversion into an aerosol suspension of sulfuric acid or ammonium sulfate.<sup>19-21</sup> The presence of sulfate in the condensed phase can then trigger chemical reactions such as acidification or substitution on organic compounds in the atmosphere, leading to the incorporation of chemical moieties such as sulfate esters, generating compounds commonly known as organosulfates.<sup>22-24</sup>

Because the main source of sulfate in the atmosphere is a consequence of human-related activities, it has been reasoned that the detection of the sulfate ester moiety is a principal molecular marker for anthropogenic pollution.<sup>25-26</sup> As such, it is imperative to understand this class of compounds with respect to their effect on the environment, chemical properties and reactivity, and eventual fate within the atmosphere. However, studying these compounds within the atmospheric community has been challenging due to the aqueous nature of the sulfate ester moiety and a lack of authentic standards for accurate comparison to field studies. Further, the compounds in question are not commercially available, making synthetic organic chemistry the only way to access these species as homogenous standards.

Recently, organic synthesis has become an essential tool for atmospheric scientists. Firstly, the generation of authentic standards for comparison to field studies allows for more conclusive and robust analysis of atmospheric measurements. Secondly, the understanding of chemical reactivity of carbon-based atmospheric constituents allows for more accurate prediction of the eventual fate of these compounds in the environment. And lastly, the use of organic synthesis allows for guided postulation for potential species within the atmosphere that are presently

unknown. Using a cross-disciplinary approach of organic synthesis and atmospheric chemistry will undoubtedly lead to the more effective study of structurally complex molecules like the organosulfates.

This chapter will provide a comprehensive analysis of organosulfates as a general class of compounds, their properties as chemical substrates, and their relevance within SOA and the atmosphere.

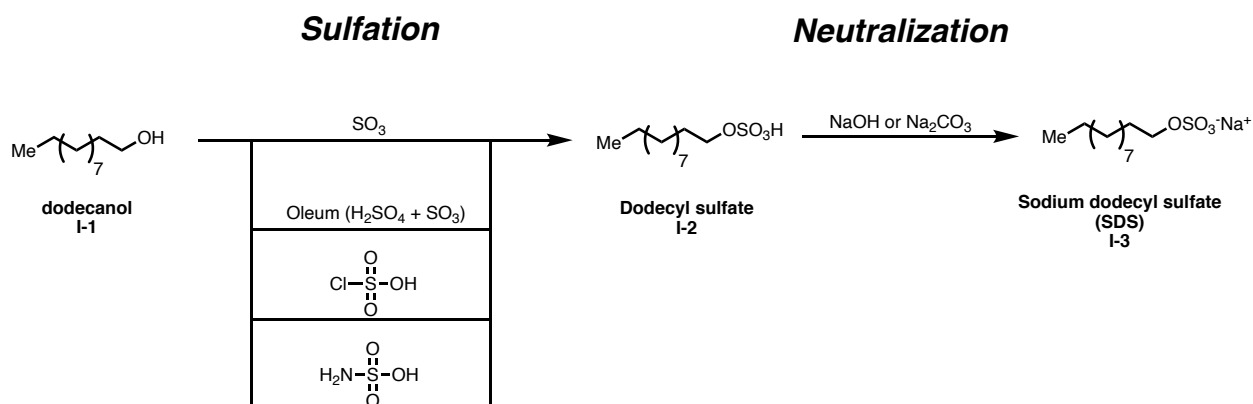
## **1.2 Prevalence of Organosulfate Compounds**

Organosulfates are generally defined as carbon-based compounds bearing one or more sulfate ester moieties ( $R-OSO_3^-$ ). The moiety is formally an alcohol bonded to a molecule of sulfuric acid via one of its protic oxygen atoms. The sulfate ester moiety generally exists as the analogous acid and is highly polar and increases the aqueous solubility of the compound bearing the functional group, which also contributes to the high hygroscopicity of sulfate esters.<sup>27-28</sup> This section will detail the prevalence of organosulfates in various fields of industry and study.

### **1.2.1 Commercial applications of Organosulfates**

Before discussion of the paramount topic of organosulfates within the atmosphere and their role as constituents within SOA, it is important to reference the general utility of this class of compounds. Because of their unique chemical properties, sulfate esters have long been chemically important in the detergent and dye industries due to high aqueous solubility and their propensity to act as surfactants when derived from alcohols bearing long, contiguous carbon chains. One of the most commonly encountered organosulfates of this type is sodium dodecyl sulfate (SDS) also

known as sodium lauryl sulfate (SLS) (**I-4**). SDS is a synthetic organosulfate derived from dodecanol bearing a sulfate ester on the terminal hydroxyl group and exists as a sodium salt. The synthesis of SDS is carried out on an industrial scale and is accomplished via treatment of the parent dodecanol **I-1** with a variety of sulfating reagents including gaseous sulfur trioxide ( $\text{SO}_3$ ), oleum ( $\text{H}_2\text{SO}_4 + \text{SO}_3$ ), chlorosulfonic acid or sulfamic acid, all of which generate dodecyl sulfate **I-2** (Scheme 1.1).<sup>29</sup> The acidic sulfate moiety is then neutralized using a sodium base such as sodium hydroxide or sodium carbonate to generate SDS **I-3**.



**Scheme 1.1** Commercial production of sodium dodecyl sulfate (SDS).

Due to the long alkyl carbon chain and water-soluble polar head group, SDS has amphiphilic properties, enabling the formation of micelles. This makes the compound a highly useful anionic surfactant and is present in a number of cleaning products in most domestic homes.<sup>30</sup> Extending beyond SDS, many long chain and branched alkyl groups bearing sulfate esters are found in

various cleaning, cosmetic and personal hygiene products.<sup>31</sup> An excellent review published by Michaels and coworkers expands further on the commercial uses of sulfate esters.

### 1.2.2 Organosulfates within Natural Products and Biological Systems

Aside from synthetic compounds used for commercial and industrial purposes, sulfate esters are also found within a number of biological systems and naturally occurring organic compounds. **Figure 1.3** shows a myriad of natural products bearing pendant sulfate esters. Within biological systems, sulfate esters are typically moieties on glycosides, polysaccharides or steroidal alcohols in some cases.<sup>32</sup> Focusing specifically on steroidal compounds, natural products of this type have been shown to have increased biological activity when decorated with a sulfate ester, likely due to the enhanced aqueous solubility.<sup>33-34</sup> For example, many chemical species derived from sea cucumbers in the Holothuroidea family are glycoside organosulfates that act as highly potent neurotoxins dependent on the presence of a sulfate ester group.<sup>32</sup> This family of sulfate esters is known as Holothurin, as the steroidal compounds Holothurin A (**I-4**) and B (**I-5**) are found in the exoskeleton of the sea cucumber and serve as a method of self-defense from predators. Other natural organosulfates include atractyloside (**I6**), which is a glycoside isolated from *Atractylis gummifera* of the daisy family that has been shown to inhibit cellular respiration.<sup>35</sup> Interestingly, the sulfate-free parent compound atractylgenin demonstrates substantially less biological activity, though the biological role of the sulfate ester remains unknown.<sup>36</sup>

Other organosulfates have been observed and have relevance within the human body and other mammalian tissues. Some have been identified as metabolites of estrogen and other sex hormones,

indicating the importance of sulfate ester formation within the endocrine system. In 1967, Acros and Lieberman isolated crystalline steroidal metabolites including **I-7** from the urine of normal human test subjects to whom pregnenolone was administered.<sup>37</sup> Sulfate ester-containing species have also been demonstrated within mammary tissue during periods of lactation, as well as brain tissue,<sup>32-34</sup> and the presence of these compounds has been extensively studied via the medicinal, synthetic and biochemical communities, and the high degree of biological relevance of organosulfates suggests that understanding the chemical properties and fate of these species could prove useful in assessing human health.

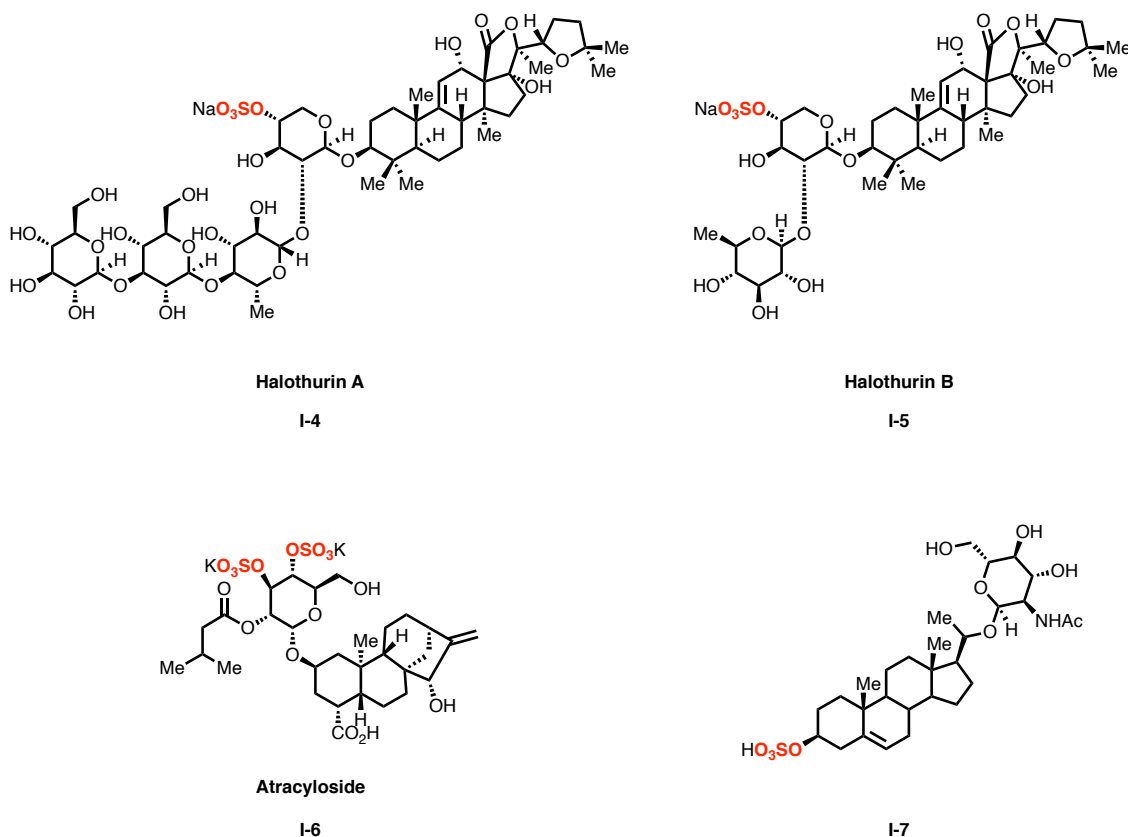


**Figure 1.3** Several natural products and biologically-relevant compounds bearing sulfate esters as functional groups.

### 1.3 Organosulfates within the Atmosphere

As mentioned earlier, aside from being compounds that demonstrate interesting biological activity and serve commercial purposes, organosulfates are commonly encountered species within the atmosphere and are suggested to represent a substantial fraction of SOA constituents. The oxidation of VOCs within the atmosphere, such as isoprene,  $\alpha$ -pinene, limonene and many other precursors, gives rise to countless oxidation products that are subject to a myriad of chemical transformations once in the particle phase. Upon exposure to acidic sulfate, these compounds are then able to form organosulfates (**Fig. 1.4**).

The presence of organosulfates in the atmosphere is highly relevant to studying the climate system because of their inherent link to atmospheric pollution. The abundance of anthropogenic pollution sources across the world, such as vehicular emissions, biomass burning, outflow from urban areas and livestock emissions, results in the emission of VOCs and other inorganic constituents that can affect naturally occurring atmospheric components, such as SOA. Although biogenic emissions of volatile organics overshadow those from man-made sources,<sup>1</sup> the presence of these anthropogenic constituents can heavily influence the chemical properties of species within atmospheric aerosols. Further, it has been shown that SOA formation is enhanced in the presence of anthropogenic emissions and acidic seed aerosol formed from the oxidation of sulfur dioxide and nitrogen oxides.<sup>10, 38-39</sup>

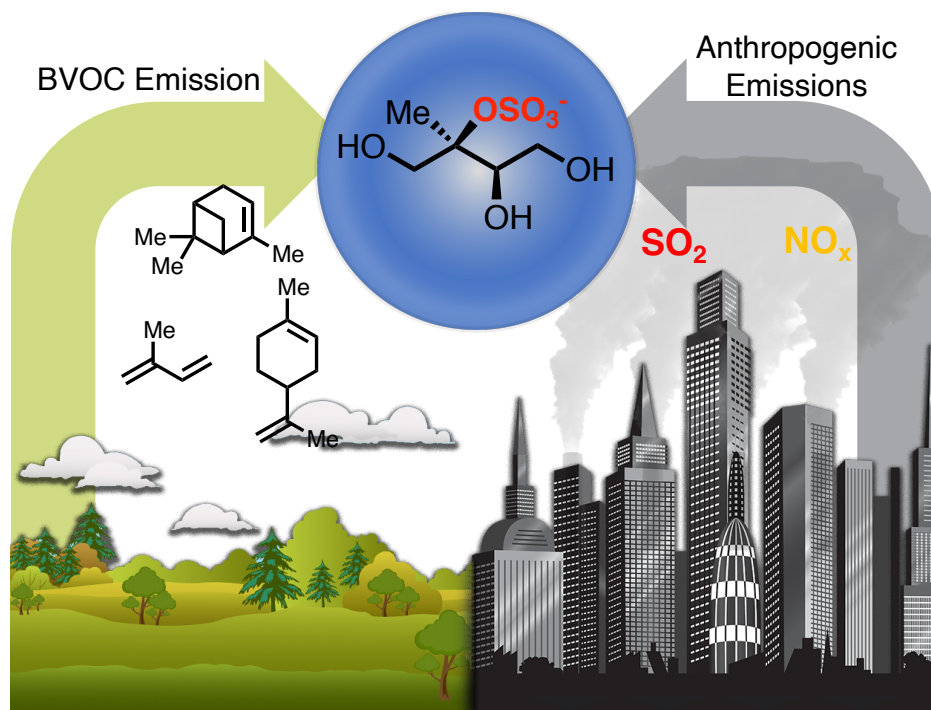


**Figure 1.4** The emission of BVOC and their resulting SOA constituents can interact with anthropogenic pollutants resulting in the generation of organosulfates, or sulfate esters

Sulfate within the atmosphere is formed from the oxidation of sulfur dioxide. As previously mentioned, there are a number of human-made sources of atmospheric  $\text{SO}_2$ , such as outflow from deforestation and fires, smelting, locomotive exhaust and energy production. Other sources of natural  $\text{SO}_2$  in the atmosphere, such as volcanic emissions, pale in comparison to those of anthropogenic activity. In a recent study disclosed by Fioletov and coworkers,  $\text{SO}_2$  levels were monitored from 2005–2014 and showed that 30% of tracked emissions originated naturally, such as degassing volcanoes as a primary source.<sup>40</sup> Though they did substantiate the fact that regulatory intervention has resulted in the sharp decline of human-made sulfur dioxide emission across the world since the 1990s,<sup>40-41</sup> the dominant sources remain anthropogenic, mostly linked to energy production and distribution (**Fig 1.5**). Therefore, the presence of organosulfates is likely an

effective molecular marker for anthropogenic pollution, as most of the atmospheric emission of SO<sub>2</sub> exists as a consequence of human civilization.

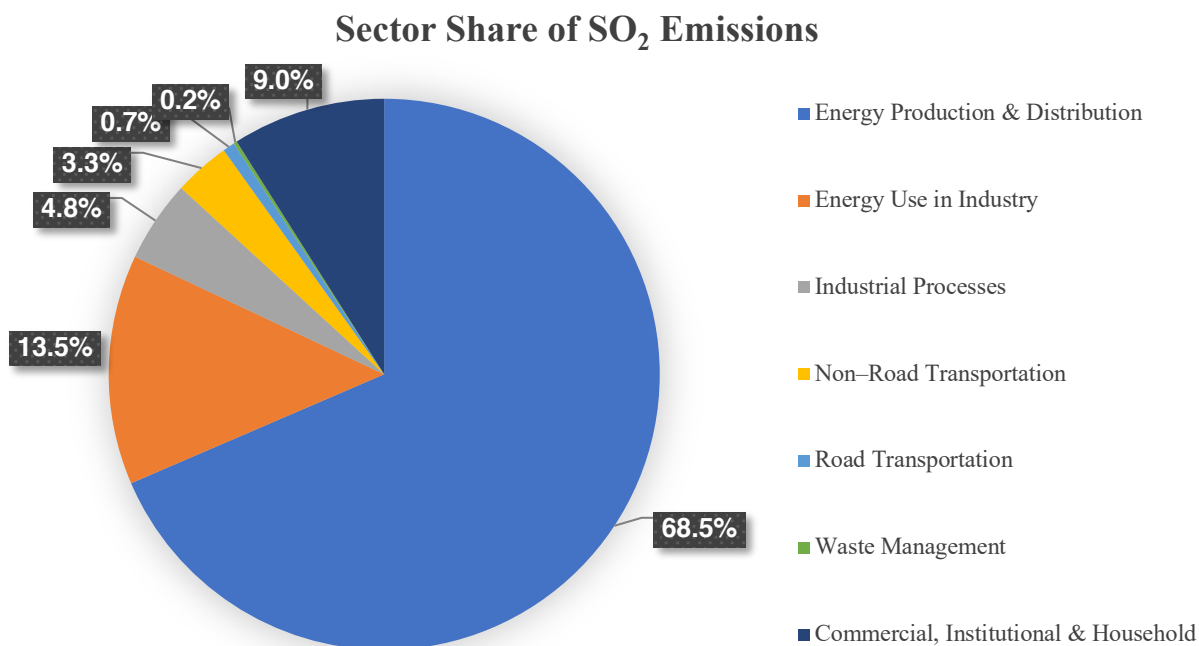


**Figure 1.5** Sector share of anthropogenic sulfur dioxide emissions measured from 2005–2014. Figure adapted from Fioletov et al, 2016.

Although organosulfates have recently been detected in various field and laboratory studies,<sup>39, 42-43</sup> the chemical implications of these compounds remain poorly understood. Only a handful of organosulfate species have been identified in the atmosphere due to the numerous potential species that can be generated from the interplay of BVOCs and acidic sulfate. Moreover, concrete identification is challenging due to a lack of pure standards to compare to field measurements, and their synthesis is challenging due to the inherent chemical properties of sulfate

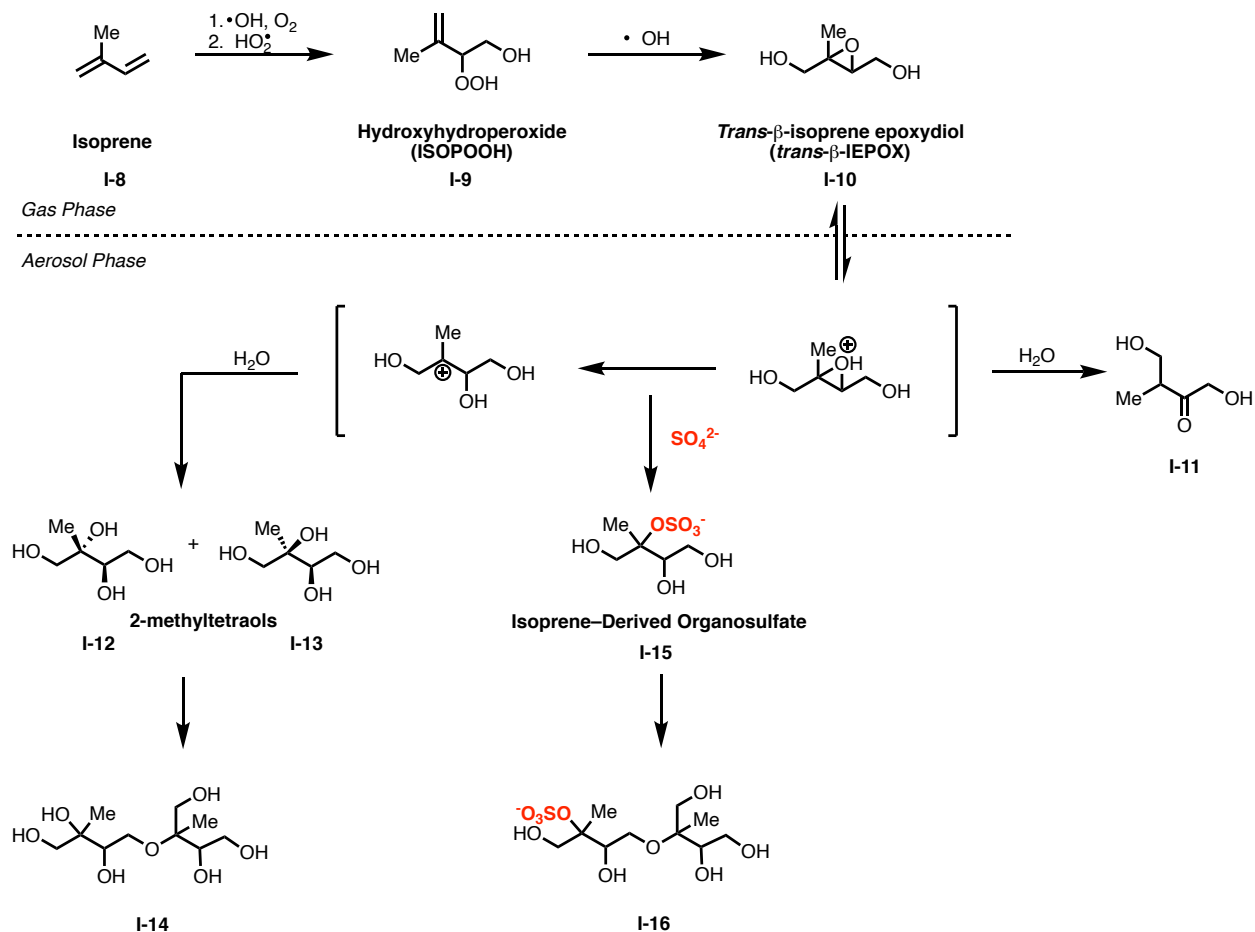
esters, such as high water solubility and fully anionic character even at acidic pH. Given that the presence of anthropogenic pollutants can not only influence the formation of SOA, but can also generate novel constituents within BVOC-derived SOA,<sup>44</sup> understanding of these species at the molecular level is essential to give a more comprehensive view of their role in the atmosphere. This section will examine some of the commonly encountered organosulfates in the atmosphere from natural and anthropogenic sources.

### 1.3.1 Isoprene (IEPOX)-Derived Organosulfates

Turning to organosulfates derived from BVOCs, one of the most relevant to consider is isoprene. Isoprene (**I-8**) is the most abundant hydrocarbon emitted into the atmosphere aside from methane. Emissions of isoprene are estimated to exceed 500 Tg yr<sup>-1</sup>,<sup>2,45-47</sup> and emissions dominate over areas of tropical vegetation. Having two double bonds of differing substitution, isoprene is highly reactive towards atmospheric oxidants. In a groundbreaking study conducted by Claeys and coworkers,<sup>48</sup> it was found that isoprene photooxidation generates significant amounts of lowly volatile oxidation products, leading to the notion that isoprene contributes significantly to the global SOA budget, estimated up to 30-50%.<sup>49</sup>

The contribution of isoprene to global SOA production has resulted in a number of illuminating studies that aim to better understand the oxidation of isoprene, its subsequent oxidation products and their fate in the atmosphere, as well as other species formed within the particle phase of isoprene-derived SOA.<sup>14, 24, 50-55</sup> **Scheme 1.2** details an oxidation pathway proposed by Surratt and coworkers involving the photooxidation of isoprene in the presence of low levels of NO<sub>x</sub> and subsequent chemical transformations within the particle phase. Once

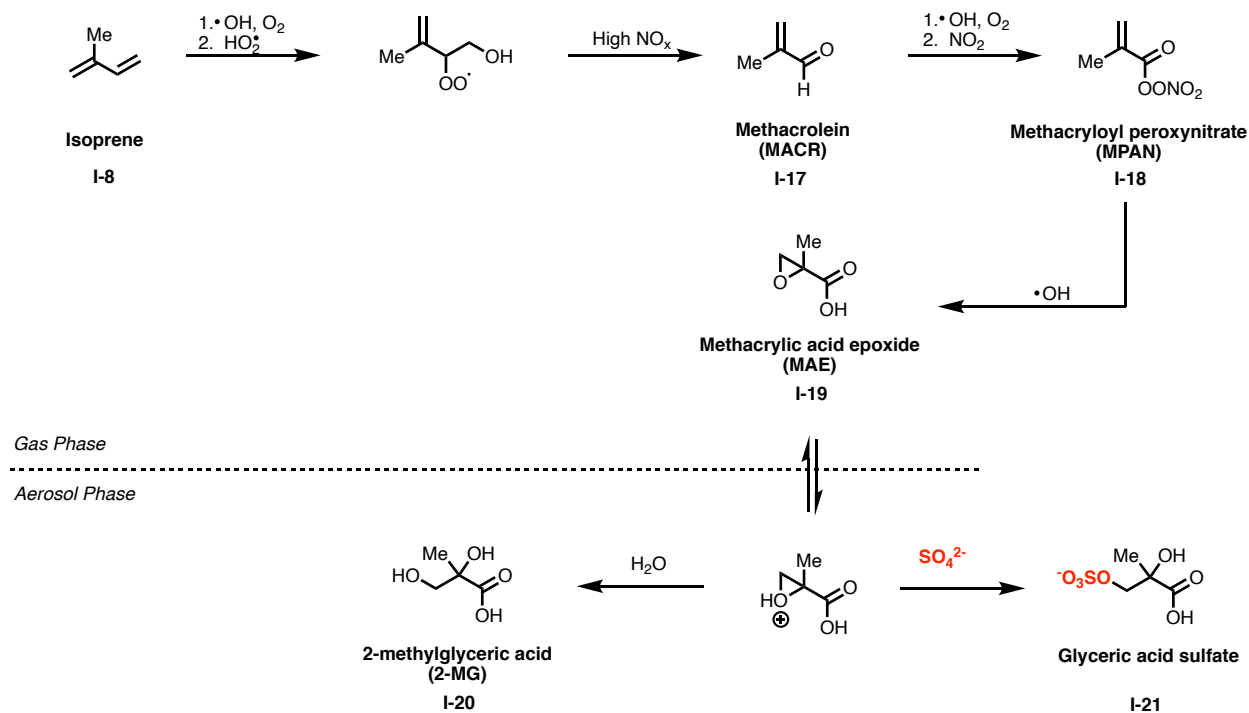
emitted into the atmosphere, isoprene **I-8** preferentially reacts with hydroxyl radical (OH) and molecular oxygen in the gas phase, followed by a reaction with hydroperoxyl radical (HO<sub>2</sub>). The result of this initial oxidation is the generation of various isomers of hydroxyhydroperoxide **I-9**, also known as ISOPOOH. This compound then can undergo decomposition through further oxidation in the presence of OH radicals, generating various isomers of isoprene epoxydiol (IEPOX), with the most stable and abundant isomer being *trans*-β-IEPOX **I-10**. These compounds have been suggested to serve as vital species for the formation of SOA particles derived from isoprene, as they are highly stable and have a surprising affinity for the interface between the gas and condensed aerosol phases.<sup>14, 56</sup> It is suggested that *trans*-β-IEPOX **I-10** partitions into the condensed aerosol phase through acid-catalyzed uptake via protonation of the internal oxiryl oxygen atom, and the resulting protonated species is then subject to a myriad of aqueous-phase chemical transformations. From the positively charged intermediate, one could imagine an elimination reaction with water to form species such as β-hydroxy ketone **I-11**, or a nucleophilic substitution on the central carbon atom to form 2-methyltetraols **I-12** and **I-13**. The formation of either diastereomeric tetraol could then be propagated towards the formation of oligomeric compounds such as **I-14**. In the presence of sulfate anion (SO<sub>4</sub><sup>2-</sup>), the acidified intermediate could serve as an electrophile for a nucleophilic substitution reaction, forming isoprene-derived organosulfate **I-15**, which could result in the formation of the corresponding oligomeric species **I-16**.



**Scheme 1.2** Formation pathway towards isoprene-derived organosulfates and other isoprene-derived oxidation products under low NO<sub>x</sub> conditions, adapted from Surratt et al, 2010.

Conversely, in high NO<sub>x</sub> environments, the formation mechanism towards postulated organosulfates is quite different. Several studies have probed the oxidation of isoprene under high NO<sub>x</sub> conditions and, as a result, the potential formation of corresponding organosulfates.<sup>57-58</sup> The presence of nitrogen oxides results in the generation of a much higher number of potential oxidation products, including nitrate esters, however these products are highly unstable and are

predicted to have short lifetimes. **Scheme 1.3** outlines a potential formation pathway for another organosulfate derived from isoprene disclosed by Lin and coworkers.<sup>58</sup> Photooxidation of **I-8** in the gas phase generates the deprotonated form of ISOPOOH, which in the presence of high NO<sub>x</sub> will oxidize further to methacrolein (MACR) **I-17**. A subsequent oxidation, followed by radical accretion via exposure to nitrate yields methacroyl peroxyxynitrate (MPAN) **I-18**, which readily collapses upon hydroxyl radical-mediated oxidation to form methacrylic acid epoxide (MAE) **I-19**. Much like the low NO<sub>x</sub> case, this epoxide can be subject to acid-mediated uptake into the condensed phase, and can be exposed to several aqueous phase transformations. Showcasing just one of the possible transformations, the protonated epoxide opening in the presence of water to generate 2-methylglyceric acid (2-MG) **I-20**. The analogous reaction can also occur in the presence of sulfate anion, generating glyceric acid sulfate **I-21**.



**Scheme 1.3** Formation pathway towards isoprene–derived organosulfates and other isoprene–derived oxidation products under high  $\text{NO}_x$  conditions, adapted from Lin et al, 2013.

In addition to the two organosulfates shown previously, several isoprene–derived sulfate esters have been detected and proposed in the literature.<sup>22-23, 50, 59-63</sup> **Figure 1.6** demonstrates a collection of frequently encountered organosulfates believed to be derived from isoprene **I-8** that are present in various field measurements and laboratory experiments. Though the detection and characterization of this family of compounds is challenging, several recent studies have suggested that the most abundant atmospheric organosulfates are derived from IEPOX.<sup>42, 58, 62, 64-68</sup> In a recent study disclosed by Hettiyadura and coworkers in which fine particulate matter ( $\text{PM}_{2.5}$ ) was collected from Centreville, AL and analyzed using hydrophilic interaction liquid exchange chromatography (HILIC) coupled with triple quadrupole mass spectrometry (TQD-MS), the organosulfate derived from IEPOX (**I-15**;  $m/z$  215) was found to contribute to over 50% of

detected bisulfite signal.<sup>61</sup> Several different studies have also suggested a similar narrative concerning the prevalence of IEPOX-derived organosulfates within SOA,<sup>22-24, 62, 69</sup> with **I-15** proposed as the most likely chemical structure. A study published by Chan and coworkers in 2010 examined filter samples collected in various cities around the state of Georgia and found that analysis using gas chromatography/time of flight mass spectrometry (GC/TOFMS) revealed the same sulfate ester **I-15** exhibited the largest signal,<sup>70</sup> though characterization of the exact structure was not possible due to a lack of authentic standards.

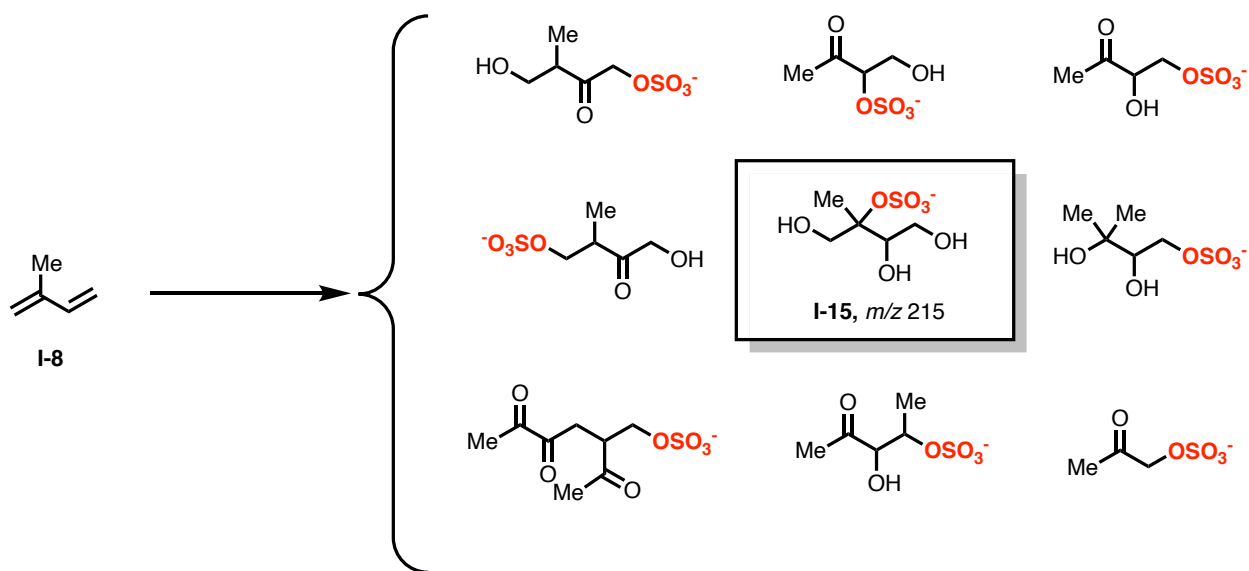


**Figure 1.6** Proposed structures of isoprene-derived organosulfates throughout the literature.

Although the ubiquity of IEPOX-derived organosulfates has generated a significant amount of inquiry from the atmospheric community, definitive characterization related to field and laboratory measurements is challenging, and there are multiple hurdles that preclude absolute confirmation. Firstly, the IEPOX-derived organosulfate attributed to  $m/z$  215 is commonly reported in the literature without having set stereochemistry, and the proposed formation mechanism shown in **Scheme 1.1** suggests that it is likely to exist as either the *syn* or *anti* diastereomer with respect to the internal hydroxyl substituents. Although it is more likely the *anti* diastereomer (derived from 2-methylerythritol) dominates due to the hypothesized mechanism proceeding through the acid-catalyzed epoxide opening of *trans*- $\beta$ -IEPOX, it is equally likely under acidic conditions to form the *syn* diastereomer (derived from 2-methylthreitol). As a result, several compounds could serve as the representative IEPOX-derived organosulfate detected in the field, shown in **Figure 1.7**.

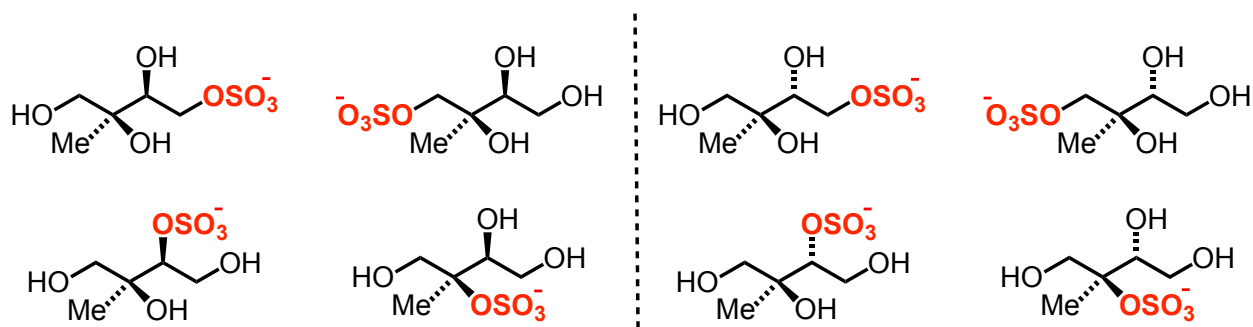


**Figure 1.7** The suite of possible structures of IEPOX-derived organosulfates attributed to  $m/z$  215.

In addition to the stereochemical complexity, this series of compounds also poses the challenge of regiochemical selectivity, as the parent tetraol structure has four hydroxyl substituents along the carbon skeleton. As mentioned earlier, though the mechanism likely proceeds towards the *anti* tertiary sulfate as a consequence of the proposed acid-mediated epoxide opening of *trans*- $\beta$ -IEPOX, it is possible that the sulfate ester moiety could be incorporated onto another hydroxyl substituent. This leads to the eight potential structures shown in **Figure 1.7** that could correspond to the dominant mass exhibited from organosulfates derived from IEPOX. Therefore, the generation of homogenous standards of these compounds is vital for understanding their impact and fate in the atmosphere, and potential synthetic procedures must be designed to selectively access all of the potential isomers.

Finally, this suite of compounds also poses the challenge of chemical composition and their inherent chemical properties. The IEPOX-derived organosulfates are suggested to bear a sulfate ester moiety coordinated to an ammonium counterion, as ammonium sulfate ( $(\text{NH}_4)_2\text{SO}_4$ ) is thought to be the dominant source of sulfate anion within the particle phase within acidic seed aerosol e.g. sulfuric acid ( $\text{H}_2\text{SO}_4$ ) + ammonium sulfate.<sup>71-74</sup> Despite this notion, in the literature, the sulfate ester moiety is shown as bearing several potential counterions; in some cases the proper ammonium cation, the free acid, or even as a free sulfate anion. Although it is common to have these cations used interchangeably, the reactivity of sulfate esters can change dramatically depending on the type of associated cation.<sup>75</sup> Therefore, a pure standard of any of the IEPOX-derived species should likely bear an ammonium counterion in order to serve as an atmospherically-relevant comparison to field samples. Further, sulfate esters as a functional group possess unique chemical properties that could contribute to further distinctions between the eight possible isomers. The sulfate ester moiety is highly acidic, retaining a negative charge at low pH,

and as a result can display various propensities towards hydrolysis and other reactivity depending on the structure of the parent compound.<sup>75</sup> The stability of an organosulfate substrate often depends on the sterics of the molecule in question, as the sulfate ester can exhibit variances in stability and properties depending on the congestion of the bonded alcohol.<sup>76</sup> In an intriguing study published by Cameron and Thatcher,<sup>77</sup> reaction dynamics simulations were used to probe the potential of intermolecular reactivity of the sulfate ester moiety across a molecule with two distinct hydroxyl groups along its backbone, showing the possibility of sulfuryl transfer. It is reasonable to assume that given the reported literature concerning sulfate esters, the IEPOX-derived species could display substantial differences dependent on the stereochemistry and regiochemistry of the compound, altering their overall chemical properties and eventual fate within the atmosphere.

In more recent literature, several studies cite the organic synthesis and use of surrogate standards of sulfate esters, as well as preliminary synthetic standards of the IEPOX-derived organosulfates specifically, the scope of which will be elaborated upon in **Section 2.2**.<sup>61-62, 78-81</sup> While these studies offer valuable insight into the detection of these species in the field, the compounds are typically mixtures of diastereomers, or bear a metallic potassium or sodium cation, or a tetrabutylammonium (TBA) ion, rather than the atmospherically-relevant free ammonium cation. Therefore, development of a synthetic method that accounts for all stereochemical, regiochemical and compositional discrepancies of this family organosulfates would assist the atmospheric community in making definitive conclusions regarding the formation, properties, and ultimate fate of these compounds in the atmosphere, as well as provide insight into the interaction of SOA and anthropogenic pollution.

### 1.3.2 Organosulfates Derived from Other BVOCs

Although organosulfates derived from isoprene oxidation products are suggested to be the most dominant and relevant within the atmosphere, species derived from other natural terpenes also contribute to the totality of BVOC-derived SOA, such as the various isomers of pinene.  $\alpha$ - and  $\beta$ - pinene (**I-22** and **I-23** respectively) are bicyclic hydrocarbons emitted into the atmosphere mainly through coniferous trees. Pinene represents a substantial amount of carbon within the atmosphere, with  $\alpha$ - and  $\beta$ - pinene emissions estimated to exceed 60 and 20 Tg yr<sup>-1</sup> respectively.<sup>45,</sup>

<sup>82</sup> Organosulfates derived from both  $\alpha$ - and  $\beta$ -pinene have been detected in several laboratory and field studies in which SOA particles from each terpene were measured and characterized.<sup>65, 83-85</sup> The mechanisms of pinene-derived organosulfate formation are not as well studied as those concerning isoprene-derived SOA due to a greater degree of molecular complexity, but a number of organosulfate masses attributed to pinene SOA constituents have been detected and proposed in the past few decades, as shown in **Figure 1.8**.

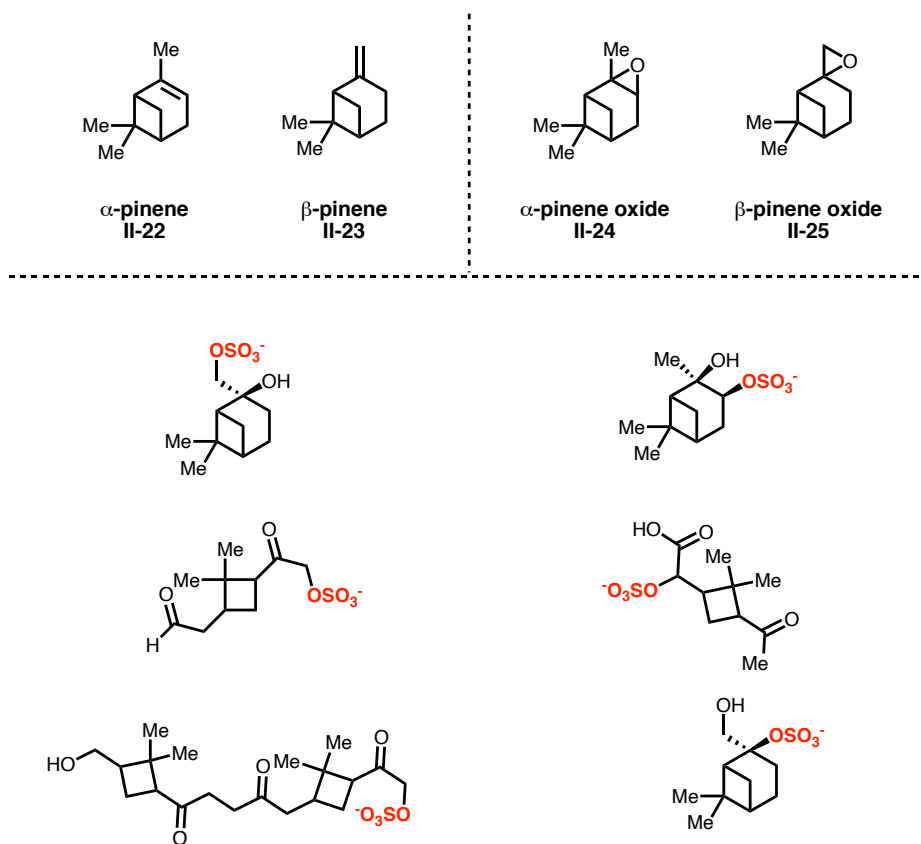


**Figure 1.8** A collection of organosulfates proposed to form from  $\alpha$ -pinene and  $\beta$ -pinene oxidation products.

Similar to the case of isoprene-derived species, a dominant formation pathway towards pinene-derived organosulfates is suggested to involve an acid-mediated epoxide opening, in which the gas phase epoxide-bearing compound partitions into the condensed phase through protonation of the oxiryl atom. Epoxides bound to exocyclic tertiary centers have been demonstrated to react quickly with acidic sulfate within aerosol, which may suggest that organosulfates derived from  $\beta$ -pinene oxide **I-25** likely form more readily than that of endocyclic epoxides like  $\alpha$ -pinene oxide **I-24**. A series of synthetic standards of hypothesized pinene-derived

sulfates have been synthesized in the past, along with a number of organosulfates derived from less abundant BVOCs such as limonene, will be elaborated upon in **Section 2.2**.<sup>86</sup>

### 1.3.3 Organosulfates Derived from Aromatic Compounds

In addition to the organosulfates derived from biogenic precursors, organosulfates bound aromatic organic compounds have also been detected in ambient aerosols from sampling around urbanized areas.<sup>87-91</sup> Some of the most commonly encountered aromatic molecules in the atmosphere include monocyclic species such as toluene, styrene, benzene, as well as polycyclic aromatic hydrocarbons (PAH) such as naphthalene.<sup>92-94</sup> Since these compounds have been known to have adverse effects on human health and the surrounding environment, the properties and ultimate fate of this family of compounds should be studied in a rapidly urbanizing society.

Aromatic compounds are emitted into the atmosphere mainly through anthropogenic activities and pollution, including combustion of fuels, commercial solvent usage, biomass burning and evaporation of gasoline and oils,<sup>93-95</sup> and several studies have shown that aromatic species represent a significant amount of carbon in the atmosphere surrounding urban sites. Of course, within these anthropogenically-influenced environments, the emissions of sulfate and nitrogen oxides can enhance the formation of SOA derived from these aromatic carbon compounds and can form aromatic species containing sulfate esters and nitrate esters within the particle phase, although the oxidation mechanisms of these compounds are not as well-studied. Aromatic organosulfates have been detected and quantified in multiple field studies. For example, Kundu and coworkers analyzed PM<sub>2.5</sub> samples collected in areas close in proximity to Lahore, Pakistan and estimated the concentration of benzyl sulfate to range from 0.05–0.50 ng m<sup>-3</sup>.<sup>87</sup> In another

campaign, Huang and coworkers determined concentrations of benzyl sulfate and phenyl sulfate in Xi'an, China to be 0.04 and 0.14–0.50  $\text{ng m}^{-3}$ , respectively. Aromatic organosulfates become more significant when anthropogenic VOCs are the dominant source of SOA precursor compounds in relation to BVOCs, dependent on factors such as level of urbanization and season. Ma and coworkers determined that benzyl sulfate contributed up to 63% of the signal attributed to detected atmospheric sulfate measured in the winter season in Shanghai, China.<sup>88</sup> The identities of these compounds and their syntheses will be discussed later in **Section 2.2**.

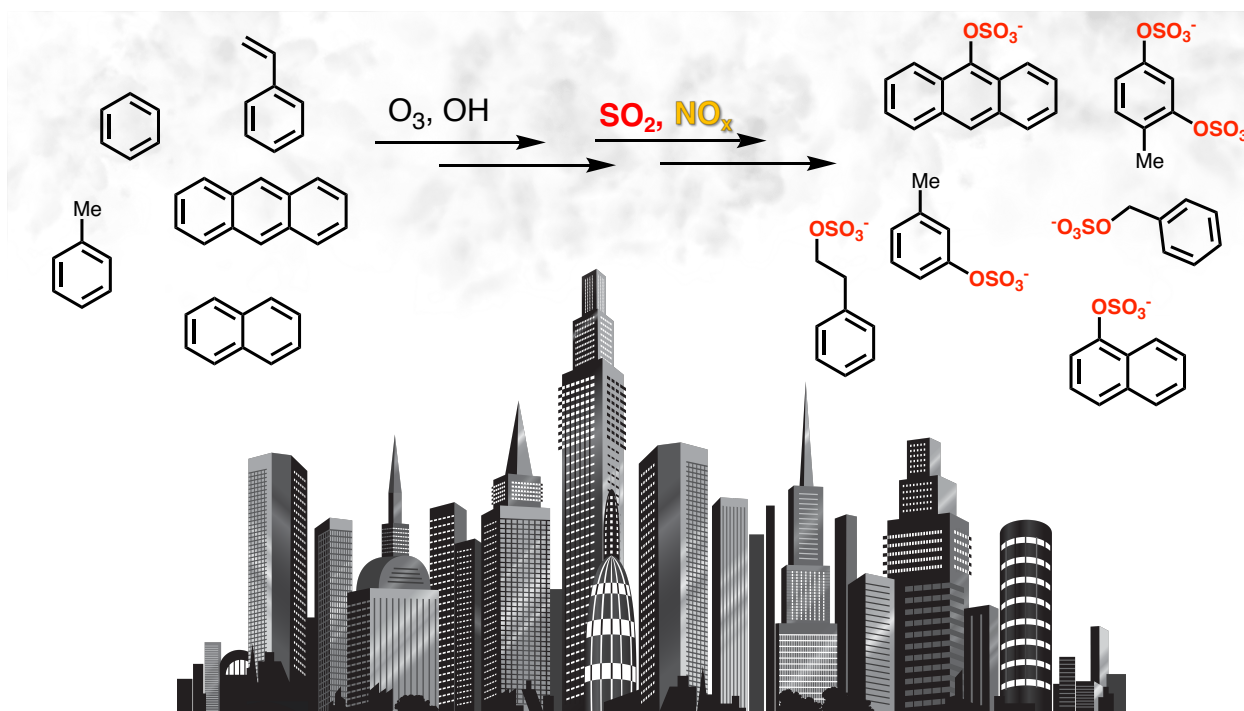


**Figure 1.9** The emission of aromatic compounds from urbanized areas can contribute to the formation of aromatic organosulfates.

## 1.4 Detection, Identification and Measurement of Organosulfates

Atmospheric organosulfates have been quantified and detected using a plethora of different techniques. The explicit measurement of these compounds is a relatively new field, with evidence of these compounds being important and abundant SOA constituents first being disclosed in 2007 in studies conducted by Seinfeld et al and Claeys et al.<sup>65, 84</sup> Prior to direct evidence of these compounds within the atmosphere, ancillary confirmation of sulfate ester functionality was shown using signatures from Fourier-transform infrared spectrometry (FTIR).<sup>96-97</sup> However, it is now widely accepted that organosulfates are abundant species within aerosol particles measured in the field, and in the recent years the methods of detection and analysis have become more exhaustive and enlightening with respect to this family of compounds. This section will briefly review a few of these techniques.

### 1.4.1 Offline Methods

The most common method to detect and quantify organosulfates as SOA constituents is analysis of atmospheric filter samples collected in the field using MS coupled with ESI and liquid-phase separation techniques.<sup>39, 65-66, 84, 98</sup> As mentioned earlier, the acidity of the sulfate ester moiety makes chemical derivatization unnecessary since the functional group bears a negative charge, leading to high ionization efficiencies in negative polarity. Specific identification of organosulfates apart from inorganic sulfate present in the sample is also accomplished using collision-induced dissociation (CID) to form characteristic fragments derived from sulfate esters, such as bisulfate ( $\text{HSO}_4^-$ ) with  $m/z \sim 96$  generated from aliphatic sulfate esters, and various sulfate radical ions generated from aromatic sulfate esters.<sup>42, 98-99</sup> Recent studies have applied high-

resolution mass spectrometry (HRMS) techniques in attempts to distinguish between structurally unique organosulfates, such as Orbitrap MS and ion cyclotron resonance (ICR) MS.<sup>25, 89, 100-101</sup> The increase in resolution has allowed for the assignment of many signals in mass spectra of filter samples to organosulfates. However, isomeric species yield a single signal and therefore cannot be differentiated from one another.

Other studies have applied ESI-MS in tandem with reversed-phase liquid chromatography (RPLC) as a method of quantification of organosulfates in filter samples,<sup>88, 102-103</sup> but the polarity of certain sulfate esters has resulted in poor chromatographic resolution. Thus, HILIC, having an extremely similar instrumental setup to RPLC, has been used as an alternative and has demonstrated utility in the resolution of highly polar organosulfates.<sup>61, 81, 104</sup> The inherent polarity and hygroscopicity of organosulfates, particularly those derived from small terpenes like isoprene, limit the utility of other liquid-phase separation techniques, highlighting the importance of developing new methodologies aside from RPLC and HILIC to assist in their detection. Approaches that have combined these separation techniques with HRMS, have resulted in characterization of organosulfate species with a higher degree of certainty,<sup>98, 105-107</sup> although the analyses were stunted due to lack of chemical standards. Despite this limitation, an interesting study published by Brüggemann and coworkers compared ionization efficiencies of several organosulfates with those of surrogate standards, allowing for the quantification of unknown sulfate ester-bearing species within filter samples taken in both urban and rural areas in China and Germany respectively.<sup>98</sup> In lieu of having pure standards, this type of approach to quantification may prove useful in future studies in determining the chemical content of atmospheric particle samples.

Finally, particle samples have also been examined using spectroscopic techniques for the detection of organosulfates, such as Raman microscopy and FTIR spectroscopy. A number of studies have utilized FTIR to quantify sulfate ester content within samples based on the characteristic absorbance of C–O–S centered at  $876\text{ cm}^{-1}$ .<sup>43, 96, 108</sup> Although the use of FTIR to visualize the presence of notable functional groups within samples can narrow the window of analysis of potential chemical compounds within particle samples, individual molecular connectivity and differentiation between isomeric organosulfates cannot be identified. However, Raman microscopy has been used to differentiate sulfate esters from inorganic sulfate present in atmospheric samples, as Bondy and coworkers recently demonstrated the use of Raman spectra taken of various organosulfate standards and spectral perturbations as a function of varying pH.<sup>79</sup> Future studies should consider the potential utility of this sort of analysis, perhaps incorporating it into existing analytical methodologies involving previously described MS-based techniques.

#### 1.4.2 Online Methods

In addition to the described offline methods of analyzing organosulfates, a number of real-time techniques have been used in recent studies. Historically, the most widely used instrumentation to acquire online organic aerosol data has been the high-resolution time-of-flight aerosol mass spectrometer (HR-ToF-AMS) from Aerodyne Research, Inc, in which quantitative real-time and size-resolved compositional analysis of particulate matter has been conducted in a number of atmospheric studies.<sup>109-113</sup> Concerning organosulfates specifically, in 2006, Liggió and coworkers employed the use of this instrument to probe the formation of organosulfates via the uptake of pinonaldehyde in the presence of acidic sulfate aerosol.<sup>114</sup> Though studies utilizing HR-

ToF-AMS have put forth intriguing results in past studies, the utility of this method is limited for when studying sulfate esters due to its hard ionization process, resulting in the fragmentation of inorganic sulfate and organosulfates being less differentiable from one another. This leads to significant limitations in the detection of organosulfates in bulk particle measurements.

Other methods aside from bulk measurements include single particle MS techniques to detect organosulfates within aerosol particles. Hatch and coworkers utilized aerosol time-of-flight (ATOF) MS in order to detect sulfate esters during field studies in the city of Atlanta, Georgia and found that real-time measurements revealed the highest organosulfate concentrations occurred during night-time acquisitions, suggesting diurnal variations in organosulfate formation.<sup>23</sup> In another study published in 2010 employing similar methods, Froyd and coworkers used laser ablation single particle MS (LA-SPAMS) and detected a significant level of the IEPOX-derived organosulfates attributed to  $m/z$  215, as well as other isoprene-derived species in the upper troposphere.<sup>22</sup> Froyd's work in particular was one of the first analytical studies to suggest the overwhelming abundance of isoprene-derived organosulfates as constituents within aerosol particles, with primary estimates of this family of sulfate esters being present in 70% of ambient particles. However, factors such as inconsistent ionization efficiencies and variable mass fragmentation prevent laser desorption methods such as LA-SPAMS from being used more generally for individual particle measurements.

## 1.5 Conclusions and Scope of Work

In this chapter, the relevance and properties of organosulfates as a class of compounds has been established both external to and within the atmosphere as SOA constituents. In particular,

although there have been a variety of sulfate esters presented that are atmospherically relevant, several studies have suggested that the most abundant and ubiquitous are derived from isoprene, with species generated from IEPOX as the most crucial to study. Although several reports have demonstrated the importance of these species, and some have even put forth synthetic standards of these compounds, chemical homogeneity and unambiguous structural specificity are crucial factors for standard development of IEPOX-derived organosulfates. This thesis reports the use of organic synthesis in order to access the organosulfates derived from IEPOX, as well as examining some physical properties of these compounds that may elucidate their effect and fate within atmospheric particles. Also, this thesis will outline the synthesis of other atmospherically relevant compounds, specifically terpenes, in order to probe certain atmospheric chemical processes.

Chapter 2 will discuss the synthesis of the suite of IEPOX-derived organosulfates shown in **Figure 1.7**. This method enables the eight isomeric sulfate esters to be generated with stereoselectivity and regiospecificity with respect to the placement of the sulfate ester moiety. This section will also cover the literature surrounding the synthesis of sulfate esters derived from atmospheric carbon compounds and their relevance as chemical standards.

Chapter 3 discusses the use of various analytical techniques to study the physical properties of the IEPOX-derived organosulfates prepared in Chapter 2. The analysis of these species using nuclear magnetic resonance (NMR) spectroscopy and measurements of aqueous acidity will provide preliminary findings regarding the characteristics and potential fate of these compounds.

Chapter 4 will briefly introduce various collaborations with the groups of Prof. Scot Martin at Harvard University and Prof. Allan Bertram at University of British Columbia to study atmospherically relevant properties of the organosulfates in question. Areas of study include the propensity of these compounds to enhance the uptake of gas-phase compounds into the condensed

phase, as well as the inherent hygroscopicity of the IEPOX-derived organosulfates. This chapter will also summarize synthetic efforts to generate various isotopologues of  $\alpha$ -pinene and ongoing collaborations with the groups of Prof. Mikael Ehn of University of Helsinki and Prof. Paul Wennberg at CalTech to probe the various oxidation pathways of these compounds.

**Chapter 2**  
Synthesis of IEPOX-derived Organosulfates

**Portions of this chapter appear in the following manuscript:**

Varelas, J. G., Vega, M. V., Geiger, F. M., Thomson, R. J. “Synthesis and Characterization of  
IEPOX-derived Organosulfates”, **2021**, *In Preparation*.

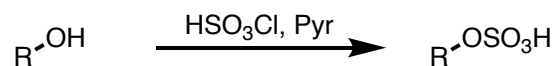
## 2.1 Synthetic Approaches Towards Sulfate Esters

As discussed in Chapter 1, sulfate esters – particularly monoesters – are an important class of molecules in a number of different areas, including biological systems, commercial use and, as pertinent to this thesis, the atmosphere and anthropogenic pollution. Due to their prevalence and importance, the chemical synthesis of several organosulfates has been disclosed throughout history. Although there is variance in the methods, the sulfate ester is typically bonded to the molecule in the penultimate or last step in the chemical synthesis, with a free alcohol being treated with one of a variety of sulfating reagents.

Before discussing the specific work conducted for this thesis, it is important to remark on the various methods of sulfate ester generation used in the context of organic synthesis. Sulfation of organic compounds has remained a challenging endeavor for synthetic chemists. The sulfate ester moiety is typically not implemented early in a chemical synthesis, because the incorporation of the functional group will typically dramatically increase the aqueous solubility of the compounds, therefore handling these species within organic solvents is quite challenging. Moreover, the aqueous solubility of these substrates presents a challenge in their purification, as typical chromatographic separation is often difficult to apply to highly polar molecules. Finally, sulfate esters have a propensity to undergo various chemical transformations depending on the reaction environment, such as pH, which makes them intolerant towards harsher reaction conditions, limiting the scope of viable synthetic procedures. This section will briefly outline the various ways in which sulfate esters have been synthesized in the past.

### 2.1.1 Chlorosulfonic Acid

One of the first reported methods of generating sulfate esters was the treatment of a free alcohol with chlorosulfonic acid ( $\text{HSO}_3\text{Cl}$ ), generating the free acidic sulfate as shown in **Scheme 2.1**. This method was first reported by Percival and coworkers in 1945, in which the sulfation of diacetone glucose was reported.<sup>115</sup> The use of this acidic sulfation had great utility in the early days of carbohydrate sulfation, but in present times does not see much use in the realm of laboratory synthesis of complex molecules due to the overly harsh acidic conditions which result in low yield and acidic hydrolysis of any protecting groups present on the larger molecule. However, certain commercial organosulfates such as SDS are sometimes generated using this acid, as the parent alcohol is a simple saturated alkane.<sup>29-30</sup>

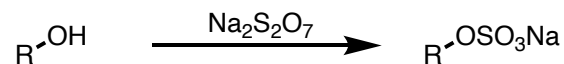


**Scheme 2.1** Synthesis of organosulfates via sulfation of an alcohol using chlorosulfonic acid.

### 2.1.2 Sodium pyrosulfate

Another early technique to access sulfate esters involved the use of sodium pyrosulfate ( $\text{Na}_2\text{S}_2\text{O}_7$ ) on a free alcohol, forming the sodium salt of the organosulfate shown in **Scheme 2.2**. Use of this reagent was first reported in the sulfation of sugars, with Turvey and coworkers accomplishing the selective sulfation of ethanolic hydroxyl groups of various monosacharrides.<sup>116</sup> Other reported uses of this reagent involved the sulfation of various pharmacological agents,

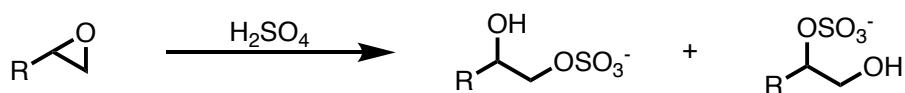
reported by Schroeter.<sup>117</sup> Similar to chlorosulfonic acid,  $\text{Na}_2\text{S}_2\text{O}_7$  is presently an inefficient reagent to produce complex sulfate esters in the laboratory due to side reactivity and the requirement of high levels of heat to force the sulfation towards full conversion.



**Scheme 2.2** Synthesis of organosulfates via sulfation of an alcohol using sodium pyrosulfate.

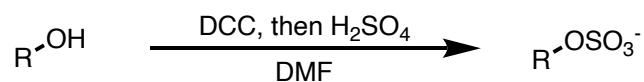
### 2.1.3 Sulfuric acid

The most intuitive reagent to consider for the generation of sulfate esters is sulfuric acid ( $\text{H}_2\text{SO}_4$ ).  $\text{H}_2\text{SO}_4$  can be used to generate sulfate esters via the opening of epoxides, shown in **Scheme 2.3**. Historically, solutions of  $\text{H}_2\text{SO}_4$  have also been used for the sulfation of free alcohols as well as alkenes. Though the use of sulfuric acid has proven useful, reaction conditions utilizing the acid as the sole reagent often lead to a variety of different side products, limiting the specificity and utility of this approach.



**Scheme 2.3** Synthesis of organosulfates via epoxide opening using sulfuric acid.

In order to achieve better selectivity, certain additives such as dicyclohexylcarbodiimide (DCC) have been used in conjunction with H<sub>2</sub>SO<sub>4</sub>. First reported by Mumma and coworkers,<sup>118</sup> the addition of DCC to the parent alcohol prior to addition of the acid generated the intended sulfate ester, as a direct combination of DCC and H<sub>2</sub>SO<sub>4</sub> would result in acidification, rendering the DCC useless. Several reports since have used the approach demonstrated in **Scheme 2.4** as a method of generating sulfate esters under relatively mild conditions. Although this method has been shown to be highly useful, it typically is geared towards the sulfation of unfunctionalized alcohols, limiting its spectrum of utility. Further, sterically congested alcohols are typically not optimal substrates for this type of sulfation due to the steric hindrance of the alcohol and DCC complex prior to acidification.

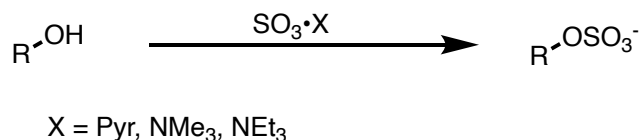


**Scheme 2.4** Synthesis of organosulfates using sulfuric acid and dicyclohexylcarbodiimide.

#### 2.1.4 Sulfur trioxide–amine complexes

Several of the aforementioned methods of sulfation utilize acidic sulfate as the means for installing the sulfate ester moiety, making these methods not amenable to sulfation onto organic scaffolds sensitive to highly acidic conditions. Conversely, direct sulfation of a free hydroxyl group using gaseous sulfur trioxide (SO<sub>3</sub>) poses several challenges, including potential polymerization and general difficulties of handling SO<sub>3</sub>.<sup>118</sup> A simpler, milder alternative that

avoids the pitfalls of both the acidic and gaseous methods of sulfation is the treatment of free alcohols with  $\text{SO}_3$ -amine adducts, the most common of which are derived from pyridine (Pyr, or Py), trimethylamine ( $\text{NMe}_3$ ) and triethylamine ( $\text{NEt}_3$ ). This highly useful method is shown in **Scheme 2.5** and has been used by organic chemists to generate a variety of monosulfated alcohols.<sup>119-122</sup>



**Scheme 2.5** Synthesis of organosulfates using sulfur trioxide amine adducts.

### 2.1.5 Masked Sulfate Esters

A drawback of the previously mentioned methods in generating sulfate esters is the need to construct a synthetic plan around the sulfation, having the sulfation normally be the final step of the synthesis due to the inconvenience posed by forming the functional group. Therefore, the use of these methods precludes the ability of synthetic chemists to manipulate the larger carbon scaffold during a total synthesis in order to prevent decomposition or labilization of the sulfate ester. In recent years, to synthesize sulfate esters with a more modular approach, there have been several reports of forming sulfate esters through a protection/deprotection strategy, in which a masked sulfate ester is bonded to a free alcohol in an intermediate step in the synthesis.<sup>123-124</sup> After

other chemical transformations to other portions of the molecule, a simple deprotection unmasks the sulfate ester moiety, shown in **Figure 2.1**.

The use of this masked sulfate ester is highly attractive for synthetic chemists. Unlike the free sulfate ester, the protected sulfate ester enables more expedient purification rather than various aqueous phase separations, as well as enabling the synthesis of more structurally diverse sulfate esters. Strategies of this type have been used several times in the synthesis of organosulfates. For example, Liu and coworkers disclosed the synthesis of several aryl organosulfates utilizing a masked sulfate ester bound to a 2,2,2-trichloroethyl (TCE) protecting group.<sup>125</sup> Shown in **Scheme 2.6**, the TCE-protected aryl sulfate **II-2** was generated through treatment of aryl alcohol **II-1** with a TCE-protected sulfonate and  $\text{NEt}_3$ , and was readily deprotected by either palladium on carbon (Pd/C) or zinc dust, coupled with ammonium formate, to afford the free organosulfate **II-3**.<sup>126</sup> While this strategy is advantageous in terms of its synthetic utility and versatility, the use of a bulky protected source of sulfate prevents this method from generating more sterically congested organosulfates.

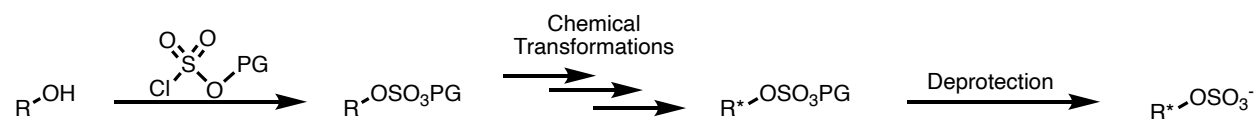
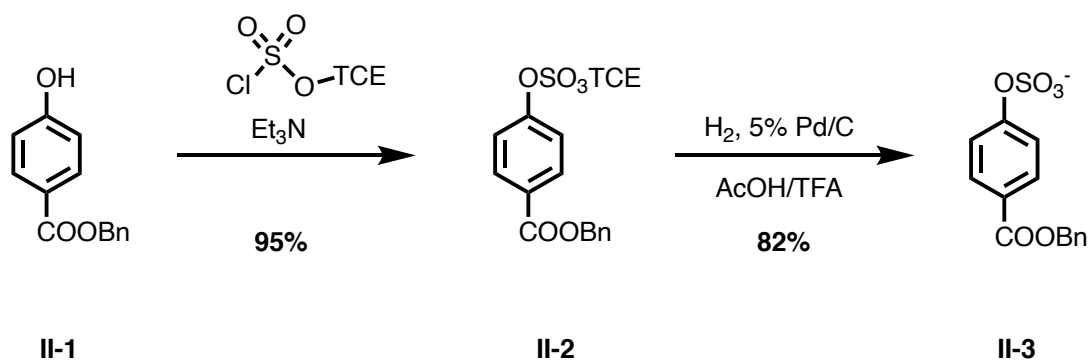


**Figure 2.1** A general synthetic strategy to access organosulfates via masked sulfate esters and subsequent deprotection.

## 2.2 Past Syntheses of Atmospherically relevant Organosulfates as Chemical Standards

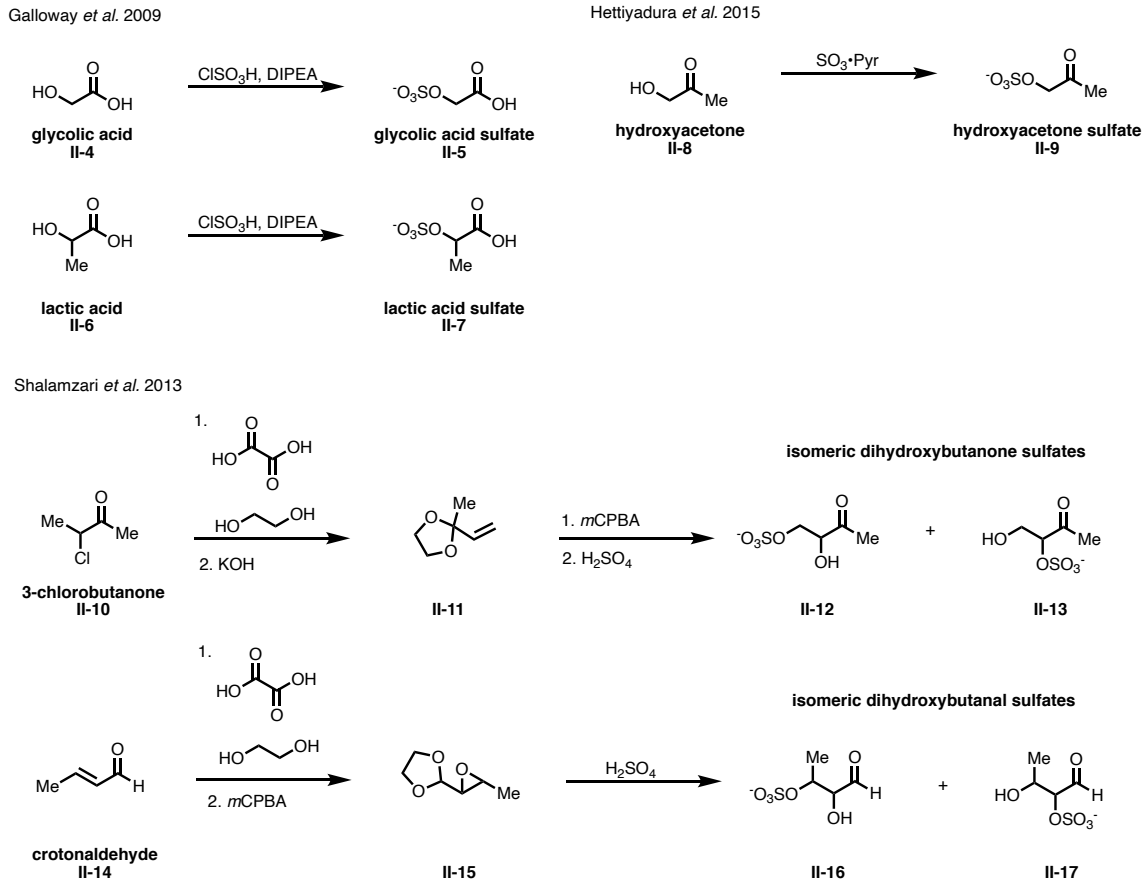
Now that some of the most common methodologies used in the synthesis of sulfate esters have been shown, the focus will turn to atmospherically relevant organosulfates. As introduced in Chapter 1, organosulfates formed from BVOCs are important constituents of SOA, yet a lack of pure standards for comparison to field studies prevents the direct characterization of species detected in the field. Several studies involving the detection of organosulfates have also disclosed synthetic procedures for synthesizing surrogate standards, a few of which are shown in **Scheme 2.7**.



**Scheme 2.6** Synthesis of aryl organosulfates utilizing a masked sulfate ester strategy disclosed by Liu and coworkers, 2004.

With respect to organosulfates believed to be derived from isoprene, the synthesis of sulfate esters derived from glycolic acid **II-4** and lactic acid **II-6**, **II-5** and **II-7** respectively, was accomplished by Galloway and coworkers in 2009 through the use of chlorosulfonic acid and diisopropylethylamine (DIPEA) in efforts to probe glyoxal uptake in acidic sulfate aerosol.<sup>127</sup> The

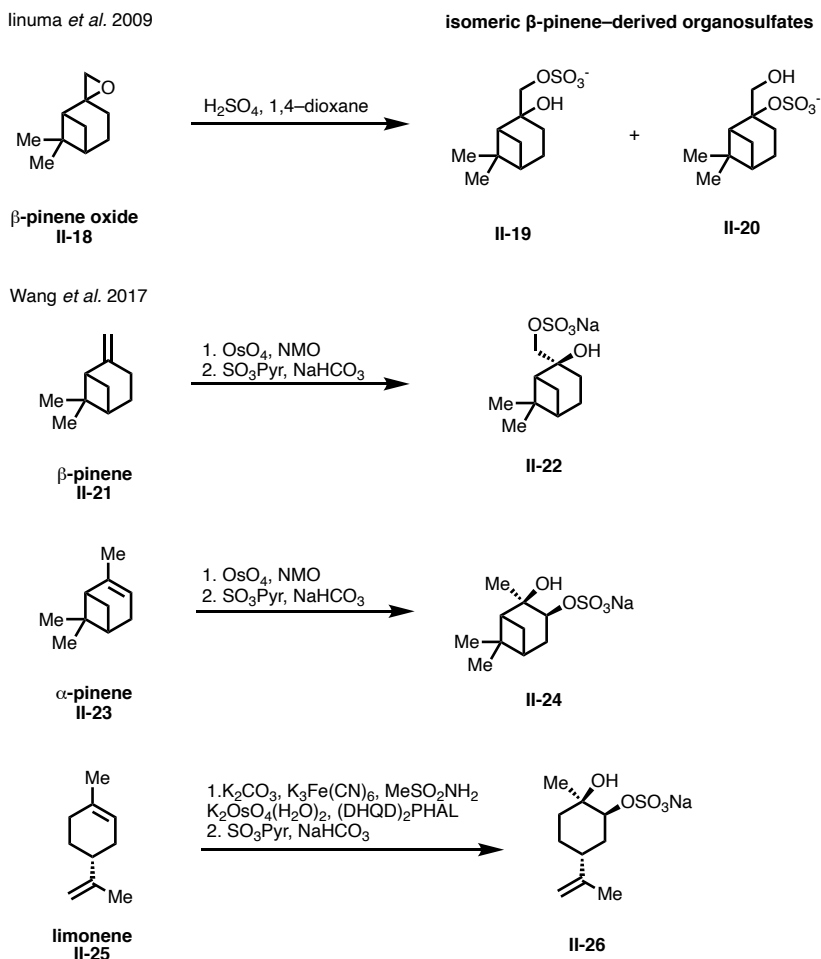
synthesis of these compounds as chemical standards allowed for a subsequent study published by Olson and workers to determine the atmospheric levels of these hydroxycarboxylic acid-derived organosulfates in urban areas.<sup>128</sup> In a later study published by Hettiyadura and coworkers, the structurally similar hydroxyacetone sulfate **II-9** was synthesized from its parent compound **II-8** through treatment with  $\text{SO}_3 \cdot \text{Pyr}$ .<sup>129</sup> In this study, the synthesis of these three carboxyorganosulfates allowed for the development of HILIC-MS procedures that have been utilized in several studies since. In 2013, Shalamzari and coworkers reported the synthesis of various organosulfates derived from dihydroxybutanone and dihydroxybutanal.<sup>130</sup> 3-Chlorobutanone **II-10** was treated with oxalic acid and ethylene glycol followed by elimination of the chlorine atom using potassium hydroxide (KOH) to afford spirocyclic ketal **II-11**. From here, epoxidation of the pendant olefin with *meta*-chloroperbenzoic acid (*m*CPBA) followed by one-pot acetal removal/sulfation using sulfuric acid led to isomeric dihydroxybutanone sulfates **II-12** and **II-13**. In the case of dihydroxybutanal sulfate isomers, crotonaldehyde **II-14** was also treated with oxalic acid and ethylene glycol, followed by epoxidation using *m*CPBA to afford internal epoxide **II-15**. This compound was then simply treated with sulfuric acid, unmasking the acetal and sulfating the hydroxyl substituents formed from the epoxide opening, forming isomeric dihydroxybutanal sulfates **II-16** and **II-17**. As stated by the authors, the generation of these four organosulfates as standards led to the identification of the dihydroxybutanone sulfates **II-12** and **II-13** within atmospheric aerosols detected within filter samples.



**Scheme 2.7** Syntheses of various organosulfates believed to be derived from isoprene.

In terms of synthetic standards of other atmospherically relevant organosulfates, species derived from BVOCs such as  $\beta$ -pinene,  $\alpha$ -pinene and limonene, **II-21**, **II-23** and **II-25** respectively, have been synthesized, shown in **Scheme 2.8**. Iinuma and coworkers reported the synthesis of isomeric  $\beta$ -pinene-derived organosulfates **II-19** and **II-20** through the treatment of  $\beta$ -pinene oxide **II-18** with sulfuric acid in attempts to probe the formation and oxidation of these species, as well as compare the respective levels of these species compared to other monoterpene-

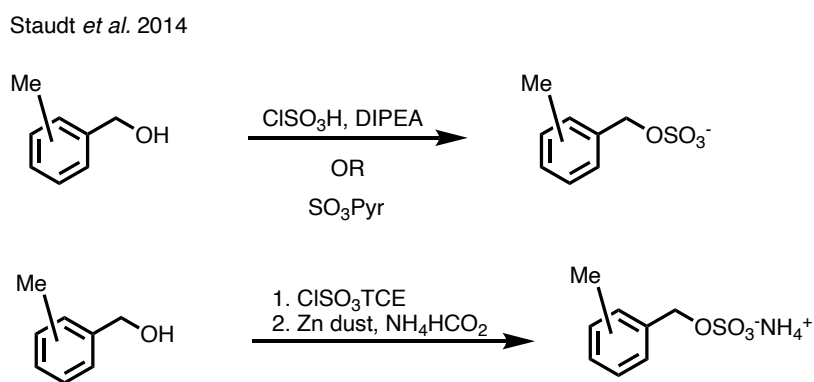
derived sulfates in the atmosphere.<sup>84</sup> In a recent study published by Wang and coworkers,<sup>102</sup>  $\beta$ - and  $\alpha$ -pinene were subjected to Upjohn dihydroxylation, followed by sulfation using sulfur trioxide pyridine complex to form respective organosulfates **II-22** and **II-24**. The authors also reported the synthesis of limonene-derived organosulfate **II-26**, in which limonene **II-25** was selectively oxidized using an asymmetric Sharpless dihydroxylation, followed by sulfation. The synthesis of these three monoterpene-derived species enabled their use as standards for comparison to field samples obtained near the Pearl River Delta in China in attempts to study the effects of anthropogenic pollution on BVOC-derived SOA. The researchers found that the limonene species was surprisingly abundant and even exceeded the levels of the species derived from  $\alpha$ - and  $\beta$ -pinene.



**Scheme 2.8** Syntheses of various organosulfates derived from  $\alpha$ - and  $\beta$ - pinene and limonene.

Synthetic efforts have also been directed towards standards of aryl organosulfates thought to be derived from anthropogenic VOCs such as toluene and benzene. As discussed in Chapter 1, the identification of aromatic sulfate esters will prove invaluable in providing insight into the molecular level effects of a rapidly urbanizing world. Staudt and coworkers synthesized and measured the levels of several aromatic organosulfates derived from several benzyl alcohol derivatives, shown in **Scheme 2.9**.<sup>131</sup> The study utilized chlorosulfonic acid, sulfur trioxide pyridine complex, as well as a TCE-protected sulfonate dependent on the functionality of the aryl

alcohol in question. Using HPLC coupled to ESI-ToF MS, the synthesis of these standards allowed for the detection of benzyl sulfate in almost all samples as the dominant aryl sulfate at measurement sites in Pakistan, Nepal, and urban California. Further development of a library of aromatic organosulfates will be highly advantageous in the identification of presently unknown species in the atmosphere.



**Scheme 2.9** Syntheses of aromatic organosulfates.

### 2.3 Development of a Regioselective and Stereocontrolled Synthesis of IEPOX-derived Organosulfates

Now that the field of sulfate ester synthesis has been described and the disclosed synthetic methodologies towards atmospheric chemical standards have been shown, the remainder of this thesis will discuss research conducted in the Thomson lab towards the synthesis of IEPOX-derived organosulfates. As previously introduced in **Section 1.3.1**, organosulfates derived from IEPOX, a highly abundant oxidation product of isoprene, are thought to represent the most abundant group

of molecules bearing sulfate esters present in the atmosphere, yet there has not been a general synthetic procedure to access all members of this family of compounds. Access to all eight IEPOX-derived organosulfates shown in **Figure 2.2** is essential for purposes of chemical standards, as well as the evaluation of their atmospherically relevant properties in order to better understand their eventual fate as SOA constituents.

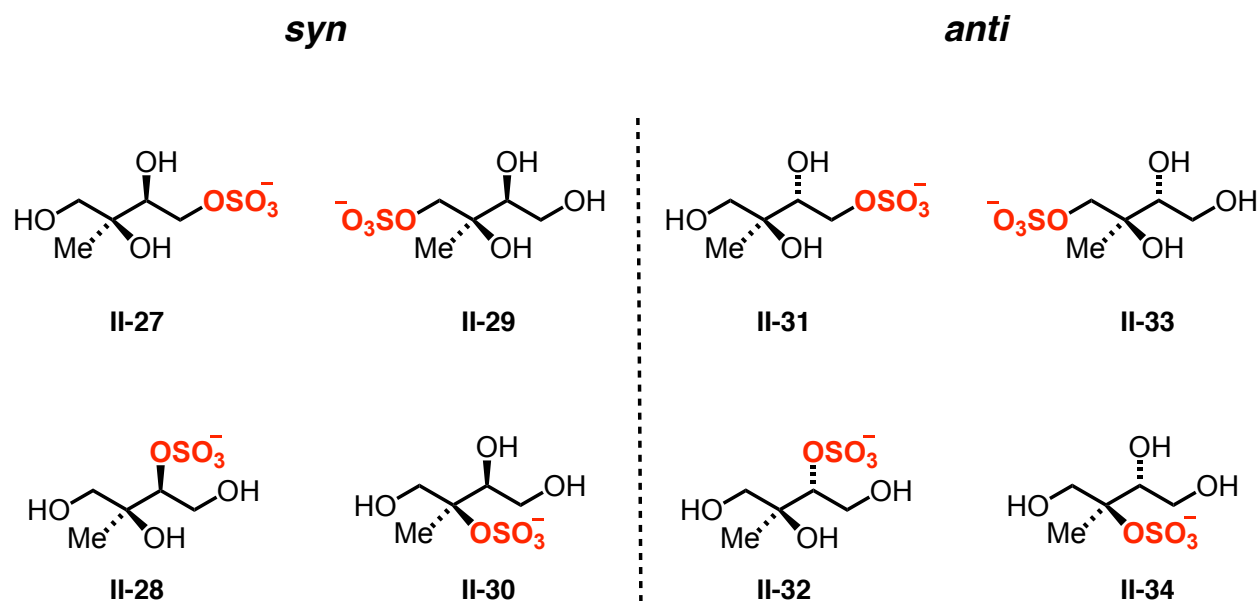


**Figure 2.2** The eight IEPOX-derived organosulfates.

We sought to devise a unified strategy to access both the anti and syn stereoisomers using prenil **II-35** as a common starting material, with stereocontrol arising from the mode of internal alkene dihydroxylation employed, and with regiocontrolled sulfation governed by a judicious choice of protecting groups. Thus, the overarching idea for the synthetic methodology described hereafter was to form a modular pathway to each organosulfate product, preparing the substrates stereoselectively with respect to the internal hydroxyl substituents, as well as controlling the

regioisomerism of the sulfate ester moiety, due to the parent tetraol compound bearing primary, secondary and tertiary sites of bonding. **Figure 2.3** shows a representation of the developed methodology, in which each of the organosulfates are derived from prenol **II-35**, also known as methallyl alcohol, as a common starting material. Hydroxyl groups are then installed across the carbon backbone and subsequently protected, with one of the hydroxyl groups bearing a more labile protecting group. The hydroxyl poised to bear the sulfate ester moiety is then selectively deprotected and sulfated, which would afford the desired organosulfate following global deprotection.

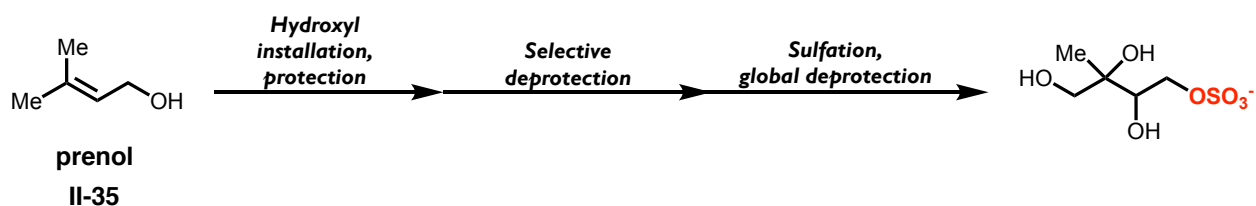


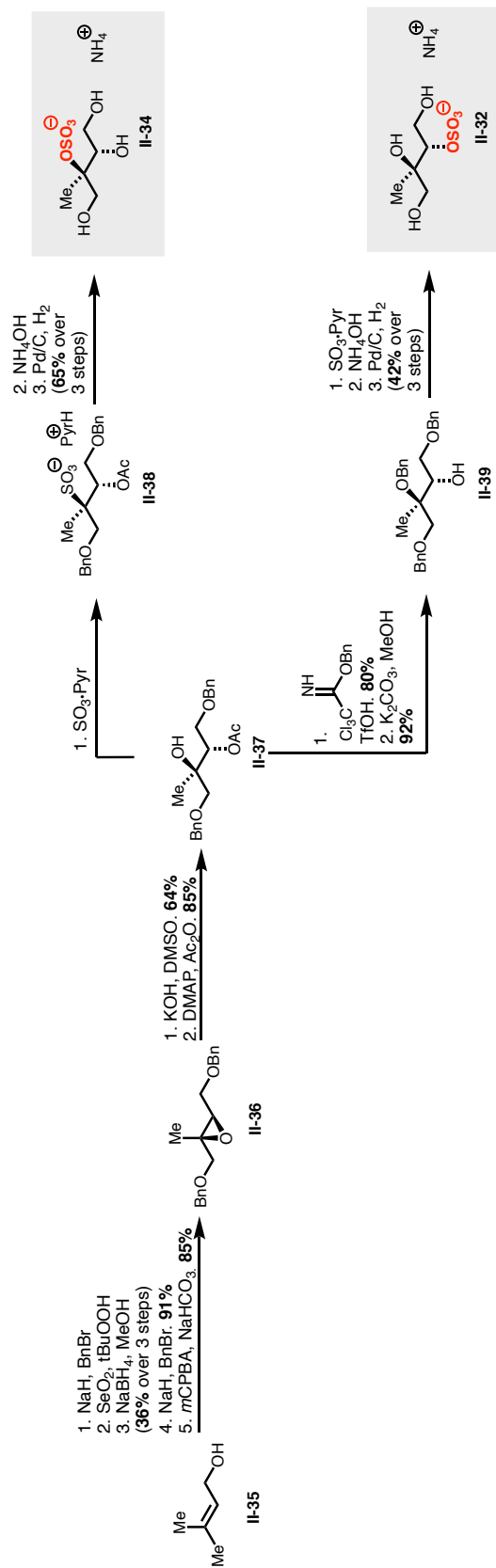
**Figure 2.3** The overall synthetic methodology to access IEPOX-derived organosulfates.

### 2.3.1 Synthesis of *anti*-IEPOX-derived organosulfates

The synthesis of the *anti* isomeric sulfates shown in **Scheme 2.10** commenced with a five-step sequence involving allylic oxidation, borohydride reduction and benzylation of prenol **II-35**, followed by epoxidation of the internal alkene using *m*CPBA afforded doubly-benzylated epoxide **II-36** in excellent yield. Subjecting the newly formed oxirane **II-36** to epoxide-opening under basic conditions using KOH:DMSO yielded the desired *anti*-configured vicinal diol, which upon selective acetylation of the secondary hydroxyl group, delivered differentially protected tertiary

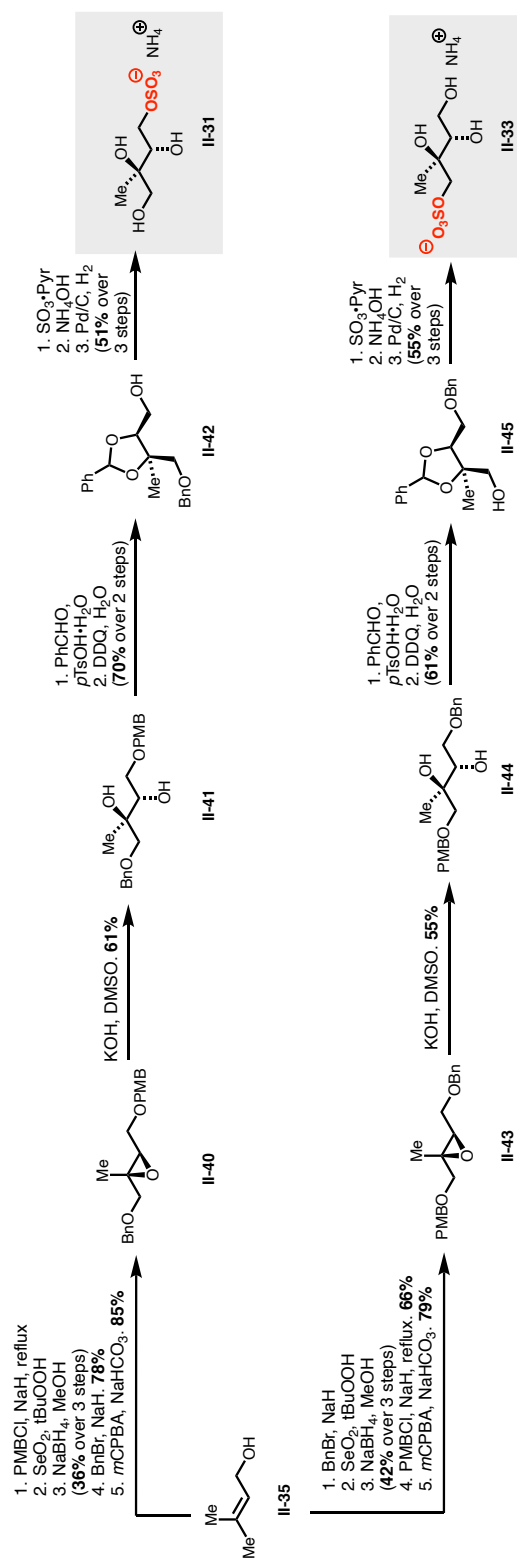
alcohol **II-37** in high yield. With the free tertiary hydroxyl, **II-37** was uniquely poised to serve as a divergent intermediate to access both the tertiary and secondary organosulfate isomers **II-34** and **II-32** respectively. Direct sulfation of **II-37** using  $\text{SO}_3 \cdot \text{Pyr}$  generated the fully protected sulfate **II-38** as the corresponding pyridine salt. To ensure our final product had the desired ammonium counterion, the pyridinium counterion was exchanged for ammonium by exposing **II-38** to stock 30% ammonium hydroxide, which also conveniently removed the acetyl group at the secondary position. As discussed in Chapter 1, the choice of the ammonium counterion was made due to the contention in the literature that the sulfate ester moiety found on atmospherically relevant organosulfates is formed from the reaction of IEPOX with ammonium sulfate under acidic conditions. A challenging logistical issue was posed by the implementation of the ammonium counterion, which will be elaborated on in Section 2.3.3. Finally, global deprotection via hydrogenolysis afforded **II-34** in good yield over 3 steps.

To access the corresponding secondary species, alcohol **II-37** was converted into trisbenzyl derivative **II-39** by a triflic acid-catalyzed benzylation of the free tertiary alcohol using benzyl 2,2,2-trichloroacetimidate, followed by removal of the acetyl group using potassium carbonate. As was the case for *anti* tertiary organosulfate **II-34**, a three-step procedure from **II-39** consisting of sulfation, installation of the desired ammonium counterion, and global hydrogenolysis afforded *anti*-secondary isomer **II-32** in reasonable yield



**Scheme 2.10** Synthesis of *anti* IEPOX-derived organosulfates **II-34** and **II-32**.

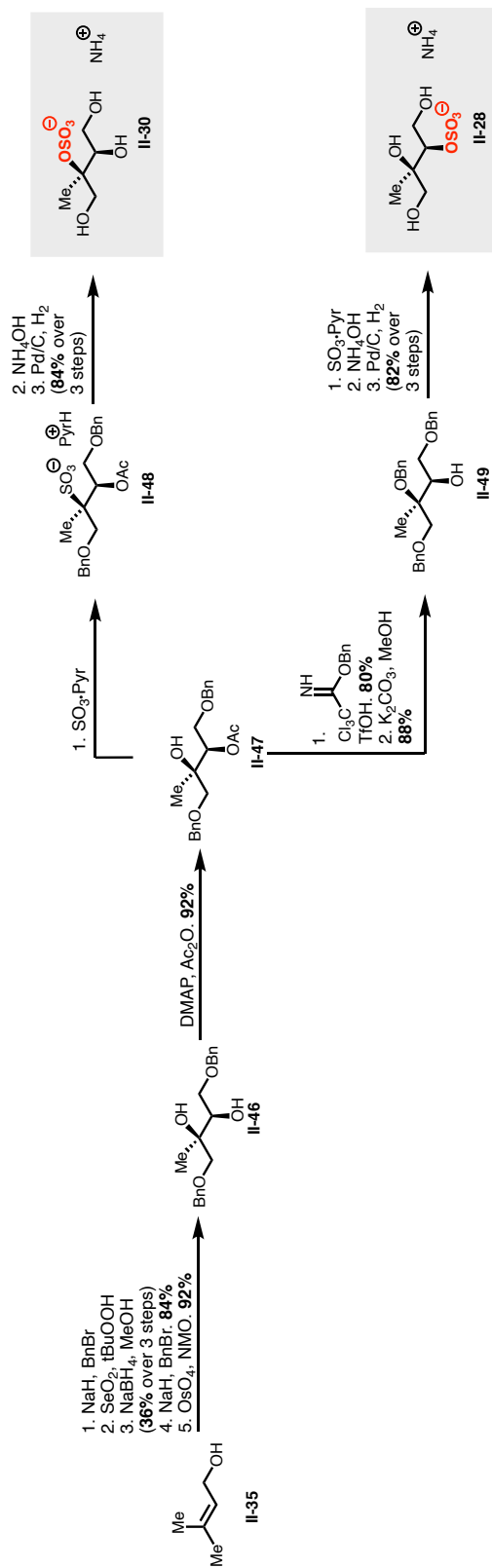
We next turned our attention to the two primary substituted *anti* organosulfates (**II-31**, **II-33**, **Scheme 2.11**). In analogy to the prior synthesis of epoxide **II-36** (**Scheme 2.10**), synthesis of **II-31** began with a five-step protocol to convert prenil **II-35** into differentially protected epoxide **II-40**. Basic hydrolysis of the epoxide furnished the requisite anti-configured diol **II-41**, setting the stage for benzylidene formation and DDQ-mediated PMB ether cleavage to deliver primary alcohol **II-42** over the three steps. Sulfation using  $\text{SO}_3 \cdot \text{Pyr}$ , followed by counterion metathesis and exhaustive hydrogenolysis of the benzyl and benzylidene groups gave **II-31** in moderate yield over the three-steps from **II-42**. With respect to the remaining primary organosulfate **II-33** through an analogous sequence, modifying the aforementioned route by swapping the positions of the benzyl and PMB ethers to generate epoxide **II-43**. From here, the synthesis followed the exact procedure described above, with *anti* vicinal diol **II-44** furnished through basic hydrolysis of **II-43**, subsequent benzylidene protection and removal of the PMB group to afford **II-45**, and finally the three step process of sulfation, counterion metathesis and global hydrogenolysis enabled access to primary sulfate **II-33**.



**Scheme 2.11** Synthesis of anti IEPOX-derived organosulfates **II-31** and **II-33**.

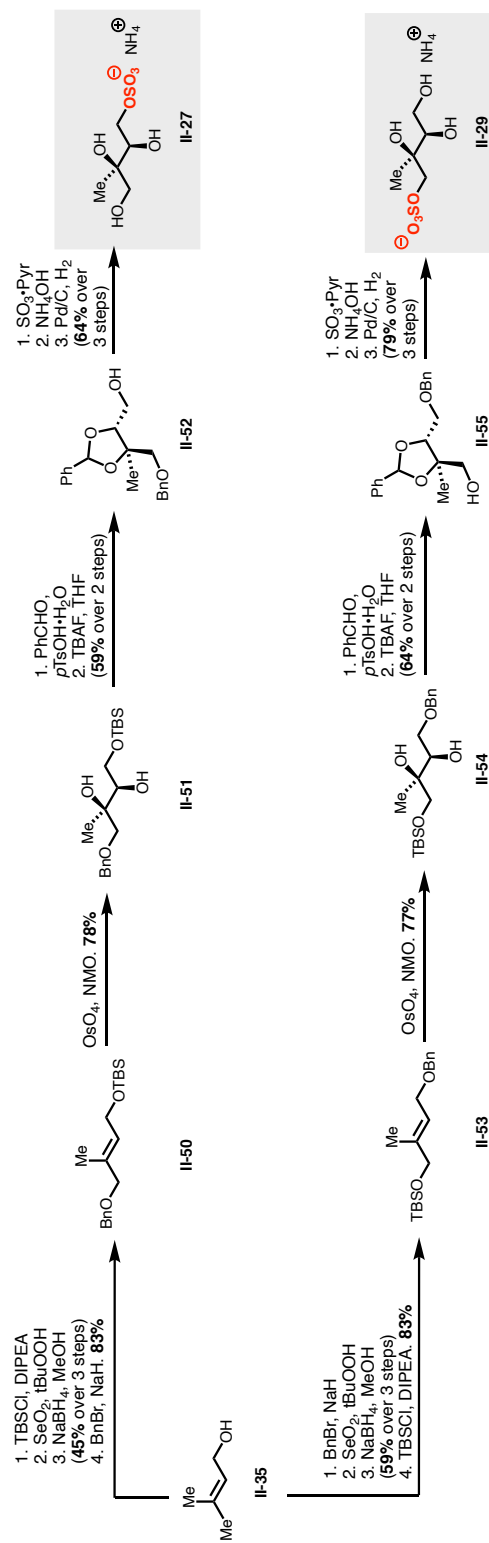
### 2.3.2 Synthesis of *syn*-IEPOX-derived organosulfates

Having established routes towards each of the four *anti*-oriented organosulfates, we wished to test the generality of our regioselective strategy by applying it to the synthesis of the corresponding *syn*-configured organosulfates (Schemes 2.12 and 2.13). We envisioned that an equivalent protecting group strategy to that used for accessing the *anti* compounds could be utilized for the desired *syn* species, with the only required modification being the method of alkene hydroxylation. To this end, *syn*-configured diol **II-46** was prepared from prenol **II-35** over five-steps with the critical relationship between the two hydroxyl stereocenters deriving from a *syn*-specific OsO<sub>4</sub>-catalyzed alkene dihydroxylation. Diol **II-46** was converted to tertiary alcohol **II-47** by selective acylation of the less hindered hydroxyl substituent, establishing the common intermediate to access to the tertiary and secondary *syn* organosulfates. Preparation of each of these regioisomeric sulfates was accomplished without incident by employing the same series of transformations as detailed for the *anti* compounds, in which alcohol **II-47** was directly sulfated to afford pyridinium salt **II-48**, and immediate counterion metathesis and hydrogenolysis yielded tertiary sulfate **II-30**. In the case of the secondary species, **II-47** was benzylated using 2,2,2-trichloroacetimidate and subsequently deprotected under basic conditions to afford free secondary alcohol **II-49**, which gave secondary organosulfate **II-28** following the three-step sequence of sulfation/ammonium installation/hydrogenolysis.



**Scheme 2.12** Synthesis of *syn* IEPOX-derived organosulfates **II-30** and **II-28**.

Finally, the remaining primary *syn*-regioisomers (**II-27** and **II-29**, **Scheme 2.13**) were synthesized in a manner analogous to their *anti* counterparts described above, with the only notable difference being the use of a TBS protecting group in place of a PMB group. The use of the TBS group was an artifact of a previously established methodology in our lab to access the *syn* organosulfates, and the use of the PMB protecting group was implemented to circumvent complications with a strategy to access the *anti* suite of compounds via an acidic epoxide opening, as well as a Prevost opening. However, once discovering the canonical basic epoxide opening proved efficient to access the *anti* species, we proceeded forward with the use of two different labile protecting groups to access the *syn* and *anti* compounds respectively. **II-35** was subjected to five step oxidation and protection sequences to afford doubly-protected olefins **II-50** and **II-53** and were subjected to *syn* Upjohn dihydroxylation to give *syn* vicinal diols **II-51** and **II-54** respectively, which were immediately protected as benzylidenes and upon deprotection using TBAF yielded their respective primary alcohols **II-52** and **II-55**. Finally, our three step sulfation/metathesis/hydrogenolysis procedure allowed for the conversion of each alcohol to the corresponding *syn* organosulfates **II-27** and **II-29** in good yield.



**Scheme 2.13** Synthesis of primary *syn* IEPOX-derived organosulfates **II-27** and **II-29**.

### 2.3.3 Challenges in the Synthesis of IEPOX-derived Organosulfates

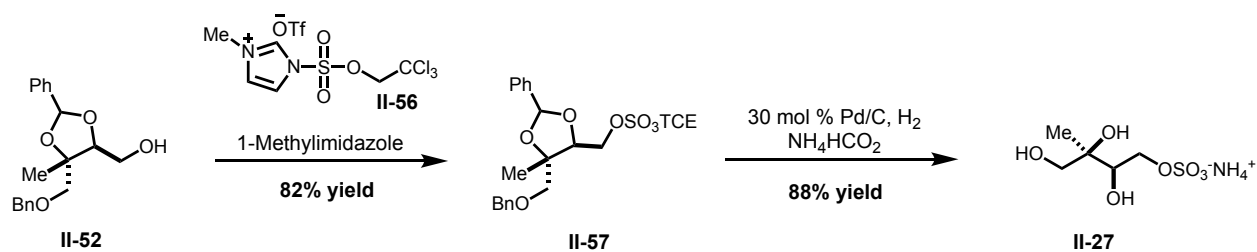
The synthetic strategy by our lab enables access to all possible stereochemical and regiospecific organosulfates derived from IEPOX shown in **Figure 2.2** through a modular method of robust functional group protections and manipulations. The completion of this endeavor marks the first synthetic approach to access this family of compounds in its entirety, avoiding the pitfalls of disclosed syntheses of sulfate esters. However, although presented in a streamlined fashion, the synthesis of these compounds posed several challenges and hurdles that resulted in the modification our method. This section will elaborate on some of the obstacles that were overcome throughout the development of our synthetic methodology.

#### *2.3.3.1 Installation of the Ammonium Counterion*

As discussed earlier, atmospherically-relevant organosulfates that are reported in the literature are commonly depicted with a high degree of variability with respect to the counterion associated with the sulfate ester functional group. Most studies that propose chemical structures of detected atmospheric species represent the pertinent moiety as the free sulfate ester bearing a negative charge with no positive counterion. Several show the sulfate ester as the parent acid despite the high level of acidity attributed to organosulfates, and others show the sulfate moiety associated with the titular ammonium counterion. Since the formation of atmospheric sulfate esters is believed to be enabled by acidic sulfate seed aerosol ( $\text{H}_2\text{SO}_4 + (\text{NH}_4)_2\text{SO}_4$ ), it is believed that the sulfate ester moiety likely bears an ammonium counterion within the particle phase. Therefore, in order to generate species of atmospheric relevance, we considered the efficient

incorporation of the ammonium cation onto the sulfate ester vital for our synthetic methodology towards IEPOX-derived organosulfates.

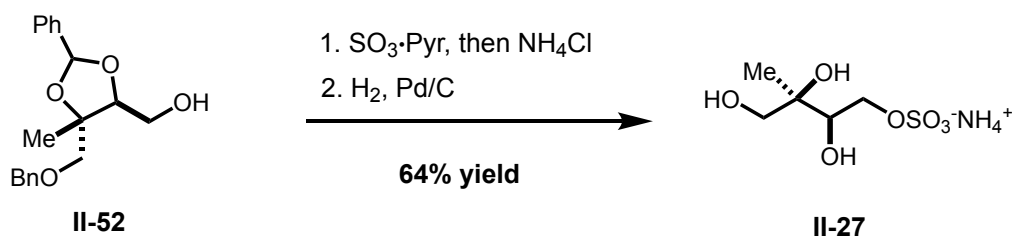
In our early synthetic attempts, the installation of the ammonium counterion in an equimolar ratio onto the sulfate ester were unsuccessful. **Scheme 2.14** shows the final steps of the initial route used to synthesize *syn* primary IEPOX-derived organosulfate **II-27** devised by former group member Dr. Marvin M. Vega. Comparing to the synthetic schemes detailed above, the major difference lies in the method of sulfation and the substrate used to incorporate the ammonium cation. Protected alcohol **II-52** was sulfated using a TCE-protected sulfation reagent **II-56** reported by Liu and coworkers,<sup>125</sup> forming masked sulfate ester **II-57** which was globally deprotected via hydrogenolysis using Pd/C and ammonium formate (NH<sub>4</sub>HCO<sub>2</sub>) to supply the ammonium cation to form *syn* primary organosulfate **II-27**.



**Scheme 2.14** Initial final steps in the synthetic route towards *syn* primary organosulfate **II-27**.

While this method of sulfation and subsequent deprotection yielded the intended organosulfate, synthetic utility was hampered by two factors: (i) the use of the protected imidazole-bound sulfating reagent **II-56** was only viable for the primary organosulfates **II-27** and **II-29**, with the more congested secondary and tertiary alcohols showing no reaction, and (ii) within

this synthetic route, the presence of the ammonium cation was never explicitly determined, as the study published by Liu suggested the  $\text{NH}_4\text{HCO}_2$  additive was sufficient to incorporate the desired ammonium counterion, and the ammonium protons were not visualized via  $^1\text{H}$  NMR (solvent:  $\text{CD}_3\text{OD}$ ). The final steps of this route were then altered in order to establish a more general sulfation method to apply to the primary, secondary and tertiary organosulfate isomers. **Scheme 2.15** depicts the revised route, in which the TCE-protected sulfating reagent is replaced with  $\text{SO}_3\cdot\text{Pyr}$ , as sulfur trioxide–amine adducts have been shown in the literature to be tolerant to hydroxyl groups of varying degrees of substitution.<sup>132-135</sup> Alcohol **II-52** was treated with  $\text{SO}_3\cdot\text{Pyr}$  to install the sulfate moiety, following quenching with saturated ammonium chloride, which gave **II-27** following hydrogenolysis. Fortunately, this method was easily applied to the *syn* secondary and tertiary isomers of the organosulfates and, later, to that of all the *anti* species.



**Scheme 2.15** Revised method of sulfation in the synthesis of *syn* primary organosulfate **II-27**.

Although this revised sulfation method was applicable to all of the IEPOX sulfates, a significant hurdle arose through the attempts to confirm the presence of the ammonium counterion. The NMR samples of the synthesized final products were prepared in deuterated methanol ( $d_4$ - $\text{CD}_3\text{OD}$ ) or deuterium oxide ( $\text{D}_2\text{O}$ ) due to the high aqueous solubility of organosulfates. Of course,

this prevented visualization of the distinct hydroxyl substituents for each sulfate ester, as the protons readily exchanged with the protic deuterium atoms. Moreover, any ammonium protons present in solution would not be visualized in an aqueous solvent. A solvent screen was therefore conducted to find a suitable NMR solvent that would dissolve the ionic organosulfate, as well as enable the visibility of the ammonium counterion. To this end, it was found that the organosulfates were soluble in  $d_6$ -DMSO. Unfortunately, this led to the realization of a significant ammonium impurity present in excess in all samples, shown in **Figure 2.4** in an NMR spectrum of *anti* primary organosulfate **II-31**. It became clear that the aqueous solubility of the suite of IEPOX-derived sulfates would pose a significant challenge in terms of the conditions necessary to install the ammonium counterion in an equimolar fashion.

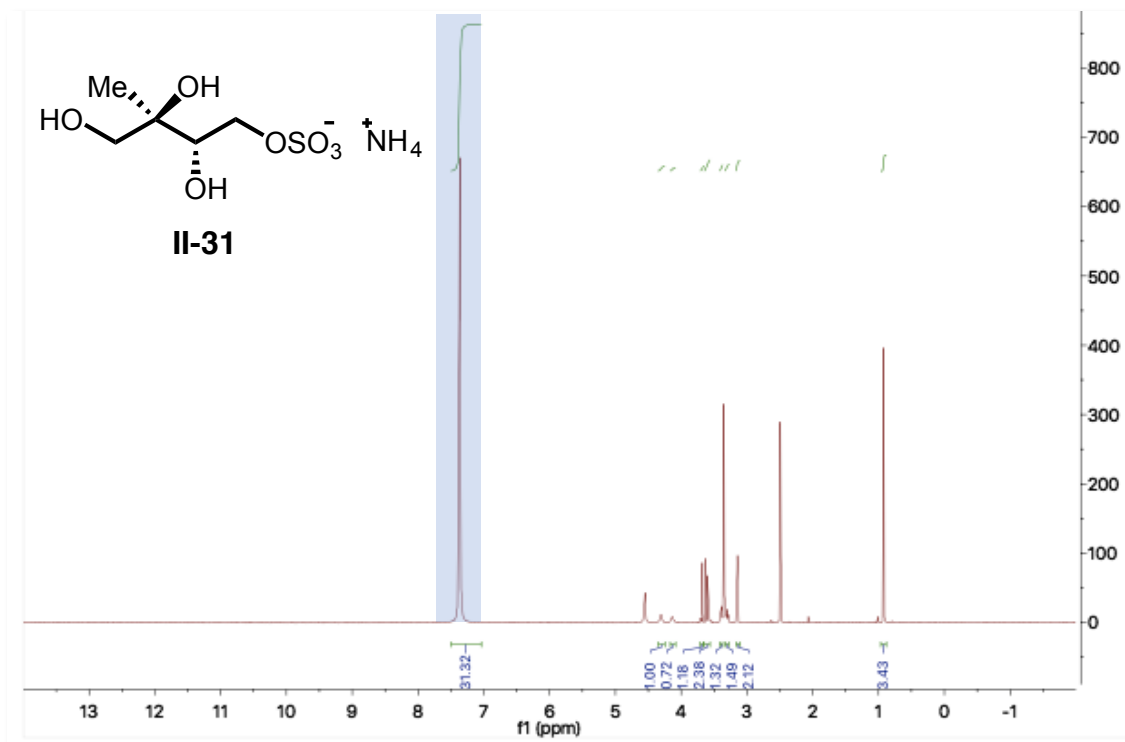


**Figure 2.4** NMR spectrum of *anti* organosulfate **II-31** in  $d_6$ -DMSO showing a substantial ammonium impurity at  $\delta$  7.45 ppm.

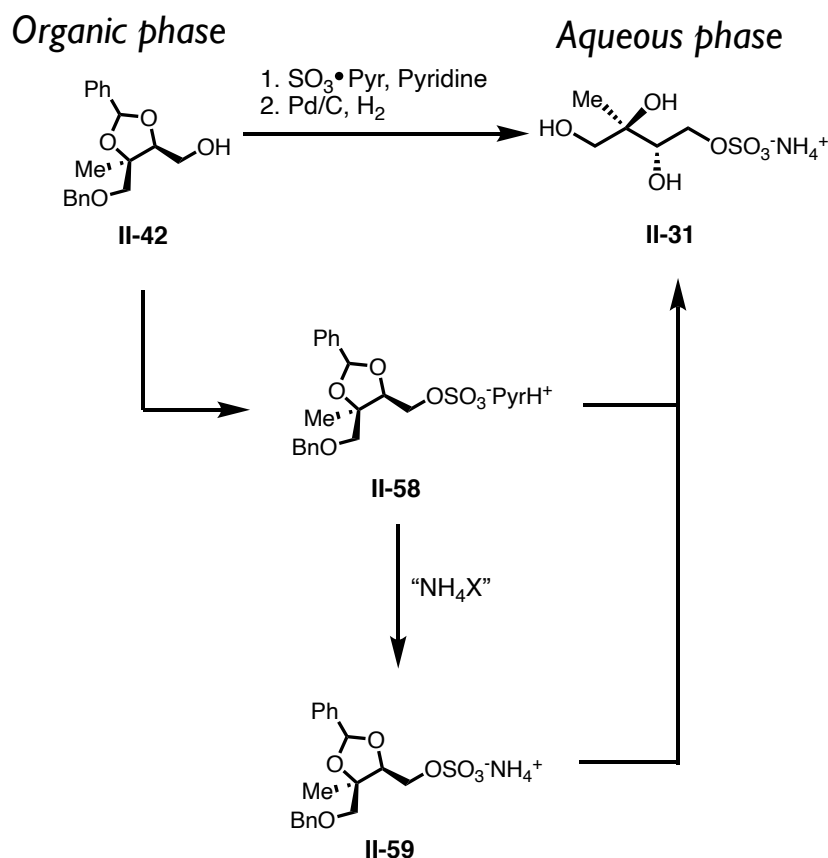
Given this circumstance, our efforts then turned towards removal of the excess ammonium impurity from the synthesized sulfates, using primary *anti* sulfate **II-31** with the hope that any established purification procedure would be suitable for the entire suite of organosulfates. These efforts are summarized in **Table 2.1**. Our initial thought was to rinse the final deprotected product using an alcohol solvent such as ethanol (EtOH) with a lower degree of aqueous solubility than that of MeOH, then simply decanting to retrieve the pure sulfate. Unfortunately, washing with EtOH displayed no change. Several attempts to use flash chromatography with the listed variety of mobile phases also proved ineffective. Extraction attempts into other polar solvents such as tetrahydrofuran (THF) were similarly unsuccessful due to the insolubility of both the organosulfate

and ammonium impurity, even when acidified using  $\text{H}_2\text{SO}_4$ . Lyophilization of the final product was attempted in case the ammonium impurity was volatile, although this also resulted in no change. Faced with the resilience of the impurity to be purified *post priori*, we then turned to methods to manipulate the method of ammonium installation by varying the quenching conditions of the sulfation reaction. Unfortunately, saturated solutions of both  $(\text{NH}_4)_2\text{SO}_4$  and  $\text{NH}_4\text{HCO}_2$  resulted in the presence of the impurity. Finally, with the failure of other saturated sources of aqueous ammonium, the quenching of the sulfation reaction was attempted using only 1 equiv. of  $\text{NH}_4\text{Cl}$ , which also failed.

**Table 2.1** Efforts to remove ammonium impurity from *anti* primary sulfate **II-31** using a variety of purification methods.

Purification Method	Result
EtOH rinse and decanting of solid material	No change
Flash chromatography, Mobile Phase - 50:50 MeOH:DCM	No change
Flash chromatography, Mobile Phase - 30:70 MeOH:DCM	No change
Flash chromatography, Mobile Phase - 100% EtOAc, followed by 30:70 MeOH:DCM	No change
Extraction from water using THF	No change (product insoluble)
Acidification with 0.1 M H <sub>2</sub> SO <sub>4</sub> , followed by extraction with THF	No change (product insoluble)
Lyophilization of final product	No change
Switching source of ammonium to saturated (NH <sub>4</sub> ) <sub>2</sub> SO <sub>4</sub>	No change
Switching source of ammonium to NH <sub>4</sub> HCO <sub>2</sub>	No change
Attempt to quench sulfation reaction with 1 molar equivalent of NH <sub>4</sub> Cl	Marginal decrease in peak area of peak at $\delta$ 7.45 ppm

Faced with the inability to manipulate or purify the ammonium species from the bulk of **II-31**, we considered the possibility of installing the appropriate counterion prior to final deprotection of the organosulfate. In this way, the ammonium group would be associated with the sulfate ester prior to unmasking the pendant hydroxyl substituents on the molecule, and any aqueous ammonium impurity would not likely be soluble with the organic sulfated compound, shown in **Scheme 2.16**. By treating protected alcohol **II-42** with the established sulfation conditions, the resultant pyridinium salt product **II-58** could be isolated in pure form, then through implementation of the ammonium counterion, the protected ammonium salt **II-59** could be purified to eliminate any excess impurity, which could then be carried directly deprotection via hydrogenolysis, resulting in the desired product **II-31**.



**Scheme 2.16** Depiction of hypothetical isolation of pyridinium salt **II-58** and subsequent counterion metathesis followed by hydrogenolysis to yield **II-59**.

Seeing as saturated ammonium sources were soluble with final product, our attention turned to the utility of volatile ammonium sources to use in this hypothesized method. In this way, the ammonium ion could be installed following sulfation, and simply concentrating off the excess ammonium would lead to all possible ammonium impurity being removed from the sample. We were pleased to see that use of excess stock ammonium hydroxide ( $\text{NH}_4\text{OH}$ ) solution (~28–30% ammonia ( $\text{NH}_3$ ) in water, Sigma Aldrich) generated protected ammonium salt **II-59** with no visible impurity within the sample, shown via NMR spectroscopy in **Figure 2.6** which easily carried

through to full deprotection, giving **II-31** as the intended ammonium salt. This method was also applicable to the other seven members of the suite of IEPOX-derived sulfate, allowing for the generation of all potential isomers as pure ammonium salts.

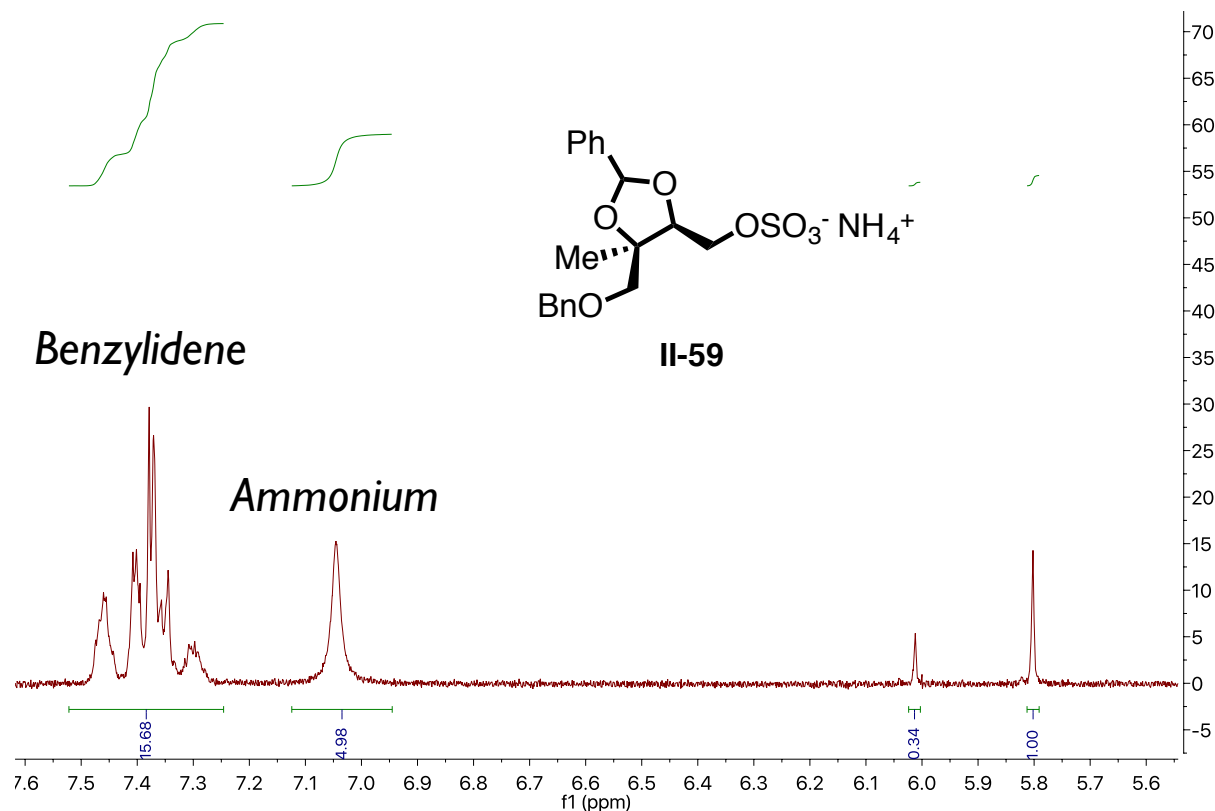


**Figure 2.5** NMR spectrum of protected ammonium salt **II-59** in *d*<sub>6</sub>-DMSO with appropriate equimolar ammonium signal at  $\delta$  7.05 ppm.

### 2.3.3.2 Stereocontrol of Internal Hydroxyl Groups

A less arduous optimization of our synthetic method came in the desire to synthesize the *anti* hydroxyl substituents of the *anti* oriented IEPOX sulfates. Methodology developed with Dr. Marvin M. Vega for the synthesis of the *syn* isomers utilized the robust method of osmium–

mediated Upjohn dihydroxylation to install the *syn* internal hydroxyl groups in excellent yield, shown in **Schemes 2.12** and **2.13**. When considering the most efficient route to take to install the *anti* substituents, several different conditions and methods were attempted before the final method of an internal epoxide opening under basic conditions.

The first method we decided to explore was the Prevost hydroxylation reaction, which is depicted generally in **Figure 2.6**. This canonical reaction disclosed by Prevost in the 1930s enabled the facile synthesis of *anti* vicinal diols from alkenes, in which the olefin is treated with silver benzoate ( $\text{AgO}_2\text{CPh}$ ) and iodine ( $\text{I}_2$ ) to generate the internal hydroxyl groups by installing two benzoate esters on the two adjacent carbon atoms. The benzoate esters are then hydrolyzed in the presence of aqueous basic conditions to afford the *anti* diol.

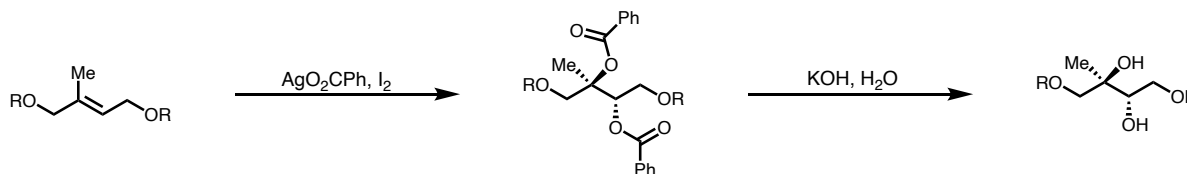
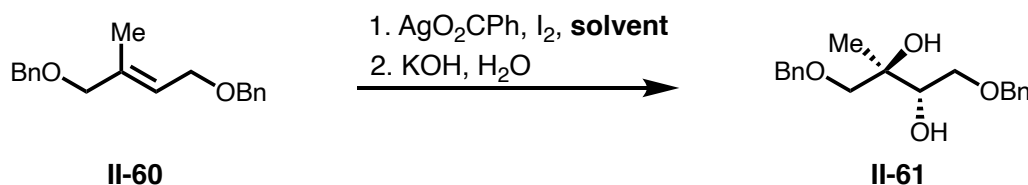


**Figure 2.6** General representation of the Prevost dihydroxylation to afford *anti* vicinal diols.

In applying this reaction to the synthesis of the *anti* IEPOX-derived organosulfates, a series of test reactions summarized in **Table 2.2** were run using doubly benzylated olefin **II-60** as the starting material. This brief screen of reaction conditions demonstrated that the Prevost reaction, although able to generate the intended *anti* diol suffered from consistently low yields in addition to requiring stoichiometric amounts of silver benzoate, which was not economically viable in terms

compared to the amount of product generated. Given these drawbacks, we turned our attention elsewhere to install the *anti* vicinal diol functionality.

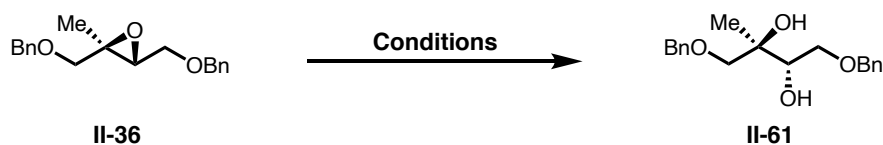
**Table 2.2** Conditions for the reaction screen of Prevost dihydroxylation of **II-60** to afford **II-61**. For all entries, the hydrolysis conditions were dissolution in 3.0 M KOH (Concentration of **II-60** in solution: 0.5 M). Entries marked with blue utilized molecular sieves in the introduction of I<sub>2</sub>.



Equiv. of AgO <sub>2</sub> CPh	Equiv. of I <sub>2</sub>	Solvent	Yield of II-61 (%)
2.0	1.0	Benzene	29 (mixture of <i>syn/anti</i> )
2.0	1.5	Benzene	31
2.5	2.0	Diethyl ether	15
2.0	1.5	Toluene	20
2.0	1.5	Toluene	36

We then began to explore the use of an epoxide opening to afford the vicinal *anti* diol, in which the same benzylated olefin **II-60** was treated with *m*CPBA to afford epoxide **II-36**, which could then be opened to generate the desired diol. **Table 2.3** summarizes the reaction screening of various epoxide opening conditions in both acidic and basic media. In general, acidic conditions used to open the epoxide involve dilute solutions of sulfuric acid dissolved in THF, only proceeding to completion under reflux conditions. Though this method resulted in full conversion

of starting material, the obvious drawback manifested in the generation of both the *syn* and *anti* isomers of desired diol, requiring careful chromatographic separation due to their very similar polarities. The exploration of basic reaction conditions proved more fruitful, though the time necessary for the reaction to proceed to completion was quite long (refluxed for 24-48 hrs) and required copious amounts of DMSO as the reaction solvent. Nevertheless, the basic epoxide opening using aqueous KOH generated *anti* diol **II-61** as the sole product in moderate yield.

**Table 2.3** Conditions for the opening of epoxide **II-36** to afford **II-61**.

Reagent	Solvent	Temperature (Celsius)	Reaction Time (hr)	Yield of II-61 (%)
1 M H <sub>2</sub> SO <sub>4</sub> (1.5 equiv)	H <sub>2</sub> O	RT	18	36 (50:50 <i>syn/anti</i> )
1 M NaOH (2 equiv)	H <sub>2</sub> O	80	22	NR
3 M NaOH (2 equiv)	DMSO (1:1 DMSO:NaOH)	190 (Reflux)	36	NR
1 M KOH (10 equiv)	DMSO (1:1 DMSO:KOH)	190 (Reflux)	48	26
3 M KOH (50 equiv)	DMSO (1:1 DMSO:KOH)	190 (Reflux)	48	64

## 2.4 Conclusions

In summary, the synthesis of all eight members of the IEPOX-derived organosulfates shown in **Figure 2.2** were successfully synthesized as pure ammonium salts. The methodology used employed the construction of the pendant hydroxyl groups from prenol **II-35** as a common starting material, with the hydroxyl groups installed and selectively protected to afford a single labile protecting group to be removed for purposes of late stage sulfation. Careful effort was put into the incorporation of the ammonium counterion on the sulfate ester moiety in order to establish a synthetic method to access these organosulfates as they are postulated to exist in the environment. Our hope is that the expedient synthesis of all isomers of the IEPOX-derived organosulfate we have described in this chapter will be an invaluable asset to the atmospheric and organic synthesis communities in the study of these species .

## 2.5 Experimentals

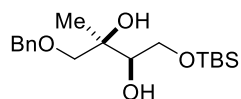
### 2.5.1 General Information

All reactions were carried out under a nitrogen atmosphere in flame-dried glassware with magnetic stirring unless otherwise stated. Anhydrous solvents (THF, Et<sub>2</sub>O, MeOH, DCM, Benzene, Toluene) were purified by passage through a bed of activated alumina.<sup>136</sup> Reagents were purified prior to use unless otherwise stated following the guidelines of Armarego and Chai.<sup>137</sup> Purification of reaction products was carried out by flash chromatography using EM Reagent silica gel 60 (230-400 mesh). Analytical thin layer chromatography was performed on EM Reagent 0.25 mm silica gel 60-F plates. Visualization was accomplished with UV light and *p*-anisaldehyde stain. Germanium ATR infrared spectra were recorded using a Bruker Tensor 37. <sup>1</sup>H NMR spectra were

recorded on a Varian Inova 500 (500 MHz) or Bruker Advance III 500 (500 MHz) spectrometer and are reported in ppm using solvent as an internal standard ( $\text{CDCl}_3$  at 7.26 ppm,  $\text{CD}_3\text{OD}$  at 3.31 ppm,  $d_6$ -DMSO at 2.50 ppm and  $\text{D}_2\text{O}$  at 4.79 ppm). Data are reported as s = singlet, d = doublet, t = triplet, q = quartet, p = pentet, hept = heptet, m = multiplet, b = broad, obs = obscured; integration; coupling constant(s) in Hz. Proton-decoupled  $^{13}\text{C}$  NMR spectra were recorded on a Bruker Advance III 500 (125 MHz) spectrometer and are reported in ppm using solvent as an internal standard ( $\text{CDCl}_3$  at 77.16 ppm). Mass spectra were obtained on an Agilent 6210 Time-of-Flight LC/MS and a Thermo Finnegan Mat 900 XL High Resolution Magnetic Sector.

## 2.5.2 Synthetic Procedures

### Compound II-51



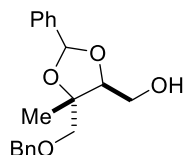
To a solution of **II-35** (5.00 g, 58.1 mmol) in dichloromethane (116 mL) was added DIPEA (18.2 mL, 104.5 mmol) and *tert*-butyldimethylsilyl chloride (9.63 g, 63.9 mmol). The reaction mixture was allowed to stir for 18 hours and then quenched with saturated ammonium chloride. The two layers were separated, and the aqueous layer was extracted with dichloromethane. The combined organic layers were washed with saturated sodium bicarbonate, brine, then dried with sodium sulfate and concentrated. The crude residue was quickly flashed through a column of silica gel (10% ethyl acetate in hexanes) to produce the appropriate silane (10.11 g, 50.5 mmol, 87%) as a clear oil. To a solution of the newly formed silane (7.69 g, 38.4 mmol) in dichloromethane (38 mL) was added selenium dioxide (0.21 g, 1.9 mmol) and salicylic acid (0.53 g, 3.8 mmol). A

solution of *tert*-butyl hydroperoxide (5.5 M in decane, 24.4 mL, 134.3 mmol) was added gradually to the solution. The reaction mixture was allowed to stir for 22 hours. Toluene was then added, and the mixture was concentrated. The resulting residue was diluted with diethyl ether and washed with saturated sodium bicarbonate and brine. The organic layer was dried with sodium sulfate and concentrated. The crude residue was diluted with methanol (77 mL) and cooled to 0 °C. Sodium borohydride (0.29 g, 7.7 mmol) was added to the solution in portions and the reaction mixture was allowed to stir at 0 °C for 30 minutes. Acetone was added to the reaction and the solution was concentrated. The resulting residue was diluted with ethyl acetate and washed with saturated ammonium chloride and brine. The organic layer was dried with sodium sulfate and concentrated. The crude residue was purified by silica gel chromatography (5% to 15% ethyl acetate in hexanes) to give the corresponding alcohol (4.33 g, 20.0 mmol, 52% over 2 reactions) as a clear oil. Sodium hydride (60% in mineral oil, 2.50 g, 63.2 mmol) was diluted with tetrahydrofuran (16 mL) and the mixture cooled to 0 °C. A solution of previously formed alcohol (4.55 g, 21.1 mmol) in tetrahydrofuran (5 mL) was cannulated over to the reaction mixture and allowed to stir for 20 minutes. Benzyl bromide (2.6 mL, 22.1 mmol) was added to the mixture. The reaction mixture was gradually brought to room temperature and allowed to stir for 16 hours. The excess sodium hydride was quenched by the slow addition of water. The mixture was diluted with ethyl acetate and added to excess water. The two layers were separated, and the aqueous layer was extracted two times with ethyl acetate. The combined organic layers were washed with brine, dried with sodium sulfate, and concentrated. The crude residue was purified by silica gel chromatography (1% to 5% ethyl acetate in hexanes) to give respective alkene (5.33 g, 17.4 mmol, 83%) as a clear oil. Then, to a solution of NMO (3.07 g, 26.2 mmol) in water (82 mL) and tetrahydrofuran (72 mL) was cannulated a solution of the alkene in tetrahydrofuran (10 mL). Osmium (VIII) oxide (2.5

w.t. % in *tert*-butyl alcohol, 2.1 mL, 0.16 mmol) was added and the reaction mixture was allowed to stir for 21 hours. Sodium thiosulfate (15.5 g, 98.2 mmol) was added to the reaction along with ethyl acetate. The mixture was allowed to stir for an additional 50 minutes before being filter through a silica gel plug with ethyl acetate. Filtrate was washed with brine, dried with sodium sulfate, and concentrated. The crude residue was purified by silica gel chromatography (10% to 20% ethyl acetate in hexanes) to give diol **II-51** (4.35g, 12.8 mmol, 78%) as a clear oil.

IR (neat): 3475, 3030, 2928, 2856, 1251, 1097, 832  $\text{cm}^{-1}$ ;  $^1\text{H}$  NMR (500 MHz,  $\text{CDCl}_3$ )  $\delta$  7.42 – 7.26 (m, 5H), 4.56 (dd,  $J = 14.8, 12.1$  Hz, 2H), 3.84 – 3.73 (m, 4H), 3.66 (q,  $J = 5.1$  Hz, 1H), 3.55 (d,  $J = 9.0$  Hz, 1H), 3.40 (d,  $J = 9.0$  Hz, 1H), 3.23 (s, 1H), 3.05 (d,  $J = 5.1$  Hz, 1H), 1.24 (s, 3H), 0.90 (s, 9H), 0.08 (s, 6H);  $^{13}\text{C}$  NMR (125 MHz,  $\text{CDCl}_3$ )  $\delta$  138.1, 128.6, 127.9, 127.8, 75.8, 73.8, 73.7, 73.5, 64.5, 26.0, 21.8, 18.3, -5.3, -5.4; HRMS (ESI): calcd for  $\text{C}_{18}\text{H}_{33}\text{O}_4\text{Si}$   $[\text{M}+\text{H}]^+$  341.2147, found 341.2156.

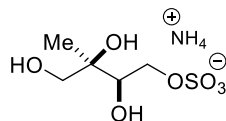
**Compound 4.89:**



To a solution of diol **II-51** (1.19 g, 3.5 mmol) in dichloromethane (12 mL) was added magnesium sulfate (0.59 g, 4.9 mmol), benzaldehyde (390  $\mu\text{L}$ , 3.9 mmol), and *p*-toluenesulfonic acid monohydrate (13 mg, 0.070 mmol), respectively. The reaction mixture was allowed to stir for 21 hours and quenched with saturated sodium bicarbonate. The mixture was diluted with dichloromethane and added to excess saturated sodium bicarbonate. The layers were separated, and the aqueous layer was extracted two times with dichloromethane. The combined organic layers were dried with sodium sulfate and concentrated.

To a solution of the crude benzylidene acetal (0.95 g, 2.2 mmol) in tetrahydrofuran (7.4 mL) was added a solution of tetrabutylammonium fluoride (1M in tetrahydrofuran, 4.4 mL, 4.4 mmol). The reaction mixture was allowed to stir for 17 hours and quenched with saturated ammonium chloride. The mixture was diluted with ethyl acetate and added to excess saturated ammonium chloride. The layers were separated, and the aqueous layer was extracted two times with ethyl acetate. The combined organic layers were washed with brine, dried with sodium sulfate, and concentrated. The crude residue was purified by silica gel chromatography (15% ethyl acetate in hexanes) to give alcohol **II-52** (0.65 g, 2.1 mmol, 59% over 2 steps) as a clear oil and mixture of diastereomers. IR (neat): 3443, 3032, 2863, 1453, 1217, 1086, 701  $\text{cm}^{-1}$ ;  $^1\text{H}$  NMR (500 MHz,  $\text{CDCl}_3$ ) For diastereomer A:  $\delta$  7.53 – 7.46 (m, 2H), 7.42 – 7.29 (m, 8H), 5.90 (s, 1H), 4.62 (s, 2H), 4.21 (dd,  $J = 6.6, 5.2$  Hz, 1H), 3.86 (dt,  $J = 11.4, 6.3$  Hz, 1H), 3.77 (ddd,  $J = 11.5, 6.3, 5.2$  Hz, 1H), 3.60 (dd,  $J = 13.0, 9.2$  Hz, 2H), 2.21 (t,  $J = 6.1$  Hz, 1H), 1.34 (s, 3H); For diastereomer B:  $\delta$  7.48 – 7.41 (m, 2H), 7.37 – 7.27 (m, 8H), 6.05 (s, 1H), 4.56 (dd,  $J = 15.3, 11.9$  Hz, 2H), 4.15 (dd,  $J = 6.7, 5.8$  Hz, 1H), 3.85 (dt,  $J = 11.4, 6.4$  Hz, 1H), 3.68 (dt,  $J = 11.6, 5.9$  Hz, 1H), 3.55 (dd,  $J = 13.9, 9.0$  Hz, 2H), 2.29 (t,  $J = 6.1$  Hz, 1H), 1.35 (s, 3H);  $^{13}\text{C}$  NMR (125 MHz,  $\text{CDCl}_3$ ) For diastereomer A:  $\delta$  137.6, 137.2, 129.5, 128.5, 128.4, 127.9, 127.7, 126.8, 102.9, 82.8, 80.9, 75.0, 73.8, 61.6, 19.3; For diastereomer B:  $\delta$  138.8, 137.6, 129.3, 128.7, 128.5, 128.1, 127.9, 126.5, 102.1, 82.1, 82.0, 75.5, 74.0, 61.2, 17.2; HRMS (ESI): calcd for  $\text{C}_{19}\text{H}_{23}\text{O}_4$   $[\text{M}+\text{H}]^+$  315.1591, found 315.1591.

**Compound II-27:**

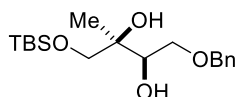


To a solution of alcohol **4.89** (0.63 g, 2.0 mmol) in pyridine (4.9 mL) was added sulfur trioxide pyridine complex (0.58 g, 2.2 mmol). The reaction mixture was allowed to stir for 14 hours. The

reaction was then concentrated under reduced pressure for 24 hours. The crude material containing the pyridinium salt was then dissolved in stock 30% NH<sub>4</sub>OH (60 mL) and stirred under N<sub>2</sub> for four hours. The crude reaction was concentrated under reduced pressure and was then left in vacuo for 16 hours to afford the sulfate ester ammonium salt. The crude material was then dissolved in MeOH (20 mL). 10% palladium on carbon was added to the reaction mixture and hydrogen gas was bubbled into the solution for 15 minutes. The reaction was allowed to stir under an atmosphere of hydrogen for an additional 20 hours. The reaction mixture was filtered through celite with excess methanol and concentrated to give organosulfate **II-27** (64% yield)

IR (neat): 3387, 3208, 3067, 1430, 1197, 980 cm<sup>-1</sup>; <sup>1</sup>H NMR (500 MHz, CD<sub>3</sub>OD) δ 4.28 (dd, *J* = 10.6, 3.1 Hz, 1H), 4.04 (dd, *J* = 10.6, 8.0 Hz, 1H), 3.82 (dd, *J* = 7.9, 3.1 Hz, 1H), 3.55 (d, *J* = 11.1 Hz, 1H), 3.47 (d, *J* = 11.1 Hz, 1H), 1.18 (s, 3H); <sup>13</sup>C NMR (125 MHz, CD<sub>3</sub>OD) δ 74.9, 74.7, 70.4, 68.0, 21.3; HRMS (ESI): calcd for C<sub>5</sub>H<sub>11</sub>O<sub>7</sub>S [M-NH<sub>4</sub>]<sup>-</sup> 215.0231, found 215.0220.

#### Compound II-54:

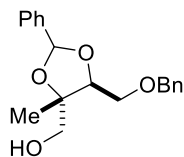


Sodium hydride (60% in mineral oil, 14.00 g, 348.3 mmol) diluted with tetrahydrofuran (116 mL) and the mixture cooled to 0 °C. **II-35** (11.8 mL, 116.1 mmol) was added over 3 minutes to the reaction mixture and allowed to stir for 15 minutes. Benzyl bromide (14.5 mL, 121.9 mmol) was added to the mixture over 5 minutes. The reaction mixture was gradually brought to room temperature and allowed to stir for 17 hours. The excess sodium hydride was quenched by the slow addition of water. The mixture was diluted with ethyl acetate and added to excess water. The two layers were separated, and the aqueous layer was extracted two times with ethyl acetate. The combined organic layers were washed with brine, dried with sodium sulfate, and concentrated.

The crude residue was diluted with dichloromethane (116 mL) and selenium dioxide (3.86 g, 34.8 mmol) and salicylic acid (3.21 g, 23.22 mmol) were added to the solution. A solution of *tert*-butyl hydroperoxide (70 w.t. % in water, 40 mL, 290.3 mmol) was added to the solution. The reaction mixture was allowed to stir for 21 hours. Toluene was then added, and the mixture was concentrated. The resulting residue was diluted with ethyl acetate and washed with saturated sodium bicarbonate and brine. The organic layer was dried with sodium sulfate and concentrated. The crude residue was diluted with methanol (116 mL) and cooled to 0 °C. Sodium borohydride (1.32 g, 34.8 mmol) was added to the solution in portions over 10 minutes and the reaction mixture was allowed to stir at 0 °C for 1 hour. Acetone was added to the reaction and the solution was concentrated. The resulting residue was diluted with ethyl acetate and washed with saturated ammonium chloride and brine. The organic layer was dried with sodium sulfate and concentrated. The crude residue was purified by silica gel chromatography (5% to 20% to 30% ethyl acetate in hexanes) to give the corresponding alcohol (13.09 g, 68.1 mmol, 59% over 3 reactions) as a clear oil. To a solution of the newly formed alcohol (4.00 g, 20.8 mmol) in dichloromethane (69 mL) was added DIPEA (5.4 mL, 31.2 mmol) and *tert*-butyldimethylsilyl chloride (3.61 g, 23.9 mmol). The reaction mixture was allowed to stir for 22 hours and then quenched with water. The two layers were separated, and the aqueous layer was extracted two times with dichloromethane. The combined organic layers were washed with brine, dried with sodium sulfate, and concentrated. The crude residue was purified by silica gel chromatography (1% to 5% ethyl acetate in hexanes) to give the desired alkene (5.29 g, 17.3 mmol, 83%) as a clear oil. To a solution of alkene (2.00 g, 6.5 mmol) in water (32 mL) and tetrahydrofuran (32 mL) was added NMO (1.22 g, 10.4 mmol) and osmium (VIII) oxide (2.5 w.t. % in *tert*-butyl alcohol, 820  $\mu$ L, 0.065 mmol), respectively. The reaction mixture was allowed to stir for 23 hours. Sodium thiosulfate (6.19 g, 39.2 mmol) was

added to the reaction along with ethyl acetate and the reaction was allowed to stir for an additional hour. The layers were separated, and the aqueous layer was extracted two times with ethyl acetate. The combined organic layers were washed with brine, dried with sodium sulfate, and concentrated. The crude residue was purified by silica gel chromatography (10% to 20% ethyl acetate in hexanes) to give diol **II-54** (1.72g, 5.1 mmol, 77%) as a clear oil. IR (neat): 3459, 3031, 2927, 2856, 1251, 1075, 834  $\text{cm}^{-1}$ ;  $^1\text{H}$  NMR (500 MHz,  $\text{CDCl}_3$ )  $\delta$  7.39 – 7.26 (m, 5H), 4.56 (s, 2H), 3.82 (dt,  $J = 6.6$ , 3.3 Hz, 1H), 3.66 (dd,  $J = 9.8$ , 4.1 Hz, 1H), 3.62 (dd,  $J = 9.8$ , 6.5 Hz, 1H), 3.60 (d,  $J = 9.7$  Hz, 1H), 3.50 (d,  $J = 9.7$  Hz, 1H), 3.13 (d,  $J = 3.5$  Hz, 1H), 3.00 (s, 1H), 1.14 (s, 3H), 0.89 (s, 9H), 0.06 (d,  $J = 1.1$  Hz, 6H);  $^{13}\text{C}$  NMR (125 MHz,  $\text{CDCl}_3$ )  $\delta$  137.8, 128.6, 128.0, 128.0, 73.8, 73.4, 73.2, 71.4, 69.0, 26.0, 21.0, 18.3, -5.4, -5.4; HRMS (ESI): calcd for  $\text{C}_{18}\text{H}_{33}\text{O}_4\text{Si}$   $[\text{M}+\text{H}]^+$  341.2143, found 341.2151.

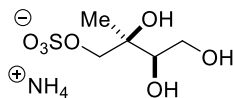
### Compound II-55:



To a solution of diol **II-54** (1.50 g, 4.4 mmol) in dichloromethane (15 mL) was added magnesium sulfate (0.74 g, 6.2 mmol), benzaldehyde (490  $\mu\text{L}$ , 4.9 mmol), and *p*-toluenesulfonic acid monohydrate (17 mg, 0.088 mmol), respectively. The reaction mixture was allowed to stir for 20 hours and quenched with saturated sodium bicarbonate. The mixture was diluted with dichloromethane and added to excess saturated sodium bicarbonate. The layers were separated, and the aqueous layer was extracted two times with dichloromethane. The combined organic layers were dried with sodium sulfate and concentrated. The crude material was then pushed forward without purification. To a solution of the crude benzylidene acetal (1.43g, 3.3 mmol) in tetrahydrofuran (11 mL) was added a solution of tetrabutylammonium fluoride (1M in

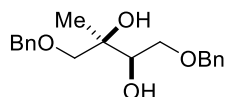
tetrahydrofuran, 6.7 mL, 6.7 mmol). The reaction mixture was allowed to stir for 17 hours and quenched with saturated ammonium chloride. The mixture was diluted with ethyl acetate and added to excess saturated ammonium chloride. The layers were separated, and the aqueous layer was extracted two times with ethyl acetate. The combined organic layers were washed with brine, dried with sodium sulfate, and concentrated. The crude residue was purified by silica gel chromatography (20% ethyl acetate in hexanes) to give alcohol **II-55** (0.88 g, 2.8 mmol, 84%) as a clear oil and mixture of diastereomers.

IR (neat): 3455, 3031, 2869, 1453, 1210, 1069, 695  $\text{cm}^{-1}$ ;  $^1\text{H}$  NMR (500 MHz,  $\text{CDCl}_3$ ) For diastereomer A:  $\delta$  7.52 – 7.44 (m, 2H), 7.44 – 7.27 (m, 8H), 5.90 (s, 1H), 4.63 (d,  $J = 11.9$  Hz, 1H), 4.55 (d,  $J = 11.9$  Hz, 1H), 4.33 (t,  $J = 6.4$  Hz, 1H), 3.80 (dd,  $J = 9.7, 6.1$  Hz, 1H), 3.74 – 3.63 (m, 2H), 3.63 (dd,  $J = 9.7, 6.6$  Hz, 1H), 2.17 (dd,  $J = 7.6, 5.5$  Hz, 1H), 1.26 (s, 3H); For diastereomer B:  $\delta$  7.46 (dd,  $J = 7.7, 1.9$  Hz, 2H), 7.42 – 7.29 (m, 8H), 6.07 (s, 1H), 4.63 (d,  $J = 11.9$  Hz, 1H), 4.57 (d,  $J = 11.9$  Hz, 1H), 4.29 (dd,  $J = 7.2, 5.6$  Hz, 1H), 3.79 (dd,  $J = 9.7, 5.7$  Hz, 1H), 3.74 – 3.55 (m, 3H), 2.29 (dd,  $J = 9.0, 4.3$  Hz, 1H), 1.31 (s, 3H);  $^{13}\text{C}$  NMR (125 MHz,  $\text{CDCl}_3$ ) For diastereomer A:  $\delta$  137.6, 137.5, 129.6, 128.6, 128.5, 128.1, 128.0, 126.9, 103.5, 82.6, 79.7, 73.9, 68.2, 67.3, 18.7; For diastereomer B:  $\delta$  138.9, 137.5, 129.4, 128.6, 128.6, 128.1, 128.0, 126.4, 102.2, 83.8, 78.3, 73.9, 68.3, 67.4, 16.1; HRMS (ESI): calcd for  $\text{C}_{19}\text{H}_{22}\text{NaO}_4$   $[\text{M}+\text{Na}]^+$  337.1410, found 337.1424.

**Compound II-29:**

To a solution of alcohol **II-55** (0.76 g, 2.4 mmol) in pyridine (5.9 mL) was added sulfur trioxide pyridine complex (0.69 g, 2.6 mmol). The reaction mixture was allowed to stir for 14 hours. The reaction was then concentrated under reduced pressure for 24 hours. The crude material containing the pyridinium salt was then dissolved in stock 30%  $\text{NH}_4\text{OH}$  (60 mL) and stirred under  $\text{N}_2$  for four hours. The crude reaction was concentrated under reduced pressure and was then left in vacuo for 16 hours to afford the sulfate ester ammonium salt. The crude material was then dissolved in MeOH (20 mL). 10% palladium on carbon was added to the reaction mixture and hydrogen gas was bubbled into the solution for 15 minutes. The reaction was allowed to stir under an atmosphere of hydrogen for an additional 20 hours. The reaction mixture was filtered through celite with excess methanol and concentrated to give organosulfate **II-29** (0.45 g, 1.9 mmol, 79% over 2 reactions) as an oily white solid.

IR (neat): 3380, 3189, 3046, 1432, 1195, 989, 818  $\text{cm}^{-1}$ ;  $^1\text{H}$  NMR (500 MHz,  $\text{CD}_3\text{OD}$ )  $\delta$  4.04 (d,  $J=9.8$  Hz, 1H), 3.87 (d,  $J=9.9$  Hz, 1H), 3.79 (dd,  $J=9.9, 1.9$  Hz, 1H), 3.66 – 3.53 (m, 2H), 1.21 (s, 3H);  $^{13}\text{C}$  NMR (125 MHz,  $\text{CD}_3\text{OD}$ )  $\delta$  76.2, 74.1, 73.0, 63.5, 21.5; HRMS (ESI): calcd for  $\text{C}_5\text{H}_{11}\text{O}_7\text{S}$  [ $\text{M}-\text{NH}_4$ ] $^-$  215.0231, found 215.0219.

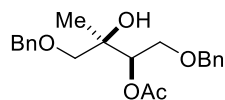
**Compound II-46:**

To a solution of alkene **II-50** (2.50 g, 8.9 mmol) in water (44 mL) and tetrahydrofuran (44 mL) was added NMO (1.66 g, 14.2 mmol). Osmium (VIII) oxide (2.5 w.t. % in *tert*-butyl alcohol, 1.1

mL, 0.089 mmol) was added dropwise over 1 minute and the reaction mixture was allowed to stir for 20 hours. Sodium thiosulfate (8.40 g, 53.1 mmol) was added to the reaction along with ethyl acetate and the reaction was allowed to stir for an additional 30 minutes. The mixture was added to excess water. The layers were separated, and the aqueous layer was extracted two times with ethyl acetate. The combined organic layers were washed with brine, dried with sodium sulfate, and concentrated. The crude residue was purified by silica gel chromatography (20% to 25% ethyl acetate in hexanes) to give diol **II-46** (2.57g, 8.1 mmol, 92%) as a white solid.

IR (neat): 3324, 3027, 2908, 2865, 1359, 1071, 696  $\text{cm}^{-1}$ ;  $^1\text{H}$  NMR (500 MHz,  $\text{CDCl}_3$ )  $\delta$  7.42 – 7.28 (m, 10H), 4.64 – 4.45 (m, 4H), 3.85 (dt,  $J = 6.0, 4.3$  Hz, 1H), 3.65 (dd,  $J = 9.8, 4.2$  Hz, 1H), 3.63 (dd,  $J = 9.8, 6.0$  Hz, 1H), 3.51 (d,  $J = 9.1$  Hz, 1H), 3.41 (d,  $J = 9.1$  Hz, 1H), 3.05 (dt,  $J = 4.4, 0.9$  Hz, 1H), 3.02 (s, 1H), 1.19 (d,  $J = 11.2$  Hz, 3H);  $^{13}\text{C}$  NMR (125 MHz,  $\text{CDCl}_3$ )  $\delta$  138.0, 137.8, 128.6, 128.6, 128.0, 128.0, 127.9, 127.8, 75.9, 73.8, 73.7, 73.3, 73.2, 71.3, 21.4; HRMS (ESI): calcd for  $\text{C}_{19}\text{H}_{25}\text{O}_4$   $[\text{M}+\text{H}]^+$  317.1747, found 317.1754.

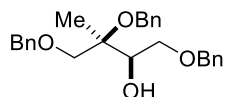
#### Compound II-47:



To a solution of diol **II-46** (2.36 g, 7.5 mmol) in dichloromethane (25 mL) was added DMAP (46 mg, 0.37 mmol) and the mixture was cooled to 0 °C. Acetic anhydride (740  $\mu\text{L}$ , 7.8 mmol) was added and the reaction mixture was gradually brought to room and allowed to stir for 18 hours. The reaction mixture was concentrated, and the crude residue was purified by silica gel chromatography (20% ethyl acetate in hexanes) to give alcohol **II-47** (2.50 g, 7.0 mmol, 94%) as a clear oil. IR (neat): 3480, 3030, 2862, 1735, 1235, 1091, 696  $\text{cm}^{-1}$ ;  $^1\text{H}$  NMR (500 MHz,  $\text{CDCl}_3$ )  $\delta$  7.36 – 7.27 (m, 10H), 5.20 (dd,  $J = 5.4, 3.9$  Hz, 1H), 4.50 (dd,  $J = 42.3, 12.0$  Hz, 2H), 4.49 (dd,

$J = 16.5, 12.0$  Hz, 2H), 3.72 (dd,  $J = 11.0, 3.9$  Hz, 1H), 3.70 (dd,  $J = 11.0, 5.4$  Hz, 1H), 3.36 (dd,  $J = 12.4, 9.1$  Hz, 2H), 3.07 (s, 1H), 2.04 (s, 3H), 1.22 (s, 3H);  $^{13}\text{C}$  NMR (125 MHz,  $\text{CDCl}_3$ )  $\delta$  170.8, 138.0, 137.8, 128.6, 128.6, 128.0, 127.9, 127.8, 74.8, 74.5, 73.7, 73.5, 73.4, 69.3, 21.8, 21.3; HRMS (ESI): calcd for  $\text{C}_{21}\text{H}_{27}\text{O}_5$   $[\text{M}+\text{H}]^+$  359.1853, found 359.1857.

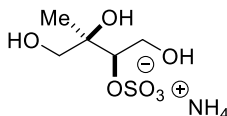
### Compound II-49:



Alcohol **II-47** (2.50 g, 7.0 mmol) and benzyl 2,2,2-trichloroacetimidate (3.52 g, 14.0 mmol) were diluted with diethyl ether (35 mL) and cooled to 0 °C. Trifluoromethanesulfonic acid (310  $\mu\text{L}$ , 3.5 mmol), cooled in an ice bath, was added dropwise to the reaction mixture over 1 minute. The reaction mixture gradually warmed to room temperature and allowed to stir for 16 hours. The reaction was quenched with saturated ammonium chloride. The reaction mixture was diluted with diethyl ether and added to excess saturated ammonium chloride. The layers were separated, and the aqueous layer was extracted two times with diethyl ether. The combined organic layers were dried with sodium sulfate and concentrated. The crude residue was purified by silica gel chromatography (10% ethyl acetate in hexanes) to give the corresponding acetate (2.50 g, 5.6 mmol, 80%) as a pale-yellow oil. To a solution of the acetate (2.44 g, 5.4 mmol) in methanol (18 mL) was added potassium carbonate (1.13 g, 8.2 mmol). The reaction mixture was allowed to stir for 21 hours. Acetone was added and the reaction mixture was concentrated. The resulting residue was diluted with ethyl acetate and water. The layers were separated, and the aqueous layer was extracted two times with ethyl acetate. The combined organic layers were washed with brine, dried with sodium sulfate, and concentrated. The crude residue was purified by silica gel chromatography (5% to 10% to 15% ethyl acetate) to give alcohol **4.103** (1.94 g, 4.8 mmol, 88%)

as a pale-yellow oil. IR (neat): 3429, 3028, 2915, 2862, 1452, 1090, 695  $\text{cm}^{-1}$ ;  $^1\text{H}$  NMR (500 MHz,  $\text{CDCl}_3$ )  $\delta$  7.40 – 7.21 (m, 14H), 4.64 – 4.53 (m, 4H), 4.50 (s, 2H), 4.03 (dt,  $J = 7.7, 3.8$  Hz, 1H), 3.76 (dd,  $J = 10.0, 3.3$  Hz, 1H), 3.68 (d,  $J = 10.0$  Hz, 1H), 3.61 (dd,  $J = 10.0, 7.5$  Hz, 1H), 3.57 (d,  $J = 10.0$  Hz, 1H), 2.82 (d,  $J = 4.6$  Hz, 1H), 1.33 (s, 3H);  $^{13}\text{C}$  NMR (125 MHz,  $\text{CDCl}_3$ )  $\delta$  139.4, 138.4, 138.1, 128.5, 128.4, 127.9, 127.8, 127.8, 127.4, 127.4, 78.2, 74.4, 73.6, 73.5, 73.2, 71.0, 65.0, 18.0; HRMS (ESI): calcd for  $\text{C}_{26}\text{H}_{31}\text{O}_4$   $[\text{M}+\text{H}]^+$  407.2217, found 407.2224.

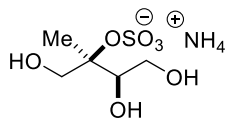
### Compound II-28:



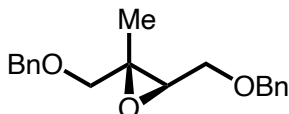
To a solution of alcohol **II-49** (1.85 g, 4.5 mmol) in pyridine (11 mL) was added sulfur trioxide pyridine complex (1.31 g, 5.0 mmol) gradually. The reaction mixture was allowed to stir for 14 hours. The reaction was then concentrated under reduced pressure for 24 hours. The crude material containing the pyridinium salt was then dissolved in stock 30%  $\text{NH}_4\text{OH}$  (120 mL) and stirred under  $\text{N}_2$  for four hours. The crude reaction was concentrated under reduced pressure and was then left in vacuo for 16 hours to afford the sulfate ester ammonium salt. The crude material was then dissolved in MeOH (45 mL). 10% palladium on carbon was added to the reaction mixture and hydrogen gas was bubbled into the solution for 15 minutes. The reaction was allowed to stir under an atmosphere of hydrogen for an additional 20 hours. The reaction mixture was filtered through celite with excess methanol and concentrated to give organosulfate **II-28** (0.87 g, 3.7 mmol, 82% over 2 reactions) as an oily white solid. IR (neat): 3374, 3210, 3044, 1405, 1204, 1008, 913  $\text{cm}^{-1}$ ;  $^1\text{H}$  NMR (500 MHz,  $\text{CD}_3\text{OD}$ )  $\delta$  4.35 (dd,  $J = 5.5, 3.8$  Hz, 1H), 3.96 (dd,  $J = 12.2, 3.8$  Hz, 1H), 3.87 (dd,  $J = 12.1, 5.5$  Hz, 1H), 3.61 (d,  $J = 11.4$  Hz, 1H), 3.42 (d,  $J = 11.4$  Hz, 1H), 1.24 (s, 3H);

$^{13}\text{C}$  NMR (125 MHz,  $\text{CD}_3\text{OD}$ )  $\delta$  83.7, 75.3, 67.8, 62.7, 22.1; HRMS (ESI): calcd for  $\text{C}_5\text{H}_{11}\text{O}_7\text{S}$   $[\text{M}-\text{NH}_4]^-$  215.0231, found 215.0221.

**Compound II-30:**



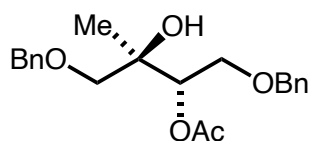
To a solution of alcohol **II-47** (1.42 g, 4.0 mmol) in pyridine (10 mL) was added sulfur trioxide pyridine complex (1.14 g, 4.4 mmol) gradually. The reaction mixture was allowed to stir for 19 hours. The reaction was then concentrated under reduced pressure for 24 hours. The crude material containing the pyridinium salt was then dissolved in stock 30%  $\text{NH}_4\text{OH}$  (105 mL) and stirred under  $\text{N}_2$  for four hours. The crude reaction was concentrated under reduced pressure and was then left in vacuo for 16 hours (vacuum  $\sim$  5 torr) to afford the sulfate ester ammonium salt without purification. The crude material was then dissolved in MeOH (40 mL) and stirred under  $\text{N}_2$ . 10% Pd/C was carefully added to the reaction.  $\text{H}_2$  gas was then bubbled through reaction for 15 minutes. The reaction was then fitted with a fresh atmosphere of  $\text{H}_2$  and the reaction was allowed to stir under  $\text{H}_2$  for 18 hours. The reaction was then filtered through a pad of celite and eluted with 50 mL MeOH. Concentration under reduced pressure afforded sulfate ester **II-30** (0.47 g, 2.0 mmol, 50% over 3 reactions) as an oily white solid. IR (neat): 3378, 3208, 3040, 1400, 1200, 1035, 878  $\text{cm}^{-1}$ ;  $^1\text{H}$  NMR (500 MHz,  $\text{CD}_3\text{OD}$ )  $\delta$  3.90 (dd,  $J = 7.2, 3.3$  Hz, 1H), 3.86 (dd,  $J = 20.8, 12.2$  Hz, 2H), 3.79 (dd,  $J = 11.6, 3.4$  Hz, 1H), 3.66 (dd,  $J = 11.6, 7.2$  Hz, 1H), 1.47 (s, 3H);  $^{13}\text{C}$  NMR (125 MHz,  $\text{CD}_3\text{OD}$ )  $\delta$  88.5, 76.8, 65.8, 63.3, 18.9; HRMS (ESI): calcd for  $\text{C}_5\text{H}_{11}\text{O}_7\text{S}$   $[\text{M}-\text{NH}_4]^-$  215.0231, found 215.0220.

**Compound II-36:**

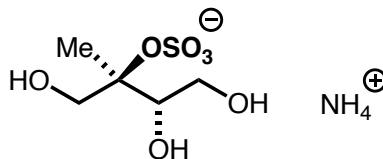
To a slurry of 60% NaH in mineral oil (6.97 g, 290.25 mmol) in THF (58 mL) at 0° C under N<sub>2</sub> was added **II-35** (5.91 mL, 58.05 mmol) over 5 minutes. The reaction was stirred at 0° C for 10 minutes. Benzyl bromide (8.32 mL, 60.95 mmol) was added to the reaction dropwise over 10 minutes and the reaction was stirred at 0° C and left to warm to room temperature over 18 hours. Saturated NaHCO<sub>3</sub> was added dropwise to the reaction to until the mixture appeared translucent. The mixture was then diluted in EtOAc and transferred to a separatory funnel. The organic phase was collected and the aqueous phase was extracted with 3 x 50 mL of EtOAc. The combined organics were washed with brine and dried with MgSO<sub>4</sub>. The crude mixture containing the benzylated species and was then carried forward without purification, and the yield was assumed to be 100% (58.05 mmol). To the crude product dissolved in DCM (58 mL) and stirred under N<sub>2</sub> was added selenium dioxide (1.31 g, 11.61 mmol) and salicylic acid (0.802 g, 5.81 mmol). A solution of *tert*-butyl hydroperoxide (5.5 M in decanes, 21.1 mL, 116.1 mmol) was added gradually to the reaction mixture. The reaction mixture was allowed to stir for 16 hours. 100 mL of toluene was then added to the reaction and was concentrated under reduced pressure to remove the decanes. The residue was then diluted with 100 mL of diethyl ether and transferred to a separatory funnel. The organic phase was collected and the aqueous phase was extracted with 3 x 50 mL diethyl ether. Combined organics were dried with MgSO<sub>4</sub> and concentrated under reduced pressure. The crude reaction mixture was then dissolved in MeOH (116 mL) and cooled to 0° C and stirred under

N<sub>2</sub>. Sodium borohydride (0.440 g, 11.6 mmol) was then added to the reaction and the reaction was stirred at 0° C for 2 hours. Acetone was added to the reaction and the solution was concentrated. The resulting residue was diluted with ethyl acetate and washed with saturated ammonium chloride and brine. The organic layer was dried with sodium sulfate and concentrated. The crude residue was purified by silica gel chromatography (5% to 20% EtOAc in hexanes) to give the resultant alcohol (5.1 g, 22.9 mmol, 36% yield over 3 reactions). The product of sodium borohydride reduction was then subjected to the same benzylation procedure used to furnish benzyl protected prenol detailed above (9.1 g, 91% yield). The doubly benzylated olefin (11 g, 33.5 mmol) was dissolved in DCM (112 mL) and stirred under N<sub>2</sub> at 0° C. NaHCO<sub>3</sub> (14 g, 167.5 mmol) was added, followed by meta-chloroperbenzoic acid (8.67 g, 50.2 mmol). The reaction was stirred at 0° C, gradually warming to room temperature over 19 hours. Saturated NaHCO<sub>3</sub> was added to the reaction and was stirred for 15 minutes. The mixture was then diluted in DCM and transferred to a separatory funnel. The organic phase was collected and the aqueous phase was extracted 3x100 mL DCM. Combined organics were dried with MgSO<sub>4</sub> and concentrated under reduced pressure. Column flash chromatography on silica gel (300 mL 10% EtOAc in hexanes) afforded **II-36** as a viscous yellow oil (8.0 g, 24.4 mmol, 85 % yield). IR (neat): 3087, 2855, 1722, 1603, 1495, 1362, 1242, 1094, 839 cm<sup>-1</sup>, <sup>1</sup>H NMR (500 MHz, Chloroform-*d*) δ 7.52 – 7.44 (m, 2H), 7.41 – 7.28 (m, 7H), 5.90 (s, 1H), 4.63 (d, *J* = 11.9 Hz, 1H), 4.55 (d, *J* = 11.9 Hz, 1H), 4.33 (t, *J* = 6.4 Hz, 1H), 3.80 (dd, *J* = 9.7, 6.2 Hz, 1H), 3.71 – 3.66 (m, 2H), 3.63 (dd, *J* = 9.7, 6.6 Hz, 1H), 2.17 (dd, *J* = 7.6, 5.5 Hz, 1H), 1.26 (s, 3H). <sup>13</sup>C NMR (125 MHz, CDCl<sub>3</sub>) δ 137.4, 137.3, 129.5, 128.5, 128.4, 127.9, 127.9, 126.8, 103.4, 82.4, 79.6, 73.8, 68.1, 67.1, 18.5., C<sub>19</sub>H<sub>22</sub>O<sub>3</sub> HRMS (ESI): calcd for C<sub>19</sub>H<sub>22</sub>O<sub>3</sub> [M+H]<sup>+</sup> 298.1569, found 298.1569.

**Compound II-37:**

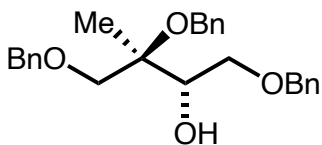


To a solution of **II-36** (1 g, 3.05 mmol) in DMSO (50.8 mL) stirred under N<sub>2</sub> was added aq. KOH (3.0 M in water, 152 mmol, 50.8 mL). The reaction was then fitted with a water condenser and heated to reflux for 46 hours. After cooling to room temperature, the reaction was diluted with Et<sub>2</sub>O and transferred to a separatory funnel. Saturated sodium chloride was added to the separatory funnel and the organic phase was collected, and the aqueous phase was extracted 3x100 mL Et<sub>2</sub>O. Combined organics were dried with MgSO<sub>4</sub> and concentrated under reduced pressure. Column flash chromatography on silica gel (400 mL 30% EtOAc in hexanes) yielded the corresponding diol a clear oil, as an equal mixture of enantiomers (0.89 g, 64% yield). To a solution of the resulting diol (1.57 g, 5.0 mmol) in dichloromethane (17 mL) was added DMAP (31 mg, 0.25 mmol) and the mixture was cooled to 0 °C. Acetic anhydride (490 μL, 5.2 mmol) was added and the reaction mixture was gradually brought to room and allowed to stir for 21 hours. The reaction mixture was concentrated, and the crude residue was purified by silica gel chromatography (20% ethyl acetate/hexanes) to give acetylated tertiary alcohol **II-37** (1.70 g, 4.2 mmol, 85%) as a clear oil. IR (neat): 3480, 3030, 2862, 1735, 1235, 1091, 696 cm<sup>-1</sup>; <sup>1</sup>H NMR (500 MHz, Chloroform-*d*) δ 7.39 – 7.24 (m, 10H), 4.83 (dd, *J* = 5.0, 4.0 Hz, 1H), 4.50 (ddt, *J* = 20.1, 7.8, 1.0 Hz, 5H), 4.05 (dd, *J* = 12.3, 8.2 Hz, 1H), 3.91 (d, *J* = 11.7 Hz, 1H), 3.55 (dd, *J* = 12.2, 8.3 Hz, 1H), 3.41 (d, *J* = 11.7 Hz, 1H), 3.29 (s, 1H), 2.02 (s, 3H), 1.38 (s, 3H). <sup>13</sup>C NMR (125 MHz, Chloroform-*d*) δ 170.2, 137.8, 137.7, 128.4, 128.3, 127.9, 127.7, 127.7, 76.3, 75.2, 74.1, 73.6, 72.5, 68.2, 21.2, 20.4. HRMS (ESI): calcd for C<sub>21</sub>H<sub>27</sub>O<sub>5</sub> [M+H]<sup>+</sup> 359.1853, found 359.1857.

**Compound II-34:**

Alcohol **II-37** (0.68 g, 1.9 mmol) was dissolved in distilled pyridine (5 mL) and stirred under N<sub>2</sub>. Sulfur trioxide pyridine complex (0.55 g, 2.1 mmol) was added to the reaction portion-wise over 3 minutes. The reaction was allowed to stir for 14 hours. The reaction was then concentrated under reduced pressure for 24 hours. The crude material containing the pyridinium salt was then dissolved in stock 30% NH<sub>4</sub>OH (50 mL) and stirred under N<sub>2</sub> for four hours. The crude reaction was concentrated under reduced pressure and was then left in vacuo for 16 hours (vacuum ~ 5 torr) to afford the sulfate ester ammonium salt without purification. The crude material was then dissolved in MeOH (19 mL) and stirred under N<sub>2</sub>. 10% Pd/C (0.03 g) was carefully added to the reaction. H<sub>2</sub> gas was then bubbled through reaction for 15 minutes. The reaction was then fitted with a fresh atmosphere of H<sub>2</sub> and the reaction was allowed to stir under H<sub>2</sub> for 18 hours. The reaction was then filtered through a pad of celite and eluted with 50 mL MeOH. Concentration under reduced pressure afforded sulfate ester **II-34** (0.29 g, 1.2 mmol, 65% yield) without purification. IR (neat): 3387, 3208, 3067, 1430, 1197, 980 cm<sup>-1</sup> <sup>1</sup>H NMR (500 MHz, Deuterium Oxide) δ 3.98 – 3.86 (m, 3H), 3.81 – 3.75 (m, 1H), 3.62 (dd, *J* = 11.8, 8.7 Hz, 1H), 1.45 (s, 3H). <sup>13</sup>C NMR (126 MHz, D<sub>2</sub>O) δ 87.8, 73.1, 63.8, 61.8, 15.4. HRMS (ESI): calcd for C<sub>5</sub>H<sub>11</sub>O<sub>7</sub>S [M–NH<sub>4</sub>]<sup>-</sup> 215.0231, found 215.0220.

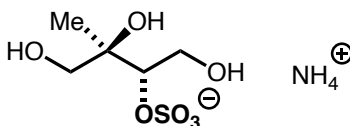
**Compound II-39**



Alcohol **II-37** (1.92 g, 5.38 mmol) and benzyl 2,2,2-trichloroacetimidate (2.70 g, 10.7 mmol) were diluted with diethyl ether (27 mL) and cooled to 0 °C. Trifluoromethanesulfonic acid (239  $\mu$ L, 2.7 mmol), cooled in an ice bath, was added dropwise to the reaction mixture over 1 minute. The reaction mixture gradually warmed to room temperature and allowed to stir for 16 hours. The reaction was quenched with saturated ammonium chloride. The reaction mixture was diluted with diethyl ether and added to excess saturated ammonium chloride. The layers were separated, and the aqueous layer was extracted two times with diethyl ether. The combined organic layers were dried with sodium sulfate and concentrated. The crude residue was purified by silica gel chromatography (10% ethyl acetate in hexanes) to give the corresponding acetate (1.92 g, 4.3 mmol, 80%) as a pale-yellow oil. To a solution of the resulting acetate (1.0 g, 2.2 mmol) in methanol (8 mL) was added potassium carbonate (0.46 g, 3.36 mmol). The reaction mixture was allowed to stir for 21 hours. Acetone was added and the reaction mixture was concentrated. The resulting residue was diluted with ethyl acetate and water. The layers were separated, and the aqueous layer was extracted two times with ethyl acetate. The combined organic layers were washed with brine, dried with sodium sulfate, and concentrated. The crude residue was purified by silica gel chromatography (5% to 10% to 15% ethyl acetate) to give alcohol **II-39** (0.82 g, 2.0 mmol, 92%) as a brown oil. IR (neat): 3309, 3001, 2890, 2854, 1450, 1118, 690  $\text{cm}^{-1}$ ;  $^1\text{H}$  NMR (500 MHz, Chloroform-*d*)  $\delta$  7.39 – 7.24 (m, 15H), 4.54 (dd,  $J = 12.1, 1.0$  Hz, 1H), 4.55 – 4.41 (m, 5H), 4.45 – 4.38 (m, 1H), 4.20 (d,  $J = 9.1$  Hz, 1H), 4.12 (d,  $J = 11.9$  Hz, 1H), 3.90 (q,  $J = 8.7$  Hz,

1H), 3.81 – 3.73 (m, 1H), 3.62 (d,  $J = 11.9$  Hz, 1H), 3.31 – 3.23 (m, 1H), 1.40 (s, 3H);  $^{13}\text{C}$  NMR (125 MHz, Chloroform-*d*)  $\delta$  139.0, 137.8, 137.7, 128.6, 128.4, 128.3, 128.1, 127.9, 127.8, 127.7, 127.7, 80.4, 74.9, 74.1, 73.4, 72.7, 69.2, 64.9, 17.8.; HRMS (ESI): calcd for  $\text{C}_{26}\text{H}_{31}\text{O}_4$   $[\text{M}+\text{H}]^+$  407.2217, found 407.1092.

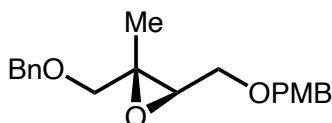
### Compound II-32



To a solution of alcohol **II-39** (1.85 g, 2.43 mmol) in pyridine (6 mL) was added sulfur trioxide pyridine complex (0.7 g, 2.7 mmol) gradually. The reaction mixture was allowed to stir for 14 hours. The reaction was then concentrated under reduced pressure for 24 hours. The crude material containing the pyridinium salt was then dissolved in stock 30%  $\text{NH}_4\text{OH}$  (78 mL) and stirred under  $\text{N}_2$  for four hours. The crude reaction was concentrated under reduced pressure and was then left in vacuo for 12 hours to afford the sulfate ester ammonium salt. The crude material was then dissolved in MeOH (24 mL). Palladium on carbon (10 w.t. %, 730 mg, 0.68 mmol) was added to the reaction mixture and hydrogen gas was bubbled into the solution for 15 minutes. The reaction was allowed to stir under an atmosphere of hydrogen for an additional 20 hours. The reaction mixture was filtered through celite with excess methanol and concentrated to give organosulfate **II-32** (0.24 g, 1.0 mmol, 42% yield) as an oily white solid. IR (neat): 3403, 3190, 3002, 1399, 1204, 1016, 913  $\text{cm}^{-1}$ ;  $^1\text{H}$  NMR (500 MHz,  $\text{D}_2\text{O}$ )  $\delta$  3.89 – 3.76 (m, 3H), 3.70 (d,  $J = 12.7$  Hz, 1H),

3.53 (dd,  $J = 11.8, 8.7$  Hz, 1H), 1.36 (s, 3H).  $^{13}\text{C}$  NMR (125 MHz,  $\text{D}_2\text{O}$ )  $\delta$  87.5, 72.9, 66.9, 61.6, 20.1; HRMS (ESI): calcd for  $\text{C}_5\text{H}_{11}\text{O}_7\text{S}$   $[\text{M}-\text{NH}_4]^-$  215.0231, found 215.0241.

### Compound II-40



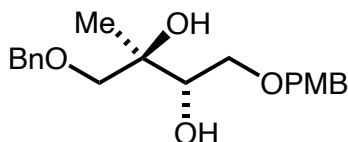
To a slurry of 60% NaH in mineral oil (6.97 g, 290.25 mmol) in THF (58 mL) at 0° C under  $\text{N}_2$  was added II-35 (5.91 mL, 58.05 mmol) over 5 minutes. The reaction was stirred at 0° C for 10 minutes. *p*-methoxybenzyl chloride (8.32 mL, 60.95 mmol) was added to the reaction dropwise over 10 minutes and the reaction was stirred at 0° C for 15 minutes. The reaction was then fitted with a water condenser and heated at reflux for 13 hours. After cooling to room temperature, saturated  $\text{NaHCO}_3$  was added dropwise to the reaction to until the mixture appeared translucent. The mixture was then diluted in EtOAc and transferred to a separatory funnel. The organic phase was collected and the aqueous phase was extracted with 3 x 50 mL of EtOAc. The combined organics were washed with brine and dried with  $\text{MgSO}_4$ . The crude mixture was then carried forward without purification, and the yield was assumed to be 100%. To the crude product dissolved in DCM (58 mL) stirred under  $\text{N}_2$  was added selenium dioxide (1.31 g, 11.61 mmol) and salicylic acid (0.802 g, 5.81 mmol). A solution of *tert*-butyl hydroperoxide (5.5 M in decanes, 21.1 mL, 116.1 mmol) was added gradually to the reaction mixture. The reaction mixture was allowed to stir for 16 hours. 100 mL of toluene was then added to the reaction and was concentrated under reduced pressure to remove the decanes. The residue was then diluted with 100 mL of diethyl ether and transferred to a separatory funnel. The organic phase was collected and the aqueous phase was extracted with 3 x 50 mL diethyl ether. Combined organics were dried

with  $\text{MgSO}_4$  and concentrated under reduced pressure. The crude reaction mixture was then dissolved in MeOH (116 mL) and cooled to  $0^\circ\text{C}$  and stirred under  $\text{N}_2$ . Sodium borohydride (0.440 g, 11.6 mmol) was then added to the reaction and the reaction was stirred at  $0^\circ\text{C}$  for 2 hours. Acetone was added to the reaction and the solution was concentrated. The resulting residue was diluted with ethyl acetate and washed with saturated ammonium chloride and brine. The organic layer was dried with sodium sulfate and concentrated. The crude residue was purified by silica gel chromatography (5% to 20% EtOAc in hexanes) to give the resulting alcohol (5.1 g, 22.9 mmol, 40% yield over 3 reactions).

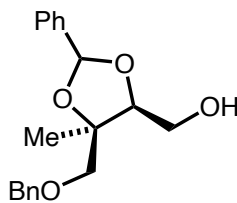
To a slurry of 60% NaH in mineral oil (2.93 g, 121.9 mmol) in THF (41 mL) at  $0^\circ\text{C}$  under  $\text{N}_2$  was added the resulting alcohol (8.41 g, 40.6 mmol) over 5 minutes. The reaction was stirred at  $0^\circ\text{C}$  for 10 minutes. Benzyl bromide (5.80 mL, 48.8 mmol) was added to the reaction dropwise over 10 minutes and the reaction was stirred at  $0^\circ\text{C}$ , gradually warming to room temperature over 16 hours. Saturated  $\text{NaHCO}_3$  was added dropwise to the reaction until the mixture appeared translucent. The mixture was then diluted in EtOAc and transferred to a separatory funnel. The organic phase was collected and the aqueous phase was extracted with 3 x 50 mL of EtOAc. The combined organics were washed with brine and dried with  $\text{MgSO}_4$ . Concentration under reduced pressure and flash column chromatography (200 mL, 10% EtOAc in hexanes) afforded the corresponding olefin. was dissolved in DCM (112 mL) and stirred under  $\text{N}_2$  at  $0^\circ\text{C}$ .  $\text{NaHCO}_3$  (14 g, 167.5 mmol) was added, followed by meta-chloroperbenzoic acid (8.67 g, 50.2 mmol). The reaction was stirred at  $0^\circ\text{C}$ , gradually warming to room temperature over 19 hours. Saturated  $\text{NaHCO}_3$  was added to the reaction and was stirred for 15 minutes. The mixture was then diluted in DCM and transferred to a separatory funnel. The organic phase was collected and the aqueous phase was extracted 3x100 mL DCM. Combined organics were dried with  $\text{MgSO}_4$  and

concentrated under reduced pressure. Column chromatography on silica gel (300 mL 10% EtOAc in hexanes) afforded **II-40** as a viscous yellow oil (8.0 g, 24.4 mmol, 85% yield). IR (neat): 3002, 2860, 1701, 1660, 1503, 1362, 1290, 1091, 910  $\text{cm}^{-1}$ ;  $^1\text{H}$  NMR (500 MHz, Chloroform-*d*)  $\delta$  7.28 (d,  $J = 4.6$  Hz, 3H), 7.24 – 7.17 (m, 4H), 6.80 (d,  $J = 8.7$  Hz, 2H), 4.57 (d,  $J = 11.8$  Hz, 1H), 4.51 – 4.36 (m, 3H), 3.73 (s, 3H), 3.65 (dd,  $J = 11.2, 4.5$  Hz, 1H), 3.51 (dd,  $J = 11.2, 6.2$  Hz, 1H), 3.43 (d,  $J = 11.1$  Hz, 1H), 3.34 (d,  $J = 11.1$  Hz, 1H), 3.08 (dd,  $J = 6.2, 4.4$  Hz, 1H), 1.24 (s, 3H).  $^{13}\text{C}$  NMR (125 MHz, Chloroform-*d*)  $\delta$  159.4, 137.8, 131.1, 128.7, 128.4, 127.9, 127.7, 113.9, 73.4, 72.6, 72.3, 66.7, 60.8, 59.2, 55.3, 16.8. HRMS (ESI): calcd for  $\text{C}_{20}\text{H}_{24}\text{O}_4$   $[\text{M}+\text{H}]^+$

## Compound II-41

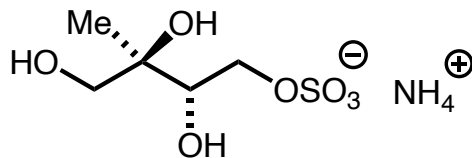


To a solution of **II-40** (2.8 g, 8.5 mmol) in DMSO (140 mL) stirred under N<sub>2</sub> was added aq. KOH (3.0 M in water, 140 mL). The reaction was then fitted with a water condenser and heated to reflux for 46 hours. After cooling to room temperature, the reaction was diluted with Et<sub>2</sub>O and transferred to a separatory funnel. Saturated sodium chloride was added to the separatory funnel and the organic phase was collected, and the aqueous phase was extracted 3x200 mL Et<sub>2</sub>O. Combined organics were dried with MgSO<sub>4</sub> and concentrated under reduced pressure. Column flash chromatography on silica gel (500 mL 30% EtOAc in hexanes) yielded the corresponding diol a clear oil, as an equal mixture of enantiomers (1.79 g, 61% yield). IR (neat): 3450, 3006, 2908, 2843, 2790, 1251, 1097, 801 cm<sup>-1</sup>; <sup>1</sup>H NMR (500 MHz, Chloroform-*d*) δ 7.38 – 7.27 (m, 5H), 7.21 (d, *J* = 8.6 Hz, 2H), 6.87 (d, *J* = 8.7 Hz, 1H), 4.52 (d, *J* = 1.8 Hz, 2H), 4.44 (s, 2H), 3.81 (s, 3H), 3.78 (td, *J* = 6.1, 3.6 Hz, 1H), 3.68 (dd, *J* = 9.8, 3.6 Hz, 1H), 3.59 (dd, *J* = 9.8, 6.4 Hz, 1H), 3.52 (d, *J* = 9.1 Hz, 1H), 3.33 (d, *J* = 9.1 Hz, 1H), 3.03 (s, 1H), 2.82 (d, *J* = 5.7 Hz, 1H), 1.18 (s, 3H). <sup>13</sup>C NMR (126 MHz, CDCl<sub>3</sub>) δ 159.5, 137.9, 130.0, 129.5, 128.6, 128.0, 128.0, 114.0, 75.4, 74.1, 73.7, 73.4, 73.3, 71.3, 55.4, 20.8. HRMS (ESI): calcd for C<sub>20</sub>H<sub>24</sub>O<sub>4</sub> [M+H]<sup>+</sup> 346.1780, found 346.1814.

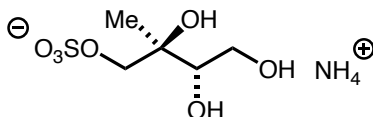
**Compound II-42**

Anti diol **II-41** (0.8 g, 2.31 mmol) was diluted in DCM (10 mL) and stirred under N<sub>2</sub>. MgSO<sub>4</sub> (0.39 g, 3.23 mmol) was added to the reaction, followed by benzaldehyde (0.3 mL, 2.77 mmol). pTsOH H<sub>2</sub>O (0.01 g, 0.046 mmol) was added to the reaction, and the reaction was allowed to stir for 19 hours. The reaction was quenched with saturated NaHCO<sub>3</sub> and diluted with DCM. The mixture was transferred to a separatory funnel. The organic phase was collected and the aqueous phase was extracted 3x20 mL DCM. Combined organics were dried with MgSO<sub>4</sub> and concentrated under reduced pressure. Column flash chromatography on silica gel (200 mL 10% EtOAc in hexanes) afforded the desired benzylidene as a collection of diastereomers. The benzylidene carried forward without purification was diluted in DCM (7.6 mL) and H<sub>2</sub>O (1.1 mL) and stirred under N<sub>2</sub> at 0° C. DDQ (0.21 g, 0.92 mmol) added to the reaction, and the reaction was allowed to stir at 0° C for 2 hours. The reaction was quenched with saturated NaHCO<sub>3</sub> and diluted with DCM. The mixture was transferred to a separatory funnel. The organic phase was collected and the aqueous phase was extracted 3x20 mL DCM. Combined organics were dried with MgSO<sub>4</sub> and concentrated under reduced pressure. Column flash chromatography on silica gel (400 mL 15% EtOAc in hexanes) yielded alcohol **II-42** as a light brown oil (0.25 mg, 0.78 mmol, 70% yield) as an inseparable mixture of diastereomers.

## Compound II-31



Alcohol diastereomers **II-42** (1.1 g, 3.4 mmol) was dissolved in distilled pyridine (9 mL) and stirred under N<sub>2</sub>. Sulfur trioxide pyridine complex (0.99 g, 3.9 mmol) was added to the reaction portion-wise over 3 minutes. The reaction was allowed to stir for 14 hours. The reaction was then concentrated under reduced pressure for 24 hours. The crude material containing the pyridinium salt was then dissolved in stock 30% NH<sub>4</sub>OH (90 mL) and stirred under N<sub>2</sub> for four hours. The crude reaction was concentrated under reduced pressure and was then left in vacuo for 16 hours (vacuum ~ 5 torr) to afford the sulfate ester ammonium salt without purification. The crude material was then dissolved in MeOH (35 mL) and stirred under N<sub>2</sub>. 10% Pd/C was added to the reaction. H<sub>2</sub> gas was then bubbled through reaction for 15 minutes. The reaction was then fitted with a fresh atmosphere of H<sub>2</sub> and the reaction was allowed to stir under H<sub>2</sub> for 18 hours. The reaction was then filtered through a pad of celite and eluted with 50 mL MeOH. Concentration under reduced pressure afforded sulfate ester **II-31** (0.51 g, 2.4 mmol, 51% yield) without purification. IR (neat): 3401, 3280, 2999, 1402, 1200, 1120, 994 cm<sup>-1</sup>. <sup>1</sup>H NMR (500 MHz, Deuterium Oxide) δ 4.20 (dd, *J* = 10.7, 2.9 Hz, 1H), 3.95 (dd, *J* = 10.7, 8.2 Hz, 1H), 3.82 (dd, *J* = 8.1, 2.8 Hz, 1H), 3.55 – 3.44 (m, 2H), 1.11 (s, 3H). <sup>13</sup>C NMR (126 MHz, D<sub>2</sub>O) δ 74.0, 72.7, 69.2, 66.0, 19.2. HRMS (ESI): calcd for C<sub>5</sub>H<sub>11</sub>O<sub>7</sub>S [M–NH<sub>4</sub>]<sup>-</sup> 215.0231, found 215.0241.

**Compound II-31**

Alcohol diastereomers **II-45** (1.8 g, 5.5 mmol) was dissolved in distilled pyridine (9 mL) and stirred under N<sub>2</sub>. Sulfur trioxide pyridine complex (1.61 g, 6.4 mmol) was added to the reaction portion-wise over 3 minutes. The reaction was allowed to stir for 14 hours. The reaction was then concentrated under reduced pressure for 24 hours. The crude material containing the pyridinium salt was then dissolved in stock 30% NH<sub>4</sub>OH (138 mL) and stirred under N<sub>2</sub> for four hours. The crude reaction was concentrated under reduced pressure and was then left in vacuo for 16 hours (vacuum ~ 5 torr) to afford the sulfate ester ammonium salt without purification. The crude material was then dissolved in MeOH (55 mL) and stirred under N<sub>2</sub>. 10% Pd/C was added to the reaction. H<sub>2</sub> gas was then bubbled through reaction for 15 minutes. The reaction was then fitted with a fresh atmosphere of H<sub>2</sub> and the reaction was allowed to stir under H<sub>2</sub> for 18 hours. The reaction was then filtered through a pad of celite and eluted with 100 mL MeOH. Concentration under reduced pressure afforded sulfate ester **II-31** (0.70 g, 3.0 mmol, 55% yield) without purification.

IR (neat): 3391, 3106, 3020, 1450, 1195, 980, 808 cm<sup>-1</sup>; <sup>1</sup>H NMR (500 MHz, Deuterium Oxide) δ 4.20 (d, *J* = 12.6 Hz, 1H), 3.74 – 3.66 (m, 3H), 3.48 (t, *J* = 8.7 Hz, 1H), 3.20 (dd, *J* = 12.1, 8.6 Hz, 1H), 1.21 (s, 3H).; <sup>13</sup>C NMR (125 MHz, Chloroform-*d*) δ 75.6, 73.3, 71.8, 63.7, 20.0; HRMS (ESI): calcd for C<sub>5</sub>H<sub>11</sub>O<sub>7</sub>S [M-NH<sub>4</sub>]<sup>-</sup> 215.0231, found 215.0209.

### **Chapter 3**

#### Evaluation of Stability and Acidity of IEPOX-Derived Organosulfates

**Portions of this chapter appear in the following manuscript:**

Varelas, J. G., Vega, M. V., Geiger, F. M., Thomson, R. J. “Synthesis and Characterization of IEPOX-Derived Organosulfates”, **2021**, *In Preparation*.

### 3.1 Inherent Acidity of IEPOX-derived Organosulfates

In chapter 2, a synthetic methodology used to access the eight possible IEPOX-derived organosulfates shown in **Figure 3.1** was described. This methodology allowed for the generation of all stereochemical and regiochemical isomers of this family of compounds as the appropriate ammonium salts postulated in the literature. Access to all relevant IEPOX-derived sulfate esters in pure form allows for measurements of their inherent chemical properties to provide meaningful insight concerning the potential impact of these molecules within the atmosphere. Preliminary findings concerning the chemical and physical properties of the IEPOX-derived sulfates will be presented in this chapter, beginning with the evaluation of inherent acidity of each compound. The following chapter then details some further collaborative investigations probing the role organosulfates might play in atmospheric processes, like particle uptake and growth.

As described in section 1.3.1, the general formation of sulfate esters derived from IEPOX is suggested to occur by acid-catalyzed uptake of *trans*- $\beta$ -IEPOX in the gas-phase through protonation of the internal epoxide, with the acidified epoxide susceptible to a myriad of aqueous-phase chemical transformations, including the nucleophilic attack of sulfate anion to generate the corresponding organosulfates.<sup>39, 49</sup> The acidity of the condensed particle is of obvious importance to the formation of IEPOX-derived organosulfates, as acidic sulfate is necessary to generate any compounds bearing sulfate ester functionality. Further, it has been shown in numerous laboratory and field studies that acidic species within atmospheric aerosols significantly enhance the rate and extent of SOA formation through processes such as increased uptake of gas-phase compounds into the condensed aerosol phase.<sup>19, 65, 114</sup> Therefore, the pH of atmospheric aerosols as a whole, as well as the acidity of the constituents within the particle phase, is an important factor in

determining the chemical properties of SOA. Accurate determination of pH of atmospheric organic aerosols is, however, a challenging endeavor due to the plethora of factors governing acidity, such as the acidity of each organic constituent within the particle phase as well as the presence of inorganic species in the condensed phase.

Organosulfates as a general class of compounds possess inherent acidity being derivatives of sulfuric acid or ammonium sulfate. Focusing specifically on the generation of sulfate esters derived from isoprene, the interaction between *trans*- $\beta$ -IEPOX and acidic sulfate seed aerosol generates IEPOX-derived organosulfates, which likely contribute substantially to overall acidity of the condensed phase particle. However, pH values of sulfate esters have been shown to vary substantially as a consequence of the degree of substitution of the parent alcohol, the overall structural features of the larger molecule, as well as the presence of the sulfate ester as either the free acid or as a salt associated with a positively charged counterion.<sup>139-141</sup> Therefore, assumptions in previously disclosed studies have suggested the IEPOX-derived family of organosulfates would demonstrate different pH values as a consequence of regiochemical and stereochemical differences between the compounds shown in **Figure 3.1**, but a historical lack of standards of all relevant compounds has made measuring acidity of these compounds impossible.

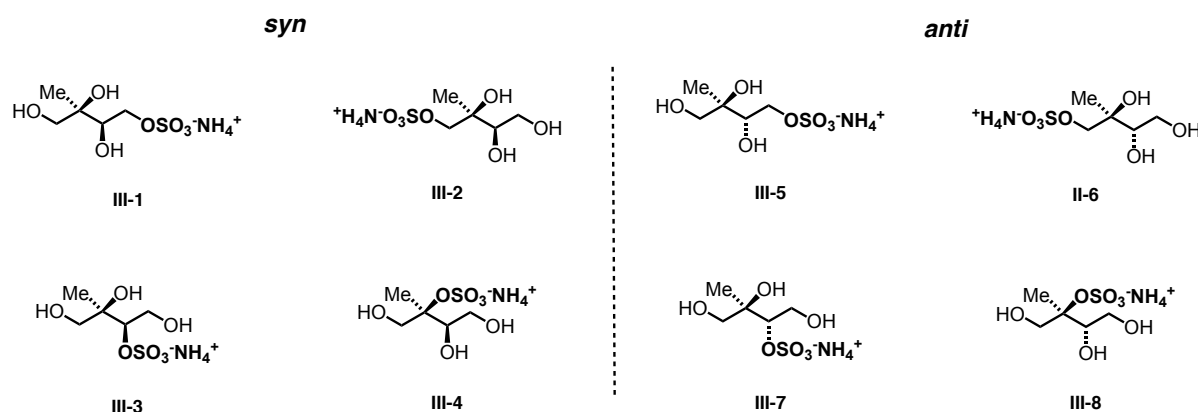


**Figure 3.1** The suite of IEPOX-derived organosulfates prepared as ammonium salts.

### 3.1.1 Measurement of pH values for IEPOX-derived Organosulfate Compounds

With the newly synthesized library of IEPOX-derived organosulfates in hand, pH values corresponding to each compound were measured to determine any differences in acidity across the different isomers. Individual 0.1 M solutions of each organosulfate were prepared by dissolving the pure compound in deionized (di) water, as each sulfate being prepared as a 0.1 M solution in D<sub>2</sub>O. The deuterium oxide solutions were not only used to evaluate pD – the equivalent value of pH applied to systems in which the protic species lies within a deuterated medium – but were also used as samples for NMR analysis of each sulfate, which will be expanded upon in section 3.2.

The measured pH and pD values for all IEPOX-derived sulfates, as well as the parent *syn* and *anti* tetraols **III-9** and **III-10** respectively, are summarized in **Table 3.1**. Measurements for each solution were conducted in triplicate, and the pH probe was calibrated using pH 4.0, 7.0 and 10.0 reference buffer solutions between each measurement to ensure accuracy and reproducibility. These results are demonstrated pictorially in **Figure 3.2**. When looking at the data set of measured pH values of the organosulfates, several conclusions can be made concerning the chemical

properties of the collection of compounds. For one, as expected, the sulfated species **III-1–8** are significantly more acidic than the respective tetraols. The organosulfate species were also more acidic than ammonium sulfate itself with pH 5.5.

The comparison of pH values measured for each organosulfate compound resulted in the realization of an interesting trend in acidity as a consequence of the location of the sulfate ester functional group along the tetraol backbone. The *syn* and *anti* primary organosulfates **III-1**, **III-2**, **III-5**, and **III-6** all demonstrated relatively correlative pH readings, centering on pH 3.0-3.1. This demonstrated the notion that acidity of the organosulfates was not significantly affected by relative *syn* or *anti* stereochemistry. However, the sterically congested *syn* and *anti* secondary sulfates **III-3** and **III-7** were found to be more acidic than all the primary isomers, with the *syn* and *anti* species measuring pH values of 2.5 and 2.4, respectively. Another increase in acidity was demonstrated when measuring solutions of *syn* and *anti* tertiary organosulfates **III-4** and **III-8**, which were found to have a pH of 2.1 and 2.0, respectively.

The results generated from the measure of the acidities of the IEPOX-derived species demonstrated that the placement of the sulfate ester functionality was the lynchpin in determining the acidity exhibited by the organosulfate compounds, with solutions of the *syn* and *anti* primary isomers displaying a higher pH (i.e., less acidic) than the more sterically congested secondary and tertiary species. A potential explanation for this structurally dependent decrease in pH would be the propensity of each compound to engage in hydrogen bonding. In the case of the primary isomers, it is possible that the optimal conformation for these isomers causes the orientation of the sulfate functional group to be far from the other adjacent hydroxyl substituents, decreasing the ability of the sulfate ester to participate in intramolecular hydrogen bonding. In the case of the secondary isomers, the placement of the moiety on the internal secondary hydroxyl substituent

moves the sulfate ester functionality towards the center of the molecule. This would theoretically result in a lower spatial and energetic barrier to hydrogen bonding with the other pendant hydroxyl groups. The increase in acidity demonstrated by the tertiary organosulfates is concordant with this notion, as the given sulfate ester functional group bound to the tertiary hydroxyl would likely have spatial constrictions that would facilitate interaction with adjacent substituents and, consequently facilitate hydrogen bonding that would make the molecule in question more acidic. This general hypothesis concerning the varying acidities of the IEPOX-derived organosulfates is summarized **Figure 3.3**. Since the *tertiary* isomers are thought to be the most abundant sulfate esters derived from IEPOX, it is interesting that our findings indicate that as the appropriate ammonium salt, these isomers also exhibit the lowest pH solutions.

In summary, the acidities of the IEPOX-derived organosulfates **III-1-8** (as ammonium salts) were quantitatively determined using pH and pD measurements. We offer the explanation of the observed trend of acidity to the interplay of regiochemical position of the sulfate ester functional group and its corresponding tendency to hydrogen bond, with the more hindered organosulfates interacting with adjacent hydroxyl substituents and thus demonstrating lower pH. To elaborate on this proposed hypothesis, future work could entail computational chemistry to determine the optimal molecular geometries for each organosulfate compound to model the extent of intramolecular hydrogen bonding. Further, the reactivity and chemical properties of sulfate esters can vary due to the positively-charged counterion associated with the sulfate functional group, as demonstrated in several reported studies.<sup>142-143</sup> Along these lines, the IEPOX-derived series of organosulfates could be prepared as salts with other cations, such as sodium, potassium, or even as the free protic acid. The pH values of these salts could then be measured and compared

to those of the environmentally-relevant ammonium salts detailed above, providing useful information concerning the variable acidities of this family of sulfates.

**Table 3.1** pH and pD measurements of the suite of IEPOX-derived organosulfates **III-1,2,...,8**, and the parent *syn* and *anti* tetraols **III-9** and **III-10** respectively. All measurements done in triplicate. Ambient temperature for all measurements was 20.3 °C.

Compound Number	Compound Structure	pH Measurements (0.1 M solution in di H <sub>2</sub> O)			Average pH Value	pD Measurements (0.1 M solution in D <sub>2</sub> O)			Average pD Value
<b>III-1</b>		3.01	3.10	2.90	3.00	3.29	3.22	3.24	3.25
<b>III-2</b>		3.11	3.03	3.01	3.05	3.23	3.22	3.19	3.21
<b>III-3</b>		2.56	2.49	2.40	2.48	2.85	2.89	2.80	2.85
<b>III-4</b>		2.20	2.09	2.10	2.13	2.47	2.48	2.40	2.45
<b>III-5</b>		3.19	3.10	3.06	3.12	3.24	3.30	3.28	3.27
<b>III-6</b>		3.20	3.00	3.00	3.07	3.14	3.26	3.16	3.19
<b>III-7</b>		2.30	2.63	2.40	2.44	2.61	2.63	2.58	2.61
<b>III-8</b>		2.00	1.92	2.14	2.02	2.30	2.31	2.37	2.33
<b>III-9</b>		6.69	6.64	6.67	6.67	7.07	7.10	7.12	7.10
<b>III-10</b>		6.63	6.61	6.61	6.62	6.90	7.20	7.10	7.07

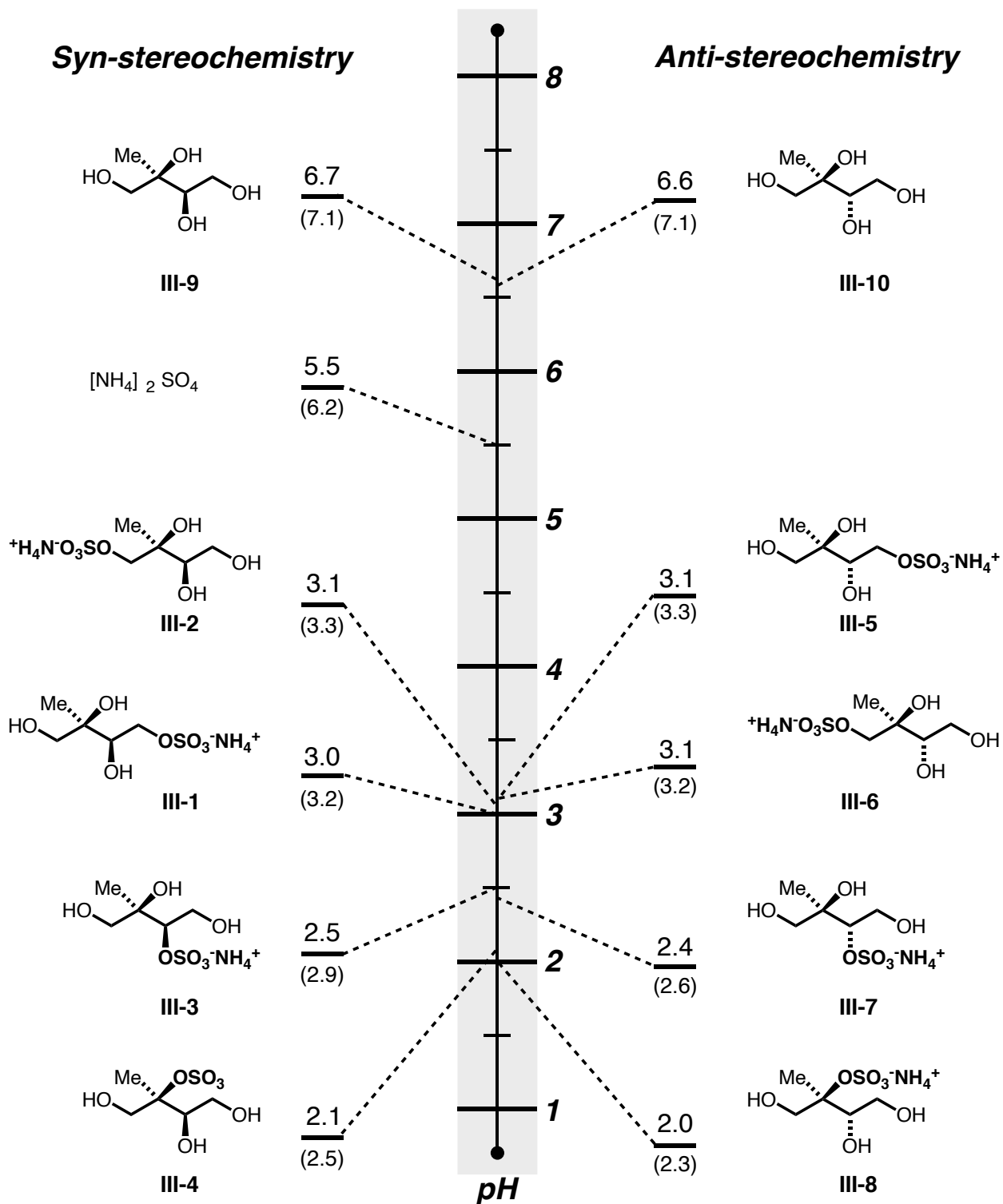


**Figure 3.2** Pictorial representation of pH and pD values measured for the suite of IEPOX-derived organosulfates and the parent tetraols. pD values are listed in parentheses under pH values. Data taken from **Table 3.1**.

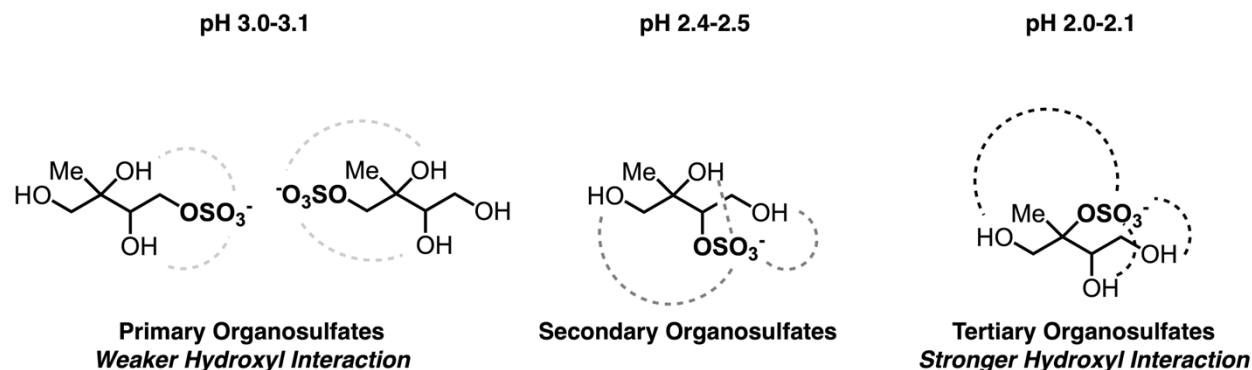


**Figure 3.3** Rationalization of the observed trend of acidity shown by the IEPOX-derived organosulfates through differing degrees of intramolecular hydroxyl interactions between the primary, secondary and tertiary isomers.

### 3.2 Stability of IEPOX-derived Organosulfates

With the pH values of the IEPOX-derived organosulfates measured and a general trend of acidity across the compounds established, we sought to evaluate the stability of each of the compounds in aqueous solution. Within the literature, organosulfates have been shown to undergo various pathways of reactivity once formed in the condensed phase of aerosol.<sup>67, 114, 144-147</sup> In 2001, Elrod and coworkers published two groundbreaking studies in which organosulfates and organonitrates derived from isoprene were studied to better characterize their formation mechanisms, inherent stability and potential chemical byproducts as a result of their decomposition and hydrolysis.<sup>145, 147</sup> Transient organosulfates and nitrates were formed *in situ* through the reaction between isoprene epoxydiols and acidic media, and the formation of various species were monitored and tracked using NMR spectroscopy. Looking specifically at the relevant organosulfates, the researchers found that the degree of substitution of the sulfate ester functional

group resulted in disparate lifetimes concerning the hydrolysis of these species, with the primary organosulfates exhibiting long lifetimes and the secondary and tertiary species vulnerable to hydrolysis in aqueous conditions. These findings resulted in the conclusion that the isomeric organosulfates derived from IEPOX will likely display different lifetimes and propensities to undergo hydrolysis in the condensed phase of SOA. However, these studies maintained a limited analytical scope, suggesting the dominant chemical byproduct of hydrolysis or decomposition of these species to be the parent tetraol compound. Further, a lack of available chemical standards precluded efficient comparison to signals detected via NMR spectroscopy.

Due to the suggested variances in hydrolytic stability, the isoprene-derived organosulfates are likely to generate different byproducts through reactions with different atmospheric constituents dependent on the regiochemical isomer in question. **Figure 3.4** shows a representation of the hydrolysis and decomposition of the tertiary IEPOX-derived organosulfate generating a plethora of chemical species such as simple hydrolysis to generate the corresponding 2-methyltetraol, elimination to form various triols or formation of hemiacetals. Moreover, although the tertiary organosulfate is hypothesized to be the most dominant of the species derived from IEPOX, the potential of the sulfate ester functionality to be bonded to any of the hydroxyl groups along the tetraol scaffold in **Figure 3.1** makes both the determination of atmospheric lifetimes and characterization of byproducts of these species challenging to study. To this end, we sought to use our library of IEPOX-derived organosulfates to study the lifetime of each compound, as well as visualize any byproducts of their aqueous phase reactions.

### 3.2.1 Time-Point NMR Spectra of IEPOX-derived Organosulfates

To monitor the stability of each compound, the synthetic organosulfates were prepared as 0.1 M solutions in deuterium oxide as well as 0.1 M solutions in  $d_2$ -sulfuric acid ( $D_2SO_4$ ). The solutions were monitored by NMR spectroscopy at both hourly and daily time intervals dependent on the visibility of spectral changes or decomposition. The results of the time-point NMR studies for each compound are summarized in **Table 3.2**. As expected in case of the primary organosulfates, both the *syn* and *anti* species (**III-1**, **III-2**, **III-5** and **III-6**) were stable under neutral aqueous conditions for upwards of six months. Even when dissolved in  $d_2$ -sulfuric acid, the NMR spectra of the primary compounds remained unchanged. This observed resistance to decomposition or hydrolysis likely stems from the slow rate of ionization of the primary carbon atom bound to the sulfate ester moiety, resulting in slower first-order nucleophilic substitution with aqueous species. Surprisingly, the secondary isomers **III-3** and **III-7** were also stable to both neutral and acidic conditions. Although these compounds are highly stable, their prevalence in the atmosphere is likely minimal due to the proposed epoxide opening mechanism, in which *trans*- $\beta$ -IEPOX is protonated at the oxiryl oxygen, from which the intermediate could be subject to nucleophilic substitution.<sup>39, 65</sup> As has been suggested countless times in the literature, though attack at both the 2 and 3 position of the erythritol backbone is possible, the tertiary isomer is likely formed predominantly due to the more stable tertiary carbocation after the opening of the epoxide.

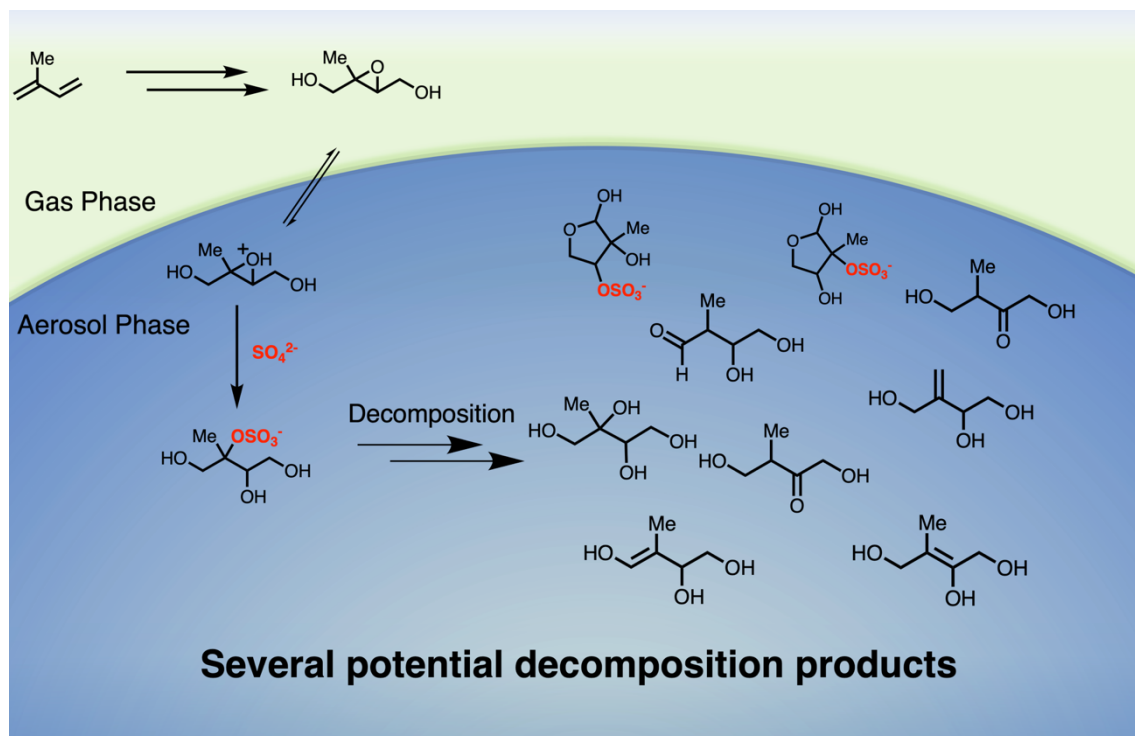


**Figure 3.4** Representation of the formation of the IEPOX-derived organosulfates from acidic uptake of *trans*- $\beta$ -IEPOX and subsequent attack of sulfate, and several chemical byproducts of decomposition of the IEPOX-derived species.

**Table 3.2** Summary of observed lifetimes of the suite of IEPOX-derived organosulfates via time-point NMR under aqueous and acidic conditions.

	<b>Syn-stereochemistry</b>		<b>Anti-stereochemistry</b>	
	<b>III-4</b>	<b>III-3</b>	<b>III-8</b>	<b>III-7</b>
<b>stability (days)</b>				
0.1 M D <sub>2</sub> O	30 (decomp)	> 60	30 (decomp)	> 60
0.1 M D <sub>2</sub> SO <sub>4</sub>	10 (decomp)	> 60	12 (decomp)	> 60
	<b>III-1</b>	<b>III-2</b>	<b>III-5</b>	<b>III-6</b>
<b>stability (days)</b>				
0.1 M D <sub>2</sub> O	> 180	> 180	> 180	> 180
0.1 M D <sub>2</sub> SO <sub>4</sub>	> 180	> 180	> 180	> 180

In the case of the tertiary organosulfates (**III-4** and **III-8**), compound stability was evaluated by monitoring the disappearance of the 3.63 ppm chemical shift of the methylene adjacent to the sulfate ester moiety. Under neutral conditions at 0.1 M in D<sub>2</sub>O, both compounds appear to be stable for approximately 28 days, shown in the NMR spectrum of **III-4** displayed in **Figure 3.5**, which coincides with studies performed by Elrod and coworkers.<sup>145, 147-148</sup> Under acidic conditions (0.1 M *d*<sub>2</sub>-sulfuric acid), our results indicate that the rate of decomposition is accelerated, as depression of the methylene signal completely disappears in approximately 10 days. In both cases, the spectra appear to be similar. It has been suggested that the decomposition of the tertiary organosulfate likely proceeds with hydrolysis of the sulfate ester group, forming the parent tetraol after substitution.<sup>145, 148</sup> However, the decomposition spectra of both tertiary species in neutral and acidic media do not match the spectra of the *syn* or *anti* 2-methyltetraols. When under vacuum, however, the NMR spectra after three days perfectly match that of the tetraol as shown in the spectrum for the *syn* tertiary organosulfate **III-4** depicted in **Figure 3.6**. These observations suggest that decomposition proceeds via different pathways when comparing *in vacuo* and aqueous conditions. Though this was a result found in laboratory conditions using a vacuum pump, this discrepancy of decomposition may have atmospheric implications, as the lower pressure in the troposphere where atmospheric organosulfates are formed predominantly could facilitate formation of the parent tetraol in addition to reactions in the condensed phase of SOA.

In the case of the *anti* tertiary organosulfate **III-8**, decomposition generated numerous products able to be visualized within the NMR spectra. However, unlike the *syn* species, the *anti* isomer appears to generate a characteristic aldehyde signal at  $\delta$  9.28 ppm, shown in **Figure 3.7**. We hypothesize that this species is the resultant product after ionization of the sulfate ester moiety

followed by a 1,2-hydride shift from the adjacent methylene group, forming aldehyde **III-11**. The propensity of sterically congested sulfate esters to labilize could lead to the generation of this compound as a result of decomposition.

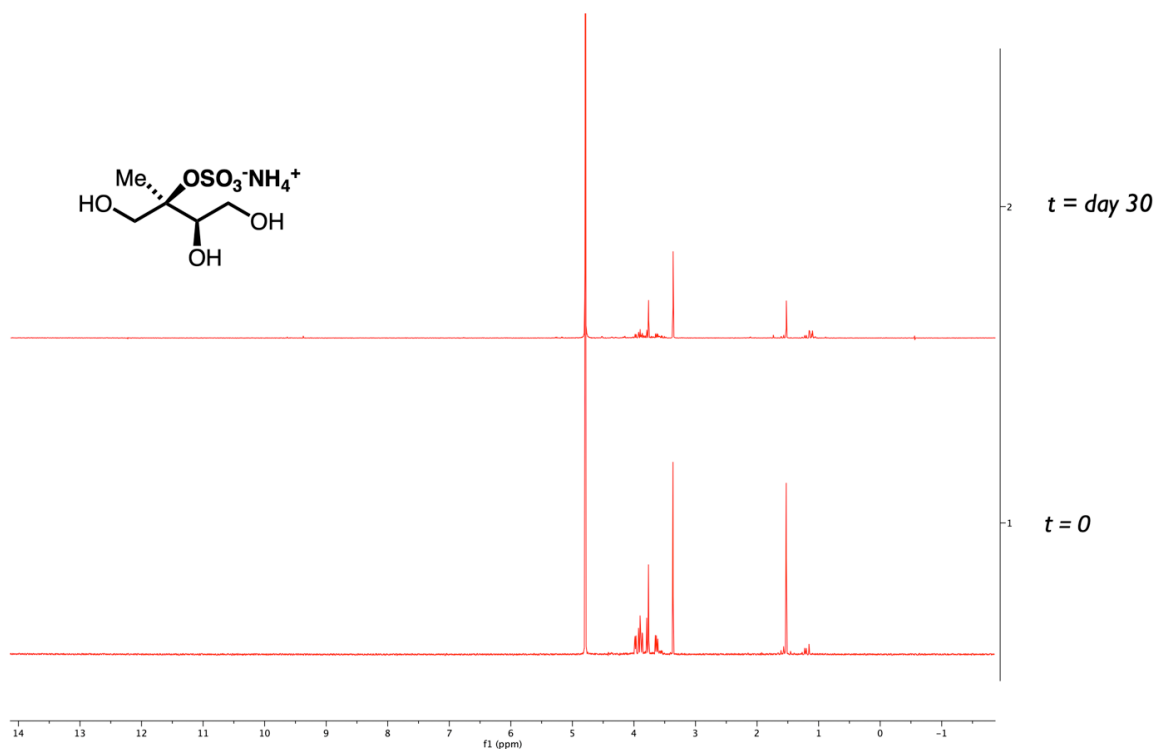


**Figure 3.5** NMR spectra of *syn* tertiary organosulfate **III-4** in D<sub>2</sub>O. Experimental duration was 30 days, with the bottom spectrum taken at day 0 and the top taken at day 30. Both spectra are normalized to the signal intensity of the deuterium oxide peak at 4.79 ppm. Disappearance of the methylene signal at 3.63 ppm was used as the baseline for decomposition.

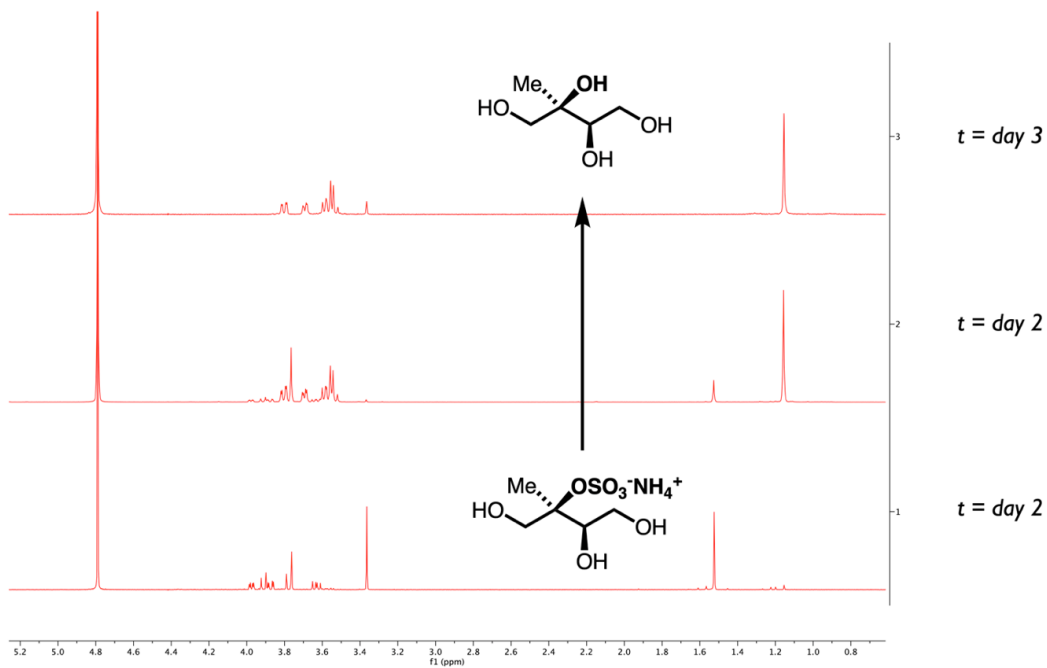


**Figure 3.6** Spectra of *syn* tertiary sulfate **III-3** and decomposition to the corresponding 2-methyltetraol held *in vacuo* using a laboratory-grade pump.

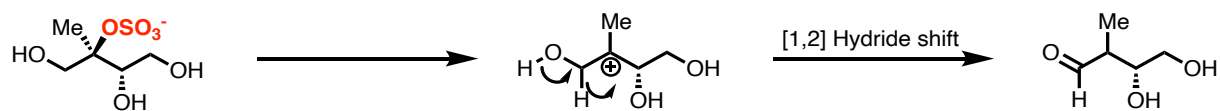
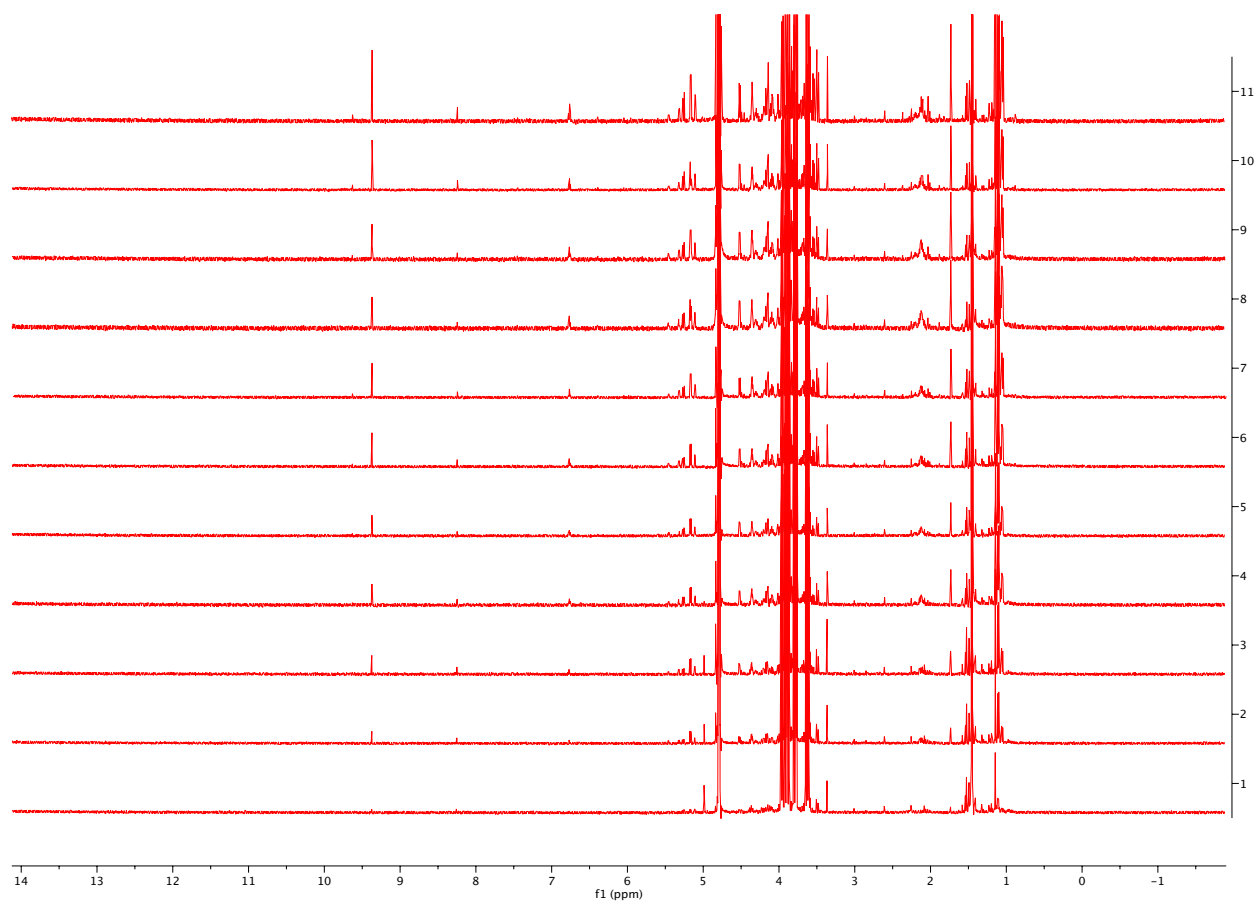
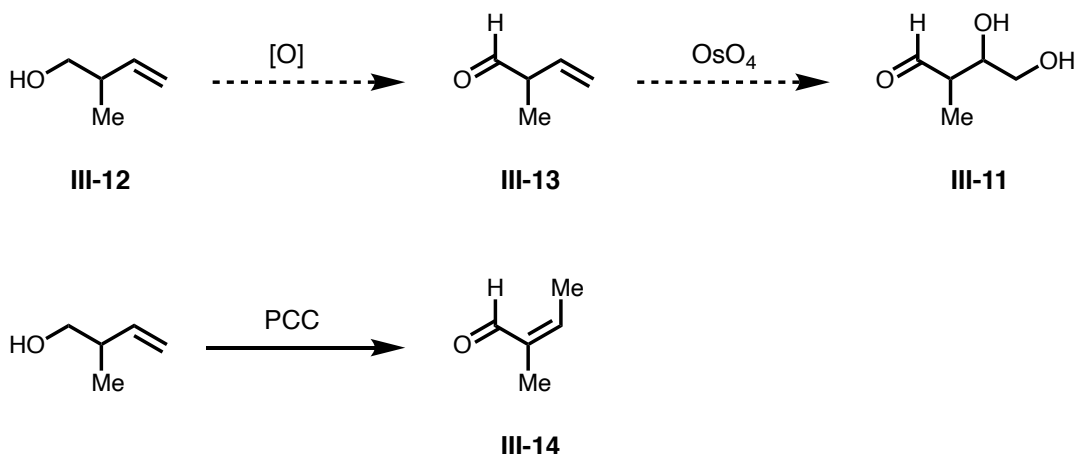


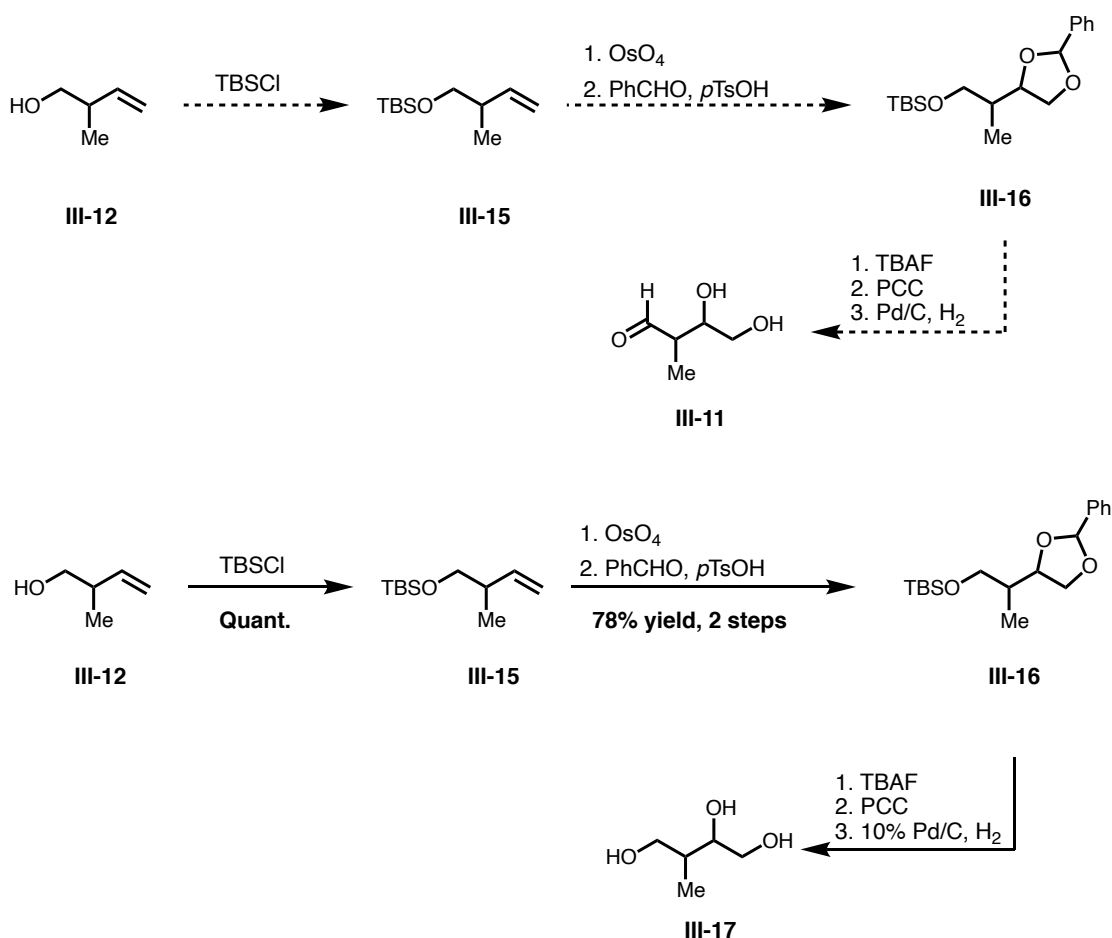
**Figure 3.7** NMR spectra of *anti* tertiary organosulfate **III-8** in D<sub>2</sub>O and the hypothesized chemical transformation leading to the signal formed in at  $\delta$  9.24 ppm.

### 3.2.2 Efforts to Synthesize Hypothesized Decomposition Product III-11

Given the presence of the characteristic aldehyde peak in the NMR spectra of **III-8**, our attention then turned to potential synthetic routes to access **III-11** in order to confirm its presence as a byproduct of decomposition. Our first idea shown in **Scheme 3.1** was to simply oxidize commercially-available 2-methylbut-3-en-1-ol **III-12** to the corresponding aldehyde **III-13**, then a simple OsO<sub>4</sub>-mediated dihydroxylation of the pendant olefin would give aldehyde **III-11**. However, oxidation of **III-12** using PCC to furnish the aldehyde resulted in isomerization to the undesired enone **III-14**. Given this unwanted result, we decided to attempt a more exhaustive strategy to access **III-11** that avoided potential side product formation.



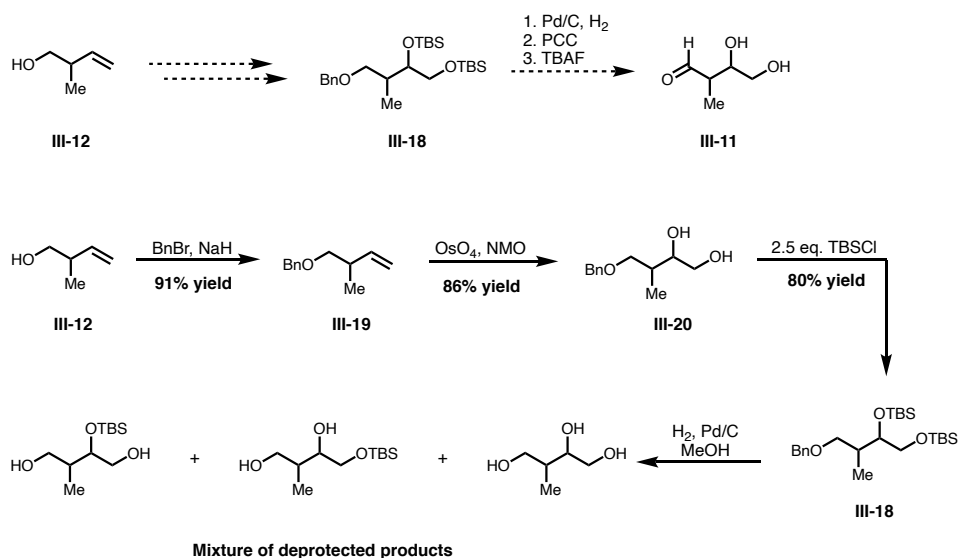
**Scheme 3.1** Initial synthetic route to access aldehyde **III-11**.



**Scheme 3.2** A revised synthetic route towards **III-11** utilizing various protecting groups.

Reforming our strategy, our intended route in **Scheme 3.2** was to begin with the same butenol **III-12** as earlier and protecting the free hydroxyl group as the silyl-protected olefin **III-15**. From here, we envisioned treatment with  $\text{OsO}_4$  followed by benzylidene protection of the vicinal diol with  $\text{PhCHO}$  and  $p\text{TsOH}$  would form **III-16** with all hydroxyl groups masked with protecting groups. Deprotection of the silyl group using TBAF, subsequent oxidation to the aldehyde using PCC and final hydrogenolysis would then afford **III-11**. This strategy in practice resulted in facile conversion in the first three steps. However, canonical Pd/C-mediated deprotection of the benzylidene group resulted in the formation of triol **III-17**, an unfortunate and

surprising result. Faced with this problem, we decided to revise our strategy once again, using different protecting groups to shield further unwanted reactivity. A final attempt at strategy revision is depicted in **Scheme 3.3**, in which butenol **III-12** would be used to afford protected species **III-18** with a benzyl group protecting the pendant hydroxyl group and the vicinal diol would be doubly-silylated. This ideally would allow deprotection of the benzyl group using catalytic hydrogenolysis, avoiding the use of these conditions in the presence of the aldehyde. Oxidation of the resulting species to the aldehyde and desilylation using TBAF would then give aldehyde **III-11**. Benzylation of **III-12** gave protected olefin **III-19**, followed by dihydroxylation to afford diol **III-20**. Subsequent protection of the resulting diol using excess TBSCl yielded the fully-protected triol **III-18**. The use of hydrogenolysis conditions once again resulted in unwanted side product formation, as mixtures of protected and deprotected species were generated, making oxidation to the desired aldehyde impossible in the presence of multiple hydroxyl substituents. It was here that we decided to halt synthetic efforts to generate the aldehyde in question. Future work will consist of obtaining a homogenous standard of the supposed aldehyde decomposition product, definitively characterizing the observed peaks in the decomposition of the *anti* tertiary organosulfate.



**Scheme 3.3** An additional revised synthetic route towards aldehyde III-11.

In lieu of a direct comparison to a standard of the aldehyde product in question, we attempted to offer some preliminary confirmation of the presence of aldehyde **III-11** by other means. **Figure 3.8** depicts the NMR spectrum of *anti* tertiary sulfate **III-8** plotted against several simulated  $^1\text{H}$  spectra of hypothesized potential decomposition products generated by the native NMR calculation plug-in within the NMR-processing program *MestreNova*<sup>TM</sup>. Simulations were completed of the hypothesized aldehyde **III-11** as well as the corresponding enol tautomers (**III-21** for both isomers). While the spectral comparisons are speculative due to inherent error in predictive NMR modeling, we saw reasonable agreement between the experimental spectrum of **III-8** and both the simulated aldehydic proton of **III-11** and the enol proton of **III-21**. Along the same lines, **Figure 3.9** shows the comparison of the experimental  $^1\text{H}$  and  $^{13}\text{C}$  NMR spectra of **III-8**. The  $\delta$  9.28 ppm and 198.84 ppm peaks are characteristic of aldehyde functionality, which could be attributed to **III-11**. Further, the upfield  $^1\text{H}$  and  $^{13}\text{C}$  peaks at  $\delta$  6.67 ppm and 154.12 ppm bolster this notion and are likely due to tautomerization of the proposed aldehyde with the corresponding enol tautomer **III-21**.

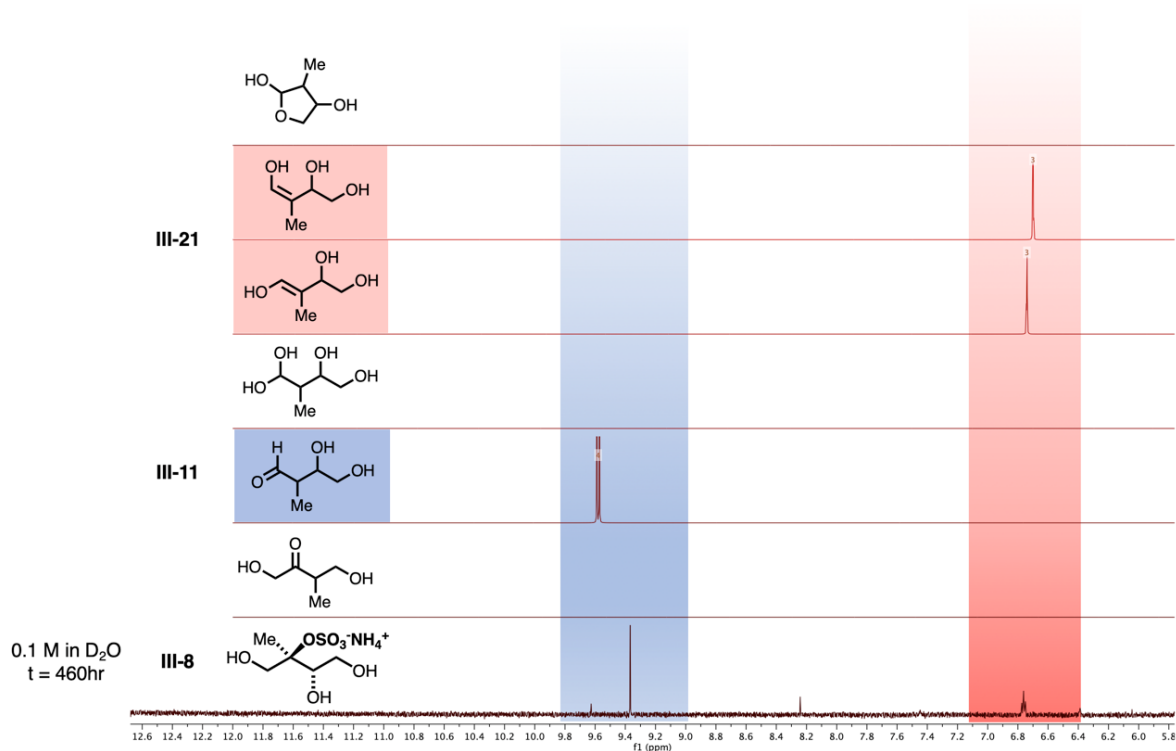


**Figure 3.8** Comparison of NMR spectrum of *anti* tertiary organosulfate **III-8** in  $\text{D}_2\text{O}$  with simulated  $^1\text{H}$  NMR spectra of several potential decomposition products, including **III-11** and its enol tautomeric forms (**III-21**). Spectra for each compound were simulated using the native NMR calculation plug-in within *MestReNova*<sup>TM</sup> NMR processing software. The confidence interval of the calculations is reported to be 95%. The relevant spectral window is shown from ~5.8 ppm – 13 ppm. The aldehydic proton of **III-11** is highlighted in blue, and the olefinic proton attributed to the enol tautomer **III-21** is highlighted in red.

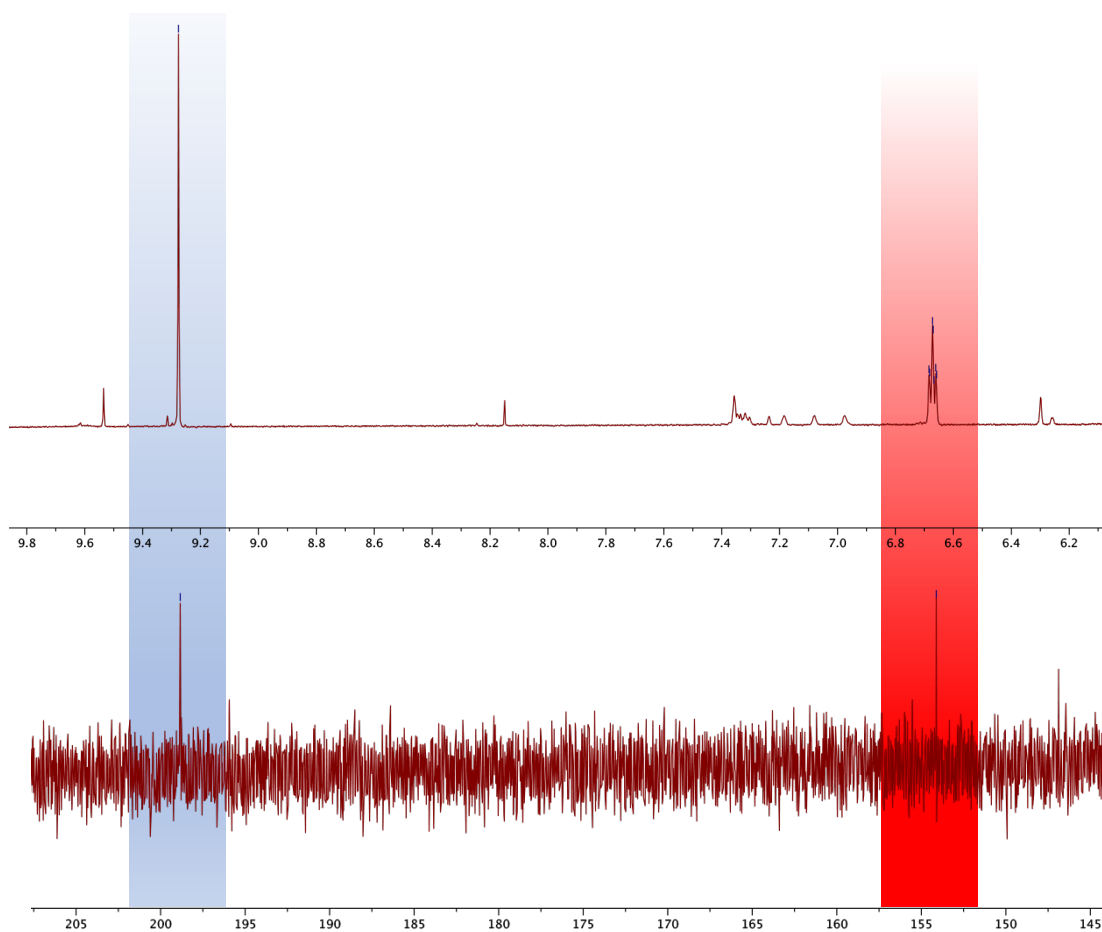
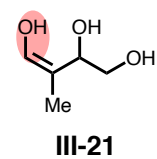
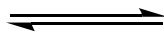
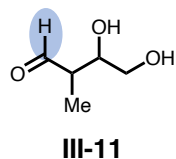
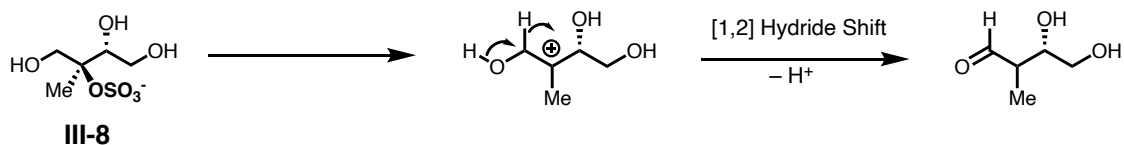


**Figure 3.9** Comparison of the <sup>1</sup>H and <sup>13</sup>C NMR spectra of *anti* tertiary organosulfate **III-8** in D<sub>2</sub>O and corresponding mechanistic explanation. The spectral windows for the proton and carbon spectra were 6.0 – 10 ppm and 145 – 205 ppm respectively. The proton and carbon spectra were taken at t = 20 days. The δ 9.28 ppm and 198.84 ppm peaks highlighted in blue are suggested to be due to **III-11**, and δ 6.67 ppm and 154.12 ppm highlighted in red due to tautomer **III-21**.

### 3.3 Conclusions

In this chapter, the acidities of the IEPOX-derived organosulfates shown in **Figure 3.1** were determined by preparing each compound as a 0.1 M solution in both di H<sub>2</sub>O and D<sub>2</sub>O and measured with a pH meter. Our findings indicate the primary isomers to be less acidic than the secondary, with the tertiary isomers demonstrating the lowest pH. We rationalized this observation through the stabilization of the conjugate base of the organosulfates with respect to the regiochemical position of the sulfate ester moiety. The primary isomers likely bear a sulfate ester group that does not interact significantly with the adjacent hydroxyl substituents along the carbon chain, while the secondary and tertiary isomers are situated in more sterically-confined areas in the molecule and thus have closer contact to the internal hydroxyl groups. Future work would ideally pertain to the accurate modeling of each compound's optimal conformation in aqueous solution to investigate any significant differences between the isomeric sulfates. Preliminary results concerning the aqueous stability of the IEPOX-derived sulfates was also presented, with time-point NMR spectra all isomers excluding the tertiary species showing resistance to hydrolysis under both aqueous and acidic conditions. The tertiary isomers were found to have different propensities of hydrolysis, with samples prepared in acidic solutions demonstrating faster degradation than those prepared with neutral D<sub>2</sub>O. The tertiary isomers also demonstrated instability when held *in vacuo*, with each converting to the respective parent tetraol. Additionally, efforts were made to characterize a potential aldehyde-containing decomposition product of the *anti* tertiary organosulfate. Although synthetic efforts to prepare this compound were unsuccessful, we offer speculative confirmation of the aldehyde by comparing <sup>1</sup>H and <sup>13</sup>C spectra, as well as comparing <sup>1</sup>H spectra with simulated spectral data. To this end, future work would

involve further efforts to access the hypothesized aldehyde for direct comparison of our experimental data to a homogenous chemical standard.

### 3.4 Experimental Information

pH and pD values for the suite of organosulfate compounds were measured using the Orion Star™ A325/Conductivity Portable Multiparameter Meter. Samples were measured under NTP conditions (ambient temperature = 20.3 °C for all measurements). Calibration curves for each sample were formed through calibration using pH 4.0, 7.0 and 10.0 standards

Time-point NMR spectra were taken using a Bruker Avance III HD system equipped with a TXO Prodigy probe for all  $^1\text{H}$  and  $^{13}\text{C}$  measurements. Parameters for each spectrum were the default instrumental settings with the number of scans increased for each nucleus ( $^1\text{H}$ , N = 1024;  $^{13}\text{C}$ , N=512).

Simulated  $^1\text{H}$  NMR spectra for studies detailed in section 3.2.2 were accomplished using *MestreNova*™ software for Macintosh (Version: 12.0.3-21384). Simulations were run using the following parameters:

- Sweep width: 10.00 – -2.00 ppm
- Number of points: 32 K
- Operating frequency: 500 MHz
- Solvent: D<sub>2</sub>O
- Spectral line width: 0.75 Hz
- Prediction entity: “MNOVA Best”

#### Chapter 4

Future Directions Regarding IEPOX-derived Organosulfates & Synthesis and Analysis of Isotopically-labelled Terpenes

**Portions of this chapter appear in the following manuscripts:**

Varelas, J. G., Vega, M. V., Geiger, F. M., Thomson, R. J. “Synthesis and Characterization of IEPOX-Derived Organosulfates”, **2021**, *In Preparation*.

Meder, M., Perakyla, O., Varelas, J. G., Cai, R., Zhang, Y., Kurten, T., Riva, M., Rissanen, M.P., Geiger, F. M., Thomson, R. J., Ehn, M. “Using Selective Deuteration to Clarify Complicated  $\alpha$ -Pinene Ozonolysis Processes Forming Highly Oxygenated Organic Molecules”, **2021**, *In Preparation*.

Xu, L., Varelas, J. G., Moller, K. H., Crouse, J. D., Kjaergaard, H. G., Geiger, F. M., Thomson, R. J., Wennberg, P. O. “Unimolecular Reactions of Peroxy Radicals Formed in the Oxidation of  $\alpha$ -Pinene by Hydroxyl Radicals”, **2021**, *In Preparation*.

## 4.1 Ongoing Work and Future Directions of IEPOX-derived Organosulfates

In Chapters 2 and 3, the synthesis of the suite of IEPOX-derived organosulfates was described and preliminary findings regarding their inherent chemical properties, such as acidity and stability, were described. It is our hope that the synthetic methodology used to access these sulfate esters will not only provide the atmospheric community with useful standards to assist in analysis of field samples, but our results concerning the stability of these structures, particularly of the *anti* tertiary organosulfate, will assist in determining the eventual fate of these compounds in the atmosphere, and will further elucidate the interaction between SOA and byproducts of anthropogenic pollution via urbanized environments. Looking beyond work described in this thesis, there are several techniques that could be used to study this series of compounds. A few of these potential applications regarding the IEPOX-derived organosulfates will be described in this section.

### 4.1.1 Surface Specific Analysis of IEPOX-derived Organosulfates – Sum Frequency Generation Spectroscopy and Pendant Drop Tensiometry

SOA constituents typically alter the surface activity of aerosol particles, as some BVOC-derived oxidation products can partition to the air-particle interface and influence macroscopic chemical properties of the condensed phase system, such as propensity to act as cloud condensation nuclei (CCN).<sup>56, 149-152</sup> Several techniques have been developed in order to examine the molecular level influence atmospheric organic compounds have on the surfaces of aerosol particles. A method that has been shown to be highly useful in studying SOA constituents and other

atmospherically-relevant organic compounds is sum frequency generation (SFG) spectroscopy. SFG spectroscopy is a nonlinear optical technique that utilizes two fields of light oscillating at different frequencies – an IR beam with a tunable frequency and a visible light beam – that are overlapped temporally and spatially.<sup>153-155</sup> This arrangement results in the generation of a light field that oscillates at the sum of the frequencies of the two aforementioned fields, as is shown pictorially in **Figure 4.1**. Because these types of second order processes are forbidden in centrosymmetric media according to the electric dipole approximation,<sup>156</sup> SFG spectroscopy is highly sensitive to surfaces and interfaces where symmetry is broken. Generally, the incident IR beam is tunable to certain frequencies in the infrared (IR) region to probe specific vibrational states of a system, while the visible beam facilitates detection of the output frequency by acting as an upconverter and provides vibrational information at a detectable wavelength.

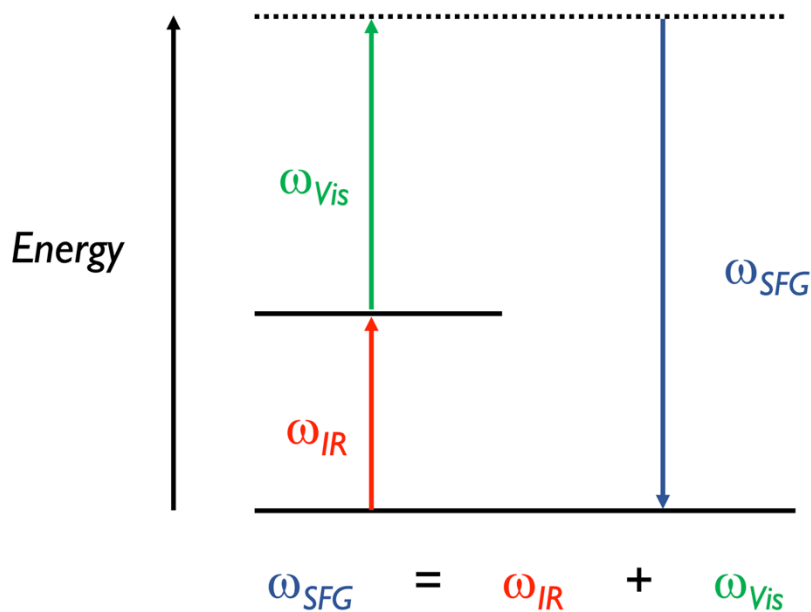


**Figure 4.1** Energy diagram depiction of SFG.  $\omega$  represents the frequency of each incident light field.  $\omega_{IR}$  represents the frequency of a tunable IR light field, and  $\omega_{Vis}$  represents a visible light field.  $\omega_{SFG}$  represents the sum frequency of the two incident light fields.

The Geiger lab at Northwestern University has successfully utilized SFG spectroscopy in a plethora of studies to investigate the chemical properties of interfaces specific to SOA constituents, and the technique has been used to provide information concerning characteristics of atmospherically-relevant systems such as molecular orientation, functional group differentiation and the probing of surface chirality.<sup>149, 157-159</sup> SFG spectra of organic aerosol particles are often less congested than those from other spectroscopies due to the inherent selectivity of detection towards surfaces, since other non-coherent spectroscopic methods produce spectra in which every oscillator contributes to the detected signal, in both the particle bulk and the surface. While its use

does not provide a complete picture of the system or interface in question, SFG is a powerful complementary technique for studying the interfaces of SOA particles.

Work in the Thomson and Geiger labs is currently underway to probe the eight isomeric IEPOX sulfates using SFG spectroscopy. While the high aqueous solubility and polarity of organosulfates likely prevents these species from being surface active, as highly polar molecules are situated within the particle bulk, the presence of these compounds in solution could have profound effects on surface properties of SOA particles which could be elucidated using SFG spectroscopy. **Figure 4.2** shows preliminary SFG spectra in the C–H stretching region of the eight relevant organosulfates taken by fellow Thomson and Geiger group member, Jana Butman. The data shown highlight clear spectral differences between each compound as a consequence of their stereochemical and regiochemical variances, in addition to significant differences when compared to the spectral features of the parent *syn* and *anti* 2-methyltetraol compounds. Intuitively, an interesting measurement for the suite of organosulfates and tetraols would be to examine the hydroxyl (O-H) region of the IR spectrum as all of the compounds are functionalized with several hydroxyl groups. Using the Tunable optical parametric amplifier set-up (TOPAS) laser in the Geiger lab, future directions will involve the measurement of the O-H and S=O stretching regions for each organosulfate, along with the parent tetraol compounds, to probe how their structural diversity affects the recorded SFG spectra.

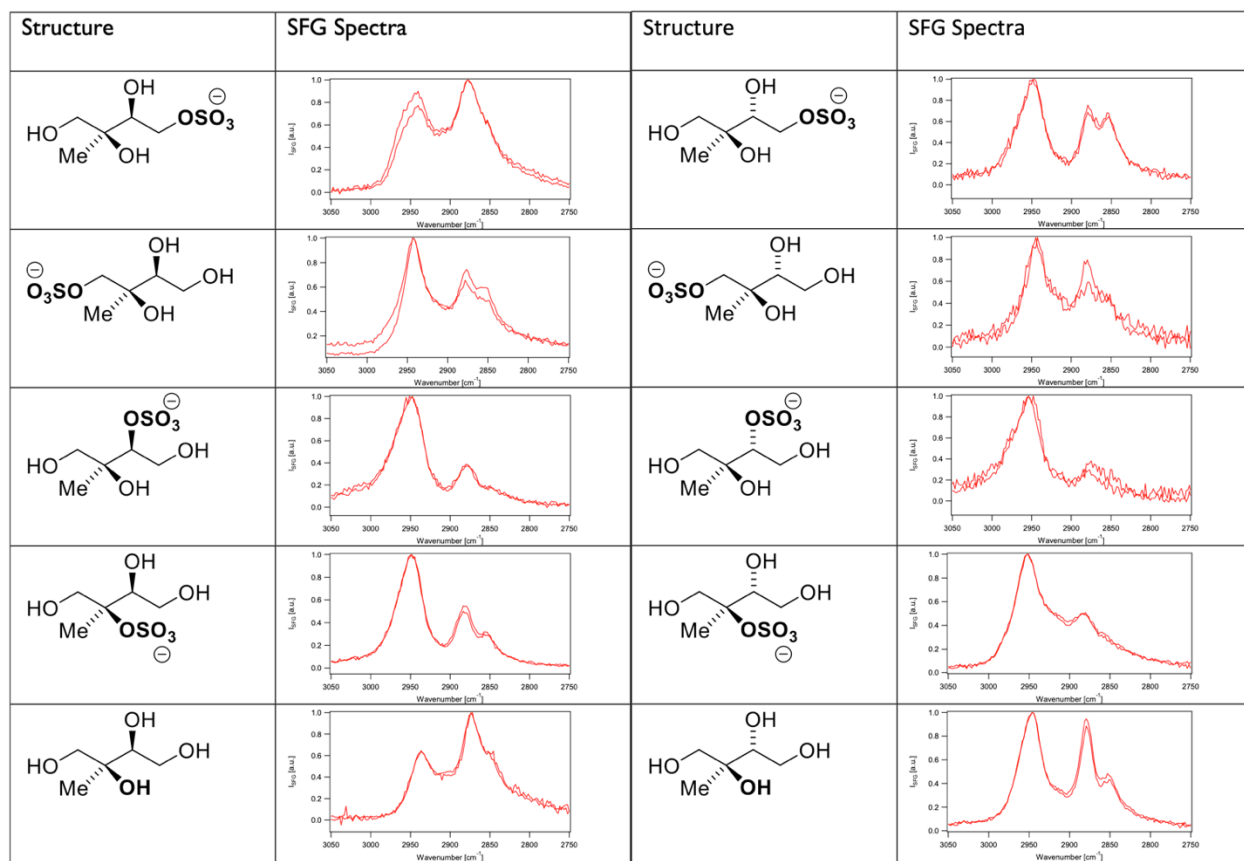


**Figure 4.2** SFG spectra of the IEPOX-derived organosulfates and the *syn* and *anti* tetraols. Each sample was spin-coated on an SiO<sub>2</sub> window and was measured in triplicate. The spectra were collected using *ssp* polarization.

In addition to the studying IEPOX-derived sulfates using spectroscopic methods such as SFG, techniques to study the behavior of this family of compounds in aqueous solution could provide valuable information concerning how organosulfates influence climate relevant properties of aerosol particles within the atmosphere. Pendant drop tensiometry (PDT) is a physical analytical technique used to determine the surface and interfacial tension of a solution. The technique consists of suspending a stagnant droplet from the bulk of a liquid sample with a syringe and measuring the perturbations of droplet geometry. In general, aqueous solutions of organic compounds are prepared at different concentrations, and the change in shape of the droplets across a series of samples is used to determine the surface activity of the molecule in solution. The apparatus used to perform these measurements is shown in **Figure 4.3**. This technique has been used successfully to probe the surface activity of atmospheric constituents throughout the literature. More specifically, the Thomson and Geiger labs have used PDT to analyze the surface activity of atmospheric oxidation products derived from terpenes such as isoprene and  $\beta$ -caryophyllene to determine climate relevant properties of these species, such as their propensity to act as cloud condensation nuclei.<sup>56, 150</sup>

As in the case with SFG spectroscopy, the polyhydroxylated IEPOX organosulfates are not likely to directly affect surface tension as substantially as SOA constituents that are known to be highly surface active, such as *trans*- $\beta$ -IEPOX, due to their hydrophilicity and high polarity.<sup>56</sup> However, these isomeric compounds could perturb solution dynamics which may be possible to discern with PDT. Further, the different isomers of the IEPOX-derived organosulfates have qualitatively exhibited differing aqueous solubilities in water as well as highly polar solvents such as DMSO as an apparent consequence of the position of the sulfate ester. PDT could allow for the

differentiation between the various organosulfate isomers, providing another piece of information concerning their chemical properties.

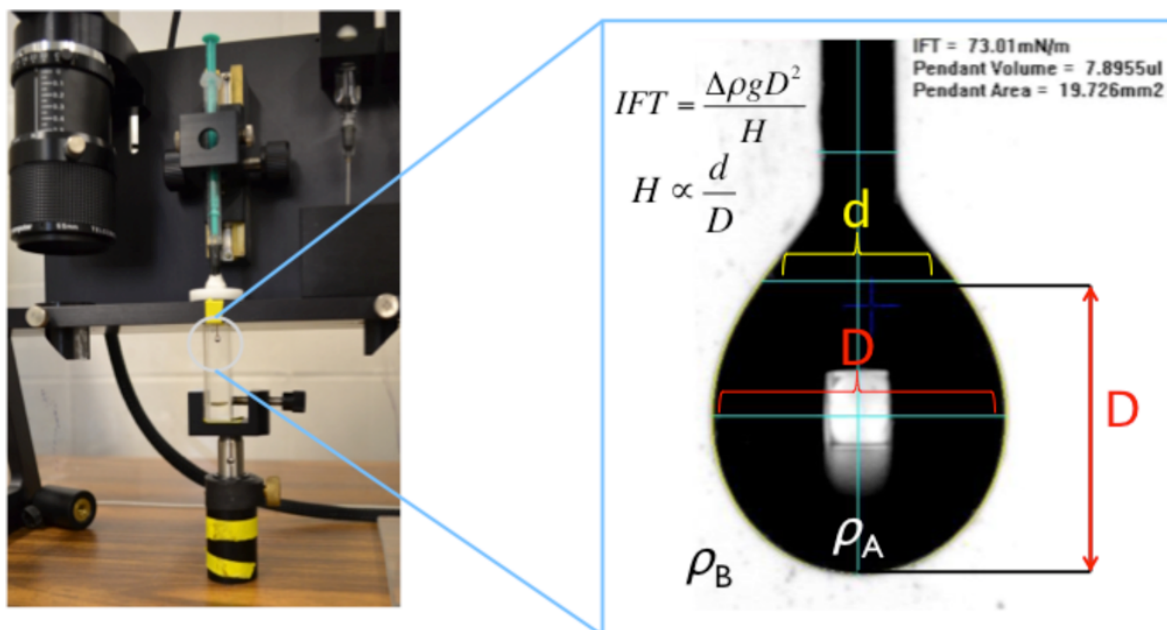


**Figure 4.3** On the left, an image of the pendant drop tensiometry instrument. On the right, an enlarged view of a pendant drop of a sample solution generated using a syringe. Figure adapted from Gray Bé et al 2017, courtesy of Dr. Ariana Gray Bé.

#### 4.1.2 Uptake of $\alpha$ -pinene-derived Semivolatile Organic Compounds by Organosulfate Particles

In addition to the experiments proposed above, access to the library of IEPOX-derived organosulfates will enable the study of these species under atmospherically-relevant conditions and may help to elucidate complex chemical processes within SOA. As discussed in chapter 1, the generation and growth of atmospheric aerosol particles are determined by a complex mix of chemical reactions and physical processes, including thermal absorption and gas-particle uptake

following atmospheric oxidation.<sup>160-161</sup> The partitioning of gas phase semivolatile organic compounds (SVOCs) into the condensed particle phase influences several properties of aerosols, including concentration of particulate matter, atmospheric processing of trace constituents, radiative scattering, and propensity to form clouds.<sup>162-163</sup> The accurate study of the processes governing gas-particle uptake of SVOCs is hampered by a number of competing factors, such as particle physicochemical properties<sup>164-165</sup> and chemical reactions within the particle phase.<sup>166-167</sup> While many laboratory studies have measured the uptake of single species such as ammonia or model organic compounds,<sup>168-169</sup> recent literature has suggested that particle-phase reactions between SVOCs can substantially increase the amount of uptake when mixtures of SVOCs are present when compared to uptake of a single organic species.<sup>167</sup> Moreover, as described earlier, uptake of organic compounds into the particle phase has been shown to be enhanced by acidic seed aerosol and acidic SOA constituents.

As described in Section 1.1, organosulfates make up a significant fraction of SOA material,<sup>39, 70, 170-171</sup> but little is known specifically about the physicochemical properties of particles containing organosulfate species predominantly. Therefore the presence of the IEPOX series of organosulfates could influence uptake of SVOCs derived from other BVOCs into the particle phase. In collaboration with Dr. Paul Ohno in the lab of Scot Martin at Harvard University, current work is underway to investigate the gas-particle uptake of SVOCs derived from  $\alpha$ -pinene by the IEPOX-derived organosulfates. In this ongoing work,  $\alpha$ -pinene-derived SVOCs are generated in the Harvard Environmental Chamber (HEC) via photooxidation of  $\alpha$ -pinene in the presence of NO. The outflow from the HEC is passed through a HEPA filter to remove the particles generated within the HEC while allowing gas-phase  $\alpha$ -pinene-derived SVOCs to remain. These SVOCs are then combined with a flow containing particles generated from through

nebulization of *anti* tertiary organosulfate **IV-1** and *syn* primary organosulfate **IV-2**. Though still ongoing, preliminary results have suggested enhanced uptake of  $\alpha$ -pinene-derived SVOCs into the particle phase in the presence of the two organosulfates. We wish to extend this analysis to all relevant IEPOX-derived sulfate isomers to probe if the uptake of SVOCs is variable between the eight different compounds.

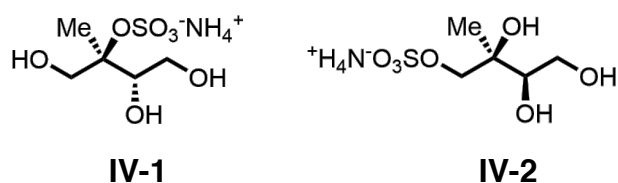


**Figure 4.4** The two organosulfates derived from IEPOX used in the study of  $\alpha$ -pinene-derived SVOC uptake in collaboration with Harvard University.

## 4.2 Synthesis of $\alpha$ -Pinene Isotopologues

In addition to the described synthesis and analysis of the series of IEPOX-derived organosulfates, work has also been done concerning the synthesis of various isotopologues of the terpene  $\alpha$ -pinene. As described earlier,  $\alpha$ -pinene is one of the most abundant sources of carbon in the atmosphere, with atmospheric emissions estimated to exceed 60 Tg yr<sup>-1</sup> and accounts for up to 34% of monoterpene emission<sup>45, 82</sup> and contributes significantly to the global SOA budget. It is therefore imperative to understand the formation mechanisms governing  $\alpha$ -pinene-derived SOA. This section will describe various ongoing domestic and international collaborations to better understand  $\alpha$ -pinene-derived SOA through the use of synthetic isotopologues.

#### 4.2.1 Using Selective Deuteration for the Investigation of $\alpha$ -Pinene-derived HOM

The oxidation of  $\alpha$ -pinene has been a fruitful area of study, and several studies disclosed in recent years have sought to probe potential reaction mechanisms. As is the case with all atmospheric terpenes, gas phase oxidation transforms BVOCs into less volatile products or SVOCs, which can partition into the condensed aerosol phase.<sup>172-173</sup> In the case of oxidation products with extremely low volatility, these compounds can even participate in the formation of new particles. Recently, some volatile have been shown to undergo autoxidation,<sup>174</sup> a series of sequential peroxy radical (RO<sub>2</sub>) hydrogen shifts and additions of molecular oxygen to the hydrocarbon chain, leading to the rapid generation of highly oxygenated organic molecules (HOM). These compounds possess several oxidized functional groups and possess very-low volatilities.<sup>175-177</sup> Recent studies have attempted to characterize the formation of HOM and measure the timespan of these fast reactions. In a publication authored by Berndt and coworkers, conversion of volatile cycloalkenes to their corresponding HOM was measured to occur on the scale of 1-2 seconds.<sup>178</sup> However, oxidation to HOM can occur even more rapidly, and autoxidation could allow HOM conversion to take place on subsecond timescales following attack via a single oxidant under natural temperature and pressure (NTP) conditions.

Due to its abundance and propensity to undergo oxidation, HOM formation from gaseous  $\alpha$ -pinene is a vital process to understand in order to accurately model relevant contributions to SOA. As stated in the introductory chapter, the atmospheric oxidation of  $\alpha$ -pinene has been extensively studied and the terpene has been shown to preferentially react with ozone (O<sub>3</sub>) over OH radical, the first steps of which are depicted in **Figure 4.5**. While it has been shown that

atmospheric oxidation of  $\alpha$ -pinene proceeds readily via ozonolysis in the presence of  $O_3$ ,<sup>10, 179-180</sup> no unambiguous reaction pathway of HOM generation from  $\alpha$ -pinene + ozone has been reported. In collaboration with the group of Prof. Mikael Ehn at University of Helsinki, work is currently underway to probe the mechanism of HOM formation from  $\alpha$ -pinene utilizing selective deuteration of the pinene skeleton via organic synthesis. **Figure 4.5** above shows the relative placement of the deuterium atoms at two sites on the carbon skeleton and their subsequent positions in the formation of various peroxy radicals. Two relevant isotopologues of  $\alpha$ -pinene shown in **Scheme 4.1** were synthesized and sent to the Ehn group to analyze using an ozonolysis flow-tube coupled to a nitrate-based chemical ionization mass spectrometer ( $NO_3$ -CIMS). The synthetic isotopologues of  $\alpha$ -pinene provide utility for the purpose of comparison of the ozonolysis of the parent terpene, monitoring the masses of the oxygenated products generated from the reaction with  $O_3$  and monitoring the potential change in reaction speed as a consequence of site-specific deuteration. The experimental apparatus created by the Ehn group for the analysis of the isotopologues is depicted and summarized in **Figure 4.6**.

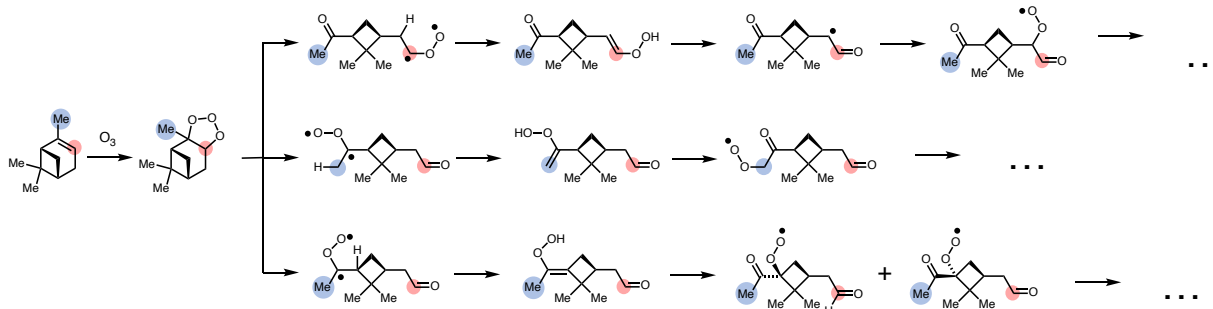
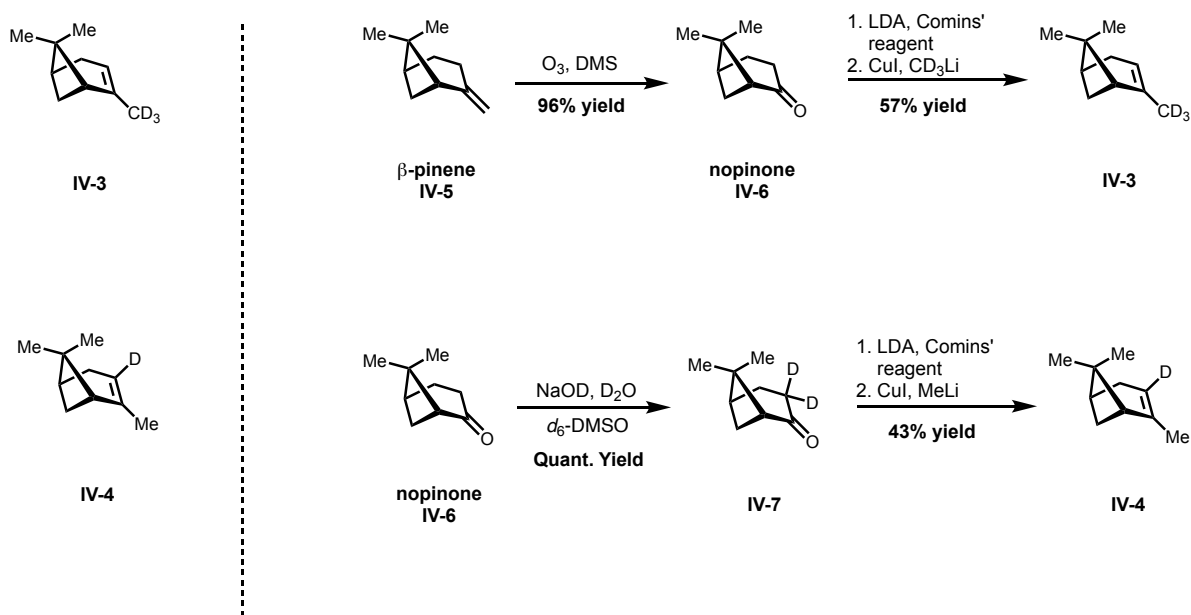


**Figure 4.5** The proposed autoxidation pathways of  $\alpha$ -pinene via ozonolysis and subsequent oxidations. Figure adapted from Iyer et al, 2021. Each of the pathways of oxidation produce structurally-unique peroxy radicals which are vital intermediates in the formation of HOM. Deuteration at certain positions of the  $\alpha$ -pinene skeleton (marked in red and blue) will assist in the elucidation of which peroxy radicals are formed and their relative rates by measuring the exchange of deuterium atoms.

The synthetic procedures used to access isotopologues vinyl-CD<sub>3</sub> **IV-3** and vinyl-deuterated **IV-4** have been previously reported by our lab and were repeated for the purposes of this collaboration.<sup>181</sup> For **IV-3**,  $\beta$ -pinene **IV-5** was converted to nopinone **IV-6** through ozonolysis with a reductive workup. From here, **IV-6** was treated with lithium diisopropylamide (LDA) and Comins' reagent to generate the respective vinyl triflate, which then gave **IV-3** in good yield upon treatment with copper iodide (CuI) and deuterated methyl lithium to install the deuterated methyl group. For **IV-4**, nopinone **IV-6** was treated with sodium deuterioxide (NaOD) and deuterium oxide (D<sub>2</sub>O) to afford **IV-7** bearing deuterium atoms on the  $\alpha$ -methylene group, which gave **IV-4** upon generation of the vinyl triflate and subsequent copper-mediated methylation. The synthesis of these compounds will be invaluable in the study of the autoxidation process of  $\alpha$ -pinene, as site-

specific deuteration will allow for the explicit formation of structurally-distinct peroxy radicals that will be able to be differentiated via detection with  $\text{NO}_3\text{-CIMS}$



**Scheme 4.1** Synthesis of  $\alpha$ -pinene IV-3 and IV-4.

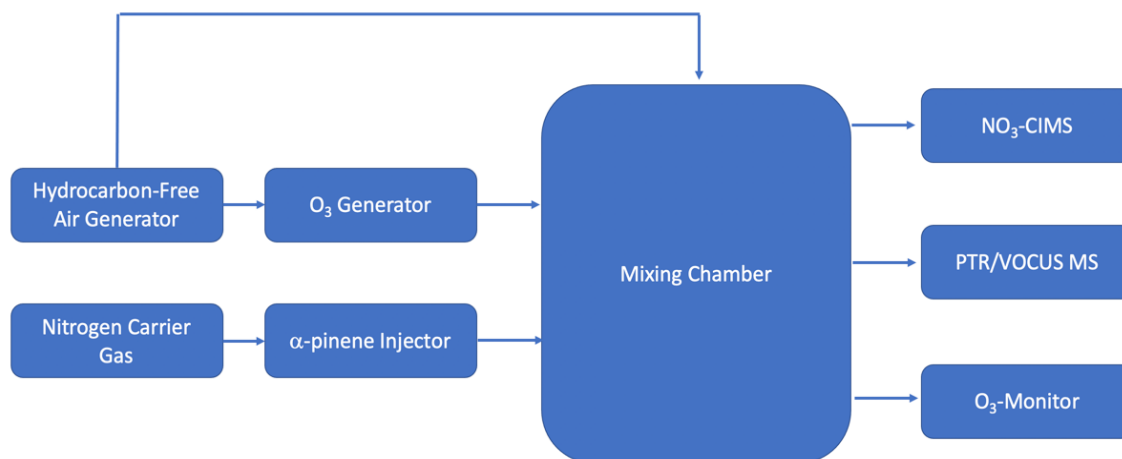


**Figure 4.6** Diagram of the experimental set-up to probe HOM formation of  $\alpha$ -pinene ozonolysis courtesy of the Ehn group at University of Helsinki.

#### 4.2.2 Unimolecular reactions of Peroxy Radicals Formed in Oxidation of $\alpha$ -pinene via Hydroxyl Radicals

In another collaboration involving the selective deuteration of  $\alpha$ -pinene, we are currently investigating the chemistry of peroxy radicals involved in  $\alpha$ -pinene oxidation. As touched upon in the previous section, the chemistry of peroxy radical ( $\text{RO}_2$ ) plays a vital role in the atmospheric oxidation of volatile organics.<sup>182-185</sup>  $\text{RO}_2$  can participate in a number of reaction pathways, such as reactions with hydroxyperoxy radical ( $\text{HO}_2$ ), nitrogen oxides, other  $\text{RO}_2$  molecules and unimolecular reactions.<sup>186-188</sup> These competing reactions have a profound effect upon the oxidation processes concerning VOCs and their corresponding oxidation products, as well as other oxidants in the atmosphere. One example of this is the interaction between  $\text{RO}_2$  and anthropogenic pollutants such as  $\text{NO}$ , which results in the generation of  $\text{NO}_2$  via radical oxidation, which generates ozone upon photolysis. Though the initial oxidation reaction mediated by  $\text{RO}_2$  leads to the formation of  $\text{O}_3$ , the unimolecular reaction involving peroxy radical does not recycle  $\text{NO}_x$ , leading to slower rates of ozone generation.<sup>189-190</sup> Also, as introduced in section 4.2.1, several studies have demonstrated that unimolecular reactions of peroxy radicals produce HOM and can subsequently generate new particle via formation of oxidation products of extremely-low volatility.

As the current landscape of environmental policies craft new regulations concerning emissions of nitrogen oxides, the emissions of  $\text{NO}_x$  are currently decreasing across the world and will continue to decline. Given the described reactivity above, unimolecular reactions involving  $\text{RO}_2$  are highly relevant to studying atmospheric constituents within the climate system.<sup>191</sup> However, the understanding of this described unimolecular reactivity is currently limited. The rates of these unimolecular reactions are incredibly sensitive to the larger structure of the peroxy

radical in question, and only a select few RO<sub>2</sub> reaction rates have been experimentally probed.<sup>174,</sup>

<sup>187, 192-193</sup> The lapse in knowledge concerning the relative reaction kinetics hinders development of any structure-activity correlations concerning the reactivity of peroxy radicals, and further study is needed in order to characterize and assess their atmospheric impact.

An ongoing collaboration with Dr. Lu Xu of the Wennberg group at CalTech is currently examining the RO<sub>2</sub> chemistry associated with atmospheric oxidation of  $\alpha$ -pinene. In 2019, Xu and coworkers demonstrated the peroxy radical reactivity of first-generation  $\alpha$ -pinene oxidation products, **IV-8**, **IV-9**, and **IV-10**.<sup>187</sup> The researchers showed that the  $\alpha$ -pinene peroxy radical **IV-9** formed from cleavage of the bridged ring could undergo three different unimolecular reactions, such as 1,5- and 1,6-hydride shifts and an endocyclization shown in **Scheme 4.2**. The total rate of unimolecular reactions is expressed as  $k_{\text{uni}} = k_{1,5\text{H}} + k_{1,6\text{H}} + k_{\text{endo}}$ , which was found to be  $4 \pm 2 \text{ s}^{-1}$ . However, the authors noted that access to isotopically-labelled  $\alpha$ -pinene derivatives would allow for the definite quantification of each unimolecular contribution to the observed overall reaction rate.

In order to investigate the mechanisms of the proposed unimolecular reactions of **IV-9**, a series of three deuterated  $\alpha$ -pinene isotopologues **IV-4**, **IV-11**, and **IV-12** shown in **Figure 4.7** were synthesized and analyzed using a gas chromatography time-of-flight chemical ionization mass spectrometer (GC-ToF-CIMS), shown in **Figure 4.9**. A full description of the instrument, including relevant reagent ions and sensitivities, can be found in work completed by Vasquez and coworkers.<sup>194</sup>

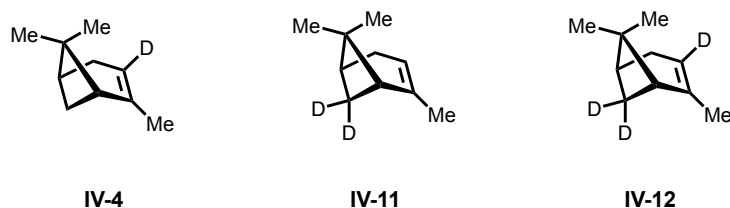
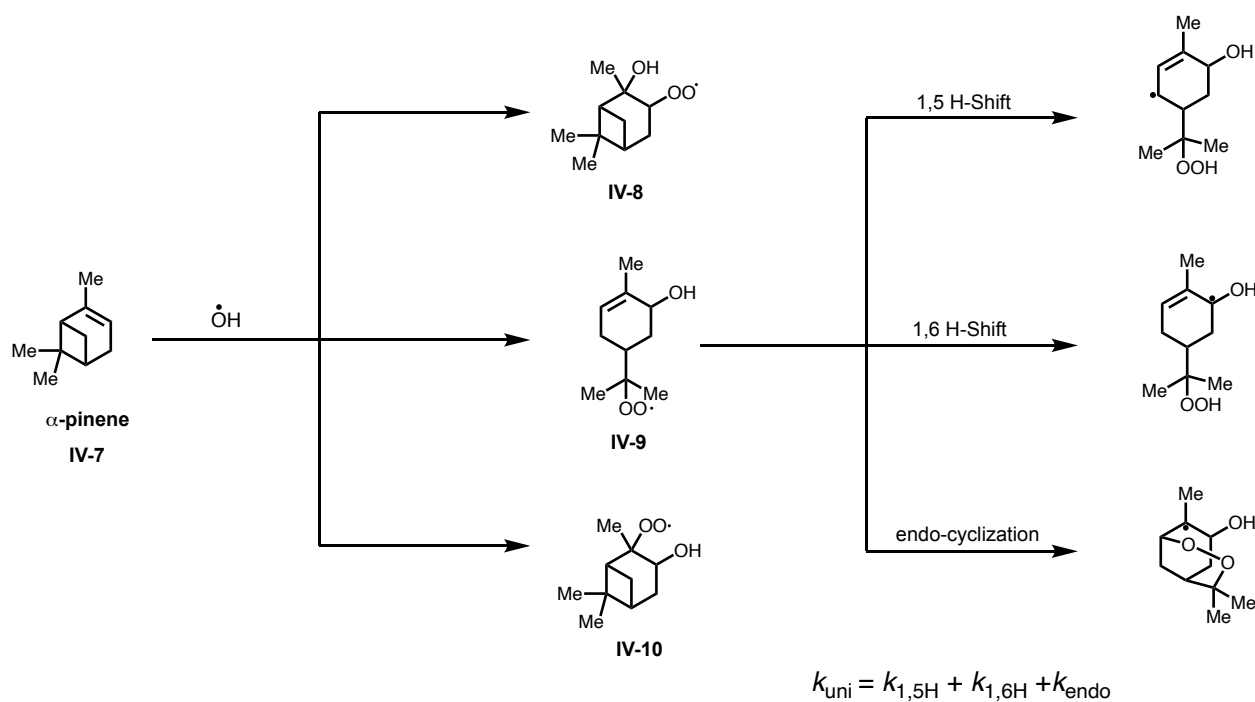


**Figure 4.7** The three isotopologues of  $\alpha$ -pinene **IV-4**, **IV-11** and **IV-12** synthesized to probe the unimolecular reactions of the  $\alpha$ -pinene-derived peroxy radicals.



**Scheme 4.2** Oxidation of  $\alpha$ -pinene via hydroxyl radical, the subsequent generation of  $\text{RO}_2$  species **IV-8**, **IV-9**, **IV-10**, and three potential unimolecular reactions from **IV-9**. The overall rate of unimolecular reactions is given by  $k_{\text{uni}} = k_{1,5\text{H}} + k_{1,6\text{H}} + k_{\text{endo}}$

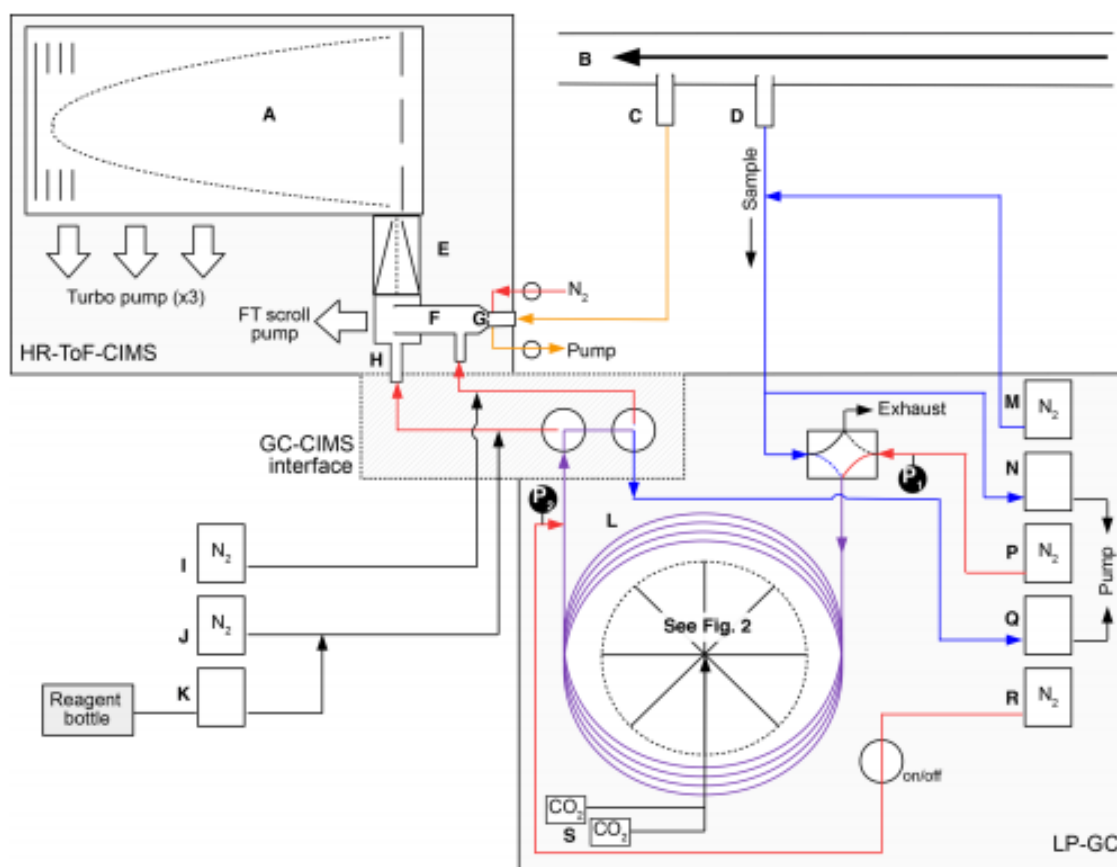
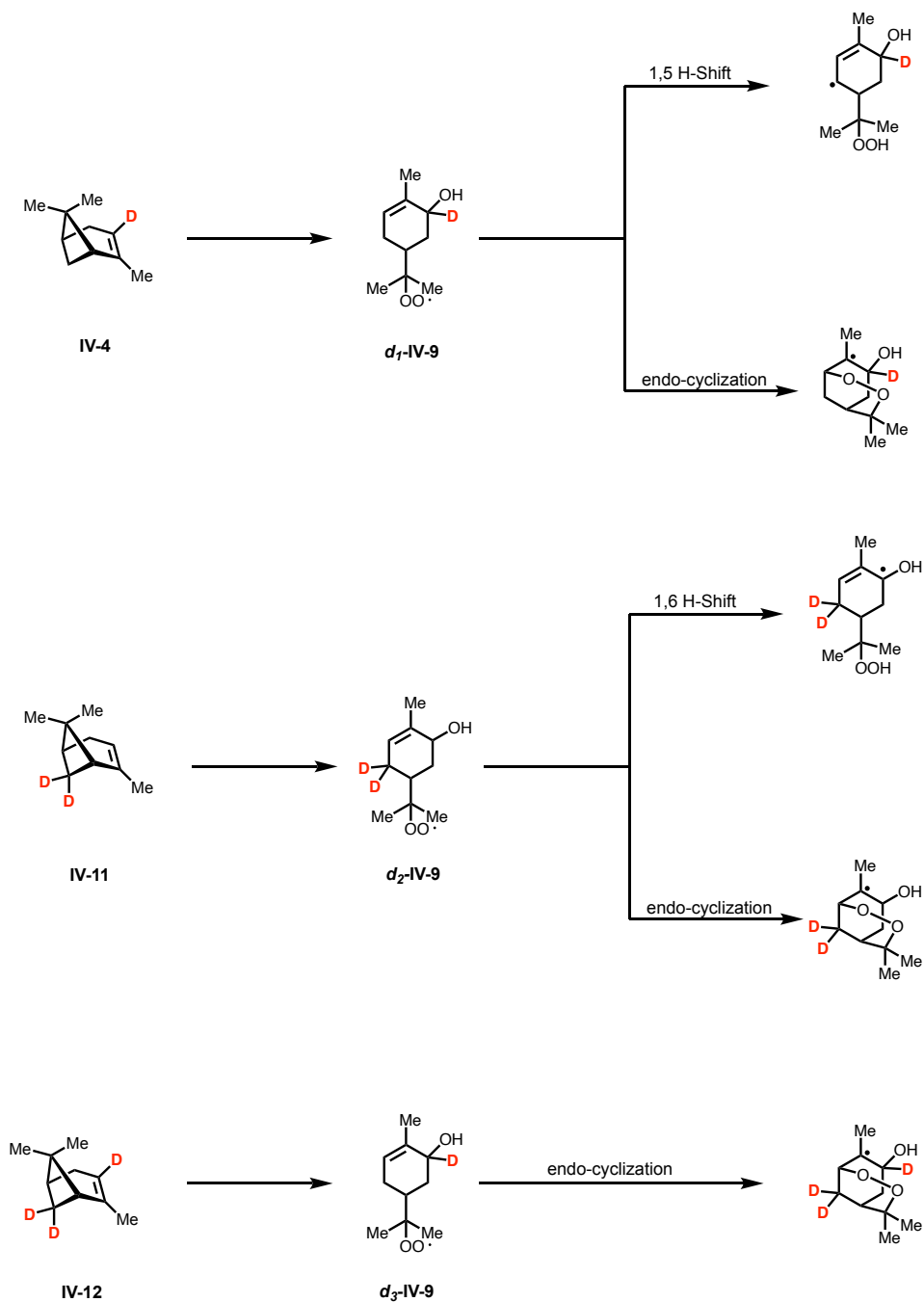


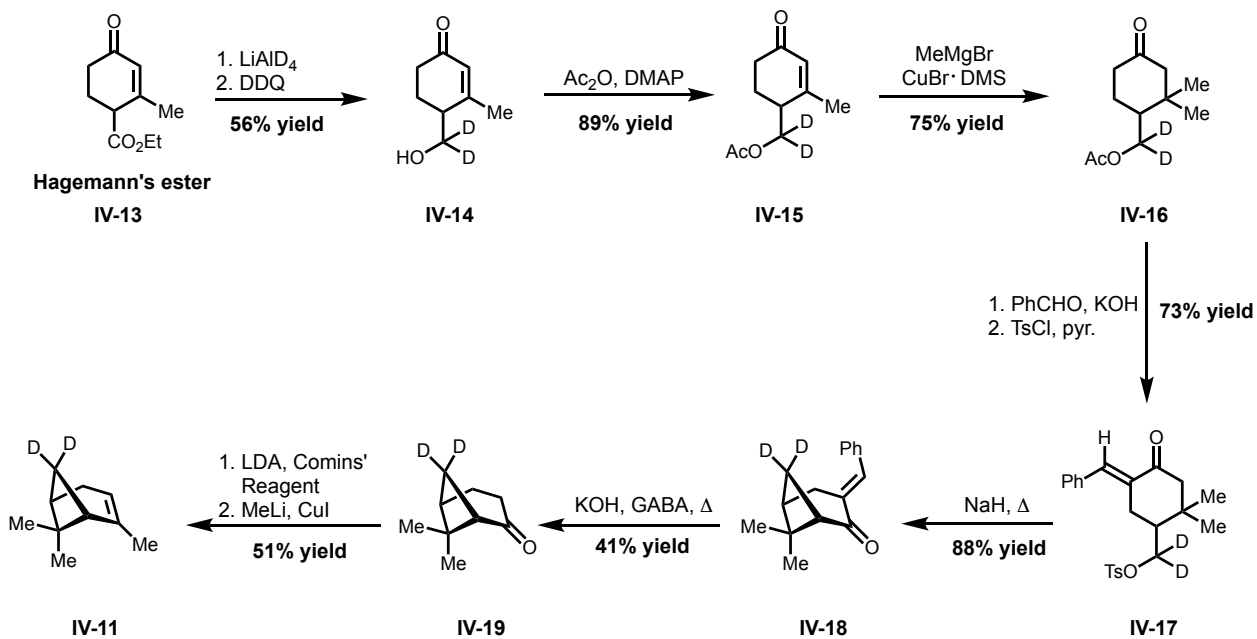
**Figure 4.8** Instrument schematic of the GC-ToF-CIMS. Figure exported from Xu et al, 2018 with permission from Dr. Lu Xu.

**Scheme 4.3** demonstrates the oxidation of each isotopologue and the relevant unimolecular reactions associated with the formation of the deuterated derivatives of **IV-9**. These isotopologues will enable the absolute confirmation of unimolecular contributions to the overall reaction rate associated with peroxy radical **IV-9** when compared to products generated from wild type  $\alpha$ -pinene. Following from the procedures detailed in section 4.2.1, synthesis of isotopologues **IV-4**, **IV-11**, and **IV-12** was completed applying methodology previously developed in our lab with a modification to access the  $d_3$  isotopologue **IV-12**.<sup>181</sup> **IV-4** was synthesized from **IV-6** using the reaction sequence shown in **Scheme 4.1**. For the synthesis of the isotopologues **IV-11** and **IV-12** bearing deuterium atoms on the methylene bridge, the method for site-specific deuteration of the carbon backbone is derived from the total synthesis of  $\alpha$ -pinene reported by Thomas and coworkers in 1976.<sup>195</sup>

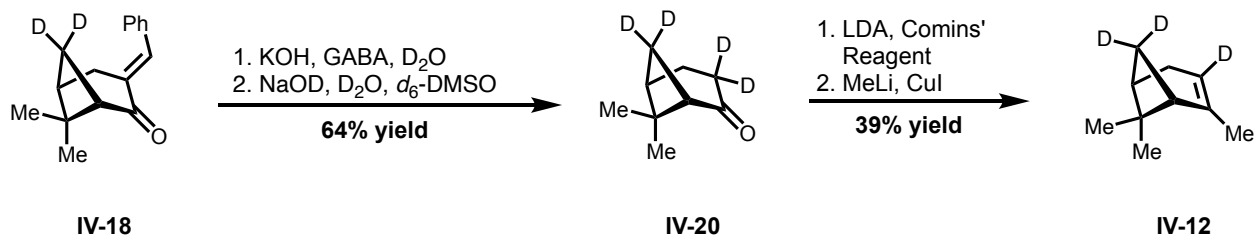


**Scheme 4.3** The oxidation of  $\alpha$ -pinene isotopologues **IV-4**, **IV-11**, and **IV-12** to form deuterated derivatives of **IV-9** and the unimolecular reactions relevant to each deuterium-labelled compound.

The synthesis of **IV-11** shown in **Scheme 4.4** began with treating Hagemann's ester **IV-13** with lithium aluminum deuteride ( $\text{LiAlD}_4$ ), reducing the ethyl ester to the primary alcohol and installing deuterium atoms on the future methylene bridgehead. The reduced product was then oxidized using DDQ to afford enone **IV-14** bearing a pendant hydroxyl group. **IV-14** was then protected using DMAP-catalyzed acetylation with acetic anhydride ( $\text{Ac}_2\text{O}$ ) which gave protected enone **IV-15**. Conjugate addition to the enone with methyl Grignard in the presence of copper (I) bromide dimethyl sulfide complex afforded carbonyl **IV-16** bearing a geminal dimethyl moiety at the 4-position of the cyclohexanone scaffold. From here, treatment with PhCHO and KOH resulted in protection of the less-hindered  $\alpha$ -methylene group as well as concomitant cleavage of the acetate group, which gave **IV-17** following tosylation of the unmasked hydroxyl group. This set the stage for the formation of the bridged methylene ring via enolate formation and subsequent intramolecular elimination of the tosyl group, affording protected bicycle **IV-18**. Deprotection of the benzylidene group using basic conditions with  $\gamma$ -aminobutyric acid (GABA) as an additive gave nopinone-derivative **IV-19** bearing deuterium atoms on the methylene bridge. The synthesis concluded with conversion of **IV-19** to the corresponding vinyl triflate using LDA and Comins' reagent, followed by copper-mediate methylation via treatment with MeLi and CuI, generating  $\alpha$ -pinene isotopologue **IV-11**. In the case of the  $\text{D}_3$  isotopologue **IV-12**, the established methodology was easily modified to incorporate the additional deuterium atom bound to the olefin. Shown in **Scheme 4.5**, bicyclic benzylidene **IV-18** was deprotected using basic conditions with GABA and  $\text{D}_2\text{O}$  as additives, followed by  $\alpha$ -deuteration using NaOD and  $\text{D}_2\text{O}$  to afford deuterated nopinone derivative **IV-20**. Copper-mediated methylation then gave **IV-12**.



**Scheme 4.4** Synthesis of  $\alpha$ -pinene isotopologue **IV-11**.



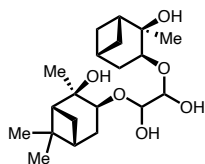
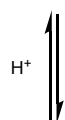
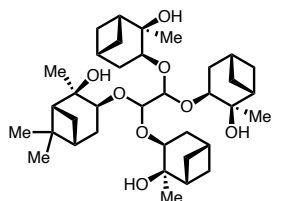
**Scheme 4.5** Synthesis of  $\alpha$ -pinene isotopologue **IV-12**.

### 4.3 Probing Synergy of Atmospheric Oxidation Products Through $^{13}\text{C}$ Isotopic-Labeling

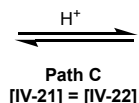
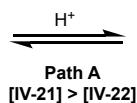
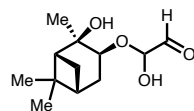
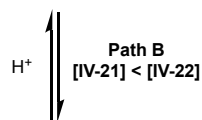
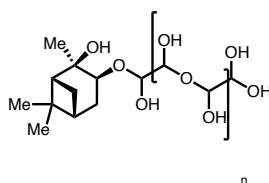
In addition to our efforts to synthesize deuterium-labeled species, ongoing and future work in the Thomson lab involves the isotopic-labeling of carbon atoms within terpene structures. As mentioned in section 4.1, SOA constituents participate in a variety of chemical reactions and physical processes, such as SOA particle formation and gas-particle partitioning. Due to the sheer variety of potential chemical transformations and physical divergences within atmospheric particles, the accurate study of these systems is a challenging endeavor. Adding to the complexity, studies has suggested that mixtures of oxidation products derived from different terpenes can lead to synergisms that can enhance SOA particle formation and greater partitioning of organic species from the gas phase into the condensed phase.

To probe the potential synergy between different atmospheric oxidation products, work is underway to probe the interactions between two oxidation products derived from  $\alpha$ -pinene and isoprene, pinanediol **IV-21** and glyoxal **IV-22** respectively. Preliminary results generated by the Martin group at Harvard University suggest that uptake of pinanediol into acidic and neutral sulfate particles was significantly enhanced in the presence of glyoxal, indicating potential positive synergy between the two oxidation products. The mechanism of this synergy is likely highly complex and difficult to elucidate due to the potential number of organic reactions possible between pinanediol and glyoxal (e.g., oligomerization, condensation, acetal formation and hydrolysis). **Figure 4.9** depicts a series of potential reaction pathways involving the hemiacetal and acetal forming reactions between pinanediol and glyoxal, potentially dependent on the concentration of each compound.

glyoxal acetal with pendant pinanediol structures



glyoxal oligomeric/polymeric species



copolymeric species

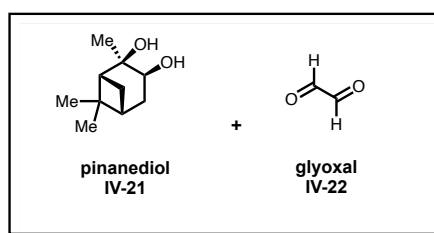
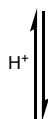
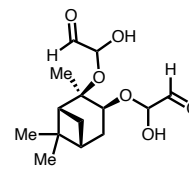
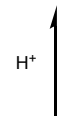
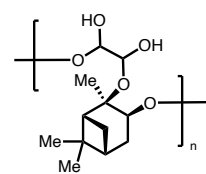
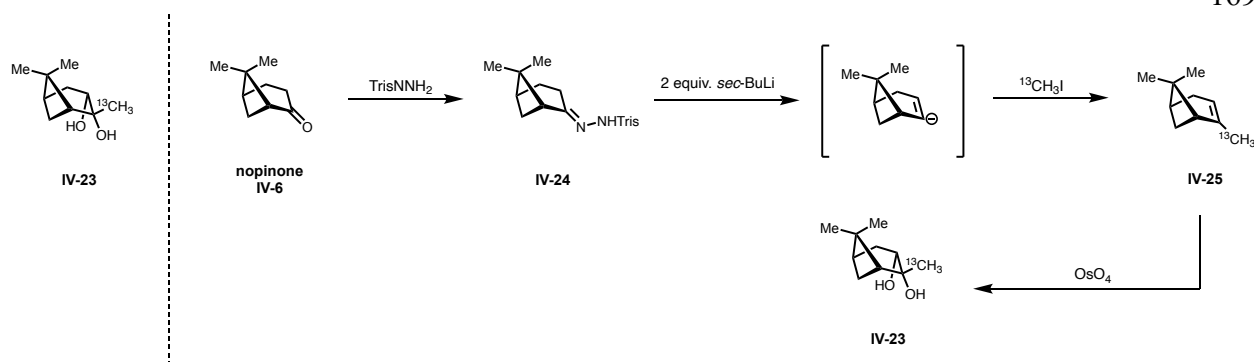


**Figure 4.9** Potential mechanisms of synergy between pinanediol **IV-21** and glyoxal **IV-22** and the subsequent formation of complex organic species.

In order to probe the formation of these species generated from hypothesized synergy between **IV-21** and **IV-22**, we envision the synthesis of a pinanediol derivative **IV-23** bearing an isotopically-labeled vinyl methyl group. Expanding on our initial collaboration with the Martin group at Harvard University, we plan to monitor the interaction of **IV-23** and glyoxal using a series of atmospheric chamber experiments. The  $^{13}\text{C}$ -labeled pinanediol will be used in the gas phase as a molecular probe to monitor uptake. These species can be observed in the AMS when they have been lost from the gas phase and transferred into the particle phase. The utility of using the proposed isotope will be demonstrated in the reliable isotopic mass shifts when compared to unlabeled precursors. In this manner, we will be able to dissect the complex reaction pathways we hypothesize are at play during particle formation and understand how varying conditions alters the synergy between **IV-21** and **IV-22**.

The synthesis of labeled pinanediol **IV-23** is currently underway. Shown in **Scheme 4.6**, our strategy is based on the use of the Shapiro reaction to generate a vinyl anion from the condensation of trisyl hydrazide onto **IV-6** to generate the trisyl hydrazone **IV-24**. From here, treatment of the hydrazone with a lithium base will result in the formation of a vinyl anion, and a subsequent treatment with a  $^{13}\text{C}$ -labeled electrophile such as methyl iodide will generate the labeled  $\alpha$ -pinene **IV-25**, from which the desired pinanediol can be easily generated via dihydroxylation. The completion of this synthesis will provide the first disclosed means to unambiguously monitor the complicated synergy between glyoxal and pinanediol, and will further elucidate the interesting and complex reactions that are suggested to occur within the atmosphere.



**Scheme 4.6** Intended synthetic route to generate labeled pinanediol **IV-23**.

#### 4.4 Conclusions

In this section, the intended future directions concerning the IEPOX-derived organosulfates were detailed. In addition to the analysis conducted within this thesis, we propose the use of robust analytical techniques to study additional physicochemical properties of the family of sulfate esters. With the use of methods such as SFG spectroscopy and PDT, the elusive chemistries of atmospheric organosulfates could be elaborated upon in a fruitful interdisciplinary manner, combining the preparative efficiency of organic synthesis with the power of analytical surface science. Additionally, several ongoing collaborations with research groups across the world were also described, in which various isotopologues of  $\alpha$ -pinene were synthesized for the purposes of studying a series of complicated atmospheric chemical processes involving oxidation and potential synergistic interplay between SVOCs derived from disparate terpenoids. It is our hope that the academic partnerships outlined here will provide the means to make meaningful, unambiguous claims about the chemistry in the atmosphere and further our understanding of constituents within the climate system at the molecular level.

## References

1. IPCC, *Climate Change 2013: The Physical Science Basis. Contribution of Working Group I to the Fifth Assessment Report of the Intergovernmental Panel on Climate Change*. Cambridge University Press: Cambridge, United Kingdom and New York, NY, USA, 2013; p 1535.
2. Kanakidou, M.; Seinfeld, J. H.; Pandis, S. N.; Barnes, I.; Dentener, F. J.; Facchini, M. C.; Van Dingenen, R.; Ervens, B.; Nenes, A.; Nielsen, C. J.; Swietlicki, E.; Putaud, J. P.; Balkanski, Y.; Fuzzi, S.; Horth, J.; Moortgat, G. K.; Winterhalter, R.; Myhre, C. E. L.; Tsigaridis, K.; Vignati, E.; Stephanou, E. G.; Wilson, J., Organic aerosol and global climate modelling: a review. *Atmos. Chem. Phys.* **2005**, *5* (4), 1053-1123.
3. Kanakidou, M.; Myriokefalitakis, S.; Tsigaridis, K., Aerosols in atmospheric chemistry and biogeochemical cycles of nutrients. *Environmental Research Letters* **2018**, *13* (6), 063004.
4. Kroll, J.; Seinfeld, J., Chemistry of secondary organic aerosol: Formation and evolution of low-volatility organics in the atmosphere. *Atmospheric Environment* **2008**, *42*, 3593-3624.
5. Jimenez, J. L.; Canagaratna, M. R.; Donahue, N. M.; Prevot, A. S.; Zhang, Q.; Kroll, J. H.; DeCarlo, P. F.; Allan, J. D.; Coe, H.; Ng, N. L.; Aiken, A. C.; Docherty, K. S.; Ulbrich, I. M.; Grieshop, A. P.; Robinson, A. L.; Duplissy, J.; Smith, J. D.; Wilson, K. R.; Lanz, V. A.; Hueglin, C.; Sun, Y. L.; Tian, J.; Laaksonen, A.; Raatikainen, T.; Rautiainen, J.; Vaattovaara, P.; Ehn, M.; Kulmala, M.; Tomlinson, J. M.; Collins, D. R.; Cubison, M. J.; Dunlea, E. J.; Huffman, J. A.; Onasch, T. B.; Alfarra, M. R.; Williams, P. I.; Bower, K.; Kondo, Y.; Schneider, J.; Drewnick, F.; Borrmann, S.; Weimer, S.; Demerjian, K.; Salcedo, D.; Cottrell, L.; Griffin, R.; Takami, A.; Miyoshi, T.; Hatakeyama, S.; Shimono, A.; Sun, J. Y.; Zhang, Y. M.; Dzepina, K.; Kimmel, J. R.; Sueper, D.; Jayne, J. T.; Herndon, S. C.; Trimborn, A. M.; Williams, L. R.; Wood, E. C.; Middlebrook, A. M.; Kolb, C. E.; Baltensperger, U.; Worsnop, D. R., Evolution of organic aerosols in the atmosphere. *Science* **2009**, *326* (5959), 1525-9.
6. Mauderly, J. L.; Chow, J. C., Health effects of organic aerosols. *Inhal Toxicol* **2008**, *20* (3), 257-88.
7. Anderson, J. O.; Thundiyil, J. G.; Stolbach, A., Clearing the air: a review of the effects of particulate matter air pollution on human health. *J Med Toxicol* **2012**, *8* (2), 166-75.
8. Kim, K. H.; Kabir, E.; Kabir, S., A review on the human health impact of airborne particulate matter. *Environ Int* **2015**, *74*, 136-43.

9. Riipinen, I.; Pierce, J. R.; Yli-Juuti, T.; Nieminen, T.; Häkkinen, S.; Ehn, M.; Junninen, H.; Lehtipalo, K.; Petäjä, T.; Slowik, J.; Chang, R.; Shantz, N. C.; Abbatt, J.; Leaitch, W. R.; Kerminen, V. M.; Worsnop, D. R.; Pandis, S. N.; Donahue, N. M.; Kulmala, M., Organic condensation: a vital link connecting aerosol formation to cloud condensation nuclei (CCN) concentrations. *Atmos. Chem. Phys.* **2011**, *11* (8), 3865-3878.
10. Hallquist, M.; Wenger, J. C.; Baltensperger, U.; Rudich, Y.; Simpson, D.; Claeys, M.; Dommen, J.; Donahue, N. M.; George, C.; Goldstein, A. H.; Hamilton, J. F.; Herrmann, H.; Hoffmann, T.; Iinuma, Y.; Jang, M.; Jenkin, M. E.; Jimenez, J. L.; Kiendler-Scharr, A.; Maenhaut, W.; McFiggans, G.; Mentel, T. F.; Monod, A.; Prévôt, A. S. H.; Seinfeld, J. H.; Surratt, J. D.; Szmigielski, R.; Wildt, J., The formation, properties and impact of secondary organic aerosol: current and emerging issues. *Atmos. Chem. Phys.* **2009**, *9* (14), 5155-5236.
11. Donahue, N. M.; Epstein, S. A.; Pandis, S. N.; Robinson, A. L., A two-dimensional volatility basis set: 1. organic-aerosol mixing thermodynamics. *Atmos. Chem. Phys.* **2011**, *11* (7), 3303-3318.
12. Baltensperger, U.; Kalberer, M.; Dommen, J.; Paulsen, D.; Alfarra, M. R.; Coe, H.; Fisseha, R.; Gascho, A.; Gysel, M.; Nyeki, S.; Sax, M.; Steinbacher, M.; Prevot, A. S. H.; Sjögren, S.; Weingartner, E.; Zenobi, R., Secondary organic aerosols from anthropogenic and biogenic precursors. *Faraday Discussions* **2005**, *130* (0), 265-278.
13. Richards-Henderson, N. K.; Pham, A. T.; Kirk, B. B.; Anastasio, C., Secondary Organic Aerosol from Aqueous Reactions of Green Leaf Volatiles with Organic Triplet Excited States and Singlet Molecular Oxygen. *Environmental Science & Technology* **2015**, *49* (1), 268-276.
14. Surratt, J. D.; Chan, A. W. H.; Eddingsaas, N. C.; Chan, M.; Loza, C. L.; Kwan, A. J.; Hersey, S. P.; Flagan, R. C.; Wennberg, P. O.; Seinfeld, J. H., Reactive intermediates revealed in secondary organic aerosol formation from isoprene. *Proceedings of the National Academy of Sciences* **2010**, *107* (15), 6640.
15. Horne, J.; Zhu, S.; Montoya-Aguilera, J.; Hinks, M.; Wingen, L.; Nizkorodov, S.; Dabdub, D., Reactive uptake of ammonia by secondary organic aerosols: Implications for air quality. *Atmospheric Environment* **2018**, *189*, 1-8.
16. Smith, S. J.; van Aardenne, J.; Klimont, Z.; Andres, R. J.; Volke, A.; Delgado Arias, S., Anthropogenic sulfur dioxide emissions: 1850–2005. *Atmos. Chem. Phys.* **2011**, *11* (3), 1101-1116.

17. Wang, Z.; Wang, T.; Fu, H.; Zhang, L.; Tang, M.; George, C.; Grassian, V. H.; Chen, J., Enhanced heterogeneous uptake of sulfur dioxide on mineral particles through modification of iron speciation during simulated cloud processing. *Atmos. Chem. Phys.* **2019**, *19* (19), 12569-12585.
18. Wang, S.; Zhou, S.; Tao, Y.; Tsui, W. G.; Ye, J.; Yu, J. Z.; Murphy, J. G.; McNeill, V. F.; Abbatt, J. P. D.; Chan, A. W. H., Organic Peroxides and Sulfur Dioxide in Aerosol: Source of Particulate Sulfate. *Environmental Science & Technology* **2019**, *53* (18), 10695-10704.
19. Weber, R. J.; Guo, H.; Russell, A. G.; Nenes, A., High aerosol acidity despite declining atmospheric sulfate concentrations over the past 15 years. *Nature Geoscience* **2016**, *9* (4), 282-285.
20. Ruprecht, H.; Sigg, L., Interactions of aerosols (ammonium sulfate, ammonium nitrate and ammonium chloride) and of gases (HCl, HNO<sub>3</sub>) with fogwater. *Atmospheric Environment. Part A. General Topics* **1990**, *24* (3), 573-584.
21. Charlson, R. J.; Vanderpol, A. H.; Covert, D. S.; Waggoner, A. P.; Ahlquist, N. C., Sulfuric Acid-Ammonium Sulfate Aerosol: Optical Detection in the St. Louis Region. *Science* **1974**, *184* (4133), 156.
22. Froyd, K. D.; Murphy, S. M.; Murphy, D. M.; de Gouw, J. A.; Eddingsaas, N. C.; Wennberg, P. O., Contribution of isoprene-derived organosulfates to free tropospheric aerosol mass. *Proceedings of the National Academy of Sciences* **2010**, *107* (50), 21360.
23. Hatch, L. E.; Creamean, J. M.; Ault, A. P.; Surratt, J. D.; Chan, M. N.; Seinfeld, J. H.; Edgerton, E. S.; Su, Y.; Prather, K. A., Measurements of Isoprene-Derived Organosulfates in Ambient Aerosols by Aerosol Time-of-Flight Mass Spectrometry—Part 2: Temporal Variability and Formation Mechanisms. *Environmental Science & Technology* **2011**, *45* (20), 8648-8655.
24. Lin, Y.-H.; Zhang, Z.; Docherty, K. S.; Zhang, H.; Budisulistiorini, S. H.; Rubitschun, C. L.; Shaw, S. L.; Knipping, E. M.; Edgerton, E. S.; Kleindienst, T. E.; Gold, A.; Surratt, J. D., Isoprene Epoxydiols as Precursors to Secondary Organic Aerosol Formation: Acid-Catalyzed Reactive Uptake Studies with Authentic Compounds. *Environmental Science & Technology* **2012**, *46* (1), 250-258.
25. Wang, K.; Zhang, Y.; Huang, R.-J.; Wang, M.; Ni, H.; Kampf, C. J.; Cheng, Y.; Bilde, M.; Glasius, M.; Hoffmann, T., Molecular Characterization and Source Identification of Atmospheric Particulate Organosulfates Using Ultrahigh Resolution Mass Spectrometry. *Environmental Science & Technology* **2019**, *53* (11), 6192-6202.

26. Li, J.; Wang, G.; Wu, C.; Cao, C.; Ren, Y.; Wang, J.; Li, J.; Cao, J.; Zeng, L.; Zhu, T., Characterization of isoprene-derived secondary organic aerosols at a rural site in North China Plain with implications for anthropogenic pollution effects. *Scientific Reports* **2018**, *8* (1), 535.
27. Estillore, A. D.; Hettiyadura, A. P. S.; Qin, Z.; Leckrone, E.; Wombacher, B.; Humphry, T.; Stone, E. A.; Grassian, V. H., Water Uptake and Hygroscopic Growth of Organosulfate Aerosol. *Environmental Science & Technology* **2016**, *50* (8), 4259-4268.
28. Peng, C.; Razafindrambinina, P. N.; Malek, K. A.; Chen, L.; Wang, W.; Huang, R. J.; Zhang, Y.; Ding, X.; Ge, M.; Wang, X.; Asa-Awuku, A. A.; Tang, M., Interactions of organosulfates with water vapor under sub- and supersaturated conditions. *Atmos. Chem. Phys.* **2021**, *21* (9), 7135-7148.
29. Takei, K.; Tsuto, K.; Miyamoto, S.; Wakatsuki, J., Anionic surfactants: lauric products. *Journal of the American Oil Chemists Society* **1985**, *62*, 341-347.
30. Bondi, C. A.; Marks, J. L.; Wroblewski, L. B.; Raatikainen, H. S.; Lenox, S. R.; Gebhardt, K. E., Human and Environmental Toxicity of Sodium Lauryl Sulfate (SLS): Evidence for Safe Use in Household Cleaning Products. *Environ Health Insights* **2015**, *9*, 27-32.
31. Lawrence, J. G., SURFACTANTS | Chromatography. In *Encyclopedia of Separation Science*, Wilson, I. D., Ed. Academic Press: Oxford, 2000; pp 4318-4327.
32. Gordon, M.; Hunter, A. S., Organic sulfate esters of potential biological interest. *Journal of Heterocyclic Chemistry* **1969**, *6* (5), 739-744.
33. Friess, S. L.; Durant, R. C.; Chanley, J. D.; Fash, F. J., Role of the sulphate charge center in irreversible interactions of holothurin A with chemoreceptors. *Biochemical Pharmacology* **1967**, *16* (8), 1617-1625.
34. Friess, S. L.; Durant, R. C., Blockade phenomena at the mammalian neuromuscular synapse. Competition between reversible anticholinesterases and an irreversible toxin. *Toxicology and Applied Pharmacology* **1965**, *7* (3), 373-381.
35. Piozzi, F.; Quilico, A.; Mondelli, R.; Ajello, T.; Sprio, V.; Melera, A., The structure and stereochemistry of atractyligenin. *Tetrahedron* **1966**, *22*, 515-529.

36. Mbaveng, A. T.; Hamm, R.; Kuete, V., 19 - Harmful and Protective Effects of Terpenoids from African Medicinal Plants. In *Toxicological Survey of African Medicinal Plants*, Kuete, V., Ed. Elsevier: 2014; pp 557-576.
37. Eriksson, H.; Gustafsson, J.-Å., Excretion of steroid hormones in adults steroids in urine from adults. *Clinica Chimica Acta* **1972**, *41*, 79-90.
38. Volkamer, R.; Jimenez, J. L.; San Martini, F.; Dzepina, K.; Zhang, Q.; Salcedo, D.; Molina, L. T.; Worsnop, D. R.; Molina, M. J., Secondary organic aerosol formation from anthropogenic air pollution: Rapid and higher than expected. *Geophysical Research Letters* **2006**, *33* (17).
39. Surratt, J. D.; Gómez-González, Y.; Chan, A. W. H.; Vermeulen, R.; Shahgholi, M.; Kleindienst, T. E.; Edney, E. O.; Offenberg, J. H.; Lewandowski, M.; Jaoui, M.; Maenhaut, W.; Claeys, M.; Flagan, R. C.; Seinfeld, J. H., Organosulfate Formation in Biogenic Secondary Organic Aerosol. *The Journal of Physical Chemistry A* **2008**, *112* (36), 8345-8378.
40. Fioletov, V. E.; McLinden, C. A.; Krotkov, N.; Li, C.; Joiner, J.; Theys, N.; Carn, S.; Moran, M. D., A global catalogue of large SO<sub>2</sub> sources and emissions derived from the Ozone Monitoring Instrument. *Atmos. Chem. Phys.* **2016**, *16* (18), 11497-11519.
41. Zhong, Q.; Shen, H.; Yun, X.; Chen, Y.; Ren, Y. a.; Xu, H.; Shen, G.; Du, W.; Meng, J.; Li, W.; Ma, J.; Tao, S., Global Sulfur Dioxide Emissions and the Driving Forces. *Environmental Science & Technology* **2020**, *54* (11), 6508-6517.
42. Stone, E. A.; Yang, L.; Yu, L. E.; Rupakheti, M., Characterization of organosulfates in atmospheric aerosols at Four Asian locations. *Atmospheric Environment* **2012**, *47*, 323-329.
43. Hawkins, L. N.; Russell, L. M.; Covert, D. S.; Quinn, P. K.; Bates, T. S., Carboxylic acids, sulfates, and organosulfates in processed continental organic aerosol over the southeast Pacific Ocean during VOCALS-REx 2008. *Journal of Geophysical Research: Atmospheres* **2010**, *115* (D13).
44. Wang, Y.; Hu, M.; Guo, S.; Wang, Y.; Zheng, J.; Yang, Y.; Zhu, W.; Tang, R.; Li, X.; Liu, Y.; Le Breton, M.; Du, Z.; Shang, D.; Wu, Y.; Wu, Z.; Song, Y.; Lou, S.; Hallquist, M.; Yu, J., The secondary formation of organosulfates under interactions between biogenic emissions and anthropogenic pollutants in summer in Beijing. *Atmos. Chem. Phys.* **2018**, *18* (14), 10693-10713.

45. Guenther, A. B.; Jiang, X.; Heald, C. L.; Sakulyanontvittaya, T.; Duhl, T.; Emmons, L. K.; Wang, X., The Model of Emissions of Gases and Aerosols from Nature version 2.1 (MEGAN2.1): an extended and updated framework for modeling biogenic emissions. *Geoscientific Model Development* **2012**, *5* (6), 1471-1492.
46. Fini, A.; Brunetti, C.; Loreto, F.; Centritto, M.; Ferrini, F.; Tattini, M., Isoprene Responses and Functions in Plants Challenged by Environmental Pressures Associated to Climate Change. *Front Plant Sci* **2017**, *8*, 1281.
47. Palmer, P. I., Mapping isoprene emissions over North America using formaldehyde column observations from space. *Journal of Geophysical Research* **2003**, *108* (D6).
48. Claeys, M.; Graham, B.; Vas, G.; Wang, W.; Vermeylen, R.; Pashynska, V.; Cafmeyer, J.; Guyon, P.; Andreae, M.; Artaxo, P.; Maenhaut, W., Formation of Secondary Organic Aerosols Through Photooxidation of Isoprene. *Science* **2004**, *303*, 1173-1176.
49. Carlton, A. G.; Wiedinmyer, C.; Kroll, J. H., A review of Secondary Organic Aerosol (SOA) formation from isoprene. *Atmospheric Chemistry and Physics Discussions* **2009**, *9* (2), 8261-8305.
50. Canaval, E.; Millet, D. B.; Zimmer, I.; Nosenko, T.; Georgii, E.; Partoll, E. M.; Fischer, L.; Alwe, H. D.; Kulmala, M.; Karl, T.; Schnitzler, J.-P.; Hansel, A., Rapid conversion of isoprene photooxidation products in terrestrial plants. *Communications Earth & Environment* **2020**, *1* (1), 44.
51. Su, L.; Patton, E. G.; Vilà-Guerau de Arellano, J.; Guenther, A. B.; Kaser, L.; Yuan, B.; Xiong, F.; Shepson, P. B.; Zhang, L.; Miller, D. O.; Brune, W. H.; Baumann, K.; Edgerton, E.; Weinheimer, A.; Misztal, P. K.; Park, J. H.; Goldstein, A. H.; Skog, K. M.; Keutsch, F. N.; Mak, J. E., Understanding isoprene photooxidation using observations and modeling over a subtropical forest in the southeastern US. *Atmos. Chem. Phys.* **2016**, *16* (12), 7725-7741.
52. Liu, Y.; Seco, R.; Kim, S.; Guenther, A. B.; Goldstein, A. H.; Keutsch, F. N.; Springston, S. R.; Watson, T. B.; Artaxo, P.; Souza, R. A. F.; McKinney, K. A.; Martin, S. T., Isoprene photo-oxidation products quantify the effect of pollution on hydroxyl radicals over Amazonia. *Science Advances* **2018**, *4* (4), eaar2547.
53. Song, M.; Zhang, C.; Wu, H.; Mu, Y.; Ma, Z.; Zhang, Y.; Liu, J.; Li, X., The influence of OH concentration on SOA formation from isoprene photooxidation. *Science of The Total Environment* **2019**, *650*, 951-957.

54. Lin, Y.-H.; Zhang, H.; Pye, H. O. T.; Zhang, Z.; Marth, W. J.; Park, S.; Arashiro, M.; Cui, T.; Budisulistiorini, S. H.; Sexton, K. G.; Vizuete, W.; Xie, Y.; Luecken, D. J.; Piletic, I. R.; Edney, E. O.; Bartolotti, L. J.; Gold, A.; Surratt, J. D., Epoxide as a precursor to secondary organic aerosol formation from isoprene photooxidation in the presence of nitrogen oxides. *Proceedings of the National Academy of Sciences* **2013**, *110* (17), 6718-6723.
55. Liu, X.; Zhang, W.; Wang, Z.; Zhao, W.; Tao, L.; Yang, X., Chemical composition and size distribution of secondary organic aerosol formed from the photooxidation of isoprene. *J Environ Sci (China)* **2009**, *21* (11), 1525-31.
56. Upshur, M. A.; Strick, B. F.; McNeill, V. F.; Thomson, R. J.; Geiger, F. M., Climate-relevant physical properties of molecular constituents for isoprene-derived secondary organic aerosol material. *Atmospheric Chemistry and Physics* **2014**, *14* (19), 10731-10740.
57. Schwantes, R. H.; Charan, S. M.; Bates, K. H.; Huang, Y.; Nguyen, T. B.; Mai, H.; Kong, W.; Flagan, R. C.; Seinfeld, J. H., Low-volatility compounds contribute significantly to isoprene secondary organic aerosol (SOA) under high-NO<sub>x</sub> conditions. *Atmos. Chem. Phys.* **2019**, *19* (11), 7255-7278.
58. Lin, Y.-H.; Knipping, E.; Edgerton, E.; Shaw, S.; Surratt, J., Investigating the influences of SO<sub>2</sub> and NH<sub>3</sub> levels on isoprene-derived secondary organic aerosol formation using conditional sampling approaches. *Atmospheric Chemistry and Physics* **2013**, *13*, 8457-8470.
59. Hyttinen, N.; Elm, J.; Malila, J.; Calderón, S. M.; Prisle, N. L., Thermodynamic properties of isoprene- and monoterpene-derived organosulfates estimated with COSMOtherm. *Atmos. Chem. Phys.* **2020**, *20* (9), 5679-5696.
60. Gao, K.; Zhu, T., Analytical methods for organosulfate detection in aerosol particles: Current status and future perspectives. *Science of The Total Environment* **2021**, *784*, 147244.
61. Hettiyadura, A. P. S.; Jayarathne, T.; Baumann, K.; Goldstein, A. H.; de Gouw, J. A.; Koss, A.; Keutsch, F. N.; Skog, K.; Stone, E. A., Qualitative and quantitative analysis of atmospheric organosulfates in Centreville, Alabama. *Atmospheric Chemistry and Physics* **2017**, *17* (2), 1343-1359.
62. Rattanavaraha, W.; Chu, K.; Budisulistiorini, S. H.; Riva, M.; Lin, Y. H.; Edgerton, E. S.; Baumann, K.; Shaw, S. L.; Guo, H.; King, L.; Weber, R. J.; Neff, M. E.; Stone, E. A.; Offenberg, J. H.; Zhang, Z.; Gold, A.; Surratt, J. D., Assessing the impact of anthropogenic pollution on isoprene-derived secondary organic aerosol formation in PM<sub>2.5</sub> collected from the Birmingham,

Alabama, ground site during the 2013 Southern Oxidant and Aerosol Study. *Atmos Chem Phys* **2017**, *16* (0), 4897-4914.

63. Xu, Z. N.; Nie, W.; Liu, Y. L.; Sun, P.; Huang, D. D.; Yan, C.; Krechmer, J.; Ye, P. L.; Xu, Z.; Qi, X. M.; Zhu, C. J.; Li, Y. Y.; Wang, T. Y.; Wang, L.; Huang, X.; Tang, R. Z.; Guo, S.; Xiu, G. L.; Fu, Q. Y.; Worsnop, D.; Chi, X. G.; Ding, A. J., Multifunctional Products of Isoprene Oxidation in Polluted Atmosphere and Their Contribution to SOA. *Geophysical Research Letters* **2021**, *48* (1), e2020GL089276.

64. Zhang, H.; Lin, Y.-H.; Zhang, Z.; Zhang, X.; Shaw, S. L.; Knipping, E. M.; Weber, R. J.; Gold, A.; Kamens, R. M.; Surratt, J. D., Secondary organic aerosol formation from methacrolein photooxidation: roles of NO<sub>x</sub> level, relative humidity and aerosol acidity. *Environmental Chemistry* **2012**, *9* (3), 247-262.

65. Surratt, J. D.; Kroll, J. H.; Kleindienst, T. E.; Edney, E. O.; Claeys, M.; Sorooshian, A.; Ng, N. L.; Offenberg, J. H.; Lewandowski, M.; Jaoui, M.; Flagan, R. C.; Seinfeld, J. H., Evidence for Organosulfates in Secondary Organic Aerosol. *Environmental Science & Technology* **2007**, *41* (2), 517-527.

66. Kristensen, K.; Glasius, M., Organosulfates and oxidation products from biogenic hydrocarbons in fine aerosols from a forest in North West Europe during spring. *Atmospheric Environment* **2011**, *45* (27), 4546-4556.

67. Lam, H. K.; Kwong, K. C.; Poon, H. Y.; Davies, J. F.; Zhang, Z.; Gold, A.; Surratt, J. D.; Chan, M. N., Heterogeneous OH oxidation of isoprene-epoxydiol-derived organosulfates: kinetics, chemistry and formation of inorganic sulfate. *Atmos. Chem. Phys.* **2019**, *19* (4), 2433-2440.

68. Liao, J.; Froyd, K. D.; Murphy, D. M.; Keutsch, F. N.; Yu, G.; Wennberg, P. O.; St. Clair, J. M.; Crouse, J. D.; Wisthaler, A.; Mikoviny, T.; Jimenez, J. L.; Campuzano-Jost, P.; Day, D. A.; Hu, W.; Ryerson, T. B.; Pollack, I. B.; Peischl, J.; Anderson, B. E.; Ziemba, L. D.; Blake, D. R.; Meinardi, S.; Diskin, G., Airborne measurements of organosulfates over the continental U.S. *Journal of Geophysical Research: Atmospheres* **2015**, *120* (7), 2990-3005.

69. Meade, L. E.; Riva, M.; Blomberg, M. Z.; Brock, A. K.; Qualters, E. M.; Siejack, R. A.; Ramakrishnan, K.; Surratt, J. D.; Kautzman, K. E., Seasonal variations of fine particulate organosulfates derived from biogenic and anthropogenic hydrocarbons in the mid-Atlantic United States. *Atmospheric Environment* **2016**, *145*, 405-414.

70. Chan, M. N.; Surratt, J. D.; Claeys, M.; Edgerton, E. S.; Tanner, R. L.; Shaw, S. L.; Zheng, M.; Knipping, E. M.; Eddingsaas, N. C.; Wennberg, P. O.; Seinfeld, J. H., Characterization and Quantification of Isoprene-Derived Epoxydiols in Ambient Aerosol in the Southeastern United States. *Environmental Science & Technology* **2010**, *44* (12), 4590-4596.
71. Duporté, G.; Flaud, P. M.; Kammer, J.; Geneste, E.; Augagneur, S.; Pangu, E.; Lamkaddam, H.; Gratien, A.; Doussin, J. F.; Budzinski, H.; Villenave, E.; Perraudin, E., Experimental Study of the Formation of Organosulfates from  $\alpha$ -Pinene Oxidation. 2. Time Evolution and Effect of Particle Acidity. *The Journal of Physical Chemistry A* **2020**, *124* (2), 409-421.
72. Tan, X.-F.; Zhang, L.; Long, B., New mechanistic pathways for the formation of organosulfates catalyzed by ammonia and carbinolamine formation catalyzed by sulfuric acid in the atmosphere. *Physical Chemistry Chemical Physics* **2020**, *22* (16), 8800-8807.
73. He, Q.-F.; Ding, X.; Fu, X.-X.; Zhang, Y.-Q.; Wang, J.-Q.; Liu, Y.-X.; Tang, M.-J.; Wang, X.-M.; Rudich, Y., Secondary Organic Aerosol Formation From Isoprene Epoxides in the Pearl River Delta, South China: IEPOX- and HMML-Derived Tracers. *Journal of Geophysical Research: Atmospheres* **2018**, *123* (13), 6999-7012.
74. Nguyen, Q. T.; Christensen, M. K.; Cozzi, F.; Zare, A.; Hansen, A. M. K.; Kristensen, K.; Tulinius, T. E.; Madsen, H. H.; Christensen, J. H.; Brandt, J.; Massling, A.; Nøjgaard, J. K.; Glasius, M., Understanding the anthropogenic influence on formation of biogenic secondary organic aerosols in Denmark via analysis of organosulfates and related oxidation products. *Atmospheric Chemistry and Physics* **2014**, *14* (17), 8961-8981.
75. Benkovic, S. J.; Benkovic, P. A., Studies on Sulfate Esters. I. Nucleophilic Reactions of Amines with p-Nitrophenyl Sulfate. *Journal of the American Chemical Society* **1966**, *88* (23), 5504-5511.
76. Fitzgerald, J., Sulfate ester formation and hydrolysis: a potentially important yet often ignored aspect of the sulfur cycle of aerobic soils. *Bacteriological reviews* **1976**, *40* 3, 698-721.
77. Cameron, D. R.; Thatcher, G. R. J., Mechanisms of Reaction of Sulfate Esters: A Molecular Orbital Study of Associative Sulfuryl Group Transfer, Intramolecular Migration, and Pseudorotation. *The Journal of Organic Chemistry* **1996**, *61* (17), 5986-5997.
78. Glasius, M.; Bering, M. S.; Yee, L. D.; de Sa, S. S.; Isaacman-VanWertz, G.; Wernis, R. A.; Barbosa, H. M. J.; Alexander, M. L.; Palm, B. B.; Hu, W.; Campuzano-Jost, P.; Day, D. A.; Jimenez, J. L.; Shrivastava, M.; Martin, S. T.; Goldstein, A. H., Organosulfates in aerosols

downwind of an urban region in central Amazon. *Environ Sci Process Impacts* **2018**, *20* (11), 1546-1558.

79. Bondy, A. L.; Craig, R. L.; Zhang, Z.; Gold, A.; Surratt, J. D.; Ault, A. P., Isoprene-Derived Organosulfates: Vibrational Mode Analysis by Raman Spectroscopy, Acidity-Dependent Spectral Modes, and Observation in Individual Atmospheric Particles. *J Phys Chem A* **2018**, *122* (1), 303-315.

80. Budisulistiorini, S. H.; Li, X.; Bairai, S. T.; Renfro, J.; Liu, Y.; Liu, Y. J.; McKinney, K. A.; Martin, S. T.; McNeill, V. F.; Pye, H. O. T.; Nenes, A.; Neff, M. E.; Stone, E. A.; Mueller, S.; Knote, C.; Shaw, S. L.; Zhang, Z.; Gold, A.; Surratt, J. D., Examining the effects of anthropogenic emissions on isoprene-derived secondary organic aerosol formation during the 2013 Southern Oxidant and Aerosol Study (SOAS) at the Look Rock, Tennessee ground site. *Atmospheric Chemistry and Physics* **2015**, *15* (15), 8871-8888.

81. Cui, T.; Zeng, Z.; Dos Santos, E. O.; Zhang, Z.; Chen, Y.; Zhang, Y.; Rose, C. A.; Budisulistiorini, S. H.; Collins, L. B.; Bodnar, W. M.; de Souza, R. A. F.; Martin, S. T.; Machado, C. M. D.; Turpin, B. J.; Gold, A.; Ault, A. P.; Surratt, J. D., Development of a hydrophilic interaction liquid chromatography (HILIC) method for the chemical characterization of water-soluble isoprene epoxydiol (IEPOX)-derived secondary organic aerosol. *Environ Sci Process Impacts* **2018**, *20* (11), 1524-1536.

82. Guenther, A.; Hewitt, C. N.; Erickson, D.; Fall, R.; Geron, C.; Graedel, T.; Harley, P.; Klinger, L.; Lerdau, M.; McKay, W. A.; Pierce, T.; Scholes, B.; Steinbrecher, R.; Tallamraju, R.; Taylor, J.; Zimmerman, P., A global model of natural volatile organic compound emissions. *Journal of Geophysical Research: Atmospheres* **1995**, *100* (D5), 8873-8892.

83. Eddingsaas, N. C.; Loza, C. L.; Yee, L. D.; Chan, M.; Schilling, K. A.; Chhabra, P. S.; Seinfeld, J. H.; Wennberg, P. O.,  $\alpha$ -pinene photooxidation under controlled chemical conditions &ndash; Part 2: SOA yield and composition in low- and high-NO<sub>x</sub> environments. *Atmospheric Chemistry and Physics* **2012**, *12* (16), 7413-7427.

84. Iinuma, Y.; Müller, C.; Berndt, T.; Böge, O.; Claeys, M.; Herrmann, H., Evidence for the Existence of Organosulfates from  $\beta$ -Pinene Ozonolysis in Ambient Secondary Organic Aerosol. *Environmental Science & Technology* **2007**, *41* (19), 6678-6683.

85. Duporté, G.; Flaud, P. M.; Geneste, E.; Augagneur, S.; Pangui, E.; Lamkaddam, H.; Gratien, A.; Doussin, J. F.; Budzinski, H.; Villenave, E.; Perraudin, E., Experimental Study of the Formation of Organosulfates from  $\alpha$ -Pinene Oxidation. Part I: Product Identification,

Formation Mechanisms and Effect of Relative Humidity. *The Journal of Physical Chemistry A* **2016**, *120* (40), 7909-7923.

86. Wang, Y.; Ma, Y.; Li, X.; Kuang, B. Y.; Huang, C.; Tong, R.; Yu, J. Z., Monoterpene and Sesquiterpene  $\alpha$ -Hydroxy Organosulfates: Synthesis, MS/MS Characteristics, and Ambient Presence. *Environmental Science & Technology* **2019**, *53* (21), 12278-12290.

87. Kundu, S.; Quraishi, T. A.; Yu, G.; Suarez, C.; Keutsch, F. N.; Stone, E. A., Evidence and quantitation of aromatic organosulfates in ambient aerosols in Lahore, Pakistan. *Atmos. Chem. Phys.* **2013**, *13* (9), 4865-4875.

88. Ma, Y.; Xu, X.; Song, W.; Geng, F.; Wang, L., Seasonal and diurnal variations of particulate organosulfates in urban Shanghai, China. *Atmospheric Environment* **2014**, *85*, 152-160.

89. Tao, S.; Lu, X.; Levac, N.; Bateman, A. P.; Nguyen, T. B.; Bones, D. L.; Nizkorodov, S. A.; Laskin, J.; Laskin, A.; Yang, X., Molecular Characterization of Organosulfates in Organic Aerosols from Shanghai and Los Angeles Urban Areas by Nanospray-Desorption Electrospray Ionization High-Resolution Mass Spectrometry. *Environmental Science & Technology* **2014**, *48* (18), 10993-11001.

90. Kuang, B. Y.; Lin, P.; Hu, M.; Yu, J. Z., Aerosol size distribution characteristics of organosulfates in the Pearl River Delta region, China. *Atmospheric Environment* **2016**, *130*, 23-35.

91. Huang, R.-J.; Cao, J.; Chen, Y.; Yang, L.; Shen, J.; You, Q.; Wang, K.; Lin, C.; Xu, W.; Gao, B.; Li, Y.; Chen, Q.; Hoffmann, T.; and Dowd, C. D.; Bilde, M.; Glasius, M., Organosulfates in atmospheric aerosol: synthesis and quantitative analysis of PM<sub>2.5</sub> from Xi'an, northwestern China. *Atmospheric Measurement Techniques* **2018**, *11* (6), 3447-3456.

92. Mögel, I.; Baumann, S.; Böhme, A.; Kohajda, T.; von Bergen, M.; Simon, J.-C.; Lehmann, I., The aromatic volatile organic compounds toluene, benzene and styrene induce COX-2 and prostaglandins in human lung epithelial cells via oxidative stress and p38 MAPK activation. *Toxicology* **2011**, *289* (1), 28-37.

93. Baek, S.-O.; Jenkins, R. A., Characterization of trace organic compounds associated with aged and diluted sidestream tobacco smoke in a controlled atmosphere—volatile organic compounds and polycyclic aromatic hydrocarbons. *Atmospheric Environment* **2004**, *38* (38), 6583-6599.

94. Kim, K.-H.; Kim, M.-Y., The distributions of BTEX compounds in the ambient atmosphere of the Nan-Ji-Do abandoned landfill site in Seoul. *Atmospheric Environment* **2002**, *36* (14), 2433-2446.
95. Sack, T. M.; Steele, D. H.; Hammerstrom, K.; Remmers, J., A survey of household products for volatile organic compounds. *Atmospheric Environment. Part A. General Topics* **1992**, *26* (6), 1063-1070.
96. Maria, S. F.; Russell, L. M.; Turpin, B. J.; Porcja, R. J.; Campos, T. L.; Weber, R. J.; Huebert, B. J., Source signatures of carbon monoxide and organic functional groups in Asian Pacific Regional Aerosol Characterization Experiment (ACE-Asia) submicron aerosol types. *Journal of Geophysical Research: Atmospheres* **2003**, *108* (D23).
97. Blando, J. D.; Porcja, R. J.; Li, T.-H.; Bowman, D.; Liroy, P. J.; Turpin, B. J., Secondary Formation and the Smoky Mountain Organic Aerosol: An Examination of Aerosol Polarity and Functional Group Composition During SEAVS. *Environmental Science & Technology* **1998**, *32* (5), 604-613.
98. Brüggemann, M.; van Pinxteren, D.; Wang, Y.; Yu, J. Z.; Herrmann, H., Quantification of known and unknown terpenoid organosulfates in PM10 using untargeted LC-HRMS/MS: contrasting summertime rural Germany and the North China Plain. *Environmental Chemistry* **2019**, *16* (5), 333-346.
99. Riva, M.; Da Silva Barbosa, T.; Lin, Y. H.; Stone, E. A.; Gold, A.; Surratt, J. D., Chemical characterization of organosulfates in secondary organic aerosol derived from the photooxidation of alkanes. *Atmos. Chem. Phys.* **2016**, *16* (17), 11001-11018.
100. Altieri, K. E.; Turpin, B. J.; Seitzinger, S. P., Oligomers, organosulfates, and nitrooxy organosulfates in rainwater identified by ultra-high resolution electrospray ionization FT-ICR mass spectrometry. *Atmos. Chem. Phys.* **2009**, *9* (7), 2533-2542.
101. Zuth, C.; Vogel, A. L.; Ockenfeld, S.; Huesmann, R.; Hoffmann, T., Ultrahigh-Resolution Mass Spectrometry in Real Time: Atmospheric Pressure Chemical Ionization Orbitrap Mass Spectrometry of Atmospheric Organic Aerosol. *Analytical Chemistry* **2018**, *90* (15), 8816-8823.
102. Wang, Y.; Ren, J.; Huang, X. H. H.; Tong, R.; Yu, J. Z., Synthesis of Four Monoterpene-Derived Organosulfates and Their Quantification in Atmospheric Aerosol Samples. *Environmental Science & Technology* **2017**, *51* (12), 6791-6801.

103. Yttri, K. E.; Simpson, D.; Nøjgaard, J. K.; Kristensen, K.; Genberg, J.; Stenström, K.; Swietlicki, E.; Hillamo, R.; Aurela, M.; Bauer, H.; Offenberg, J. H.; Jaoui, M.; Dye, C.; Eckhardt, S.; Burkhardt, J. F.; Stohl, A.; Glasius, M., Source apportionment of the summer time carbonaceous aerosol at Nordic rural background sites. *Atmos. Chem. Phys.* **2011**, *11* (24), 13339-13357.
104. Hettiyadura, A. P. S.; Al-Naiema, I. M.; Hughes, D. D.; Fang, T.; Stone, E. A., Organosulfates in Atlanta, Georgia: anthropogenic influences on biogenic secondary organic aerosol formation. *Atmos. Chem. Phys.* **2019**, *19* (5), 3191-3206.
105. Brüggemann, M.; Poulain, L.; Held, A.; Stelzer, T.; Zuth, C.; Richters, S.; Mutzel, A.; van Pinxteren, D.; Iinuma, Y.; Katkevica, S.; Rabe, R.; Herrmann, H.; Hoffmann, T., Real-time detection of highly oxidized organosulfates and BSOA marker compounds during the F-BEACh 2014 field study. *Atmos. Chem. Phys.* **2017**, *17* (2), 1453-1469.
106. Vogel, A. L.; Schneider, J.; Müller-Tautges, C.; Klimach, T.; Hoffmann, T., Aerosol Chemistry Resolved by Mass Spectrometry: Insights into Particle Growth after Ambient New Particle Formation. *Environmental Science & Technology* **2016**, *50* (20), 10814-10822.
107. Wang, K.; Zhang, Y.; Huang, R.-J.; Cao, J.; Hoffmann, T., UHPLC-Orbitrap mass spectrometric characterization of organic aerosol from a central European city (Mainz, Germany) and a Chinese megacity (Beijing). *Atmospheric Environment* **2018**, *189*, 22-29.
108. Frossard, A. A.; Shaw, P. M.; Russell, L. M.; Kroll, J. H.; Canagaratna, M. R.; Worsnop, D. R.; Quinn, P. K.; Bates, T. S., Springtime Arctic haze contributions of submicron organic particles from European and Asian combustion sources. *Journal of Geophysical Research: Atmospheres* **2011**, *116* (D5).
109. Huang, S.; Poulain, L.; van Pinxteren, D.; van Pinxteren, M.; Wu, Z.; Herrmann, H.; Wiedensohler, A., Latitudinal and Seasonal Distribution of Particulate MSA over the Atlantic using a Validated Quantification Method with HR-ToF-AMS. *Environmental Science & Technology* **2017**, *51* (1), 418-426.
110. Huang, X.; He, L. Y.; Hu, M.; Zhang, Q.; Zhu, T.; L, X.; L.-W, Z.; X.-G, L.; Y.-H, Z.; Jayne, J.; Ng, N.; Worsnop, D., Highly time-resolved chemical characterization of atmospheric submicron particles during 2008 Beijing Olympic Games using an Aerodyne High-Resolution Aerosol Mass Spectrometer. *Atmospheric Chemistry and Physics Discussions* **2010**, *10*.
111. Hu, W. W.; Hu, M.; Yuan, B.; Jimenez, J. L.; Tang, Q.; Peng, J. F.; Hu, W.; Shao, M.; Wang, M.; Zeng, L. M.; Wu, Y. S.; Gong, Z. H.; Huang, X. F.; He, L. Y., Insights on organic

aerosol aging and the influence of coal combustion at a regional receptor site of central eastern China. *Atmos. Chem. Phys.* **2013**, *13* (19), 10095-10112.

112. DeCarlo, P. F.; Kimmel, J. R.; Trimborn, A.; Northway, M. J.; Jayne, J. T.; Aiken, A. C.; Gonin, M.; Fuhrer, K.; Horvath, T.; Docherty, K. S.; Worsnop, D. R.; Jimenez, J. L., Field-deployable, high-resolution, time-of-flight aerosol mass spectrometer. *Anal Chem* **2006**, *78* (24), 8281-9.

113. Huang, D. D.; Li, Y. J.; Lee, B. P.; Chan, C. K., Analysis of organic sulfur compounds in atmospheric aerosols at the HKUST supersite in Hong Kong using HR-ToF-AMS. *Environ Sci Technol* **2015**, *49* (6), 3672-9.

114. Liggió, J.; Li, S.-M., Organosulfate formation during the uptake of pinonaldehyde on acidic sulfate aerosols. *Geophysical Research Letters* **2006**, *33* (13).

115. Percival, E. G. V., 31. Carbohydrate sulphuric esters. Part III. The hydrolysis of isopropylidene glucofuranose sulphates and methylglucofuranoside sulphates. *Journal of the Chemical Society (Resumed)* **1945**, (0), 119-123.

116. Turvey, J. R., Sulfates of the Simple Sugars. In *Advances in Carbohydrate Chemistry*, Wolfrom, M. L., Ed. Academic Press: 1965; Vol. 20, pp 183-218.

117. Schroeter, L. C., Sulfurous Acid Salts as Pharmaceutical Antioxidants. *Journal of Pharmaceutical Sciences* **1961**, *50* (11), 891-901.

118. Mumma, R. O., Preparation of sulfate esters. *Lipids* **1966**, *1* (3), 221-223.

119. Nair, V.; Bernstein, S., A CONVENIENT PROCEDURE FOR THE PREPARATION OF TRIETHYLAMINE-SULFUR TRIOXIDE. *Organic Preparations and Procedures International* **1987**, *19* (6), 466-467.

120. Dusza, J. P.; Joseph, J. P.; Bernstein, S., The preparation of estradiol-17 $\beta$  sulfates with triethylamine-sulfur trioxide. *Steroids* **1985**, *45* (3), 303-315.

121. Kitagawa, K.; Aida, C.; Fujiwara, H.; Yagami, T.; Futaki, S.; Kogire, M.; Ida, J.; Inoue, K., Facile solid-phase synthesis of sulfated tyrosine-containing peptides: total synthesis of human big gastrin-II and cholecystokinin (CCK)-39. *J Org Chem* **2001**, *66* (1), 1-10.

122. Lee, J.-C.; Lu, X.-A.; Kulkarni, S. S.; Wen, Y.-S.; Hung, S.-C., Synthesis of Heparin Oligosaccharides. *Journal of the American Chemical Society* **2004**, *126* (2), 476-477.
123. Simpson, L. S.; Widlanski, T. S., A Comprehensive Approach to the Synthesis of Sulfate Esters. *Journal of the American Chemical Society* **2006**, *128* (5), 1605-1610.
124. Karst, N. A.; Islam, T. F.; Avci, F. Y.; Linhardt, R. J., Trifluoroethylsulfonate protected monosaccharides in glycosylation reactions. *Tetrahedron Letters* **2004**, *45* (34), 6433-6437.
125. Liu, Y.; Lien, I. F.; Ruttgaizer, S.; Dove, P.; Taylor, S. D., Synthesis and protection of aryl sulfates using the 2,2,2-trichloroethyl moiety. *Org Lett* **2004**, *6* (2), 209-12.
126. Ingram, L. J.; Taylor, S. D., Introduction of 2,2,2-trichloroethyl-protected sulfates into monosaccharides with a sulfuryl imidazolium salt and application to the synthesis of sulfated carbohydrates. *Angew Chem Int Ed Engl* **2006**, *45* (21), 3503-6.
127. Galloway, M. M.; Chhabra, P. S.; Chan, A. W. H.; Surratt, J. D.; Flagan, R. C.; Seinfeld, J. H.; Keutsch, F. N., Glyoxal uptake on ammonium sulphate seed aerosol: reaction products and reversibility of uptake under dark and irradiated conditions. *Atmos. Chem. Phys.* **2009**, *9* (10), 3331-3345.
128. Olson, C. N.; Galloway, M. M.; Yu, G.; Hedman, C. J.; Lockett, M. R.; Yoon, T.; Stone, E. A.; Smith, L. M.; Keutsch, F. N., Hydroxycarboxylic acid-derived organosulfates: synthesis, stability, and quantification in ambient aerosol. *Environ Sci Technol* **2011**, *45* (15), 6468-74.
129. Hettiyadura, A. P. S.; Stone, E. A.; Kundu, S.; Baker, Z.; Geddes, E.; Richards, K.; Humphry, T., Determination of atmospheric organosulfates using HILIC chromatography with MS detection. *Atmos. Meas. Tech.* **2015**, *8* (6), 2347-2358.
130. Safi Shalamzari, M.; Ryabtsova, O.; Kahnt, A.; Vermeylen, R.; Hérent, M. F.; Quetin-Leclercq, J.; Van der Veken, P.; Maenhaut, W.; Claeys, M., Mass spectrometric characterization of organosulfates related to secondary organic aerosol from isoprene. *Rapid Commun Mass Spectrom* **2013**, *27* (7), 784-94.
131. Staudt, S.; Kundu, S.; Lehmler, H.-J.; He, X.; Cui, T.; Lin, Y.-H.; Kristensen, K.; Glasius, M.; Zhang, X.; Weber, R. J.; Surratt, J. D.; Stone, E. A., Aromatic organosulfates in atmospheric aerosols: synthesis, characterization, and abundance. *Atmos Environ (1994)* **2014**, *94*, 366-373.

132. Gilbert, E. E., The Reactions of Sulfur Trioxide, and Its Adducts, with Organic Compounds. *Chemical Reviews* **1962**, 62 (6), 549-589.
133. Gill, D. M.; Male, L.; Jones, A. M., Sulfation made simple: a strategy for synthesising sulfated molecules. *Chemical Communications* **2019**, 55 (30), 4319-4322.
134. Alshehri, J. A.; Benedetti, A. M.; Jones, A. M., A novel exchange method to access sulfated molecules. *Scientific Reports* **2020**, 10 (1), 16559.
135. Tserng, K. Y.; Klein, P. D., Synthesis of sulfate esters of lithocholic acid, glycolithocholic acid, and tauroolithocholic acid with sulfur trioxide-triethylamine. *J Lipid Res* **1977**, 18 (4), 491-5.
136. Pangborn, A. B.; Giardello, M. A.; Grubbs, R. H.; Rosen, R. K.; Timmers, F. J., Safe and Convenient Procedure for Solvent Purification. *Organometallics* **1996**, 15 (5), 1518-1520.
137. Armarego, W. L. F.; Perrin, D. D., *Purification of Laboratory Chemical*. 3rd ed.; Pergamon Press: Oxford, 1988.
138. Völkert, M.; Uwai, K.; Tebbe, A.; Popkirova, B.; Wagner, M.; Kuhlmann, J.; Waldmann, H., Synthesis and Biological Activity of Photoactivatable N-Ras Peptides and Proteins. *J. Am. Chem. Soc.* **2003**, 125 (42), 12749-12758.
139. Wolfenden, R.; Yuan, Y., Monoalkyl sulfates as alkylating agents in water, alkylsulfatase rate enhancements, and the "energy-rich" nature of sulfate half-esters. *Proc Natl Acad Sci U S A* **2007**, 104 (1), 83-6.
140. Benkovic, S. J.; Hevey, R. C., Studies in sulfate esters. V. Mechanism of hydrolysis of phenyl phosphosulfate, a model system for 3'-phosphoadenosine 5'-phosphosulfate. *Journal of the American Chemical Society* **1970**, 92 (16), 4971-4977.
141. Benkovic, S. J., Studies on Sulfate Esters. II. Carboxyl Group Catalysis in the Hydrolysis of Salicyl Sulfate. *Journal of the American Chemical Society* **1966**, 88 (23), 5511-5515.
142. Tcacenco, C. M.; Zana, R.; Bales, B. L., Effect of the nature of the counterion on the properties of anionic surfactants. 5. Self-association behavior and micellar properties of ammonium dodecyl sulfate. *J Phys Chem B* **2005**, 109 (33), 15997-6004.

143. Tabatabai, M. A., Physicochemical Fate of Sulfate in Soils. *JAPCA* **1987**, *37* (1), 34-38.
144. Xu, R.; Ge, Y.; Kwong, K. C.; Poon, H. Y.; Wilson, K. R.; Yu, J. Z.; Chan, M. N., Inorganic Sulfur Species Formed upon Heterogeneous OH Oxidation of Organosulfates: A Case Study of Methyl Sulfate. *ACS Earth and Space Chemistry* **2020**, *4* (11), 2041-2049.
145. Hu, K. S.; Darer, A. I.; Elrod, M. J., Thermodynamics and kinetics of the hydrolysis of atmospherically relevant organonitrates and organosulfates. *Atmospheric Chemistry and Physics* **2011**, *11* (16), 8307-8320.
146. Aoki, E.; Sarrimanolis, J. N.; Lyon, S. A.; Elrod, M. J., Determining the Relative Reactivity of Sulfate, Bisulfate, and Organosulfates with Epoxides on Secondary Organic Aerosol. *ACS Earth and Space Chemistry* **2020**, *4* (10), 1793-1801.
147. Darer, A. I.; Cole-Filipiak, N. C.; O'Connor, A. E.; Elrod, M. J., Formation and Stability of Atmospherically Relevant Isoprene-Derived Organosulfates and Organonitrates. *Environmental Science & Technology* **2011**, *45* (5), 1895-1902.
148. Darer, A. I.; Cole-Filipiak, N. C.; O'Connor, A. E.; Elrod, M. J., Formation and stability of atmospherically relevant isoprene-derived organosulfates and organonitrates. *Environ Sci Technol* **2011**, *45* (5), 1895-902.
149. Bé, A. G.; Liu, Y.; Tuladhar, A.; Bellcross, A. D.; Wang, Z.; Thomson, R. J.; Geiger, F. M., Surface-Active  $\beta$ -Caryophyllene Oxidation Products at the Air/Aqueous Interface. *ACS Earth and Space Chemistry* **2019**, *3* (9), 1740-1748.
150. Gray Bé, A.; Upshur, M. A.; Liu, P.; Martin, S. T.; Geiger, F. M.; Thomson, R. J., Cloud Activation Potentials for Atmospheric  $\alpha$ -Pinene and  $\beta$ -Caryophyllene Ozonolysis Products. *ACS Cent Sci* **2017**, *3* (7), 715-725.
151. Tang, C.; Ding, K.; Liu, Y.; Yu, S.; Chen, J.; Feng, X.; Zhang, C.; Chen, J., Quantitative relationship between the structures and properties of VOCs and SOA formation on the surfaces of acidic aerosol particles. *Physical Chemistry Chemical Physics* **2021**, *23* (21), 12360-12370.
152. Zhu, J.; Penner, J. E.; Lin, G.; Zhou, C.; Xu, L.; Zhuang, B., Mechanism of SOA formation determines magnitude of radiative effects. *Proceedings of the National Academy of Sciences* **2017**, *114* (48), 12685-12690.

153. Jubb, A. M.; Hua, W.; Allen, H. C., Environmental Chemistry at Vapor/Water Interfaces: Insights from Vibrational Sum Frequency Generation Spectroscopy. *Annual Review of Physical Chemistry* **2012**, *63* (1), 107-130.
154. Geiger, F. M., Second Harmonic Generation, Sum Frequency Generation, and  $\chi(3)$ : Dissecting Environmental Interfaces with a Nonlinear Optical Swiss Army Knife. *Annual Review of Physical Chemistry* **2009**, *60* (1), 61-83.
155. Reddy, S. K.; Thiriaux, R.; Wellen Rudd, B. A.; Lin, L.; Adel, T.; Joutsuka, T.; Geiger, F. M.; Allen, H. C.; Morita, A.; Paesani, F., Bulk Contributions Modulate the Sum-Frequency Generation Spectra of Water on Model Sea-Spray Aerosols. *Chem* **2018**, *4* (7), 1629-1644.
156. Shen, Y. R., Surface properties probed by second-harmonic and sum-frequency generation. *Nature* **1989**, *337* (6207), 519-525.
157. Ebben, C. J.; Ault, A. P.; Ruppel, M. J.; Ryder, O. S.; Bertram, T. H.; Grassian, V. H.; Prather, K. A.; Geiger, F. M., Size-Resolved Sea Spray Aerosol Particles Studied by Vibrational Sum Frequency Generation. *The Journal of Physical Chemistry A* **2013**, *117* (30), 6589-6601.
158. Ebben, C. J.; Shrestha, M.; Martinez, I. S.; Corrigan, A. L.; Frossard, A. A.; Song, W. W.; Worton, D. R.; Petäjä, T.; Williams, J.; Russell, L. M.; Kulmala, M.; Goldstein, A. H.; Artaxo, P.; Martin, S. T.; Thomson, R. J.; Geiger, F. M., Organic Constituents on the Surfaces of Aerosol Particles from Southern Finland, Amazonia, and California Studied by Vibrational Sum Frequency Generation. *The Journal of Physical Chemistry A* **2012**, *116* (32), 8271-8290.
159. Martinez, I. S.; Peterson, M. D.; Ebben, C. J.; Hayes, P. L.; Artaxo, P.; Martin, S. T.; Geiger, F. M., On molecular chirality within naturally occurring secondary organic aerosol particles from the central Amazon Basin. *Physical Chemistry Chemical Physics* **2011**, *13* (26), 12114-12122.
160. Shiraiwa, M.; Zuend, A.; Bertram, A. K.; Seinfeld, J. H., Gas-particle partitioning of atmospheric aerosols: interplay of physical state, non-ideal mixing and morphology. *Phys. Chem. Chem. Phys.* **2013**, *15* (27), 11441-11453.
161. Shrivastava, M.; Cappa, C. D.; Fan, J.; Goldstein, A. H.; Guenther, A. B.; Jimenez, J. L.; Kuang, C.; Laskin, A.; Martin, S. T.; Ng, N. L.; Petaja, T.; Pierce, J. R.; Rasch, P. J.; Roldin, P.; Seinfeld, J. H.; Shilling, J.; Smith, J. N.; Thornton, J. A.; Volkamer, R.; Wang, J.; Worsnop, D. R.; Zaveri, R. A.; Zelenyuk, A.; Zhang, Q., Recent advances in understanding secondary organic aerosol: Implications for global climate forcing. *Rev. Geophys.* **2017**, *55* (2), 509-559.

162. Liu, P.; Song, M.; Zhao, T.; Gunthe, S. S.; Ham, S.; He, Y.; Qin, Y. M.; Gong, Z.; Amorim, J. C.; Bertram, A. K.; Martin, S. T., Resolving the mechanisms of hygroscopic growth and cloud condensation nuclei activity for organic particulate matter. *Nat. Commun.* **2018**, *9* (1), 4076.
163. Gray Bé, A.; Upshur, M. A.; Liu, P.; Martin, S. T.; Geiger, F. M.; Thomson, R. J., Cloud Activation Potentials for Atmospheric  $\alpha$ -Pinene and  $\beta$ -Caryophyllene Ozonolysis Products. *ACS Cent. Sci.* **2017**, *3* (7), 715-725.
164. Reid, J. P.; Bertram, A. K.; Topping, D. O.; Laskin, A.; Martin, S. T.; Petters, M. D.; Pope, F. D.; Rovelli, G., The viscosity of atmospherically relevant organic particles. *Nat. Commun.* **2018**, *9* (1), 956.
165. Liu, P.; Li, Y. J.; Wang, Y.; Bateman, A. P.; Zhang, Y.; Gong, Z.; Bertram, A. K.; Martin, S. T., Highly Viscous States Affect the Browning of Atmospheric Organic Particulate Matter. *ACS Cent. Sci.* **2018**, *4* (2), 207-215.
166. Jang, M.; Czoschke, N. M.; Lee, S.; Kamens, R. M., Heterogeneous Atmospheric Aerosol Production by Acid-Catalyzed Particle-Phase Reactions. *Science* **2002**, *298* (5594), 814-817.
167. Qin, Y.; Ye, J.; Ohno, P. E.; Lei, Y.; Wang, J.; Liu, P.; Thomson, R. J.; Martin, S. T., Synergistic Uptake by Acidic Sulfate Particles of Gaseous Mixtures of Glyoxal and Pinanediol. *Environ. Sci. Technol.* **2020**, *54* (19), 11762-11770.
168. Gong, Z.; Han, Y.; Liu, P.; Ye, J.; Keutsch, F. N.; McKinney, K. A.; Martin, S. T., Influence of Particle Physical State on the Uptake of Medium-Sized Organic Molecules. *Environ. Sci. Technol.* **2018**, *52* (15), 8381-8389.
169. Han, Y.; Gong, Z.; Ye, J.; Liu, P.; McKinney, K. A.; Martin, S. T., Quantifying the Role of the Relative Humidity-Dependent Physical State of Organic Particulate Matter in the Uptake of Semivolatile Organic Molecules. *Environ. Sci. Technol.* **2019**, *53* (22), 13209-13218.
170. Surratt, J. D.; Chan, A. W. H.; Eddingsaas, N. C.; Chan, M.; Loza, C. L.; Kwan, A. J.; Hersey, S. P.; Flagan, R. C.; Wennberg, P. O.; Seinfeld, J. H., Reactive intermediates revealed in secondary organic aerosol formation from isoprene. *Proc. Natl. Acad. Sci. U.S.A.* **2010**, *107* (15), 6640-6645.

171. Hettiyadura, A. P. S.; Jayarathne, T.; Baumann, K.; Goldstein, A. H.; de Gouw, J. A.; Koss, A.; Keutsch, F. N.; Skog, K.; Stone, E. A., Qualitative and quantitative analysis of atmospheric organosulfates in Centreville, Alabama. *Atmos. Chem. Phys.* **2017**, *17* (2), 1343-1359.
172. Kroll, J. H.; Donahue, N. M.; Jimenez, J. L.; Kessler, S. H.; Canagaratna, M. R.; Wilson, K. R.; Altieri, K. E.; Mazzoleni, L. R.; Wozniak, A. S.; Bluhm, H.; Mysak, E. R.; Smith, J. D.; Kolb, C. E.; Worsnop, D. R., Carbon oxidation state as a metric for describing the chemistry of atmospheric organic aerosol. *Nat Chem* **2011**, *3* (2), 133-9.
173. Bianchi, F.; Kurtén, T.; Riva, M.; Mohr, C.; Rissanen, M. P.; Roldin, P.; Berndt, T.; Crouse, J. D.; Wennberg, P. O.; Mentel, T. F.; Wildt, J.; Junninen, H.; Jokinen, T.; Kulmala, M.; Worsnop, D. R.; Thornton, J. A.; Donahue, N.; Kjaergaard, H. G.; Ehn, M., Highly Oxygenated Organic Molecules (HOM) from Gas-Phase Autoxidation Involving Peroxy Radicals: A Key Contributor to Atmospheric Aerosol. *Chemical Reviews* **2019**, *119* (6), 3472-3509.
174. Crouse, J. D.; Nielsen, L. B.; Jørgensen, S.; Kjaergaard, H. G.; Wennberg, P. O., Autoxidation of Organic Compounds in the Atmosphere. *The Journal of Physical Chemistry Letters* **2013**, *4* (20), 3513-3520.
175. Iyer, S.; Rissanen, M. P.; Valiev, R.; Barua, S.; Krechmer, J. E.; Thornton, J.; Ehn, M.; Kurtén, T., Molecular mechanism for rapid autoxidation in  $\alpha$ -pinene ozonolysis. *Nature Communications* **2021**, *12* (1), 878.
176. Roldin, P.; Ehn, M.; Kurtén, T.; Olenius, T.; Rissanen, M. P.; Sarnela, N.; Elm, J.; Rantala, P.; Hao, L.; Hyttinen, N.; Heikkinen, L.; Worsnop, D. R.; Pichelstorfer, L.; Xavier, C.; Clusius, P.; Öström, E.; Petäjä, T.; Kulmala, M.; Vehkamäki, H.; Virtanen, A.; Riipinen, I.; Boy, M., The role of highly oxygenated organic molecules in the Boreal aerosol-cloud-climate system. *Nature Communications* **2019**, *10* (1), 4370.
177. Wang, Y.; Riva, M.; Xie, H.; Heikkinen, L.; Schallhart, S.; Zha, Q.; Yan, C.; He, X. C.; Peräkylä, O.; Ehn, M., Formation of highly oxygenated organic molecules from chlorine-atom-initiated oxidation of alpha-pinene. *Atmos. Chem. Phys.* **2020**, *20* (8), 5145-5155.
178. Berndt, T.; Richters, S.; Kaethner, R.; Voigtländer, J.; Stratmann, F.; Sipilä, M.; Kulmala, M.; Herrmann, H., Gas-Phase Ozonolysis of Cycloalkenes: Formation of Highly Oxidized RO<sub>2</sub> Radicals and Their Reactions with NO, NO<sub>2</sub>, SO<sub>2</sub>, and Other RO<sub>2</sub> Radicals. *The Journal of Physical Chemistry A* **2015**, *119* (41), 10336-10348.

179. Docherty, K. S.; Wu, W.; Lim, Y. B.; Ziemann, P. J., Contributions of organic peroxides to secondary aerosol formed from reactions of monoterpenes with O<sub>3</sub>. *Environ Sci Technol* **2005**, *39* (11), 4049-59.
180. Aljawhary, D.; Zhao, R.; Lee, A. K. Y.; Wang, C.; Abbatt, J. P. D., Kinetics, Mechanism, and Secondary Organic Aerosol Yield of Aqueous Phase Photo-oxidation of  $\alpha$ -Pinene Oxidation Products. *The Journal of Physical Chemistry A* **2016**, *120* (9), 1395-1407.
181. Upshur, M. A.; Vega, M. M.; Bé, A. G.; Chase, H. M.; Zhang, Y.; Tuladhar, A.; Chase, Z. A.; Fu, L.; Ebben, C. J.; Wang, Z.; Martin, S. T.; Geiger, F. M.; Thomson, R. J., Synthesis and surface spectroscopy of  $\alpha$ -pinene isotopologues and their corresponding secondary organic material. *Chemical Science* **2019**, *10* (36), 8390-8398.
182. Tomaz, S.; Wang, D.; Zabalegui, N.; Li, D.; Lamkaddam, H.; Bachmeier, F.; Vogel, A.; Monge, M. E.; Perrier, S.; Baltensperger, U.; George, C.; Rissanen, M.; Ehn, M.; El Haddad, I.; Riva, M., Structures and reactivity of peroxy radicals and dimeric products revealed by online tandem mass spectrometry. *Nature Communications* **2021**, *12* (1), 300.
183. Zhao, Y.; Thornton, J. A.; Pye, H. O. T., Quantitative constraints on autoxidation and dimer formation from direct probing of monoterpene-derived peroxy radical chemistry. *Proceedings of the National Academy of Sciences* **2018**, *115* (48), 12142-12147.
184. Schervish, M.; Donahue, N. M., Peroxy radical chemistry and the volatility basis set. *Atmos. Chem. Phys.* **2020**, *20* (2), 1183-1199.
185. Berndt, T.; Hyttinen, N.; Herrmann, H.; Hansel, A., First oxidation products from the reaction of hydroxyl radicals with isoprene for pristine environmental conditions. *Communications Chemistry* **2019**, *2* (1), 21.
186. Müller, J.-F.; Liu, Z.; Nguyen, V. S.; Stavrou, T.; Harvey, J. N.; Peeters, J., The reaction of methyl peroxy and hydroxyl radicals as a major source of atmospheric methanol. *Nature Communications* **2016**, *7* (1), 13213.
187. Xu, L.; Møller, K. H.; Crouse, J. D.; Otkjær, R. V.; Kjaergaard, H. G.; Wennberg, P. O., Unimolecular Reactions of Peroxy Radicals Formed in the Oxidation of  $\alpha$ -Pinene and  $\beta$ -Pinene by Hydroxyl Radicals. *The Journal of Physical Chemistry A* **2019**, *123* (8), 1661-1674.

188. Ren, X.; Brune, W. H.; Cantrell, C. A.; Edwards, G. D.; Shirley, T.; Metcalf, A. R.; Leshner, R. L., Hydroxyl and Peroxy Radical Chemistry in a Rural Area of Central Pennsylvania: Observations and Model Comparisons. *Journal of Atmospheric Chemistry* **2005**, *52* (3), 231-257.
189. He, S.; Carmichael, G., Sensitivity of photolysis rates and ozone production in the troposphere to aerosol properties. *Journal of Geophysical Research* **1999**, *104*, 26307-26324.
190. Thornton, J.; Wooldridge, P.; Cohen, R.; Martínez, M.; Harder, H.; Brune, W.; Williams, E.; Roberts, J. M.; Fehsenfeld, F.; Hall, S.; Shetter, R.; Wert, B.; Fried, A., Ozone production rates as a function of NO<sub>x</sub> abundances and HO<sub>x</sub> production rates in the Nashville urban plume. *Journal of Geophysical Research* **2002**, *107*, 4146.
191. Praske, E.; Otkjær, R. V.; Crouse, J. D.; Hethcox, J. C.; Stoltz, B. M.; Kjaergaard, H. G.; Wennberg, P. O., Atmospheric autoxidation is increasingly important in urban and suburban North America. *Proceedings of the National Academy of Sciences* **2018**, *115* (1), 64-69.
192. Teng, A. P.; Crouse, J. D.; Wennberg, P. O., Isoprene Peroxy Radical Dynamics. *Journal of the American Chemical Society* **2017**, *139* (15), 5367-5377.
193. Møller, K. H.; Praske, E.; Xu, L.; Crouse, J. D.; Wennberg, P. O.; Kjaergaard, H. G., Stereoselectivity in Atmospheric Autoxidation. *J Phys Chem Lett* **2019**, *10* (20), 6260-6266.
194. Vasquez, K.; Allen, H.; Crouse, J.; Praske, E.; Xu, L.; Noelscher, A. C.; Wennberg, P., Low-pressure gas chromatography with chemical ionization mass spectrometry for quantification of multifunctional organic compounds in the atmosphere. *Atmospheric Measurement Techniques* **2018**, *11*, 6815-6832.
195. Thomas, M. T.; Fallis, A. G., The total synthesis of (+)-.alpha.- and (+)-.beta.-pinene. A general route to bicyclic mono- and sesquiterpenes. *Journal of the American Chemical Society* **1976**, *98* (5), 1227-1231.

**Appendix**

## Investigation of the binding mode of Eudistomin U to DNA

Jonathan Gregory Varelas

### Abstract

Eudistomin U is a naturally-occurring indole alkaloid within a chemical family known as  $\beta$ -carboline. These molecules have a wide array of biological activity and have been seen as valuable pharmacophores for drug targeting. Though the compound has been suggested to have multiple biological targets, eudistomin U has exhibited a high binding affinity to DNA. This has made eudistomin U and other  $\beta$ -carboline attractive targets for total synthesis. Though there have been evaluations of the interaction between this compound and DNA, the specific binding profile of eudistomin U to DNA – whether acting as an intercalator, groove binder or binds electrostatically – remains elusive.

Here, a series of biological experiments and a potential synthetic methodology to derivatize eudistomin U are proposed. In order to better understand the variables influencing the binding affinity of the natural compound to DNA, a series of mutant strands containing only complementary base pairs will be generated (e.g. GCGC...,ATAT...). The use of these simplified sequences will enable the determination of eudistomin U to act as an intercalator between specific base pairs of DNA, and the comparison with known intercalators will provide further information regarding the binding interaction in question. A crystalline structure of eudistomin U to DNA will also be evaluated once the optimal base pair configuration is understood.

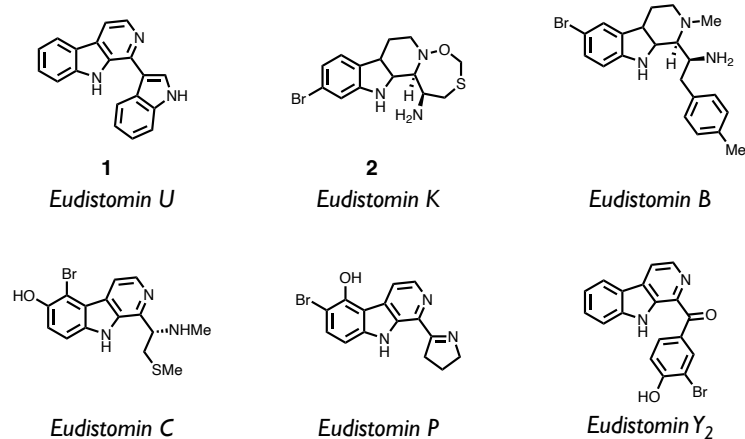
In order to probe other potential interactions with DNA, a synthetic methodology employing a “tethered” strategy will also be investigated. The proposed method is based on functionalizing the natural eudistomin U compound to join the pyridyl nitrogen and the adjacent 2-position of the indole ring to lock the spatial conformation into place. This methodology could

provide further evidence towards classifying eudistomin U as an intercalator or provide evidence of major or minor groove binding if the newly annulated molecule has high complementarity with the inner or outer groove of DNA.

## Introduction

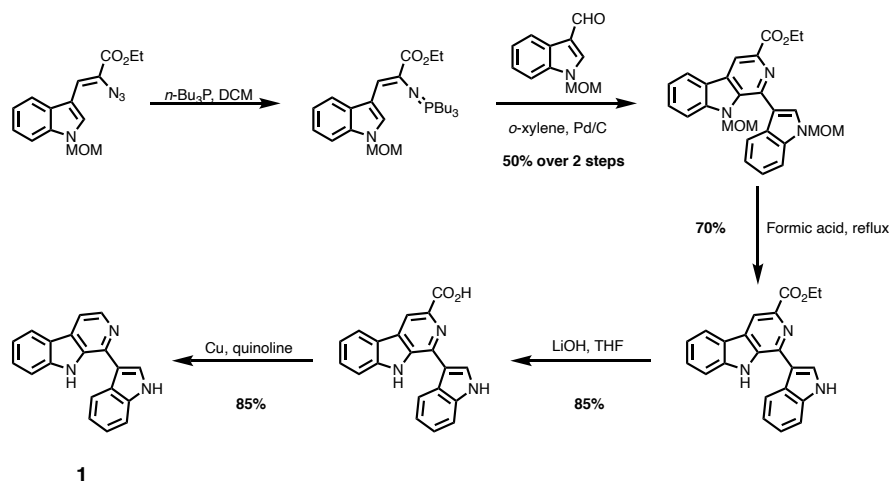
Pyrido[3,4-b]indole alkaloids, commonly known as  $\beta$ -carbolines, are a class of alkaloids that exist as secondary metabolites in many living organisms.<sup>1</sup> Members of a particular family of  $\beta$ -carboline natural products known as the eudistomins have been isolated from several species of marine ascidians,<sup>2</sup> and the group of compounds has a wide array of structural diversity (**Figure A.1**). The eudistomins also show a wide-ranging biological activity profile, making them attractive targets for synthetic chemists. Nearly half of all eudistomin alkaloids exhibit antimicrobial activity,<sup>1,3</sup> while others demonstrate affinity as antivirals against herpes simplex-1 and polio type-1 virus.<sup>4-6</sup> Selective inhibition of mammalian cancer cell lines has also been shown by many family members. Extending beyond naturally occurring species such as eudistomin U (**1**), a synthetic analogue of eudistomin K (**2**) was shown to exhibit subnanogram potency towards various leukemic cells, demonstrating the utility of eudistomin compounds as privileged lead structures in drug development.<sup>7</sup>

**Figure A.1.** Several examples of the eudistomin family that exhibit potent biological activity.



Due to their planar, drug-like structure and potent activity towards several diverse organisms, it has been suggested that the eudistomins interact with their biological targets primarily through binding to DNA.<sup>8</sup> Focusing specifically on one member of this family of compounds, eudistomin U (**1**) was first isolated in 1994 along with its saturated derivative isoeudistomin U from the caribbean ascidian *Lissoclinum fragile*.<sup>8-9</sup> Eudistomin U is the only naturally occurring eudistomin with a fully aromatic group at the 1 position on the pyridine ring of the β-carboline core. Structural features such as the free rotation around the σ-bond joining the carboline scaffold with the indole moiety has sparked the interest of the synthetic community, and a number of total syntheses of eudistomin U have been reported.

The first successful synthesis of eudistomin U was completed by Molina and coworkers in 1995 which employed an aza-Wittig-electrocyclic ring closure strategy which led to the target alkaloid (**Scheme A.1**).<sup>10</sup> In the past decades, a number of additional syntheses towards eudistomin U have been disclosed.<sup>11-13</sup>

**Scheme A.1** Molina's synthesis of Eudistomin U, 1995

Although the synthesis of eudistomin U has been the focus of many synthetic efforts, the mechanism of action towards its wide variety of biological targets remains poorly understood. As previously stated, it has been suggested that eudistomins primarily interact via binding to DNA, but efforts to elucidate relationship between DNA and eudistomins has not been sufficiently investigated. In 2016, Giulietti and coworkers disclosed a series of experiments to investigate the binding of eudistomin U and various strains of representative DNA.<sup>14</sup> While this study confirmed a weak complexing between the two, the specific interaction between eudistomin U and DNA requires a more in-depth inquiry.

### Specific Aims and Intellectual Merit

The goal of this proposal is to provide a definitive binding mode between eudistomin U and DNA. If successful, this work will not only offer the first conclusive model between this alkaloid and its potential target, but will also illuminate the general binding profile of other structurally related eudistomins. This work will also enable more informed drug development procedures utilizing eudistomins as promising leads and will potentially result in a more robust

approach to structural derivatization and improved structure-activity profiling of these species upon their pharmacological targets.

***Specific Aim 1:*** Illumination of the interaction between eudistomin U and DNA will employ the use of synthetic mutant strands of DNA generated by the polymerase chain reaction (PCR). In order to definitively model this interaction, DNA strands consisting solely of complementary base pairs will be assigned the interaction mechanism. Using this approach will provide insight into the potential of eudistomin U to act as an intercalator between certain base pair arrangements, as it will suggest a preferred binding to certain sequences within DNA. Comparison with known intercalators will also enable the definitive classification of eudistomin U as a possible intercalating compound.

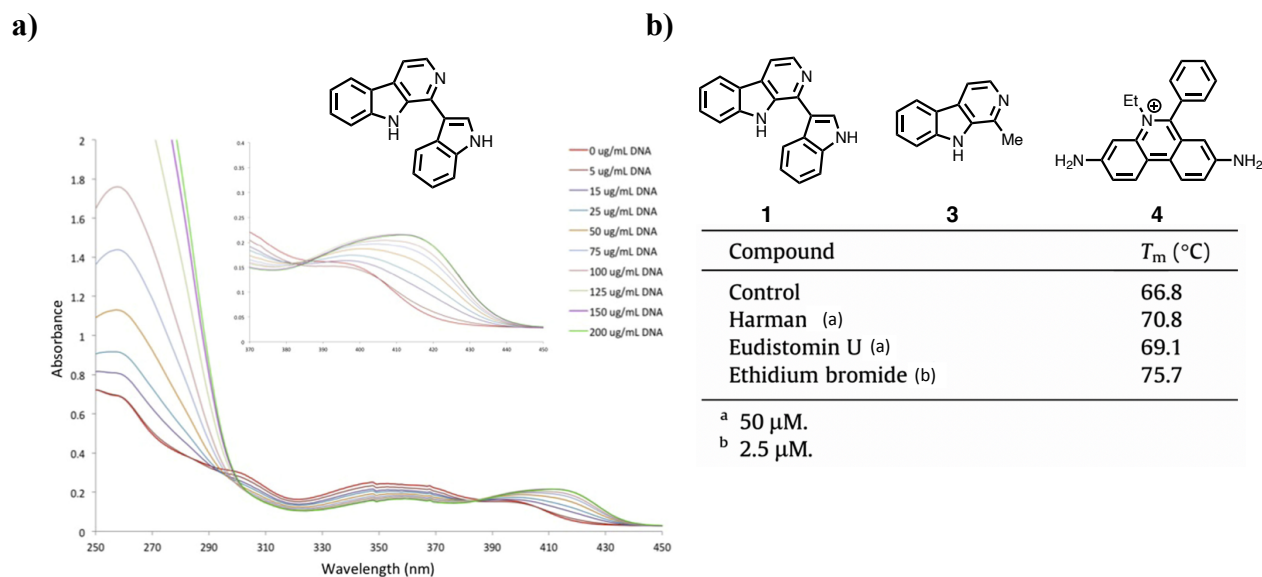
***Specific Aim 2:*** Once the general profile of preferential interfacing of eudistomin U towards DNA is established with the model strands in specific aim 1, a synthetic methodology to derivatize eudistomin U will be used to evaluate how potential structural changes will bolster or diminish binding affinity. Applying an extension of indole functionalization methodology disclosed by Pan and coworkers will enable an additional annulation to join the pyridyl nitrogen of the carboline scaffold with the indole substituent to restrict rotational movement of the molecule, forcing a helical geometry. The generation of this species will enable the definitive assignment of eudistomin U as a potential major or minor groove binder if the geometries of the DNA strand and the proposed analogue of eudistomin are highly complementary.

### **Previous Work**

***With respect to specific aim 1:*** While the synthesis of eudistomin U is a mature field, the evaluation of its preferential interaction with DNA remains elusive. In 2016, Giulietti and coworkers disclosed their findings concerning eudistomin U and calf thymus DNA using a

synthetic standard made in house.<sup>14</sup> The authors first evaluated spectral changes to samples of eudistomin U after doping with increasing concentrations of calf thymus DNA using UV-Vis spectroscopy. It was found that the spectra containing higher concentrations of DNA revealed a dramatic hyperchromic shift, indicative of a simple interaction with DNA (**Figure A.2a**). These results were in line with behavior exhibited by small molecules known to be intercalators, such as harman (**3**) and ethidium bromide (**4**).

**Figure A.2 (a)** UV-Vis spectra of calf thymus DNA and eudistomin U. **(b)** Thermal denaturation of DNA in the presence of eudistomin U compared to known intercalators. Figures adapted from Giulietti and coworkers, 2016.<sup>14</sup>

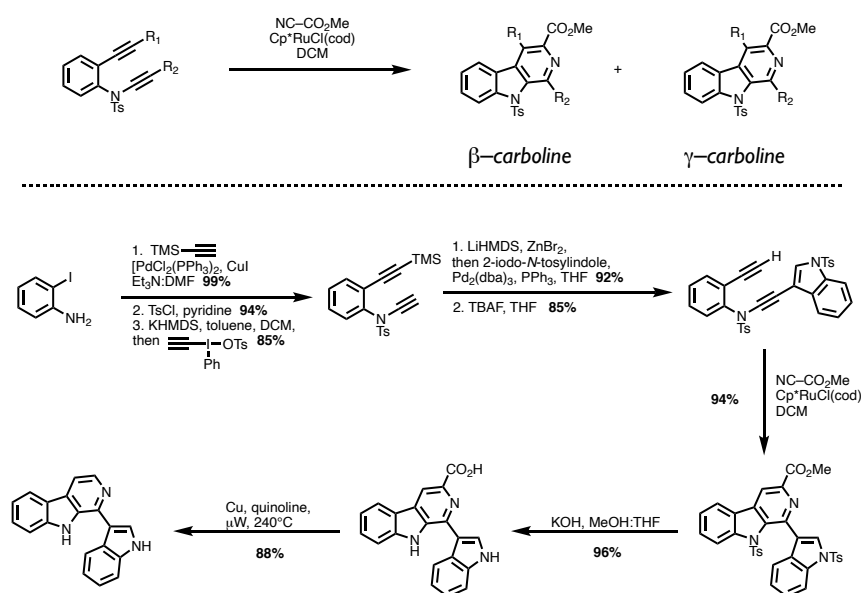


In the same study, the thermal denaturation of calf thymus DNA in the presence of eudistomin U was carried out. Canonically, thermal denaturation is used to measure disruptions to the double helix of DNA, resulting in higher or lower thermal energy required to denature if the

molecule stabilizes or destabilizes the strands respectively. It was found that eudistomin U disrupted the integrity of DNA on a level comparable to harman, a lowly intercalating molecule, having demonstrated a similar  $T_m$ , or the temperature at which a double helix unwinds to two single helices (**Figure A.2b**).

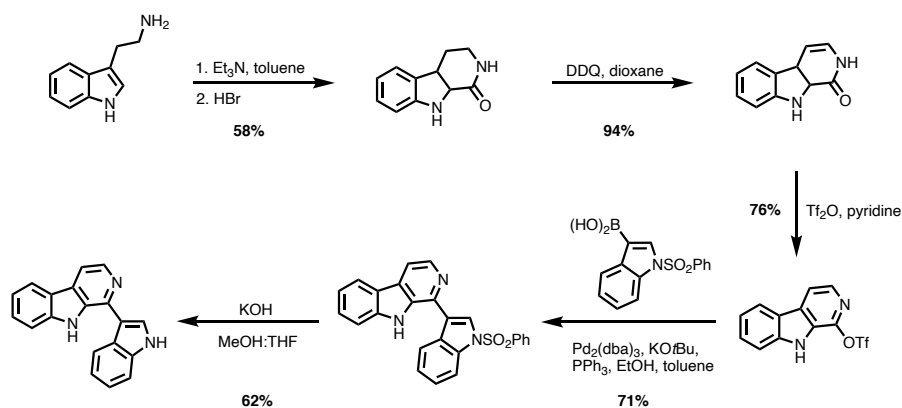
**With respect to specific aim 2:** The synthesis of eudistomin U has been completed several times. Molina's synthesis in 1995 was the first reported synthesis of the molecule (**Scheme A.1**). More recently, Nissen and coworkers disclosed a method to generate  $\beta$ - and  $\gamma$ -carbolines in 2011.<sup>11</sup> Their method involved ruthenium and rhodium catalyzed intermolecular [2+2+2] cycloadditions to afford both isomeric carbolines and extended this methodology further towards the synthesis of eudistomin U (**Scheme A.2**)

**Scheme A.2** Methodology to afford  $\beta$ - and  $\gamma$ -carbolines using transition metal catalyzed [2+2+2] cyclization and its use in the synthesis of eudistomin U. Scheme adapted from Pan *et al*, 2011.<sup>11</sup>



In 2014, Roggero and coworkers disclosed a synthesis of eudistomin U utilizing a Bischler-Napieralski cyclization to form the core  $\beta$ -carboline as an aryl triflate, and a Suzuki cross-coupling with an indole bearing a pendant boronic acid to form the target molecule.<sup>15</sup> This particular synthesis remains the shortest linear sequence towards eudistomin U (**Scheme A.3**).

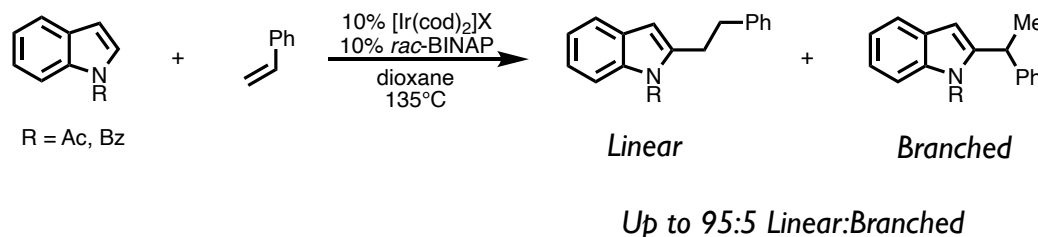
**Scheme A.3** Synthesis of eudistomin U reported by Roggero and coworkers, 2014.<sup>15</sup>



In 2018, Zhang and coworkers disclosed a synthetic methodology towards the synthesis of 2 and 3-substituted indoles using carbazole-based conjugated microporous polymers with tunable redox potentials. This powerful methodology resulted in functionalized indoles bearing pendant formyl and thiocyanide functional groups (**Figure A.3**).



**Scheme A.4** Methodology to afford C-2 functionalized indoles disclosed by Pan *et al*, 2012.



### Proposed Research

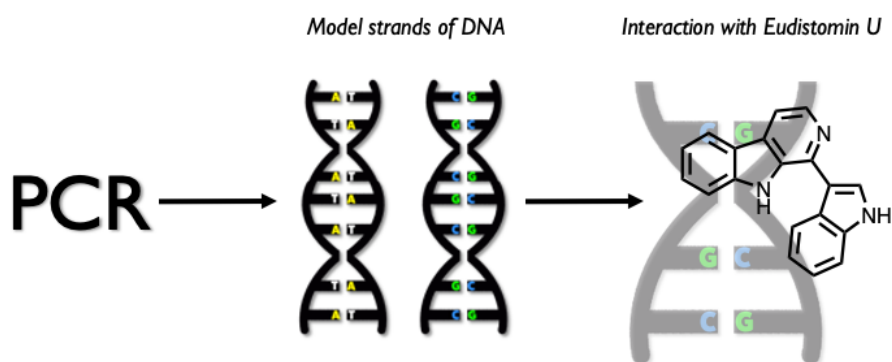
With the landscape of research concerning eudistomin U, its synthesis and its potential activity with DNA laid out, the proposed research will entail two phases. Phase one will involve the synthesis of model, highly idealized strands of DNA in order to probe the propensity of eudistomin U to act as an intercalator as a function of specific basepairs. Phase two will involve the structural derivatization of eudistomin U via organic synthesis in order to restrict the conformation of the molecule to better probe its specific interaction with DNA.

*Phase one* will begin with the generation of model strands of DNA. There are several covalent and non-covalent modes in which small molecules interact with and bind to DNA. Molecules such as eudistomin U and other small, planar alkaloids have been shown to interact non-covalently with DNA.<sup>18-19</sup> Some of the most frequently encountered modes include: intercalation, or insertion of molecular moieties between base pairs; electrostatic, or the exterior complex of a small molecule and DNA via innate charge; and major/minor groove binding, or the exterior binding of a molecule to the respective groove of DNA. In order to eliminate some complexity likely to preclude the observation of a specific binding interaction, idealized strands of DNA will be produced using the polymerase chain reaction, or PCR, a canonical method of generating synthetic strands of DNA with a desired sequence of base pairs.<sup>20</sup>

The two idealized DNA strands will consist of solely complementary base pairings in order to examine which base pairs facilitate a stronger interaction with eudistomin U (**Figure A.4**). Di-

nucleotide repeats (e.g ATAT..., CGCG...) will be used as the primers for replication. A process disclosed by Lorenz will be utilized in order to produce these strands.<sup>20</sup> This will likely be a relatively simple procedure to carry out, but in case the complementarity of the strands results in some geometric abnormalities in the resultant strands of DNA, a slightly modified primer will be used such that there will be a repeating sequence of four base pairs, followed by the inverse of the pattern (e.g TATAATATTATA..., CGCGGCGCCGCG...). The use of this slightly modified strand will still eliminate most other variables as model systems to probe the interaction between DNA and eudistomin U.

**Figure A.4** The use of the polymerase chain reaction will enable the synthesis of two model DNA strands in order to accurately describe their interactions with eudistomin U as a consequence of base pairing.



Upon synthesizing the two model systems, each strand will be subject to a suite of experiments with eudistomin U, as well as other small molecules known to interact with DNA. First, UV-Vis spectroscopy will be used in order to examine a series of titrations of each strand of DNA being added to a solution of eudistomin U. When a small molecule binds to DNA through binding mechanisms such as intercalation or groove binding, spectral changes such as hyperchromic shifts will occur that are known to be concentration-dependent.<sup>21</sup> Therefore, titrations of each strand into solution with eudistomin U followed by examination with UV-Vis

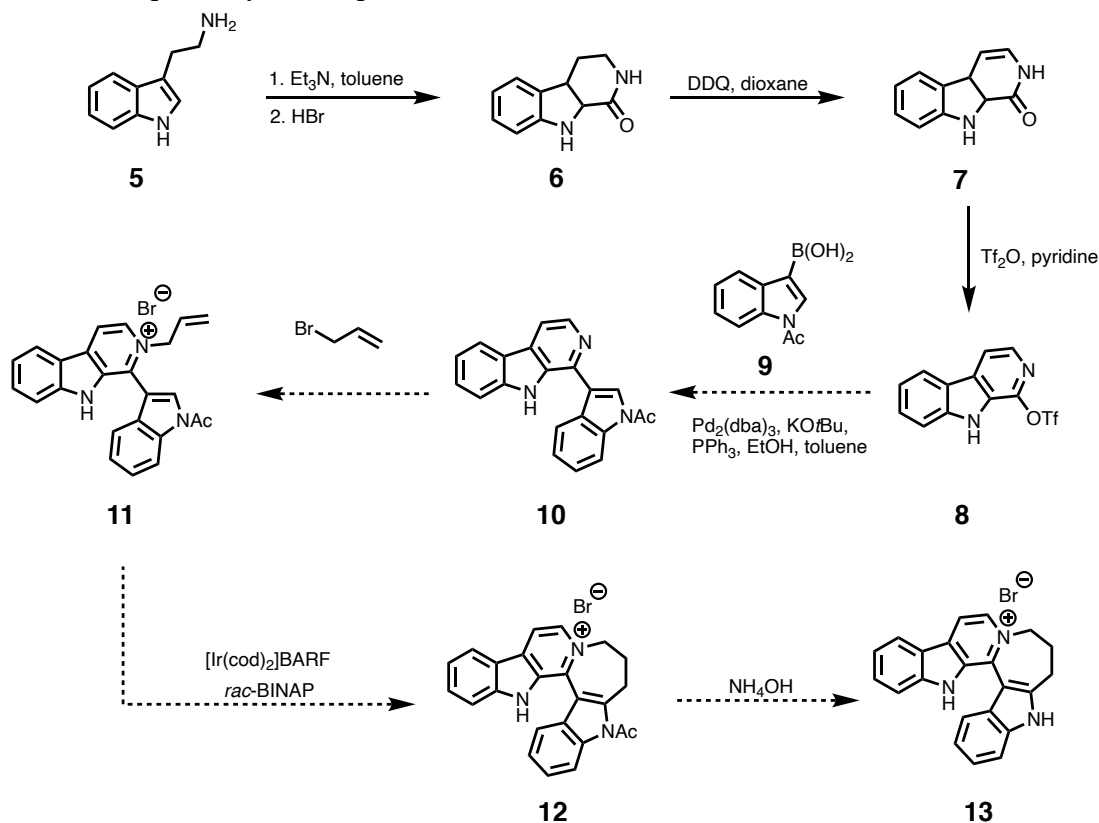
spectroscopy will be conducted in order to visualize such changes. In a recent paper, eudistomin U was subjected to a series of titrations of calf thymus DNA.<sup>14</sup> While the reported experiments demonstrated a simple reaction between the natural product and DNA, the control of base pairings present in the proposed model strands will enable a more complete understanding of how the chemical structure of DNA relates to the binding of the target molecule. Further, the comparison of the titrations using eudistomin U compared with known molecular intercalators such as harman, ethidium bromide and tilorone will provide even greater elucidation into the binding mode of the target molecule. Assignment of eudistomin U as an intercalator may be possible if comparable to the response from known intercalators.

Another method that will enable study of the molecular interaction between the natural product and the model strands of DNA is 1- and 2-dimensional NMR spectroscopy. NMR spectroscopy has been instrumental in the elucidation the binding modes of several biologically active molecules known to interact with DNA.<sup>22-24</sup> Depending on the type of covalent or non-covalent interaction, the NMR spectrum of a DNA strand will be perturbed in the presence of a binding molecular agent. Therefore, a study will be conducted involving the NMR spectroscopy of each model DNA strand complexed with eudistomin U compared to that of ethidium bromide and harman. The change in spectral features will enable robust assignment of the effect of base pairing on the propensity of eudistomin U to bind, while also enabling a direct comparison to strong intercalating agents. With the results of the two sets of proposed experiments, the strand exhibiting the strongest interaction with the natural product will allow the assignment of which base pairings are most hospitable to eudistomin U as an intercalator: A–T or C–G.

As a contingency, if the previously described experiments provide little insight into the specific binding mode as a function of base pairing, a series of more general experiments will be

conducted, such as thermal denaturation. It is known that small molecules affect the stability of DNA when complexed, and the change in melting temperature in the presence of a binding agent indicates the relative strength of a molecular interaction.<sup>25</sup> This experiment provides insight into interaction strength, but does not account for the specific molecular processes responsible for the change in stability.

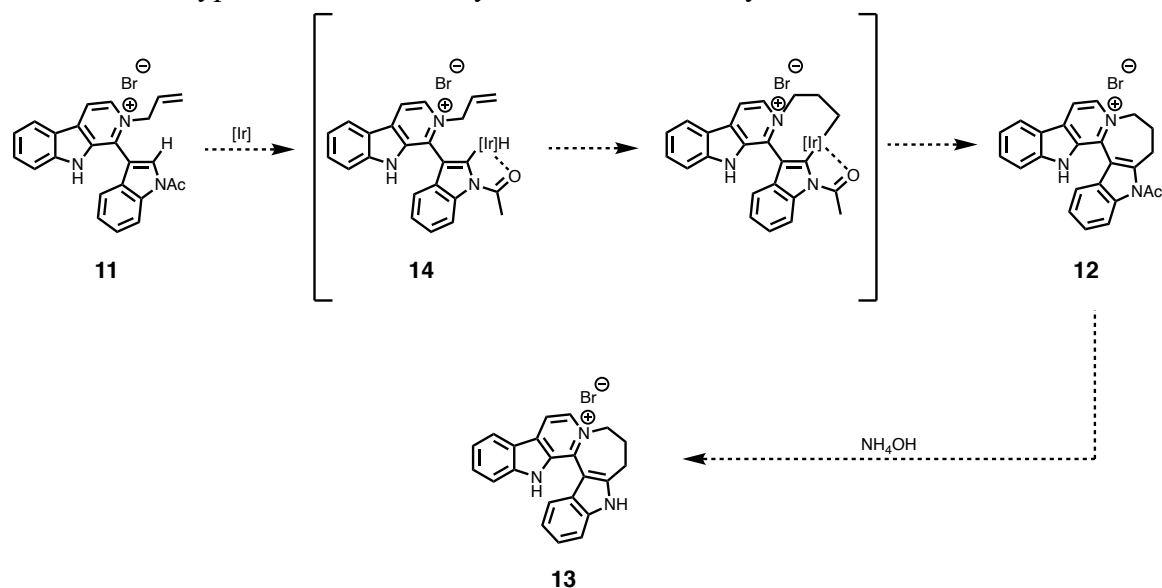
*Phase two* will involve the synthesis of analogues of eudistomin U in order to investigate the effect of structure on binding to DNA. As referenced above, the synthesis of members of the eudistomin family is a mature field with several reported syntheses. Therefore, the proposed research will primarily utilize the shortest reported synthesis of eudistomin U reported by Roggero and coworkers (**Scheme A.3**)<sup>15</sup>, with a change in the boronic acid substrate in order to facilitate substitution at the C-2 position of the indole similarly reported by Pan and coworkers.<sup>17</sup> The proposed synthetic sequence is presented in **Scheme A.5**.

**Scheme A.5** Proposed synthetic plan towards an annulated eudistomin U derivative.

Taking inspiration from both the synthetic plan disclosed by Roggero and coworkers,<sup>15</sup> along with the methodology reported by Pan and coworkers,<sup>17</sup> the proposed synthetic plan will begin with tryptamine **5** being converted to lactam **6** through a Bischler-Napieralski cyclization. DDQ oxidation of **6** will afford pyridoindolone **7**, which through reaction with triflic anhydride will give aryl triflate **8**. It is at this point that efforts will diverge from previously disclosed syntheses. Suzuki cross coupling with *N*-acetylated indole-based boronic acid **9** will yield protected eudistomin **10**. Then, reaction with allyl bromide will yield the corresponding pyridonium indole **11**. Given that the pyridonium species will bear both a pendant olefin and indole that is unsubstituted at the C-2 position, the use of a C-2 specific indole coupling reaction will allow for the formation of annulated compound **12**, which following deacetylation using  $\text{NH}_4\text{OH}$  will afford the final annulated eudistomin U analogue **13**. Rationalization of the

selectivity of the iridium-catalyzed C-2 substitution can be seen in **Scheme A.6**, in which oxidative insertion of iridium into the C-2 C–H indole bond will result in species **14** poised to direct the iridium substitution via the pendant acetyl group.

**Scheme A.6** Hypothesized selectivity of the iridium-catalyzed C-2 indole substitution.



With the newly synthesized eudistomin analogue **13**, the intended direction is to compare its binding affinity to wild type calf thymus DNA to that of unsubstituted eudistomin U. Having previously established the preferential binding to one of the model DNA strands in phase one, the use of wild type DNA will enable the evaluation of eudistomin binding under more natural conditions. As in the case with phase one, the comparison of the annulated eudistomin analogue **13** with known intercalators such as ethidium bromide and visualization techniques such as UV-Vis, 2-dimensional NMR and, perhaps, a potential crystal structure of either the unsubstituted eudistomin U or its annulated analogue, will enable the concrete elucidation of the preferential binding mode of the natural product to DNA.

## Summary and Conclusions

Eudistomin U is a  $\beta$ -carboline natural product with a unique and diverse biological activity profile, such as cytotoxic, antibacterial, antifungal and antiviral affinities. Like many  $\beta$ -carboline alkaloids, it has been suggested that the primary mechanism of action for eudistomin U is its interaction with DNA. However, the exact binding mode of the natural product is not well understood and has not been specifically elucidated. In this proposed work, the demonstration of the binding mode of the molecule will be attempted, first through the assay of eudistomin U with idealized model strands of DNA, and the synthesis of an annulated analogue of the natural product, and their respective comparisons to known intercalating molecules, will enable a more complete depiction of its binding mode. If successful, the proposed research will provide the first assignment of the binding mode of the molecule and will enable the more robust study of biologically-active and pharmacologically-relevant compounds in the future.

### Appendix References

1. Cao R, Peng W, Wang Z, Xu A. beta-Carboline alkaloids: biochemical and pharmacological functions. *Current Medicinal Chemistry*. 2007 ;14(4):479-500.
2. Eudistomidins B, C, and D: novel antileukemic alkaloids from the Okinawan marine tunicate *Eudistoma glaucus*.
3. Eudistomins W and X, Two New  $\beta$ -Carbolines from the Micronesian Tunicate *Eudistoma* sp.
4. Eudistomin K sulfoxide - an antiviral sulfoxide from the New Zealand ascidian *Ritterella sigillinoides*.
5. Eudistomin C, an Antitumor and Antiviral Natural Product, Targets 40S Ribosome and Inhibits Protein Translation.
6. Eudistomins C, E, K, and L, potent antiviral compounds containing a novel oxathiazepine ring from the Caribbean tunicate *Eudistoma olivaceum*.
7. Antiviral and antitumor structure-activity relationship studies on tetracyclic eudistomines.
8. Eudistomin U and Isoeudistomin U, New Alkaloids from the Caribbean Ascidian *Lissoclinum fragile*.
9. V. Serdyuk, O.; A. Kolodina, A., Eudistomin U, Isoeudistomin U, and Related Indole Compounds: Synthesis and Biological Activity. *Heterocycles* **2018**, *96* (7).
10. An iminophosphorane-mediated efficient synthesis of the alkaloid eudistomin U of marine origin.
11. F. Nissen, V. Richard, C. Alayrac, and B. Witulski, *Chem. Commun.*, 2011, 47, 6656.
12. P. Rocca, F. Marsais, A. Godard, G. Quéguiner, L. Adams, and B. Alo, *Tetrahedron Lett.*, 1995, 36, 7085. .

13. Massiot, S. Nazabadioko, and C. Bliard, *J. Nat. Prod.*, 1995, 58, 1636; (b) H. Kang and W. Fenical, *Nat. Prod. Lett.*, 1996, 9, 7.
14. DNA-binding studies of the natural b-carboline eudistomin U.
15. Roggero, C. M.; Giulietti, J. M.; Mulcahy, S. P., Efficient synthesis of eudistomin U and evaluation of its cytotoxicity. *Bioorg Med Chem Lett* **2014**, 24 (15), 3549-51.
16. Directed palladation: fine tuning permits the catalytic 2-alkenylation of indoles.
17. Pan, S.; Ryu, N.; Shibata, T., Ir(I)-catalyzed C-H bond alkylation of C2-position of indole with alkenes: selective synthesis of linear or branched 2-alkylindoles. *J Am Chem Soc* **2012**, 134 (42), 17474-7.
18. Almaqwashy, A. A.; Paramanathan, T.; Rouzina, I.; Williams, M. C., Mechanisms of small molecule-DNA interactions probed by single-molecule force spectroscopy. *Nucleic Acids Res* **2016**, 44 (9), 3971-88.
19. Nafisi, S.; Bonsaii, M.; Maali, P.; Khalilzadeh, M. A.; Manouchehri, F., Beta-carboline alkaloids bind DNA. *J Photochem Photobiol B* **2010**, 100 (2), 84-91.
20. Lorenz, T. C., Polymerase chain reaction: basic protocol plus troubleshooting and optimization strategies. *J Vis Exp* **2012**, (63), e3998.
21. Tu, L. C.; Chen, C. S.; Hsiao, I. C.; Chern, J. W.; Lin, C. H.; Shen, Y. C.; Yeh, S. F., The beta-carboline analog Mana-Hox causes mitotic aberration by interacting with DNA. *Chem Biol* **2005**, 12 (12), 1317-24.
22. Nishimura, T.; Okobira, T.; Kelly, A. M.; Shimada, N.; Takeda, Y.; Sakurai, K., DNA Binding of Tilorone: <sup>1</sup>H NMR and Calorimetric Studies of the Intercalation. *Biochemistry* **2007**, 46 (27), 8156-8163.
23. Nielsen, C. B.; Petersen, M.; Pedersen, E. B.; Hansen, P. E.; Christensen, U. B., NMR Structure Determination of a Modified DNA Oligonucleotide Containing a New Intercalating Nucleic Acid. *Bioconjugate Chemistry* **2004**, 15 (2), 260-269.

24. Laskowski, T.; Czub, J.; Sowiński, P.; Mazerski, J., Intercalation complex of imidazoacridinone C-1311, a potential anticancer drug, with DNA helix d(CGATCG)<sub>2</sub>: stereostructural studies by 2D NMR spectroscopy. *Journal of Biomolecular Structure and Dynamics* **2016**, *34* (3), 653-663.
25. Hayashi, K.; Nagao, M.; Sugimura, T., Interactions of norharman and harman with DNA. *Nucleic Acids Research* **1977**, *4* (11), 3679-3686.